Self-Assembled Monolayers of Metal Complexes Attached to Gold Electrodes

A Thesis Submitted for the Degree of

Doctor of Philosophy

by

Maria Pilar Calatayud Sanz

School of Chemistry
University of Edinburgh
King's Buildings
West Mains Road
Edinburgh, EH9 3JJ

March 2009

Abstract

Self-assembled monolayers (SAMs) of organo-sulfur compounds on gold surfaces offer the possibility of creating controlled surface chemistries with high molecular organization. These nanostructured materials are useful for studying interfacial phenomena and for the development of new devices, sensors and catalysts.

In this thesis, ten different ligands were designed and synthesized in such a way as to provide metal containing SAMs.
The metal binding sites of these ligands are derivatives of the tripodal ligand tris(2-pyridylmethyl)amine (TPA) and the tridentate amine bis(2-pyridylmethyl)amine (BPA), which have good molecular recognition properties in solution. As the interface separating the electrode from the metal binding site and gold anchor group we have chosen thiophenyl, thioethyl and thioctic acid groups.

Electrochemical studies with $[Fe(CN)_6]^{3-/4-}$ as redox probe in solution were carried out on SAMs of the TPA thioctic acid derivative **L4** and its complexes Cu**L4**, Zn**L4** and Fe**L4**. The electron-transfer properties were evaluated by measuring the charge transfer resistance "R_{ct}" across the SAMs, and this parameter was used to calculate the apparent rate constant for the solution redox couple, k_{app}. For SAM-**L4** k_{app} was found to be 3.87×10^{-5} cm/s, and was compared with the electron-transfer blocking behaviour of SAMs obtained with decanethiol ($k_{app} = 1.54 \times 10^{-4}$ cm/s) and thiophenol ($k_{app} = 5.95 \times 10^{-4}$ cm/s). Monolayers containing redox active Cu(II/I) ions accelerated the electron-transfer reaction ($k_{app} = 2.78 \times 10^{-2}$ cm/s) more than those containing Zn(II) ($k_{app} = 1.51 \times 10^{-4}$ cm/s) and Fe(II) ($k_{app} = 1.40 \times 10^{-3}$ cm/s) ions. This is consistent with a mechanism for electron-transfer in which the Cu ions exist in different coordination environments and with different redox potentials, and are rapidly undergoing interconversion.
The ability of this system to facilitate the electron-transfer process to the redox probe was used to develop a new cyanide sensor. Addition of cyanide ions increases the blocking behaviour of the SAM, suggesting the elimination of Cu from the SAM to form $[Cu(CN)_n]^{(n-1)-}$ complexes. This was corroborated by the surface technique X-

ray photoelectron spectroscopy (XPS), which revealed that after the addition of increasing concentrations of cyanide the presence of the Cu(II/I) on the SAM surface decreases. The cyanide detection limit was found to be 1 nM.

Electrodes modified with the binucleating ligand 2,6-bis[bis(2-pyridylmethyl)amino-methyl]phenol thioctic acid derivative (bearing two BPA arms) **L7** were also investigated. Good blocking properties of SAM-**L7** in solution were observed. SAM-Zn**L7** complexes showed slower electron transfer ($k_{app} = 4.93 \times 10^{-5}$ cm/s) compared to SAM-**L7** ($k_{app} = 1.75 \times 10^{-4}$ cm/s). Electrochemical studies using different electrolytes suggested the formation of a negatively charged metal complex resulting in the generation of a film of counter cations between the SAM-Zn**L7** and the redox probe, which slows down the electron-transfer process.
The blocking behaviour of the SAM-Zn**L7** decreases in the presence of μM concentrations of phosphate and pyrophosphate at pH = 7. The response to pyrophosphate was found to be larger, presumably because Zn**L7** binds pyrophosphate more strongly than phosphate. This is consistent with recently reported pyrophosphate binding studies in solution for related metal complexes.

The results presented in this work show that metal containing SAMs can influence the electron-transfer process through the SAM to a solution containing a redox probe. This property can be used to develop new anions sensors in aqueous system.

Acknowledgements

This work would never have been accomplished without the support and guidance of my supervisor Dr. Juan Mareque-Rivas. Above all, I want to thank him for giving me the opportunity of developing this thesis. I am very grateful for his advice, kind assistance and for the things I have learnt from him. Gracias por todo Juan.

I would like to thank all the members of Mareque's group from the past and present. Especially Emiliano and Laurent, for their help in the early stage of my research work and for the good times in and out the lab. I would like to express my gratitude to Dr. Ganesh who worked with me on the electrochemical experiments and for the numerous helpful discussions. Manish, thank you for your enjoyable conversations, happiness and cheerfulness. I want to also thank other labmates who were members of the group for short periods, Jordan, Jose, Nina and Carmen. Thank you for the pleasant time that we spent together. It was a great joy to work with all of them.

To Daniela and Maria, the most important people that have been with me during my whole phD. They were my labmates, flatmates and my best friends. I want to thank you for your support, company and patience during these three years. Without you I don't know how I would have survived in Edinburgh. I will never forget our time together, and I hope we will have many other nice moments in the future. I don't have words to express how grateful I am and how happy I feel for having you in my life.

Agustinos, thanks for your friendship and your individuality, you are unforgettable. I also want to thank my friends, Giorgios and Alessandro for a good and enjoyable time together. I hope that we will be able to stay in touch in the future despite the distance.

A very special thank goes to my colleagues at the department who have made Edinburgh a very special place over all these years: Michele, Mike, Iria, Alex, Pekka, Andrea, Isabel, Oscar, Gordon, Uma, Kiara, Cecile, Javi, Luis, Davide and Filipa.

I would also like to thank other good friends I have made during this period like Eleni, Jordi, Andoni, Xios, Bea, Jöao and Max, with whom I also had great moments in Edinburgh.

My gratitude to the School of Chemistry and Leverhulme Trust for financial support during these years and to all the technical staff. In particular Mr. John Millar from the NMR services for his help. I also want to express my sincere appreciation to Professor Lesley Yellowless for allowing me to use the electrochemical equipment.

To my adoptive family in Edinburgh, Malcolm and Ann. Thanks for always being so kind, for your company, friendship and for making me feel at home. This really helped during my last period in Edinburgh.

Angeles, gracias por tu ayuda y tu apoyo dentro y fuera del laboratorio, por tu amistad y por estar siempre cuando te necesito.

No puedo dejar de mencionar al Dr. Angel Lopez Molinero, profesor de la Universidad de Zaragoza, quien contribuyó a mi formación académica y quien me inicié en el mundo de la investigación. Mi más sincero agradecimiento por su aprecio, consejos y apoyo.

A mis amigas, Silvia Chueca, con la que viví mis primeras experiencias en Edimburgo y a Nuria, Ester, Adriana, Sara y Silvia, con las que compartí los años de carrera y sigo compartiendo gratos momentos. Mil gracias por vuestro cariño y amistad que siempre me habéis demostrado.

Finalmente, doy gracias a las personas más importantes en mi vida. A mi hermano Ignacio, por tu apoyo durante este periodo, por tu cariño y por transmitirme siempre tu optimismo. A mis padres, José Antonio y Pilar, a vosotros os dedico este trabajo y todos mis esfuerzos. Gracias por haber creído siempre en mí, por animarme a sacar este proyecto adelante, por escucharme y por vuestros consejos.

Abbreviations

ac	Alternating current
ADP	Adenosine diphosphate
AFM	Atomic force microscope
AIBN	2,2'-azobis(2-methyl-propionitrile)
AMP	Adenosine monophosphate
ATP	Adenosine triphosphate
BBPAP	2,6-bis[bis(2-pyridylmethyl)aminomethyl]-4-aminophenol
BPA	Bis(2-pyridylmethyl)amine
BPAP	2-[bis(2-pyridylmethyl)aminomethyl]-4-aminophenol
ca.	Circa
cAMP	2',3'-cyclic adenosine monophosphate
CcO	Cytochrome c oxidase
C_{dl}	Double layer capacitance
CTV	Cyclotriveratrylene
CV	Cyclic voltammetry
dc	Direct current
DCC	1,3-dicyclohexylcarbodiimide
DβM	Dopamine β-monooxygenase
DMSO	Dimethyl sulfoxide
DNA	Deoxyribonucleic acid
E_b	Binding energy
E_{kin}	Kinetic energy
EIS	Electrochemical impedance spectroscopy
EIS-MS	Electrospray ionisation mass spectroscopy
et al.	And others
EtOH	Ethanol
eV	Electron volts
FT	Fourier transform
HEPES	4-(2-hydroxyethyl)-1-piperazineethanesulfonic acid
HREELS	High resolution electron energy loss spectroscopy
His	Histidine
I	Current

I_A	Light absorbed
I_c	Charging current
I_f	Faradaic current
I_0	Incident light
I_R	Reflected light
I_T	Transmitted light
IR	Infrared
Is	Scattered light
MCT	Mercury cadmium telluride
MeOH	Methanol
NBS	*N*-bromosuccinimide
NEXAFS	Near edge X-ray absorption fine structure spectroscopy
NMR	Nuclear magnetic resonance
NTA	Nitrilotriacetic acid
OPE	Oligo(phenyleneethynylene)
3,4-PCD	Enzyme 3,4 - dioxygenase
PENP	*N,N*-bis(2-pyridylmethyl)ethane-1,2-diamine
PHM	Peptidylglycineα-hydroxylating monooxygenase
Pi	Inorganic phosphate
PM-RAIRS	Polarization-modulation reflection absorption infrared spectroscopy
PPi	Pyrophosphate
RAIRS	Reflection absorption infrared spectroscopy
R_{ct}	Charge transfer resistance
R_s	Solution resistance
RT	Room temperature
SAM	Self-assembled monolayer
SCE	Saturated calomel electrode
STM	Scanning tunneling microscopy
THF	Tetrahydrofuran
TPA	Tris(2-pyridylmethyl)amine
TPA-(NH_2)	*N,N*-bis(2-pyridylmethyl)-*N*-(6-amino-2-pyridylmethyl)amine
TPA-(NH_2)$_2$	*N,N*-bis(6-amino-2-pyridylmethyl)-*N*-(2-pyridylmethyl)amine
Tyr	Tyrosine

UV-vis	Ultraviolet visible spectroscopy
V	Potential
XPS	X-ray photoelectron spectroscopy
Z	Impedance
Z_{Im}	Imaginary part of impedance
Z_{Re}	Real part of impedance
Z_w	Warburg impedance
Z_f	Faradaic impedance

Table of Contents

Chapter 1

INTRODUCTION

1.1 Host-guest chemistry

A molecule (a 'host') binding to another molecule (a 'guest') is generally considered a 'host-guest' complex or supramolecule.[1]

The host is defined as the molecular entity possessing convergent binding sites (e.g. Lewis basic donor atoms, hydrogen bond donors, etc.), whereas the guest posseses divergent binding sites (e.g. a spherical, Lewis acidic metal cation or a hydrogen bond acceptor halide anion).

The relationship with the resulting host-guest complex has been defined by Donald Cram as follows:[2]

Complexes are composed of two or more molecules or ions held together in unique structural relationships by electrostatic forces other than those of full covalent bonds. Molecular complexes are usually held together by hydrogen bonding, by ion pairing, by π-acid to π-base interactions, by metal to ligand binding, by van der Waals attractive force, by solvent reorganising, and by partially made and broken covalent bonds (transition states).
High structural organisation is usually produced only through multiple binding sites.
A highly structured molecular complex is composed of at least one host and one guest component.
A host-guest relationship involves a complementary stereo electronic arrangement of binding sites in host and guest.
The host component is defined as an organic molecule or ion whose binding sites converge in the complex. The guest component is any molecule or ion whose binding sites diverge in the complex.

In order to bind, a host must have binding sites with an electronic character (polarity, hydrogen bond donor/acceptor ability, hardness, softness, etc.) that complements those of the guest. For instance, hydrogen bond donors must match acceptors and Lewis acids must match Lewis bases. Furthermore, those binding sites must be spaced out in such a way as to make it possible for them to interact with the guest in the binding conformation of the host molecule. Of a host that fulfils these criteria, it is said to be *complementary* of a guest.

If a host molecule does not undergo a significant conformational change upon guest binding, it is said to be *preorganised.* Host preorganisation is a key concept in host:guest chemistry because it represents a major enhancement in the overall free energy of guest complexation.

A host-guest binding process may be divided into two stages. An activation stage in which the host undergoes conformational readjustment in order to arrange its binding sites in a fashion complementary to the guest. This is energetically unfavourable, and because the host must remain in this binding conformation throughout the lifetime of the host-guest complex, this energy is never paid back. Following rearrangement, binding occurs which is energetically favourable because of the enthalpically stabilizing attraction between mutually complementarity binding sites of host and guest. The overall free energy of complexation represents the difference between the unfavorable reorganization energy and the favourable binding energy. If the reorganization energy is large, then the overall energy is reduced, disestablishing the complex. If the host is preorganized, this rearrangement energy penality is small.
However, rigidly preorganized hosts may have significant difficulty in passing through a complexation transition state, so they generally exhibit slow guest binding kinetics. Conformationally mobile hosts are able to adjust rapidly to changing conditions, and both complexation and decomplexation are rapid. Solvation enhances the effects of preorganisation since the solvation stabilization of the unbound host is often greater than when it is wrapped around the guest.

The goal of supramolecular host design, both in nature (enzymes, transport proteins) and in artificial systems is the achievement of selectivity, that is, the discrimination between one guest and another.

We can readily assess the affinity of a host for a particular receptor by its binding constant, which represents the thermodynamic equilibrium constant for the binding process, Host + Guest ↔ (Host.Guest):

$$K = \frac{[Host.Guest]}{[Host]\cdot[Guest]}$$

In thermodynamic terms, selectivity is the ratio of the binding constant for one guest over another:

$$Selectivity = \frac{K_{Guest1}}{K_{Guest2}}$$

1.2 Host-guest chemistry in anion recognition and sensing

Anion receptor chemistry is a vigorous area of research due to the importance of anions in biological systems.[3] They carry genetic information (DNA is a polyanion) and the majority of enzyme substrates and co-factors are anionic. Anions also play roles in the areas of medicine and catalysis, whilst pollutant anions have been linked to eurotrophication of rivers (from the over use of phosphate-containing fertilizers) and carcinogenesis (metabolites of nitrate).

The design of anion receptors is particularly challenging.[4] There are a number of reasons for this. Anions are larger than cations, and therefore have a lower charge to radius ratio. This means that electrostatic binding interactions are less effective than for cations. Additionally anions may be sensitive to pH values (becoming protonated at low pH and so losing their negative charge). This means that receptors must function within the pH window of their target anion. Anionic species have a wide range of geometries and therefore a higher degree of design may be required to make

receptors complementary to their anionic guest. Solvation also plays a crucial role in controlling anion binding strength and selectivity, and is greater for anions than for cations of the same size. Electrostatic interactions generally dominate in anion solvation, and hydroxylic solvents in particular can form strong hydrogen bonds with anions. A potential anion receptor must therefore effectively compete with the solvent environment in which the anion recognition event takes place.

The design of selective hosts for anions requires the geometry and basicity of the anion and the nature of the solvent medium all to be taken into account. Complementarity between the receptor and the anion is crucial in determining selectivity.

1.2.1 Anion recognition

Anion receptors employ noncovalent interactions to complex the anion guest. These include electrostatic interactions, hydrogen bonding, the use of metal complexes as anion binding sites and combination of these interactions working together.

Electrostatic interactions with anions are found when positively charged receptors having for instance guanidinium groups or quaternary ammonium groups are used. Some examples are shown in Figure 1.1.

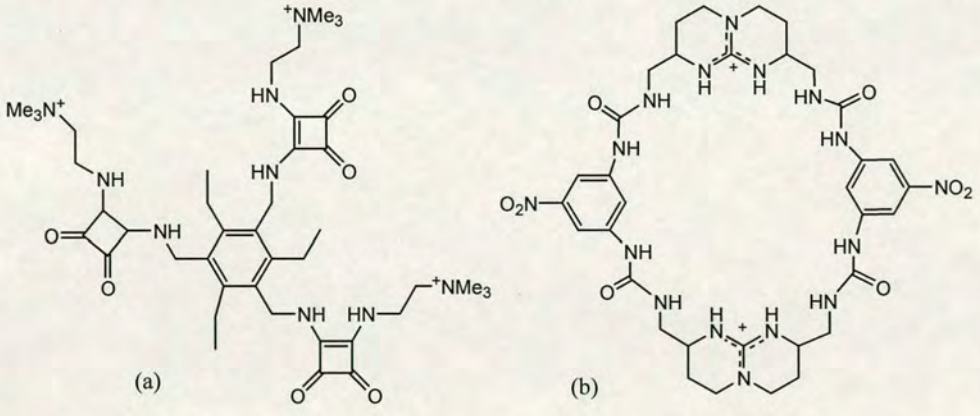

Figure 1.1: Ammonium and guanidinium based anion receptors.

The quaternary ammonium containing squaramido-functionalized tripodal receptor was designed by Anslyn and co-workers, and is able to form stable complexes with

tricarboxylate anions.[5] Jadhav and Schmidtchen synthesised the macrocycle containing two chiral guanidinium anchor groups linked via four urea groups,[6] which also binds carboxylates.

Hydrogen-bonding groups have been widely used in binding sites for anion recognition. A hydrogen bond can be established when a hydrogen covalently attached to a highly electronegatively atom interacts with another electronegatively atom (of the same or different molecule) having lone pairs. Typical hydrogen-bonding sites used for anion binding are: ureas,[7] thioureas,[8] calix[4]pyrroles,[9] porphyrins[10] and amides.[11] Figure 1.2 shows two examples of organic receptors based on hydrogen bonding groups.

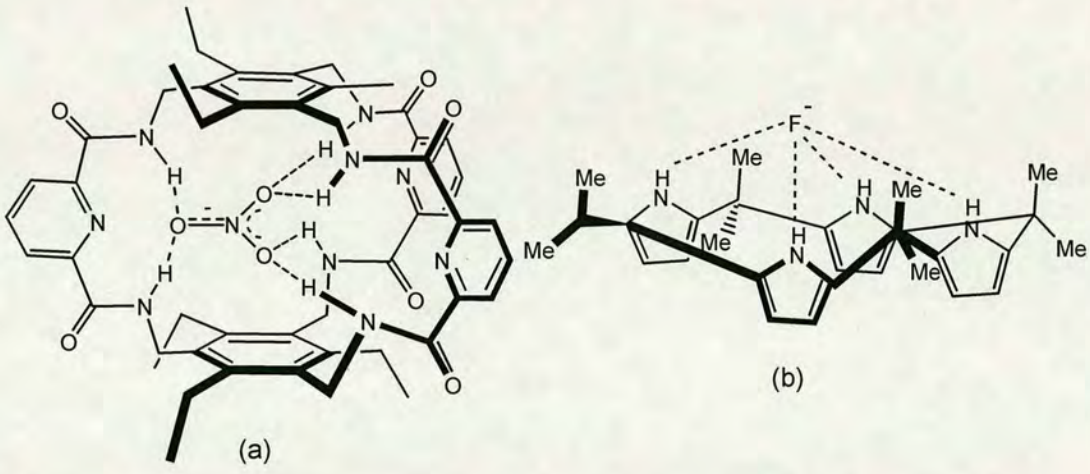

Figure 1.2: Anions receptors based on amido groups and calix[4]pyrrole.

Anslyn and co-workers developed the anion receptor shown in Figure 1.2 (a).[12] Because the amide NH groups are arranged in a trigonal prismatic array, they are able to coordinate to the π-electron system of planar anions such as carboxylates and nitrate. The octamethylcalix[4]pyrrole (Figure 1.2 (b)) was developed by Gale and Sessler,[9] and is selective for fluoride anions.

These organic receptors provide efficient hosts for anions due to strong complementary hydrogen bonding in non-aqueous solutions. However, since hydrogen bonds are typically disrupted in water, it is generally difficult to achieve strong binding of guest molecules with organic hosts. Thus, recently, several groups

have opted for coordination complexes due to the potentially strong interactions that they can form with anions even in water.

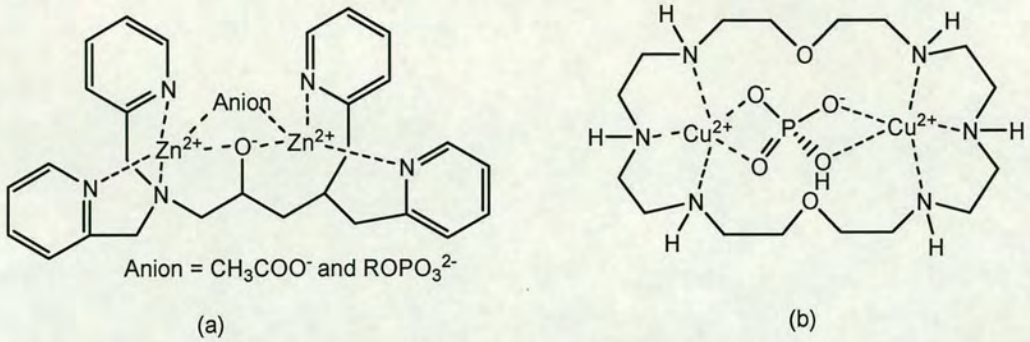

Figure 1.3: (a) Recognition of anions by an alkoxide-bridged dinuclear Zn(II) complex (b) Macrocyclic bis-dien dinuclear Cu(II) complex binding hydrogen phosphate.

An example is the bis(2-pyridylmethyl)amine (BPA) based ligand shown in Figure 1.3 (a) where two Zn(II) ions are used to bind anions such as acetate and phosphate.[13] Macrocycles containing two metal centers (Figure 1.3 (b)) also allows the binding of small anions, such as hydrogen phosphates, phosphates,[14] pyrophosphates,[15] glycinate, or malonate.[16]

Even more recently, a few groups have shown that the combination of hydrogen bonding and metal coordination could be an even more powerful strategy to increase the affinity of host molecules for anions.[17]

An example is the Zn(II) complex developed by Torres Martin de Rosales et al. [18] (Figure 1.4), which shows enhanced affinity for phosphate esters due to two amino hydrogen bonding groups.

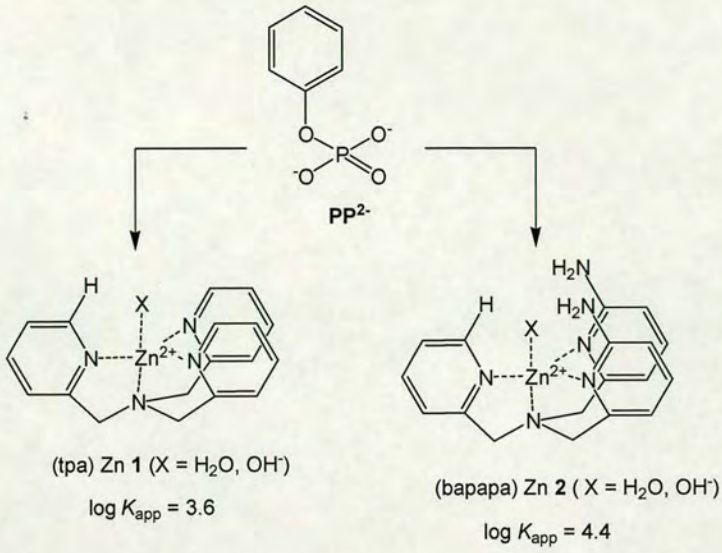

Figure 1.4: Phosphate ester binding to Zn(II) complexes with and without amino groups.

1.2.2 Anion sensors

Recognition sites can be coupled to certain groups that are capable of "reporting" the anion coordination process. In this case, the binding process is transduced into a signaling event. Receptors specifically designed for sensing purposes are generally called chemosensors (Figure 1.5).

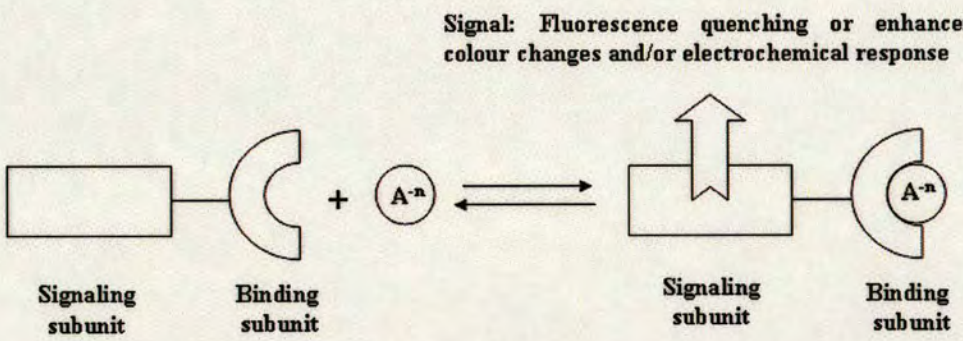

Figure 1.5: Anion chemosensors based on the binding site-signaling subunit approach.

The coordination site binds the anion in such a way that the properties of the signaling subunit are changed, sensing anion binding through an electrochemical or optical response (fluorescence, colour change).

1.2.2.1 Electrochemical recognition of anions

A variety of organic, organometallic, and inorganic redox-active centers have been incorporated into various host frameworks and they have been shown to electrochemically detect charged and neutral guests.[19] Beer and co-workers developed receptors containing cobaltocenium (Figure 1.6).[20]

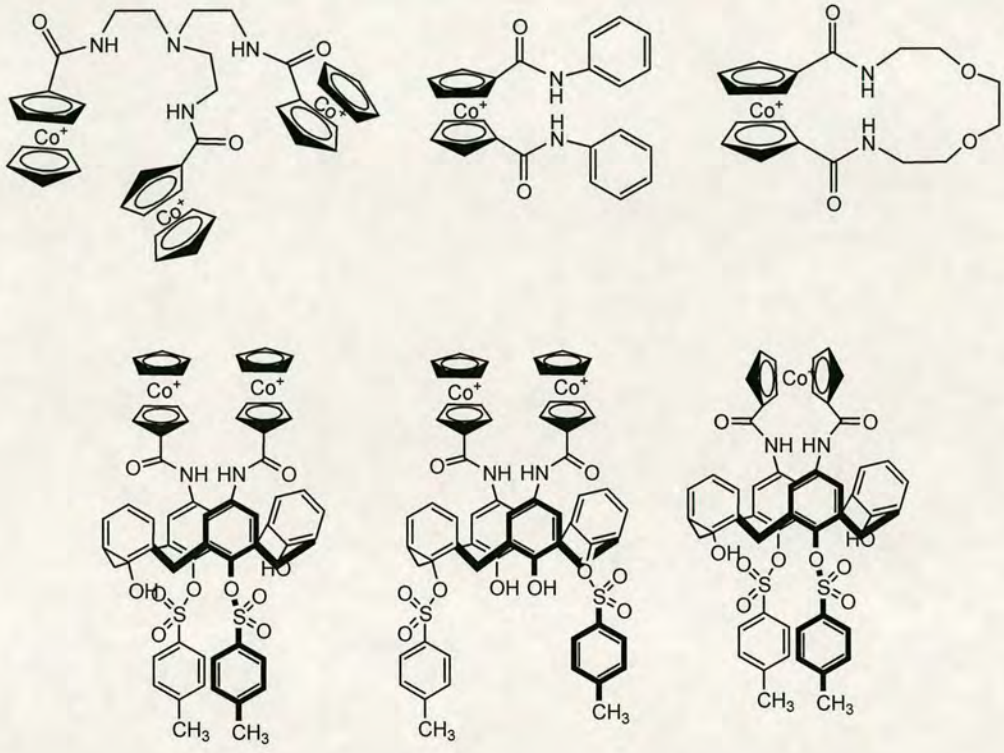

Figure 1.6: Cobaltocenium derivatives for anion receptors.

Cyclic voltammetric experiments demonstrated that all these receptors could electrochemically detect anions. The addition of anions to solutions of the receptors in acetonitrile resulted in significant cathodic shifts of the reversible Cp_2Co^+/Cp_2Co redox couple. The complexed anionic guest effectively stabilizes the positively charged cobalt center making it more difficult to reduce.

The redox-active ferrocene moiety has also been exploited in the electrochemical detection of anions, both in organic and aqueous media.[19]

For example, the receptors shown in Figure 1.7 synthesized by Beer et al. can selectively bind and electrochemically detect phosphate and sulphate (in various states of protonation) as well as nucleotide ions in water.[21]

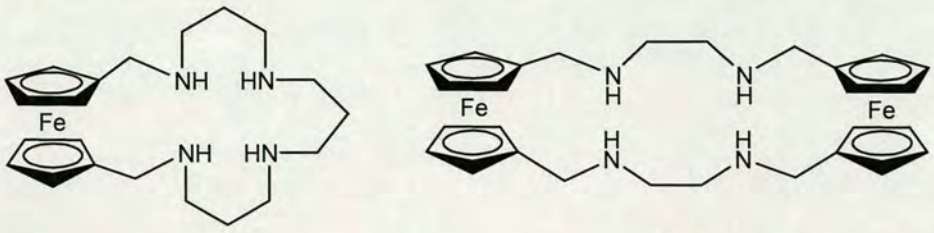

(a) (b)

Figure 1.7: Ferrocene derivatives capable of detecting of phosphates (a) and sulphate (b) anions.

In all these examples, the anion guest is complexed to the receptor through hydrogen bonding interactions, which induces changes in the redox potential of the ferrocene or cobaltocene unit. Tucker and co-workers have also shown that the charge of these redox active units can control the hydrogen bonding strength with the guest.[22] For instance, the ferrocene or cobaltocene receptors containing an amidopyridine group (Figure 1.8) on each Cp ring have been shown to exhibit enhanced glutaric acid binding when they are oxidized.[23]

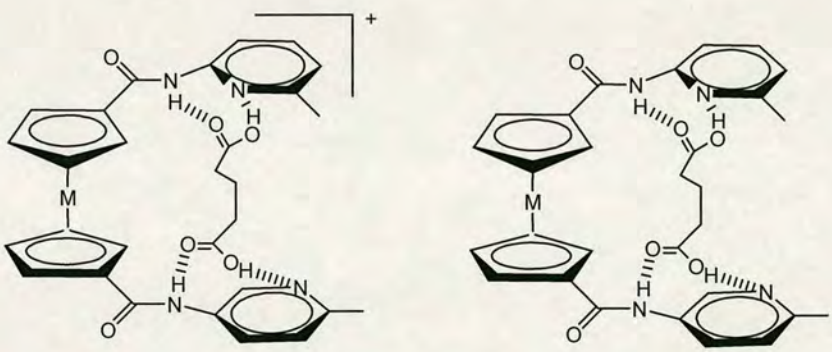

Stronger binding M = Fe, Co Weaker binding

Figure 1.8: Ferrocene and cobaltocene derivatives capable of varying the binding strength by switching their charge.

1.2.2.2 Optical sensing of anions

Another possibility is to use spectroscopic signaling subunits to transduce the coordination event into changes in either colour or fluorescence emission. Fluorescence detection has been widely used as a versatile tool in analytical chemistry, biochemistry, cell biology, etc., due to its high sensitivity. Colour changes as signaling events have been widely used because it requires the use of inexpensive

equipment or no equipment at all as they can be detected by naked eye. Figure 1.9 shows an example of a fluorescent chemosensor.[24]

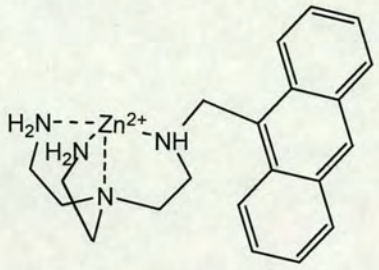

Figure 1.9: Example of a fluorescent chemosensor.

Methanolic solutions of the fluorescence receptors shown in Figure 1.9 are fluorescent, but addition of N,N-dimethylaminobenzoate induces a near complete quenching. A similar effect was observed upon addition of other benzoate anions. In contrast, addition of anions such as nitrate, thiocyanate or chloride did not have any effect. The quenching was ascribed to an intramolecular electron transfer process from the benzoate to the photoexcited anthracene unit.

Two examples of chromogeneic receptors are illustrated in Figure 1.10.[25]

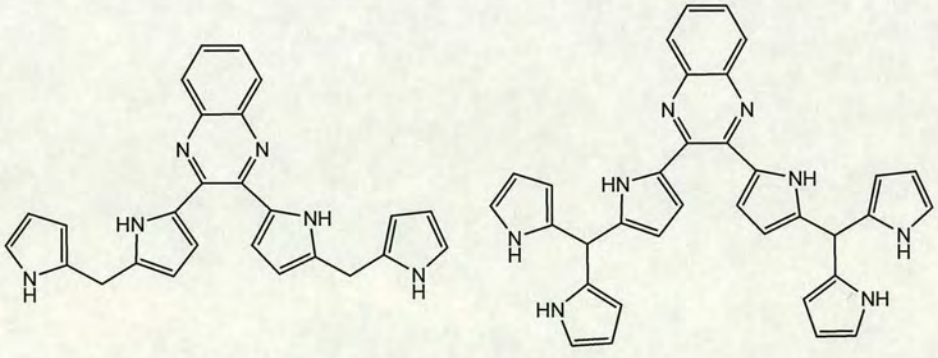

Figure 1.10: Examples of chromogenic chemosensors.

Using UV-visible absorption spectroscopy it was found that these two receptors form 1:1 complexes with fluoride, chloride and dihydrogenphosphate.

1.3 Self-assembled monolayers (SAMs)

The field of self-assembled monolayers (SAMs) has grown over the past 15 years. The field began much earlier than is generally recognized. In 1946 Zisman published the preparation of a monomolecular layer by adsorption (self-assembly) of a surfactant onto a clean metal surface.[26]At that time, the potential of self-assembly was not recognized, and this publication generated only a limited level of interest. Early work initiated in Kuhn's laboratory applying many years of experience in using chlorosilane derivatives on glass,[27] was followed by the more recent discovery by Nuzzo and Allara that SAMs of alkanethiolates on gold can be prepared by adsorption of di-n-alkyl disulfides from dilute solutions.[28] Getting away from the moisture-sensitive alkyl trichlorosilanes, as well as working with crystalline gold surfaces, were two important reasons for the success of these SAMs.

The formation of monolayers by self-assembly of surfactant molecules on surfaces is just one example of the general phenomena of self-assembly. SAMs offer unique opportunities to increase fundamental understanding of self-organisation, structure-properties relationships, and interfacial phenomena.

1.3.1 Concept of self-assembly

SAMs are layers formed on a solid surface by spontaneous organization of molecules (Figure 1.11). SAMs are prepared by immersion of a substrate into a solution of an organic molecule. They are usually composed of molecules which are chemically bound to the substrate via a head group while the molecular chain points away from the substrate. Their inherent organisation, packing, well-defined pattern and versatility allow establishing the correlation between structure and functional behaviour of terminal groups. The functionality at the end of the spacer (end group) mainly defines the surface properties of the film.

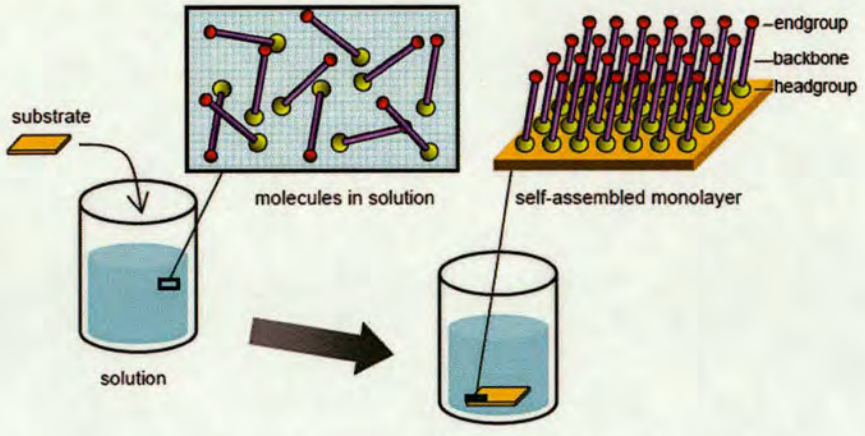

Figure 1.11: Scheme of SAM-preparation and the constituents of a SAM-molecule (headgroup, backbone or bridge and endgroup).

SAM formation provides an easy route towards surface functionalization by organic molecules (both aliphatic and aromatic) containing suitable functional groups like - SH, - CN, - COOH, - NH_2 and silanes on selected metallic (Au, Cu, Ag, Pd, Pt, Hg, and C) as well as semiconducting surfaces (Si, GaAs, indium coated tin oxides, etc.). Two types of these self-assembled monolayers have been extensively studied: alkanethiolates on gold and alkylsilanes on silica or glass. Thiols on gold are the most extensively studied class of SAM due to their ease of preparation and the high order of the monolayer obtained.[29] The thiol groups serve as nucleation centers for the growth of the monolayer film.

1.3.2 SAMs of thiolates on gold

Molecules containing thiols are widely used for self-assembly on gold. This is due to the high affinity of Au for these groups. Among these molecules are di-n-alkylsulfides, di-n-alkyldisulfide, thiophenols, mercaptopyridines, mercaptoanilines, thiophenes, thiocarbaminates, thioureas etc., but the most studied and understood SAM is that of alkanethiolates on Au(111) surfaces. Despite extensive research, the nature of the sulphur-gold bond and the arrangement of the sulphur groups on the underlying surface are still not completely understood. It is assumed that the formation of S-Au bond requires the loss of the hydrogen from the -SH group[30] and that the thiolate ($R\text{-}S^-$) is bound to the gold surface by a covalent bond.[29]

$$R\text{-}S\text{-}H + Au^0_n \rightarrow R\text{-}S^-Au^+ \cdot Au^0_{n-1} + 1/2\ H_2$$

The bonding of the thiolate group to the gold surface is very strong ca. 40 kcal/mol. The most common procedure for preparing SAMs of thiolates on gold is immersion of a clean gold substrate into a thiol solution for several hours. There are two distinct stages in the formation of the monolayer: first a fast process, which takes a few minutes, when the thiol is adsorbed and interacts with the gold surface, and then a relatively slow process, which lasts several hours, when the molecules organize to reach equilibrium and form an ordered film. The structure of the monolayers is determined by the intermolecular chain-chain and headgroup-substrate interactions.

There are a number of experimental factors that can affect the structure of the resulting SAM and the rate of formation:[31]

-*Solvent*: Ethanol is the most widely used solvent for preparing SAMs. SAMs formed from solutions of thiols in non-polar organic solvents are less organized.

-*Temperature*: Forming SAMs at temperatures above 25 °C can improve the kinetics of formation and reduce the number of defects in them. But elevated temperatures also increase the rate of desorption.

-*Concentration and immersion time*: Low concentrations of thiols in solution require long immersion time, however, the coverage of the surface increases with extended immersion times.

-*Oxygen content of solution*: The degasing of the solvent prior to preparing the solutions of thiols and maintaining an inert atmosphere over the solution during formation generally improves the reproducibility of the SAMs.

-*Cleanliness of the substrate*: SAMs have reproducible properties when formed on substrates that are cleaned with strongly oxidizing chemicals ("piranha" solution H_2SO_4:H_2O_2).

Most structural investigations have been carried out on SAMs of alkanethiols ($CH_3(CH_2)_nSH$) on Au(111) surfaces.[29,32] The structure and high coverage of these SAMs was first reported by Strong and Whitesides.[33] An average tilt angle of ~27°-

35° was observed for alkanethiol molecules on Au(111). The headgroup-substrate interaction plays a dominant role for the structure and packing in alkanethiol SAMs.

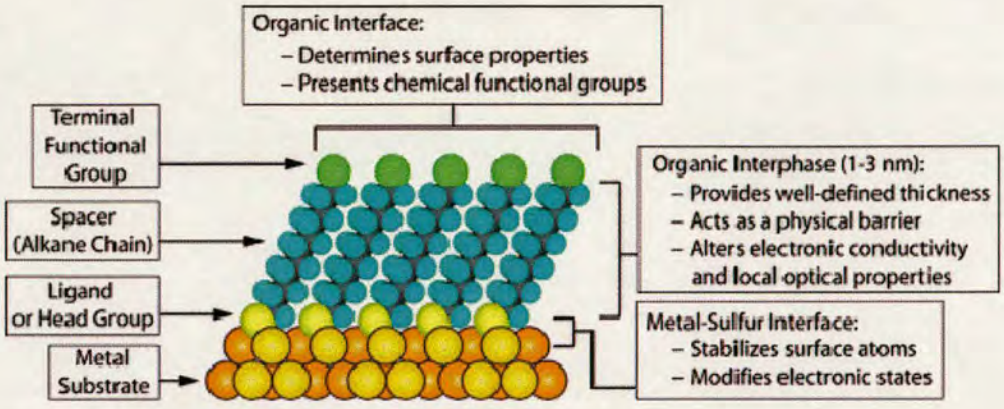

Figure 1.12: Schematic diagram of an ideal SAM of alkanethiolate supported on a gold surface with a (111) texture. The anatomy and the characteristics of the SAM are highlighted.

In the case of thioaromatic SAMs these parameters are mainly determined by the intermolecular interaction. For the SAMs of the simplest thioaromatic molecule, thiophenol (C_6H_5SH), on Au(111), strongly inclined adsorption geometry of the phenyl rings has been reported.[34] With increasing number of the phenyl rings in the aromatic chain, the monolayers become more densely packed and well-ordered.[29]

1.3.3. Electrochemical desorption of SAMs

Thiols undergo reductive desorption when a negative potential is applied to the supporting metallic film.[35] For electrochemical desorption SAMs are typically immersed in an aqueous or ethanolic solution with an electrolyte at a neutral or basic pH. The electrochemical half-reaction for alkanethiolates adsorbed on metals is:

$$RS\text{-}M + e^- \longrightarrow RS^- + M^0$$

Both the thiolate and the bare metal surface become solvated, and the thiolate diffuses away from the surface. The process is reversible: removing the applied negative potential can result in re-adsorption of the thiolates onto the metal surface.[36]

1.3.4 Characterization of SAMs: structure, assembly and defects

The structures of SAMs and the mechanism by which they assemble are subjects that have evolved considerably over the past two decades due to substantial advances in the experimental methods suitable for characterizing them. The development of scanning probe microscopies (AFM, STM, etc.) provided powerful new capacities to study both the structural organization of SAMs and the assembly process at a molecular level. These techniques have greatly extended the initial structural understandings derived mainly from spectroscopic techniques such as: reflection absorption infrared spectroscopy (RAIRS),[37] Raman spectroscopy,[38] X-ray photoelectron spectroscopy (XPS),[39] high resolution electron energy loss spectroscopy (HREELS),[40] near edge X-ray absorption fine structure spectroscopy (NEXAFS),[41] ellipsometry,[42] etc.

1.3.5 SAMs on gold electrodes: mechanism of electron-transfer phenomena studies

Processes that transfer electrons from one location to another over nanometer-scale distances (1-100 nm) are fundamental to important redox processes in biology (photosynthesis, respiration) and to the operation of a wide range of devices, including transistors and catalysts.[43]

Charge transfer processes in biological systems are often mediated by organic molecules and future electronic systems may also involve electron transport through organic matter, but the mechanism for charge transfer in these types of systems are not well established.

SAMs on gold electrodes are useful systems to study the transport through molecules, giving information about the fundamental mechanism (tunneling, hopping, thermionic conduction), the rates of electronic transport, how the structure and the composition affect the transfer process, and allow to investigate how the mechanism and rate of electron transfer changes as a function of distance.

Chemical modification of an electrode makes it possible to generate barrier layers that prevent free diffusion of electroactive species to the surface of the electrode and to immobilize electroactive species on the electrode itself. There are two experimental configurations commonly used in electrochemistry for studying electron transfer processes with SAM-modified electrodes. One strategy uses a hydrophobic SAM to block a redox species (dissolved in the surrounding electrolyte solution) from diffusing to the surface of the electrode itself.[44] A second approach uses SAMs were the molecular components terminates with an electroactive group (for example, ferrocene or ruthenium pentaamine).[45]

Some of the charge-transfer phenomena studied with SAM-modified electrodes include:

-The parameters (distance from the surface, electrolyte, temperature, metal) affecting electron-transfer process.

-Proton-coupled electron-transfer reactions.

-Effect of solvation of electroactive species in hydrophobic environments on redox reactions.

-Effect of counter ion motion on the rates of electron transfer.

-The effect of orientation and conformation of electroactive proteins (e.g. cytochrome c, glucose oxidase) on the rates of electron transfer across SAMs.

1.3.6 SAMs of redox molecules on gold electrodes

Self-assembled monolayers of redox molecules on gold electrodes create the electrochemical analogue of a bridged donor-acceptor molecule and allow the study of kinetic parameters of long-range electron transfer processes.[46] These studies may also help the development of the fields of molecular electronics,[47] electro catalysis,[48] and sensor design.[49]

Electrochemical techniques like cyclic voltammetry (CV) and electrochemical impedance spectroscopy (EIS) can be used to understand the packing density and

surface coverage of the molecular films, and to measure kinetic parameters associated with the electron-transfer across the SAM.

For instance, Creager and co-workers studied the influence of the length of the bridge in the rate of electron transfer in a series of ferrocene-containing monolayers on gold electrodes by cyclic voltammtery (CV) (Figure 1.13).[50]

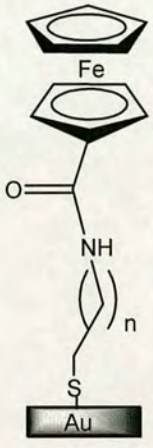

number of methylenes (n)	7	10	15
k_0, s^{-1}	6.6×10^4	6×10^3	6.6

Figure 1.13: Rate constants for ferrocene-containing monolayers.

The ferrocene groups were linked to a gold electrode by alkane chains of different lengths. The clear trend is that as the chains become longer, the rate is slower. This reflects a decrease in the electronic coupling between the ferrocene group and the electrode as the length of the alkane chain linking the ferrocene group to the electrode increases.

Although there are fewer reports on aromatic thiol monolayers,[51] they represent interesting systems because of the highly delocalized electron density and structural rigidity of the π -bonds.

It has been shown that the kinetics of electron-transfer of the ferrocene redox couple through oligo(phenyleneethynylene) (OPE) bridges vary significantly depending on their molecular conformations and length (Figure 1.14).[52]

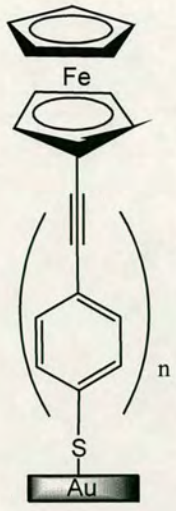

number of units (n)	1	2	3
k_0, s^{-1}	1.5×10^7	3.3×10^6	6.4×10^4

Figure 1.14: Electron transfer rate constants for monolayers containing OPE bridging unit.

From these studies it is possible to compare the values obtained for the electron transfer rate across an aromatic and aliphatic domain (Figure 1.15).

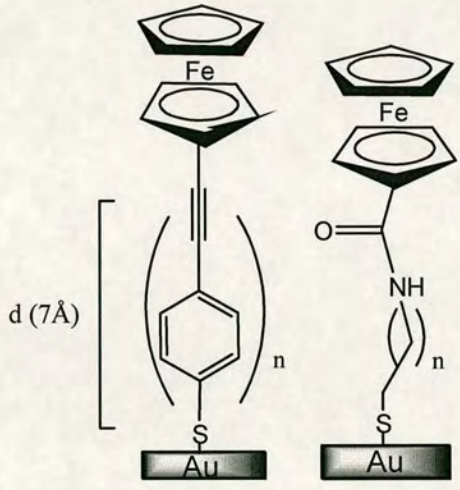

n = 1 Aromatic chain k_0, $s^{-1} = 1.5 \pm 0.1 \times 10^7$

n = 7 Aliphatic chain k_0, $s^{-1} = 6.6 \times 10^4$

Figure 1.15: Electron transfer rates across aromatic and aliphatic interfaces.

The values of k_0 are orders of magnitude (10^3-fold) larger for an OPE spacer than for alkanes spacer of comparable length. This is because the electron transport through π-conjugated materials such as OPEs is faster. Because of this property, these types of materials have been the subject of considerable recent study for the design and construction of molecular-scale electronic devices.[53]

Studies with SAMs have also shown that interchain interactions (i.e. electronic coupling through nonbonded contacts) can affect the rate of electron transfer across molecular films.[54]

For instance, in a recent study the effect of hydrogen bonds formed by amide groups in the monolayer on the electronic coupling between ferrocene and gold electrodes was found to be significant.[55] To obtain the hydrogen bond network, two component monolayers were prepared using functionalized alkanethiols (Figure 1.16).

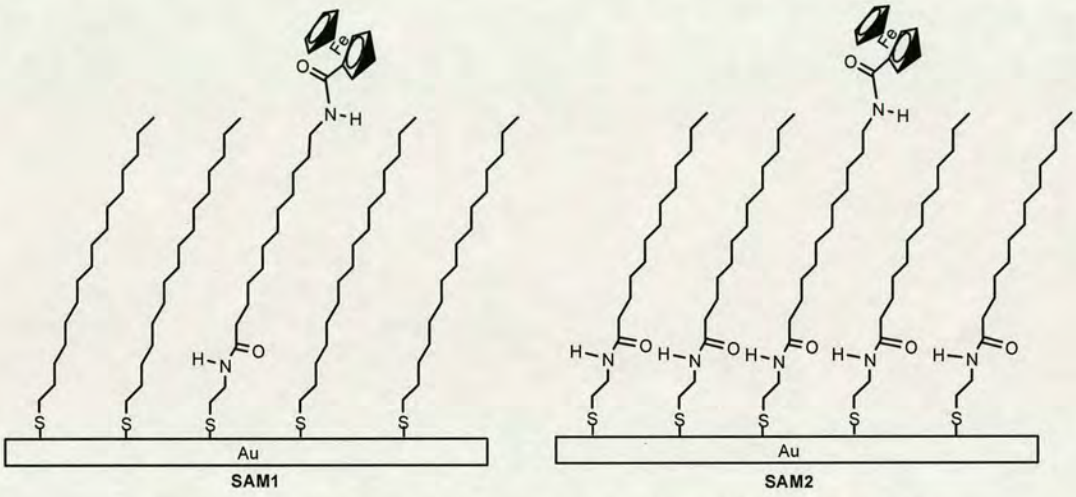

Figure 1.16: Scheme of the monolayer assemblies SAM1 and SAM2.[54]

In the case of SAM1 with an amide moiety situated only in the electroactive component, the rate constant obtained by cyclic voltammetry was 4.5 s^{-1}, which is close to the value of 6.6 s^{-1} obtained by Creager for monolayers lacking the amide group. This indicates that the introduction of a -CONH bond into the electroactive molecules does not lead to an increase of the electron-transfer rate. SAM2 with amide groups both in the electroactive molecules and in the diluent thiol present a rate constant of 17 s^{-1}. It was suggested that the increase of coupling is due to the presence of a hydrogen bond network inside the layer, and that the contribution of the coadsorbate, or diluent, to the electronic coupling may be significant when additional electron delocalization is introduced by the lateral bonds formed by the diluent molecules. Such cooperative effects confirm the importance of hydrogen bonding for long-range electron transfer.

1.4 Metal containing SAMs: applications in chemical sensing and catalysis

The immobilization of functional metal complexes onto gold electrodes can be used to develop molecular recognition systems and catalysts.[56] SAMs offer the possibility of modulating the length and the nature of the bridge that connects the metal unit and the electrode, promoting or decreasing the electron transfer process. This can be used to regulate the properties of the system depending on the desired applications.

For instance, Collman and co-workers have recently reported the immobilization of a complex onto gold which mimics the coordination environment and relative locations of Fe_{a3}, Cu_B and Tyr^{244} of cytochrome c oxidase (CcO) (Figure 1.17).[57]

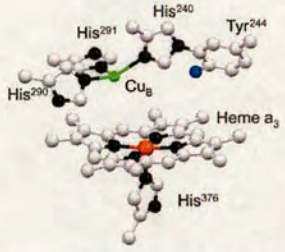

Figure 1.17: Crystal structure of the active site of CcO.

These chemically modified gold electrodes were found to act like the enzyme as a catalyst for the reduction of oxygen to water (Figure 1.18).

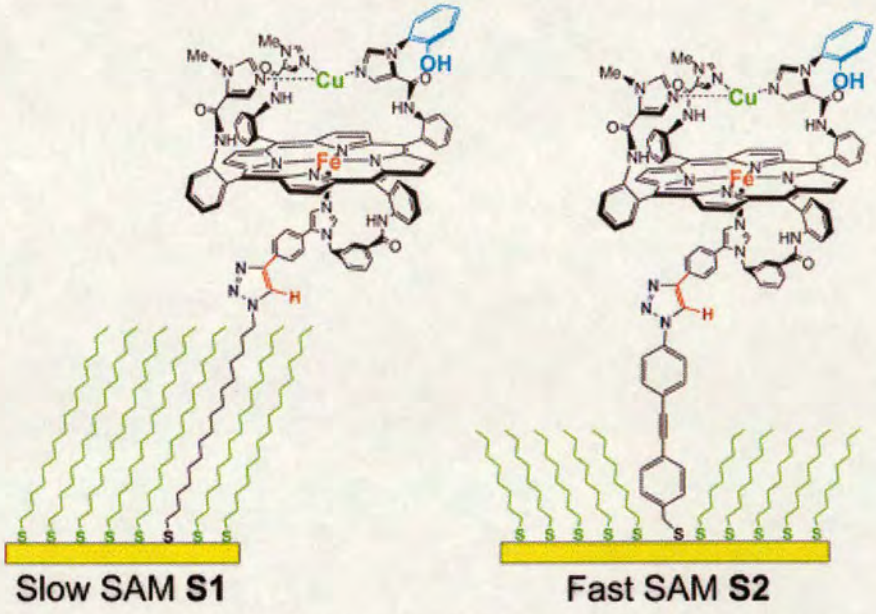

Figure 1.18: Slow SAM S1 and fast SAM S2 functionalized with a synthetic model of cytochrome c enzyme.

The model of CcO was covalently attached to the gold surfaces by mixed SAMs. SAM S1 was composed of 1-azidohexadecanethiol and hexadecanethiol ("slow SAM S1") and SAM S2 of a highly conjugated SAM composed of azido phenylleneethynylenebenzyl thiol and octanethiol ("fast SAM S2").

The standard electron-transfer rate constant, k_0, between the gold electrode and the iron center of these models was $6 \pm 0.1\ s^{-1}$ for SAM S1. In contrast, k_0 for SAM S2 was too fast to measure with conventional electrochemical methods[58] but is at least $1 \times 10^4\ s^{-1}$. These results show again how the nature of the SAM influences the electron transfer process to the metal centers of the CcO model. Both SAMs were found to be selective at reducing oxygen to water releasing only a small percentage of partially reduced oxygen species.

Another example of metal containing SAMs that can act as catalyst was developed by Yamaguchi et al.[59] In this case it is a gold electrode modified with copper complexes containing a tridentate aromatic amine compound bis(6-methyl-2-pyridylmethyl)amine ethyl sulphide (Figure 1.19). This SAM was able to catalyse the conversion of nitrite to nitrogen monoxide under acidic conditions.

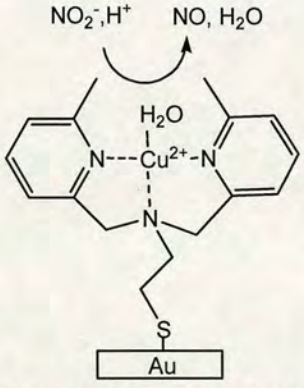

Figure 1.19: Gold electrode modified with Cu(II) bound to the tridentate aromatic amine ligand bis(6-methyl-2-pyridylmethyl)amine ethyl sulphide.

The combination of molecular recognition elements and SAMs generates a powerful tool for sensing applications. Incorporating SAMs in sensing devices offers several advantages[60] including ease of preparation, reproducibility, fast response, amplification of sensing, and pre-organization of receptors on the surfaces. Sensing is achieved with SAMs containing redox active and inactive receptors using

techniques such as fluorescence spectroscopy, cyclic voltammetry and electrochemical impedance spectroscopy.

SAMs have been used to immobilize macromolecules, including DNA,[61] proteins,[62] and enzymes.[63] For instance, Whitesides et al. developed procedures to modify the surface of gold films with Ni(II)NTA (NTA = nitrilotriacetic) complex. [64] Using this complex they were able to selectively immobilize proteins with His-tags (Figure 1.20).

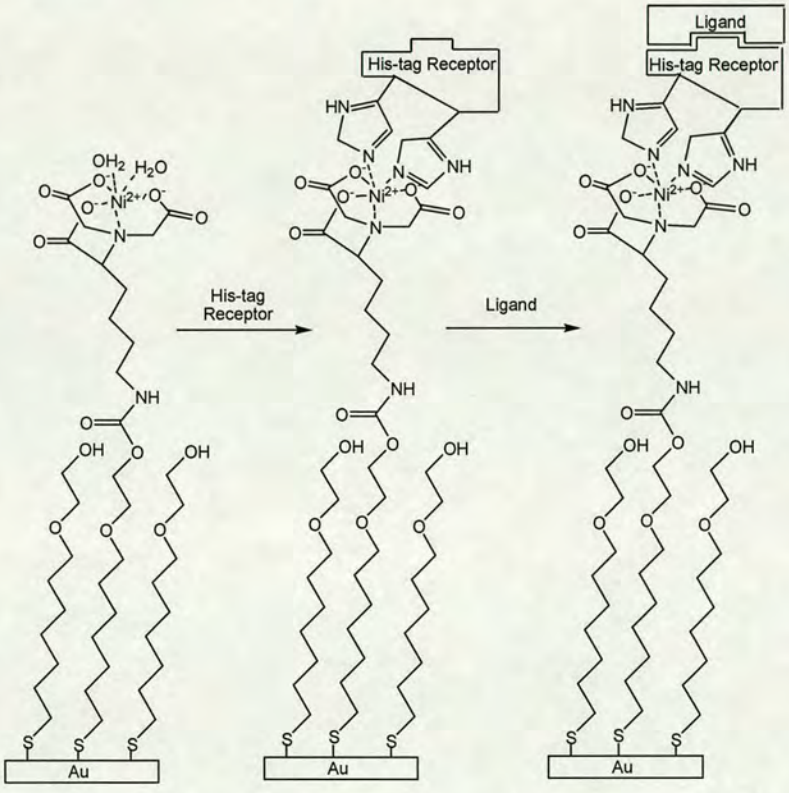

Figure 1.20: Protocol for immobilization of proteins onto surfaces to probe the ability of immobilized proteins to interact with ligands in solution.

SAMs are also useful to detect environmentally and biologically important anionic species. Compared to the well developed cation binding and sensing,[65] anion recognition both in bulk solution and at monolayer/solution interfaces is a more challenging field due to their variable sizes, shapes and strong solvation.

The advantage of immobilizing receptors was demonstrated by Beer and co-workers assembling disulfide functionalized Zn(II) metalloporphyrins on gold nanoparticles

(Figure 1.21). UV-visible experiments carried out in CH_2Cl_2, DMSO and DMSO-aqueous solutions, revealed that the modified nanoparticles have higher affinity for anions than the free metalloporphyrin.[66]

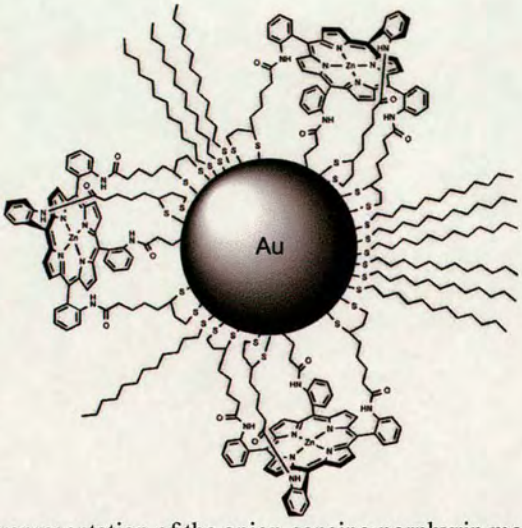

Figure 1.21: Schematic representation of the anion-sensing porphyrin modified gold nanoparticle.

Such enhancement in anion binding was attributed to the pre-organization of receptors and/or solvation effects.

Most anion sensors reported thus far have been investigated in organic media. However, specific sensors for small inorganic anions that exist in neutral aqueous environments are needed; SAMs can serve as efficient sensors in aqueous medium. For example, Gobi and Ohsaka prepared SAMs of a Ni(II) azamacrocyclic complex on gold electrodes to investigate anionic recognition in water (Figure 1.22).[67]

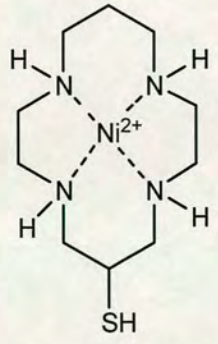

Figure 1.22: Structure of the Ni(II) complex with a surface anchoring group.

The electrochemical response of these monolayers was susceptible to the type of anions present in solution as well as the anion concentration. These changes were attributed to the axial coordination of the anions with the nickel center, inducing changes in its E^{o}. Based on the concentration dependent electrochemical response, the binding constants of the macrocyclic complex with different anions were measured. Also, their electrochemical investigation indicated that the monolayer could distinguish between several different anions including NO_3^-, CF_3COO^-, SO_4^{2-}, $H_2PO_4^-$, ClO_4^-, PF_6^-, SCN^-, and even biologically important anion such as adenosine triphosphate (ATP).

Echegoyen and co-workers have developed sensing systems that work in aqueous environments without the need for electroactive reporting groups. In this case electrochemical impedance spectroscopy (EIS) is employed to investigate anion sensing.[68]

EIS is based upon measurements of the response of the electrochemical cell to an alternating potential. Binding of charged analytes to the receptors immobilized on the electrode surfaces can affect the electron transfer process between the electrodes and charged redox probes in solution due to the electrostatic attraction or repulsion between the SAM surface and the redox active probe. The impedance response can be analysed using a Randles equivalent circuit (Figure 1.23).

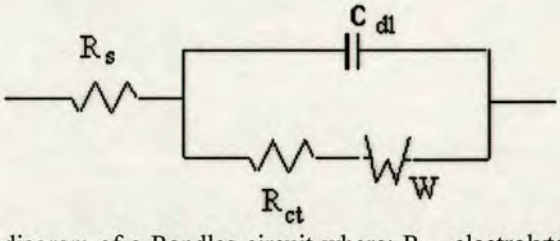

Figure 1.23: Schematic diagram of a Randles circuit where: R_s - electrolyte resistance, C_{dl}- double-layer capacitance, R_{ct}-electron transport, W-ions diffusion impedance.

The Randles circuit consists of a charge-transfer resistance across the SAM, R_{ct}, in series with a Warburg impedance and in parallel with a total interfacial capacitance. The R_{ct} reflects the charge-transfer resistance across the SAMs and can be used to detect the binding events occuring at the interface between the electrode and the

analyte-containing electrolytes. Typically, the deposition of the monolayer leads to a significant increase in the charge transfer resistance.

This principle was applied to SAMs of an electrochemically inactive cyclotriveratrylene (CTV) (Figure 1.24) for anion sensing.[69]

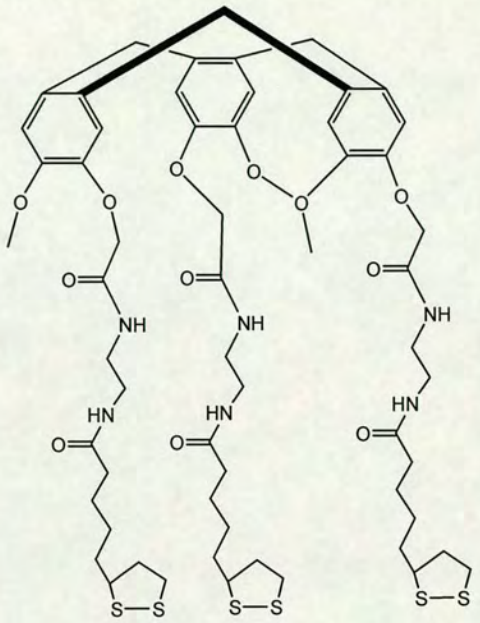

Figure 1.24: CTV thioctic acid derivative.

Figure 1.25 shows the impedance response of this SAM-modified electrode using $[Ru(NH_3)_6]^{3+/2+}$ as the redox probe in the presence of different anions.

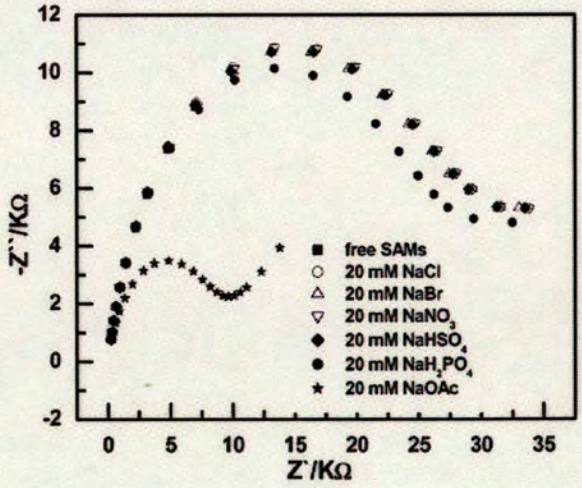

Figure 1.25: Impedance response of $[Ru(NH_3)_6]^{3+/2+}$ at the monolayer-modified gold electrode in the absence and presence of 20 mM of Cl^-, Br^-,NO_3^-,HSO_4^-, $H_2PO_4^-$ and AcO^-.[68]

The electrostatic attraction between the positively charged probes and the negatively charged SAM surface created due to anion binding increases the local concentrations of the redox probe near the electrode and thus facilitates the electron transfer reaction.

In this case the responses revealed the selective anion sensing properties of the SAM for acetate, having a detection limit of 3 mM. The efficiency of the sensor, however, was limited by the receptor, which only binds acetate with relatively low affinity.

This example shows that the use of impedance spectroscopy offers advantages for ion recognition such as: (1) ion sensing can be conducted in aqueous environments, (2) receptors can be designed exclusively for binding without consideration of the need to incorporate electrochemical or fluorescent active groups, thus broadening the options for the development of more selective and sensitive anion sensors and (3) practical anion sensors are possible by assembling receptors on surfaces. Therefore, to overcome problems of the sensitivity or selectivity it is necessary to develop better receptors. This could be achieved by using better recognition units like metal complexes or combining metal complexes and hydrogen bonding groups.

1.5 References

(1) J. W. Steed, J. L. Atwood, *Supramolecular Chemistry*, John Wiley & Sons, Ltd, 2000.

(2) E. P. Kyba, R. C. Helgeson, K. Madan, G. W. Gokel, T. L. Tarnowski, S. S. Moore and D. J. Cram, *J. Am. Chem. Soc.*, 1977, **99**, 2564.

(3) P. A. Gale, S. E. García-Garrido and J. Garric, *Chem. Soc. Rev.*, 2008, **37**, 151.

(4) P. D. Beer and P. A. Gale, *Angew. Chem. Int. Ed.*, 2001, **40**, 486.

(5) A. Frontera, J. Morey, A. Oliver, M. N. Piña, D. Quiñonero, A. Costa, P. Ballester, P. M. Deya and E. V. Anslyn, *J. Org. Chem.*, 2006, **71**, 7185.

(6) V. D. Jadhav and F. P. Schmidtchen, *Org. Lett.*, 2006, **8**, 2329.

(7) T. R. Nelly and M. H. Kim, *J. Am. Chem. Soc.*, 1994, **116**, 7072.

(8) S. Bulmann, K. Nishizawa, P. Xiao and Y. Umezawa, *Tetrahedron*, 1997, **53**, 1647.

(9) P. A. Gale, J. L. Sessler, V. Kral and V. Lynch, *J. Am. Chem. Soc.*,1996, **118**, 5140.

(10) M. Takeuchi, T. Shioya and T. M. Swager, *Angew. Chem. Int. Ed.*, 2001, **40**, 3372.

(11) (a) C. Raposo, N. Pérez. M. Almaraz, L. Mussons, M. C. Caballero and J. R. Morán, *Tetrahedron Lett.*, 1995, **36**, 3255; (b) S. I. Kondo, Y. Hiraoka, N. Kuumatani and Y. Yano, *Chem. Commun.*, 2005, 1720; (c) M. R. Sambrook, P. D. Beer, J. A. Wisner, R. L. Paul, A. R. Cowley, F. Szemes and M. G. B. Drew, *J. Am. Chem. Soc.*, 2005, **127**, 2292.

(12) A. P. Bisson,V. M. Lynch, M. K. C Monahan and E. V. Anslyn, *Angew. Chem. Int. Ed. Engl.*, 1997, **36**, 2340.

(13) (a) E. Kinoshita, M. Takahashi, H. Takeda, M. Shiro and T. Koike, *Dalton Trans.*, 2004, **8**, 1189; (b) H. Adams, D. Bradshaw and D. E. Fenton, *J. Chem. Soc., Dalton, Trans.*, 2002, 925.

(14) R. J. Motekaitis and A. E. Martell, *Inorg. Chem.*, 1994, **33**, 1032.

(15) P. E. Jurek, A. E. Martell, R. J. Motekaitis and R. D. Hancock, *Inorg. Chem.*, 1995, **34**, 1823.

(16) R. J. Motekaitis and A. E. Martell, *Inorg. Chem.*, 1992, **31**, 5534.

(17) (a) S. L. Tobey, B. D. Jones and E. V. Anslyn, *J .Am. Chem. Soc.*, 2003, **125**, 4026; (b) J. C. Mareque-Rivas, R. Torres Martin de Rosales and S. Parsons, *Dalton Trans.*, 2003, 4385; (c) E. Kimura, S. Aoki, T. Koike and M. Shiro, *J. Am. Chem. Soc.*,1997, **119**, 3068.

(18) J. C. Mareque-Rivas, R. Torres Martin de Rosales and S. Parsons, *Chem Commun.*, 2004, 610.

(19) P. D. Beer, P. A. Gale and G. Z. Chen, *Coord. Chem. Rev.*, 1999, **185**, 3.

(20) (a) P. D. Beer, D. Hesek, J. Hodacova and S. E. Stokes, *J. Chem. Soc., Chem. Commun.*, 1992, 270; (b) P. D. Beer, C. Hazlewood, D. Hesek, J. Hodacova and S. E. Stokes, *J .Chem. Soc., Dalton Trans.*, 1993, 1327; (c) P. D. Beer, M. G. B. Drew, A. R. Graydon and D. K. Smith, *J. Chem. Soc., Dalton Trans.*, 1995, 403, (d) P. D. Beer, D. Hesek, J. E. Kingston, D. K. Smith, S. E. Stokes and M. G. B. Drew, *Organometallics*, 1995, **14**, 3288; (e) P. D. Beer, M. G. B. Drew, J. Hodacova and S. E. Stokes, *J. Chem. Soc., Dalton Trans.*, 1995, 3447.

(21) (a) P. D. Beer, Z. Chen, M. G. B. Drew, J. Kingston, M. I. Ogden and P. Spencer, *J. Chem. Soc., Chem. Commun.*, 1993, 1046; (b) P. D. Beer, Z. Chen, M. G. B. Drew, A. O. M. Johnson, D. K. Smith and P. Spencer, *Inorg. Chim. Acta*, 1996, **246**, 143; (c) P. D. Beer, J. Cadman, J. M. Lloris, R. Martínez-Máñez, M. E. Padilla-Tosta, T. Pardo, D. K. Smith and J. Soto, *J. Chem. Soc., Dalton Trans.*, 1999, 127.

(22) S. R. Collinson, T. Gelbrich, M. B. Hursthouse and J. H. R. Tucker, *Chem. Commun.*, 2001, 555.

(23) J. D. Carr, S. J. Coles, M. B. Hursthouse, M. E. Light, J. H. R. Tucker and J. Estwood, *Angew. Chem. Int. Ed.*, 2000, **39**, 3296.

(24) G. De Santis, L. Fabbrizzi, M. Licchelli, A. Poggi and A. Taglietti, *Angew. Chem. Int. Ed. Engl.*, 1996, **35**, 202.

(25) J. L. Sessler, H. Maeda, T. Mizuno, V. M. Lynch and H. Furuta, *Chem. Commun.*, 2002, 862.

(26) W. C. Bigelow, D. L. Pickett and W. A. J. Zisman, *Colloid Interface Sci.*, 1946, **1**, 513.

(27) H. Kuhn, D. Mobius and H. Bucher, *Techniques of Chemistry*; Wiley: New York, 1973.

(28) R. G. Nuzzo and D. L. Allara, *J. Am. Chem. Soc.*, 1983, **105**, 4481.

(29) A. Ulman, *Chem. Rev.*, 1996, **96**, 1533.

(30) M. Hasan, D. Bethell and M. Brust, *J. Am. Chem. Soc.*, 2002, **124**, 1132.

(31) J. Christopher Love, L. A. Estroff, J. K. Kriebel, R. G. Nuzzo and G. M. Whitesides, *Chem. Rev.*, 2005, **105**, 1103.

(32) (a) L. H. Dubois and R. G. Nuzzo, *Annu. Rev. Phys. Chem.*, 1992, **43**, 437; (b) T. Ederth, P. Claesson and B. Liedberg, *Langmuir*, 1998, **14**, 4782.

(33) L. Strong and G. M. Whitesides, *Langmuir*, 1988, **4**, 546.

(34) (a) E. Sabatini, J. Cohenboulakai, M. Bruening and I. Rubinstein, *Langmuir*, 1993, **9**, 2974; (b) J. Y. Gui, D. A. Stern, D. G. Frank, F. Lu, D. C. Zapien and A. T. Hubbard, *Langmuir*, 1991, **7**, 955.

(35) (a) H. O.Finklea, *Electroanal. Chem.*, 1996, **19**, 109; (b) T. W. Schneider and D. A. Buttry, *J. Am. Chem. Soc.*, 1993, **115**, 12391; (c) J. L. Shepherd, A. Kell, E. Chung, C. W. Sinclar, M. S. Workentin and D. Bizzotto, *J. Am. Chem. Soc.*, 2004, **126**, 8329.

(36) C. B. Gorman, H. A. Biebuyck and G. M. Whitesides, *Langmuir*, 1995, **11**, 2242.

(37) D. L. Allara and R. G. Nuzzo, *Langmuir*, 1985, **1**, 52.

(38) M. A. Bryant and J. E. Pemberton, *J. Am. Chem. Soc.*, 1991, **113**, 8284.

(39) C. D. Bain and G. M. Whitesides, *J. Phys. Chem.*, 1989, **93**, 1670.

(40) A. S. Duwez, *J. Electron Spectrosc. Relat. Phenom.*, 2004, **134**, 97.

(41) H. Rieley and G. K. Kendall, *Langmuir*, 1999, **15**, 8867.

(42) M. D. Porter, T. B. Bright, D. L. Allara and C. E. D. Chidsey, *J. Am. Chem. Soc.*, 1987, **109**, 3559.

(43) (a) J. H. Schön, H. Meng and Z. Bao, *Adv. Mater.*, 2002, **14**, 323; (b) J. H. Schön, H. Meng and Z. Bao, *Nature*, 2001, **413**, 713; (c) J. Das, Md. A. Aziz and H. Yang, *J. Am. Chem. Soc.*, 2006, **128**, 16022.

(44) M. D. Porter, T. B. Bright, D. L. Allara and C. E. D. Chidsey, *J. Am. Chem. Soc.*, 1987, **109**, 3559.

(45) (a) C. E. D. Chidsey, *Science*, 1991, **251**, 919; (b) C. E. D. Chidsey, C. R. Bertozzi, T. M. Putvinski and A. M. Mujsce, *J. Am. Chem. Soc.*, 1990, **112**, 4301; (c) E. Tran, M. A. Rampi and G. M. Whitesides, *Angew. Chem. Int. Ed. Engl.*, 2004, **43**, 3835.

(46) (a) V. Ganesh and V. Lakshminarayanan, *J. Phys. Chem. B*, 2005, **109**, 16372; (b) M. S. Ravenscroft and H. O. Flinkea, *J. Phys. Chem.*, 1994, **98**, 3843; (c) S. P. Dudek, H. D. Sikes and C. E. D. Chidsey, *J. Am. Chem. Soc.*, 2001, **123**, 8033.

(47) (a) L. Brus, C. E. D. Chidsey, S. Creager, C. Creutz, C. R. Kagan, P. V. Kamat, M. Lieberman, S. Lindsay, R. A. Marcus, R. M. Metzger, M. E. Michel-Beyerle, J. R. Miller, M. D. Newton, D. R. Rolison, O. Sankey, K. S. Schanze, J. Yardley and X. Zhu, *J. Phys. Chem. B*, 2003, **107**, 6668; (b) A. Nitzan and M. A. Ratner, *Science,* 2003, **300**, 1384.

(48) J. E. Hutchison, T. A. Postlethwaite and R. W. Murray, *Langmuir,* 1993, **9**, 3277.

(49) (a) I. Willner, V. Heleg-Shabtai, R. Blonder, E. Katz and G. L. Tao, *J. Am. Chem. Soc.*, 1996, **118**, 10321; (b) E. J. Calco, C. Danilowicz, C. M. Lagier, J. Manrique, and M. Otero, *Biosensors and Bioelectronics,* 2004, **19**, 1219.

(50) K. Weber, L. Hockett and S. Creager, *J. Phys. Chem. B*, 1997, **101**, 8286.

(51) (a) E. Sabatani, J. Cohen-Boulakia, M. Bruening and I. Rubistein, *Langmuir,* 1993, **9**, 2974; (b) S. P. Dudek, R. P. Hsung, L. R. Sita, J. F. Smalley, M. D. Newton, S. W. Feldberg and C. E. D. Chidsey, *J. Am. Chem. Soc.*, 1997, **119**, 10563; (c) H. D. Sikes, J. F. Smalley, S. P. Dudek, A. R. Cook, M. D. Newton, C. E. D. Chidsey and S. W. Felderg, *Science*, 2001, **291**, 1519.

(52) J. F. Smalley, S. B. Sachs, C. E. D. Chidsey, S. P. Dudek, H. D. Sikes, S. E. Creager, C. J. Yu, S. W. Feldberg and M. D. Newton, *J. Am. Chem. Soc.*, 2004, **126**, 14620.

(53) C. Joachim, J. K. Gimzewski and A. Aviram, *Nature*, 2000, **408**, 541.

(54) (a) R. Bilewicz, S. Sek, and I. Zawisza, *Russ. J. Electrochem.*, 2001, **38**, 35; (b) R. S. Clegg and J. E. Hutchison, *Langmuir*, 1996, **12**, 5239.

(55) S. Sek, A. Misicka and R. Bilewicz, *J. Phys. Chem. B,* 2000, **104**, 5399.

(56) (a) L. Xiaoquan, L. Baoqiang, X. Zhonghua, L. Minrui, Z. Limin and K. Jingwan, *Thin Solid Films,* 2005, **488**, 230; (b) M. Nielsen, N. B Larsen and K. V. Gothelf, *Langmuir,* 2002, **18**, 2795.

(57) J. P. Collman, N. K. Devaraj, R. A. Decréau, Y. Yang, Y. L. Yan, W. Ebina, T. A. Eberspacher and C. E. D. Chidsey, *Science*, 2007, **315**, 1565.

(58) N. Devaraj, R. A. Decreau, W. Ebina, J. P. Collman and C. E. D. Chidsey, *J. Phys. Chem. B*, 2006, **110**, 15955.

(59) T. Hiratsu, S. Suzuki and K. Yamaguchi, *Chem. Commun.*, 2005, 4534.

(60) (a) R. M. Crooks and A. J. Ricco, *Acc. Chem. Res.*, 1998, **31**, 219; (b) M. Crego-Calama and D. N. Reinhoudt, *Adv. Mater.*, 2001, **13**, 1171; (c) R. C. Major and X. Y. Zhu, *J. Am. Chem. Soc.*, 2003, **125**, 8454.

(61) (a) N. Higashi, M. Takahashi and M. Niwa, *Langmuir*, 1999, **15**, 111; (b) C. Z. Li, Y. T. Long, J. S. Lee and H. B. Kraatz, *Chem. Commun.*, 2004, 574.

(62) (a) H. Chen , M. Lee , S. Choi, J. H. Kim, H. J. Choi, S. H. Kim, J. Lee and K. Koh, *Sensors*, 2007, **7**, 1091; (b) J. Ladd, C. Boozer, Q. Yu, S. Chen, J. Homola and S. Jiang, *Langmuir*, 2004, **20**, 8090.

(63) (a) Y. P. Sun, J. Q. Sun, X. Zhang, C. Q. Sun, Y. Wang and J. C. Shen, *Thin Solid Films*,1998, **329**, 730; (b) E. J. Calvo, R. Etchenique, L. Pietrasanta, A. Wolosiuk and C. Danilowicz, *Anal. Chem.*, 2001, **73**, 1161; (c) O. Pierrat, N. Lechat, C. Bourdillon and J. M. Laval, *Langmuir*, 1997, **13**, 4112.

(64) G. B. Sigal, C. Bamdad, A. Barberis, J. Strominger and G. M. Whitesides, *Anal. Chem.*, 1996, **68**, 490.

(65) (a) A. P. de Silva, B. McCaughan, B. O. F. McKinney and M. Querol, *Dalton Trans.*, 2003, 1902; (b) K. Rurack and U. Resch- Genger, *Chem. Soc. Rev.*, 2002, **31**, 116; (c) A. P. de Silva, H. Q. N. Gunaratne, T. Gunnlaugsson, A. J. M. Huxley, C. P. McCoy, J. T. Rademacher and T. E. Rice, *Chem. Rev.*, 1997, **97**, 1515.

(66) P. D. Beer, D. P. Cormode and J. J. Davis, *Chem. Commun.*, 2004, 414.

(67) K. V. Gobi and T. Ohsaka, *J. Electroanal. Chem.*, 2000, **485**, 61.

(68) S. Zhang, A. Palkar and L. Echegoyen, *Langmuir*, 2006, **22**, 10732.

(69) S. Zhang and L. Echegoyen, *J. Am. Chem. Soc.*, 2005, **127**, 2006.

Chapter 2

Experimental techniques

2.1 Introduction

Several techniques have been used in this thesis to characterize the structure and investigate the properties of the monolayer films. The electrochemical properties of the modified gold electrodes have been studied using cyclic voltammetry (CV) and electrochemical impedance spectroscopy (EIS). Complementary surface analysis was performed using X-ray photoelectron spectroscopy (XPS) and polarization modulation infrared reflection-absorption spectroscopy (PM-RAIRS). In this chapter a brief description on each of these experimental methods is provided.

2.2 Electrochemical techniques

2.2.1 The electrochemical cell

In the electrochemical measurements a three-electrode set-up was used. A saturated calomel electrode as a reference electrode, a platinum rod electrode as a counter electrode, and a gold electrode as a working electrode were used. All measurements were performed at room temperature.

2.2.2 Cyclic voltammetry (CV)

Cyclic voltammetry (CV) is the most extensively used electrochemical technique among the potential sweep techniques.[1] CV involves sweeping the electrode potential with time and recording the current. The potential is varied linearly with time over a potential range of interest and the potential sweep is reversed and this can be repeated. A typical potential-time profile is shown in Figure 2.1. The rate at which the potential is varied is known as scan rate, ν.

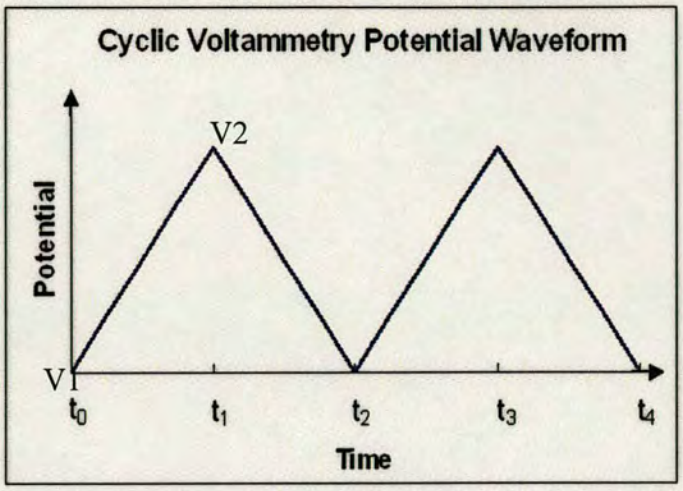

Figure 2.1: Potential-Time profile for cyclic voltammetry.

Cyclic voltammetry concerns with scanning of working electrode potential between two potential limits at a known scan rate ν, in both the forward and reverse direction and measuring the current of the electrochemical cell. The resultant current of the system involves the faradaic current due to the various electrochemical processes occurring on the electrode surface such as electron transfer redox reactions and adsorption processes in addition to the capacitative current due to the double layer charging at these potentials. A plot of measured current as a function of applied potential is known as "cyclic voltammogram" (Figure 2.2). It is an electrochemical spectrum indicating the potentials at which several processes occur.

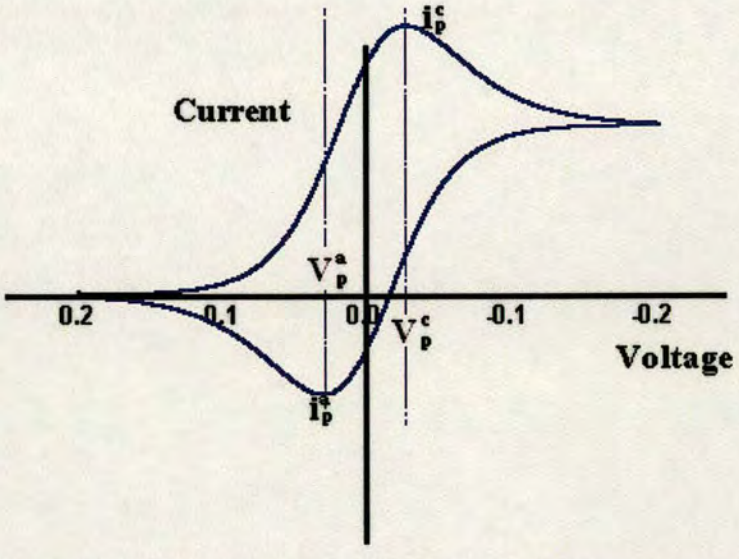

Figure 2.2: Cyclic voltammogram for a single electron reversible process.

For a typical single electron reversible redox reaction of the type,

$$O + ne^- \leftrightarrow R$$

the rate of charge transfer is always greater than the rate of mass transfer at all potentials and the redox reaction is under diffusion control. The ratio of concentrations of oxidant and reductant species of a reversible reaction is given by Nernst equation and a concentration gradient exists within the region near the electrode surface known as Nernst diffusion layer, where the concentration gradient of the electroactive species is linear. Also the Nernstian equilibrium is always maintained at the electrode surface at all the potentials. The shape of current-potential profile for a one-electron reversible redox reaction as shown in Figure 2.2 can be understood in the following way. When the potential of the electrode is made more negative, the surface concentration of the reactant O decreases progressively, thereby the concentration gradient is increased which results in increase in the current. On reaching the electrode potential where O is reduced, the surface concentration of O decreases from its bulk value in order to satisfy the Nernst equation and the concentration gradient is setup. As a result a current proportional to the concentration gradient at the electrode surface flows. Due to the diffusion of ions, the concentration gradient does not remain constant and it starts to decrease. At the same time, the electrode potential is also continuously changing leading to a further decrease of surface concentration of O until it effectively reaches zero concentration. Once the concentration of O reaches zero, the gradient decreases due to the accumulation of reduced species R, in the vicinity of the electrode surface (relaxation effect) and hence the current also decreases. Overall, this behaviour gives rise to a peak shaped current-potential profile as shown in Figure 2.2. Using similar arguments used for the forward sweep, it can be shown that the current change on reverse sweep also exhibit a similar peak shaped response though of the opposite sign.

CV is often used to study redox reactions and other electrochemical reactions that may occur on the electrode surface or at the interface. The reversibility of an

electrochemical reaction can be evaluated from the corresponding oxidation and reduction peaks. The resistive and capacitive characteristics of the interface can be understood by the potential-dependence of the current. Moreover, the CV can be performed at different potential sweep rates, which provide information about the influence of the sweep rate on the electrochemical reactions as well as on resistive and capacitive characteristics of the interface.

Cyclic voltammetry technique has been used in this work to study the electron-transfer reactions across SAM modified gold electrodes.

2.2.3 Electrochemical impedance spectroscopy (EIS)

Electrochemical impedance spectroscopy (EIS) is a powerful and non-destructive technique for investigating electrochemical systems.[2] EIS can provide information on a vast variety of electrochemical processes, such as charge transfer or polarisation resistance, corrosion, interfacial and bulk capacitance, transport of species in electrolyte and solids, coatings,[3] polymer degradation,[4] hydrogen adsorption[5] and lipid bilayers.[6]

2.2.3.1 General aspects of EIS

This method comes under the category of ac techniques. In contrast to cyclic voltammetry, which is a dc technique, where the electrochemical system is perturbed far from the equilibrium, this method involves the application of a very small perturbation close to the steady state equilibrium. The electrochemical impedance spectroscopy measurements involve essentially a small perturbation of the electrode potential from the equilibrium potential by the application of a sinusoidal signal with 5-10 mV peak to peak amplitude and measuring the response of the electrochemical cell. Using small amplitude excitation signals allows the response of the electrochemical system to be regarded as linear where the current response to a sinusoidal potential will be a sinusoid at the same frequency, but shifted in phase.

Figure 2.3 shows the sinusoidal signals of perturbation and response of the electrochemical cell.

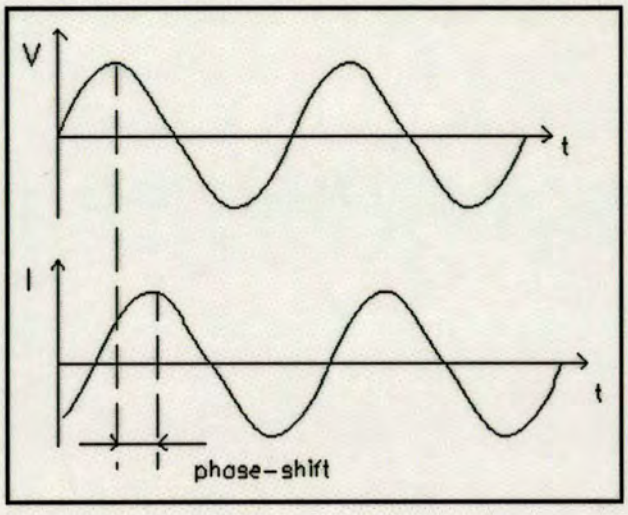

Figure 2.3: Sinusoidal signal of perturbation and response obtained in EIS.

Many concept used in the analysis of electrical circuits can be applied in analysing electrochemical impedance spectroscopy data. However, since few real electrochemical interfaces can be regarded as ideal, the analogy between electrochemical and electrical systems should be treated with care. For complex responses and to more accurate determination of the characteristics of the interface, it is better to use an adequate equivalent circuit representing the interface and then evaluate the values of the circuit component by fitting the experimental data using the equivalent circuit.

2.2.3.2 Principles of ac circuits

The electrochemical response of a cell to an ac perturbation can be understood by knowing the fundamental principles of ac circuits. If a sinusoidal signal of voltage $V = V_0 \sin \omega t$ is applied to an electrical circuit that contains a combination of resistors and capacitors, the response is a current, which is given by, $I = I_0 \sin (\omega t + \theta)$, where V_0 is the maximum amplitude, I_0 is the maximum current, ω is the angular frequency and θ is the phase angle between the perturbation and response. The proportionality factor between V and I is known as impedance Z. In phasor terms the rotating vectors are separated in the polar diagram by the angle θ.

In the case of a pure resistor, R, the phase angle θ is zero. According to Ohm's law, V = IR, which leads to $I = V_0 \sin \omega t / R$. There is no phase difference between the potential and the current (Figure 2.4).

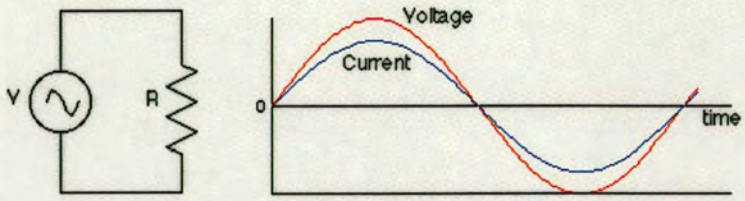

Figure 2.4: Relationship between the voltage across a resistor and current through the resistor.

For a pure capacitor, C, the current I is given by,

$$I = C\, dV/dt$$

On substituting the value V as $V_0 \sin \omega t$ and differentiating, we obtain:

$$I = V_0\, \omega\, C \sin(\omega t + \pi/2)$$

$$I = V_0 \sin(\omega t + \pi/2) / X_c$$

where $X_c = 1/\omega C$ is known as the capacitive reactance. Here we find that the phase angle is $\pi/2$, implying that the current leads the potential by 90^0 or $\pi/2$ in the case of a pure capacitor (Figure 2.5). In a complex notation this can be written as $V = - jX_cI$ ($j = \sqrt{-1}$). A comparison of this equation and V = IR shows that X_c must carry dimensions of resitance, unlike R, its magnitude falls with increasing frequency.

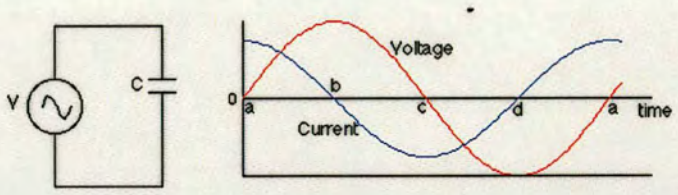

Figure 2.5: Relationship between an alternating voltage across a capacitor and the alternating current through the capacitor.

Thus, for the case of a resistor and a capacitor in series, the voltage applied across them must be the sum of the individual voltage drops across the resistor and capacitor, i.e. $V = I (R - j X_c)$ in which $R - jX_c$ is called impedance $Z(\omega)$.

2.2.3.3 Equivalent circuit of an electrochemical cell

In general, an electrode-solution interface can be considered as an impedance to a small sinusoidal excitation. The impedance of such a kind of electrochemical interface is a complex number $Z(\omega)$, that is expressed using a complex notation:

$$Z(\omega) = Z_{Re} - j\, Z_{Im} = R - j\, 1/\omega C$$

Where $Z_{Re} = R$ and $Z_{Im} = 1/\omega C$ are the real and imaginary parts of the impedance, respectively.

The magnitude of Z is given by:

$$Z^2 = (Z_{Re})^2 + (Z_{Im})^2 = R^2 + X_c^2$$

And the phase angle, θ, is given by:

$$\tan\theta = Z_{Im}/Z_{Re} = X_c/R = 1/\omega RC$$

The impedance is a kind of generalized resistance.

Hence the electrode-electrolyte interface of the electrochemical cell can be represented by a suitable equivalent circuit consisting of resistors and capacitors that pass current with the same amplitude and the same phase angle under a given excitation. A typical equivalent circuit for an electrochemical system is shown in Figure 2.6.

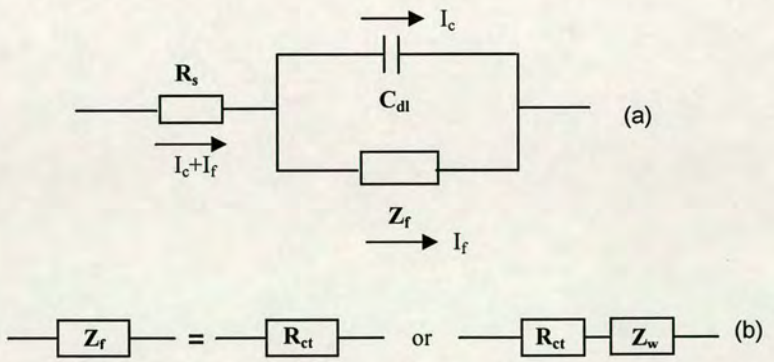

Figure 2.6: (a) Equivalent circuit of an electrochemical cell. (b) Two possibilities of Z_f consideration, as R_{ct} or subdivided as R_{ct} and Z_w.

In Figure 2.6 (a), an equivalent circuit popularly known as Randles equivalent circuit with the double layer capacitance C_{dl}, the solution resistance, R_s and the faradaic impedance Z_f is shown.

The total current of the working electrode is obtained by the sum of distinct contributions from the faradaic current I_f and the double layer charging current I_c. The double layer capacitance arises from the charges stored at the interface between an electrode and its surrounding electrolyte. The charges in the electrode are separated from the charges of the bulk ions. In many cases, the double layer capacitance closely resembles a pure capacitance and hence it is represented by the element C_{dl} in the equivalent circuit. The faradaic impedance Z_f can be separated into two components namely, the charge transfer resistance, R_{ct} and the Warburg impedance, Z_w. The simplest representation is to consider the faradaic impedance as the pure resistance R_{ct}, where the double layer capacity is in parallel with the impedance due to the charge transfer reaction. Another alternative circuit model is when a general impedance, Z_w, is considered and represents a kind of resistance to mass transfer because of diffusion. This impedance depends on the frequency of the perturbation in terms of the applied potential. At high frequencies, the Warburg impedance is small because the reactants do not have to diffuse very far. In contrast, at low frequencies, the diffusing reactants have to move very far, thereby increasing the Warburg impedance.

The uncompensated solution resistance denoted by R_s exits between the working electrode and the reference electrode. In the equivalent circuit representation, the uncompensated solution resistance, R_s is inserted as a series element because all the current must pass through it. In contrast to R_s and C_{dl}, which are nearly ideal circuit elements, the components of faradaic impedance, Z_f namely the charge transfer resistance, R_{ct} and Warburg impedance, Z_w are not ideal because they change with frecuency ω.

For a planar diffusion, the value of R_{ct} can be expressed as,

$$R_{ct} = RT / nFI_0$$

Where I_0 is the exchange current density.

The relative values of R_{ct} and Z_w at a given frequency are the measure of the balance between kinetic and diffusion control. If the exchange current density I_0 is very large, then R_{ct} will tend to zero and its value will be too small to measure so that only the Warburg impedance will be observed.

The variation of the impedance with frequency is often of interest and can be displayed in different ways. In a *Bode plot*, Log Z and θ are both plotted against log ω. An alternative presentation, a *Nyquist Plot* displays Z_{Im} vs Z_{Re} for different values of ω, and it is the one we have used for our analysis. Figure 2.7 shows a *Nyquist plot* for a charge transfer control and diffusion control reaction.

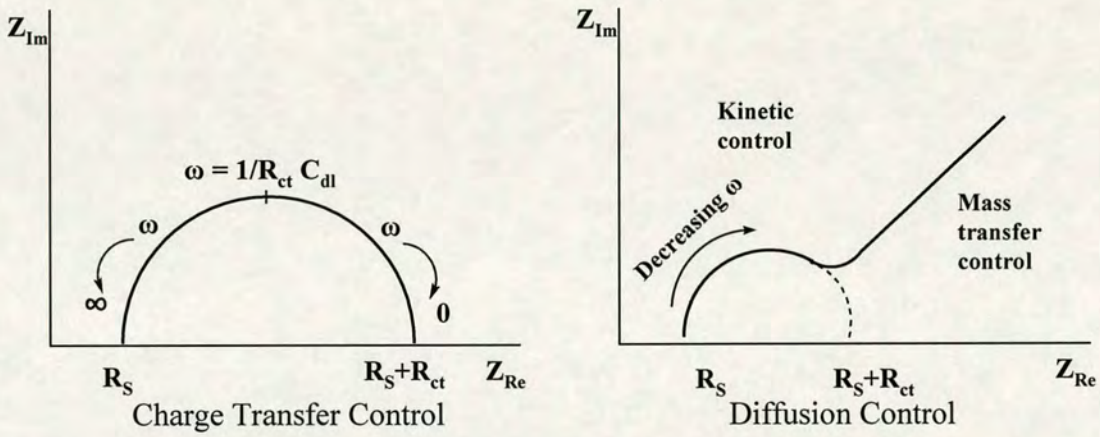

Figure 2.7: Nyquist plots obtained for circuits shown in Figure 2.6. Regions of mass-transfer and kinetic control are found at low and high frequencies, respectively.

The Nyquist plot for a Randles cell shows a semicircle when the process is charge transfer controlled ($Z_f = R_{ct}$) and a small semicircle and a straight line at low frequencies when the process is diffusion controlled ($Z_f = R_{ct} + Z_w$). R_s can be determined by reading out the real axis value at the high frequency intercept. C_{dl} can be obtained from the maximum value of Z_{Im} in the semicircular region where $\omega = 1/ R_{ct} C_{dl}$. The diameter of the semicircle provides the value of R_{ct}.

In this work, we have extensively used impedance spectroscopy to study the electron-transfer reactions on the SAM modified surfaces and to calculate its rate constant.

2.3 Surface characterization techniques

2.3.1 X-ray photoelectron spectroscopy (XPS)

X-ray photoelectron spectroscopy (XPS) is a surface analysis technique that provides information about the presence of elements and its electronic state within a material.[7] In this thesis work, XPS is employed to study core levels of adsorbates on gold surfaces by ionizing the core electron and measuring their kinetic energy distribution. When a sample is irradiated with a flux of X-ray photons of known energy (e.g., Al Kα line at 1486.6 eV or Mg Kα at 1253.6 eV), photoelectrons are emitted from the sample after direct transfer of energy from the photon to the core-level electron. This is known as 'photoionization process'. A typical XPS experimental setup is depicted in Figure 2.8.

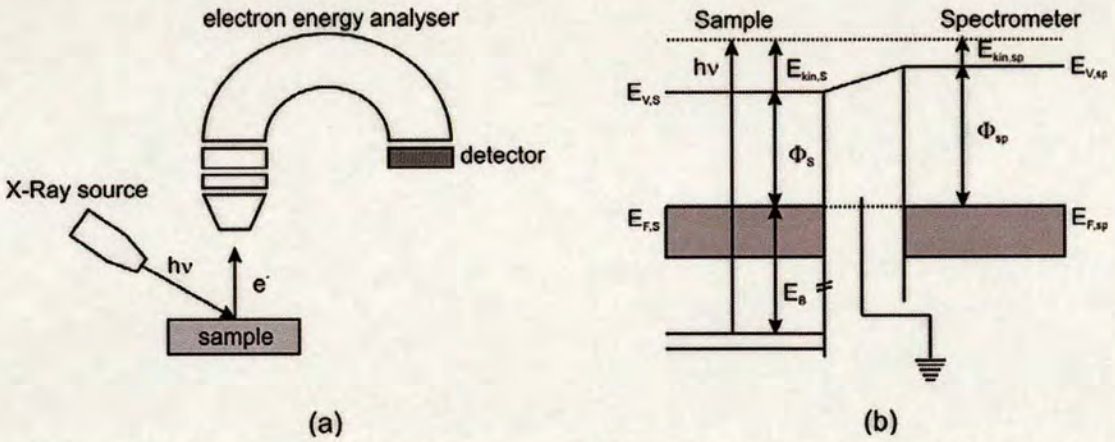

Figure 2.8: (a) Setup of a typical XPS experiment; (b) Energy level diagram for the XPS process.

The emitted electrons are subsequently separated based on the difference in their kinetic energies. The energy of the photons is related to the atomic and molecular environment from which they originate. The number of electrons emitted is related to the concentration of the emitting atoms present in the sample. An example of XPS spectra is shown in Figure 2.9.

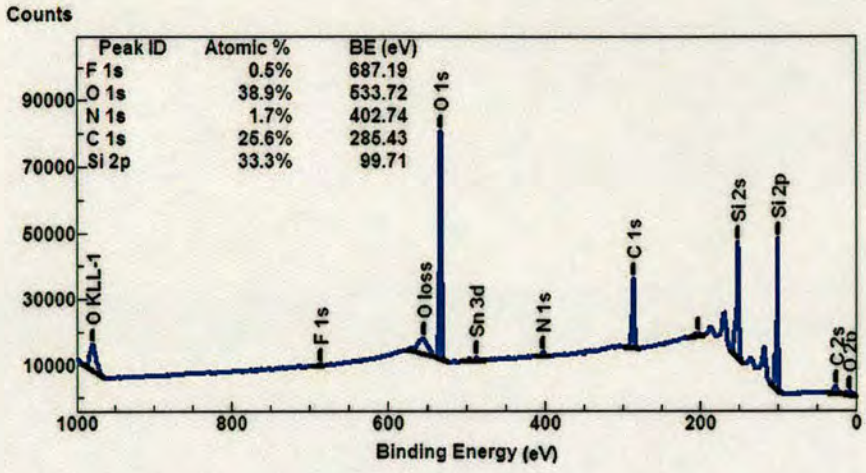

Figure 2.9: Example of X-ray photoelectron spectra.

The physical principle behind the photoemission process is illustrated in the energy level diagram shown in Figure 2.8 (b). Conducting samples like metals are placed in electrical contact with the spectrometer, usually by simply grounding the sample and the spectrometer. Under these conditions the Fermi level of the sample and the spectrometer are at the same reference level.

Accordingly, the relation governing the interaction between an impinging photon and an emitted electron can be written as:

$$h\upsilon = E_{kin,s} + E_{b,s} + \emptyset_{sp}$$

The most important parameters are the kinetic energies $E_{kin,s}$ of the electrons and the energies required to remove the electrons from the initial state, that is, the *binding energies*, E_b. Since the value of E_b is discrete and is well defined for different atomic levels, one can expect discrete kinetic energies $E_{kin,s}$ corresponding to these levels.
The binding energy associated with a given peak is approximately $h\upsilon$- $E_{kin,s}$. Minor correction for the spectrometer *work function* (which is the energy needed to move an electron from the Fermi level into vacuum), $\emptyset_{sp}$ (3-4 mV), must be applied for accurate binding energy assignment. This value, $\emptyset_{sp}$, can be obtained by putting a standard in the spectrometer, usually a clean gold sample with a binding energy of 84 eV (Au 4f).

The physical principle of XPS is even more complicated than reported here. In fact, removing an electron from an atom causes a perturbation, leading to relaxation processes in which the remaining electrons try to screen the created hole. There are many possibilities of how the system can react to the removal of an electron, influencing differently the kinetic energy of the photoemitted electron.

A schematic diagram of an X-ray photoelectron spectrometer is shown in Figure 2.10.

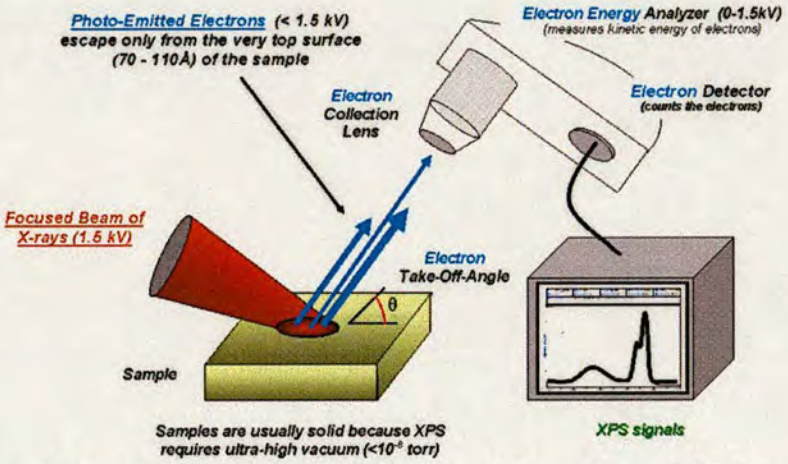

Figure 2.10: Example of the basic components of a monochromatic XPS system.

Siegbahn and co-workers (who pioneered the technique of XPS) showed that XPS can also be used to probe the chemical environment or 'oxidation state' of surface species.[8] The precise binding energy of the core levels of an atom or molecule depends critically on the species to which it is bonded. Charge transfer may leave atoms with partial positive (or negative) charges, leading to a shift in core levels to higher (or lower) binding energies associated with increased (or decreased) columbic attraction between the core electrons and the nucleus. Hence, atoms in a high formal oxidation state shows XPS peaks at high binding energy relative to the same atom in a low oxidation state. The magnitude of this so called 'chemical shift' is dependent on the local environment surrounding the atom and can, in certain cases, be as large as 10 eV.

2.3.2 Reflection-absorption infrared spectroscopy (RAIRS)

The fact that infrared (IR) spectroscopy provides specific information on the types of bonds present in a molecule and is non-destructive has made it a highly versatile technique for surface analysis.[7]

The principle of infrared spectroscopy is based on the vibrational excitation of molecules by absorption of infrared light.

In general, there are four ways by which incident light (I_0) can interact with a sample. It can be reflected from the sample surface (with intensity I_R), scattered by the surface or bulk of the sample (I_S) and absorbed (I_A) or transmitted though the sample (I_T). Conservation of energy requires that the intensities associated with these processes must sum to the intensity (I_0) of the incident light on the sample:

$$I_0 = I_R + I_S + I_A + I_T$$

Each of the intensities on the right hand side of the equation contains information about the sample. The most commonly used is the absorbed intensity, but I_A can not normally be measured directly. Instead, it is inferred by measuring other intensities. In a typical absorption spectrum, only I_0 and I_T are measured and the sum of I_S and I_R is assumed to be negligible. If I_R is measured instead of I_T it results in a reflection spectrum.

There are two types of mid-IR spectrometers; dispersive and Fourier transform (FT). The majority of modern IR spectrometers are FT instruments, which have the advantage that data are collected at many wavelengths simultaneously (rather than consecutively) resulting in faster and more sensitive measurements.[9]

Many surfaces are opaque to infrared radiation, so transmission experiments are not viable. IR reflection absorption spectroscopy (know as reflection absorption infrared spectroscopy (RAIRS)) is the most suitable technique for the study of adsorbed layers on metal surfaces.

RAIRS was pioneered by researchers such as Greenler[10] and Francis and Ellison,[11] who found that it could be used to investigate thin films and even monolayers adsorbed on metal substrates.[12]

Since a monolayer film of molecular adsorbate has a coverage of about 10^{15} molecules/cm^2, and the total area of a typical sample probed is less than a square centimetre, sensitivity is the major problem encountered in RAIRS measurements. Hence, in order to study the structure and orientation of molecular adsorbates on the metal surface, the incident radiation is used at a grazing angle, which maximizes surface sensitivity.[13]

A typical experimental setup for a vacuum RAIRS experiment is shown in Figure 2.11.

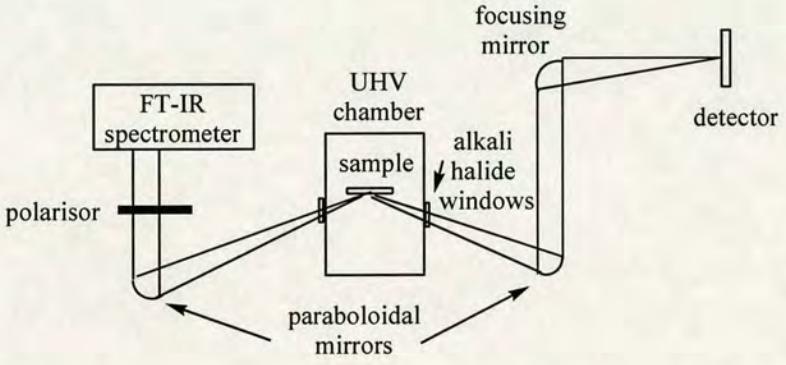

Figure 2.11: Schematic diagram of the experimental configuration used in reflection-absorption infrared spectroscopy.

Infrared radiation is focused through an IR –transparent window (usually an alkali halide) onto the sample surface at grazing incident. The light is generally polarized prior to focusing. The sample, acting as a mirror, reflects the beam out of a second vacuum-sealed window, where it is recollimated on to a photoconductive semiconductor detector such as mercury cadmium telluride (MCT) (5000-800 cm^{-1}).

2.3.2.1 Surface analysis using infrared spectroscopy: polarization-modulation reflection absorption infrared spectroscopy (PM-RAIRS)

PM-RAIRS is used in this work to investigate the adsorbed monolayer films onto gold surface. PM-RAIRS is based on the modulation of a linearly polarized infrared beam, which is divided into an s-polarized beam (with its electric field parallel to the sample surface), and a p-polarized beam (with its electric field perpendicular to the sample surface).[14] According to metal surface selection rules, species on a metal surface can only absorb p-polarized IR light, while molecule in an isotropic gaseous

(or liquid) environment can absorb both p- and s-polarized IR light. So, it is possible to obtain a surface specific IR absorption spectrum, virtually independent of the surrounding conditions, by subtracting s-polarized absorptions from the p-polarized ones. The predominance of p-polarized light over s-polarized light at the metal surface has been utilized to obtain the reflectance spectrum of the adsorbed surface species.[15] An example of the PM-RAIRS setup is shown in Figure 2.12.

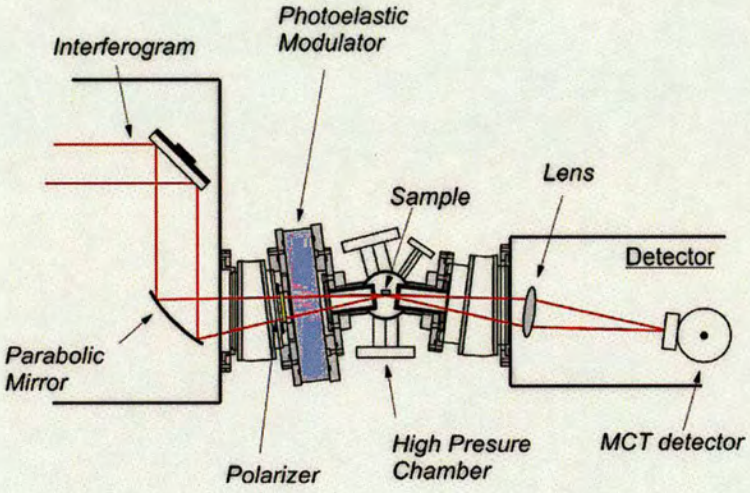

Figure 2.12: Schematic top view of the PM-IRAS optical setup.

2.4 References

(1) *Instrumental Methods in Electrochemistry*, Edited by Southampton Electrochemistry Group, Horwood Publishing, Chichester, 2001.

(2) A. J. Bard and L. R. Faulkner, *Electrochemical methods: Fundamental and applications*, John Wiley & Sons Inc., New York, 2001.

(3) E. P. M. Van Westing, G. M. Ferrari and J. H. W. De Wit, *Electrochim. Acta,* 1994, **39**, 899.

(4) C. Fernández-Sánchez, C. J. McNeil and K. Rawson, *TrAC Trends Anal. Chem.,* 2005, **24**, 37.

(5) J. S. Chen, J. P. Diard, R. Durand and C. Montella, *J. Electroanal. Chem.*, 1996, **406**, 1.

(6) M. Naumowicz, A. D. Petelska and Z. A. Figaszewski, *Electrochim. Acta,* 2005, **50**, 2155.

(7) D. P. Woodruff, *Modern Techniques of Surface Science*, Cambridge University Press, 1994.

(8) K. Siegbahn in ESCA-*Atomic, molecular and solid state structure studied by means of electron spectroscopy*, Almquist and wiksells, Uppsala, 1967.

(9) P. R. Griffiths and J. A. Haseth, *Fourier Transform Infrared Spectroscopy*, John Wiley & Sons: New York, 1986.

(10) R. G. Greenler, *J. Chem. Phys.*, 1966, **44**, 310.

(11) S. A. Francis and A. H. Ellison, *J. Opt. Soc. Am.*, 1959, **49**, 131.

(12) R. G. Greenler, R. R. Rahn and J. P. Schwartz, *J. Catal.*, 1971, **23**, 42.

(13) (a) R. G. Greenler, *J. Chem. Phys.*, 1966, **44**, 310; (b) R. G. Greenler, *J. Chem. Phys.*, 1969, **50**, 1963.

(14) B. J. Barner, M. J. Green, E. I. Sáez and R. M. Corn, *Anal. Chem.*, 1991, **63**, 55.

(15) (a) G. A. Beitel, A. Laskov, H. Oosterbeek and E. W. Kuipers, *J. Phys. Chem.*, 1996, **100**, 12494; (b) W. G. Golden, D. S. Dunn and J. Overend, *J. Catal.*, 1981, **77**, 395; (c) K. P. Pang, J. B. Benziger, M. P. Sorlaga and A. T. Hubbard, *J. Phys. Chem.*, 1964, **88**, 4503.

Chapter 3

Ligands design and synthesis

3.1 Introduction

There are many examples in the literature of metal complexes with open coordination sites for use in molecular recognition. They serve as binding sites in the development of new chemosensors to study metalloenzyme function in bioinorganic chemistry or to direct supramolecular assembly. As a first step for metal-complex based molecular recognition at surfaces, we chose some ligands which form metal complexes with interesting properties for catalysis and molecular recognition and we derivatized them with thiol groups for attachment to gold surfaces. Thus, the attachment of these ligands to gold should provide metal complexes with interesting sensing, electronic and catalytic properties.

This chapter describes the design and synthesis of these ligands, which are based upon the ligands tris(2-pyridylmethyl)amine (TPA) and bis(2-pyridylmethyl)amine (BPA) derivatized with different spacers and thiols.

3.1.1 Metal binding units selected

3.1.1.1 Tris(2-pyridylmethyl)amine (TPA) based ligands and metal complexes

Metal complexes of the tripodal ligand TPA (Figure 3.1) and related ligands exhibit interesting redox-induced changes in molecular geometry[1] and excellent properties for catalysis[2] and molecular recognition.[3]

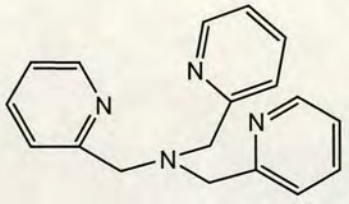

Figure 3.1: Tris(2-pyridylmethyl)amine (TPA).

This ligand was first reported in 1969 by da Mota[4] and a large number of derivatives have been used for complexation of metal ions. Most reports cover investigations of Cu(II),[5] Zn(II)[6] and Fe(III)[7] ion complexation.

Properties in molecular recognition

Metal complexes of TPA typically have one or two available sites for coordination of external molecules and as a result they have shown good properties for anion binding.[8,9]

The binding properties of the TPA metal complexes can be improved by introducing in the ligand other functional groups. An example was reported in our group, where the modification of the TPA ligand with H-bonding groups was shown to influence the properties of the Zn(II) metal complex formed, including its ability to bind phosphates.[10]

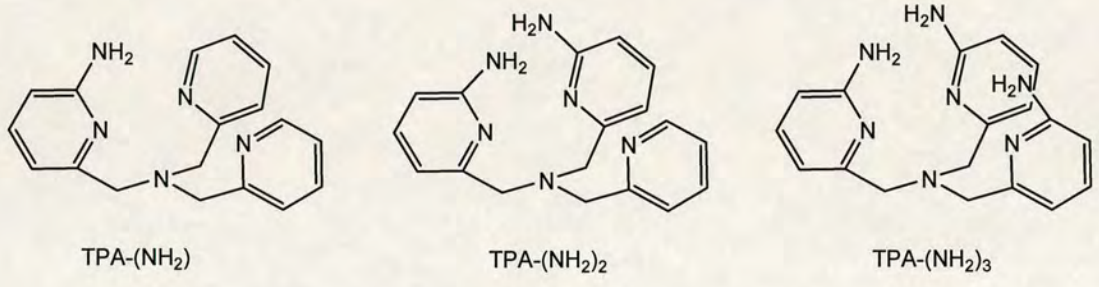

Figure 3.2: TPA ligand modified with amino groups.

A related Cu(II) complex developed by Anslyn et al. has also been shown to exhibit improved binding properties due to H-bonding interactions with guanidinium moieties.[11]

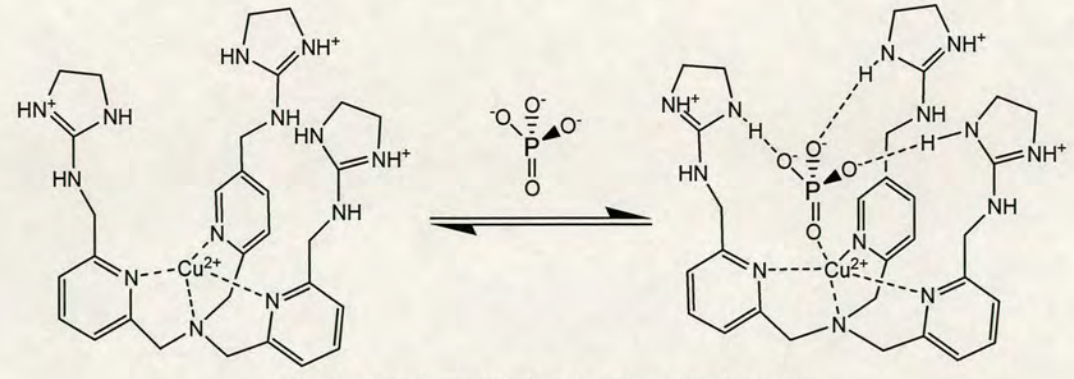

Figure 3.3: Assembly for phosphate ion detection.

Properties as catalysts

Cu and Fe complexes of TPA have been used to model biological oxygen binding and activation. Karlin et al. synthesized the first structurally-characterized copper-dioxygen complex, a trans-(μ-1,2-peroxo)dicopper(II) using TPA.[12] Since then, other TPA-based ligands have been used to study a range of ligand effects in the reactivity and structure of Cu-dioxygen adducts.[2a,13]

Masuda et al. have created a synthetic model of the enzymes dopamine β-monooxygenase (DβM) and peptidylglycineα-hydroxylating monooxygenase (PHM) based on the mononuclear Cu(II)-hydroperoxo complex obtained from reaction of the Cu(I) complex of a TPA derivative with pivaloylamido groups (H_2BPPA) with dioxygen (Figure 3.4).[14]

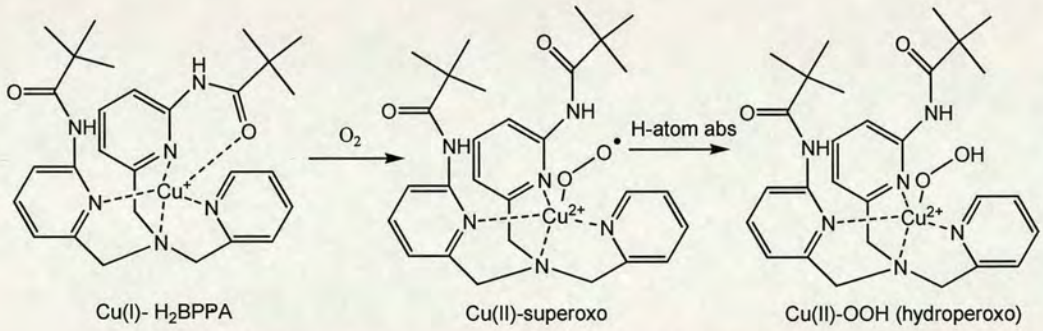

Figure 3.4: TPA-Cu(II)-peroxo stabilized by pivaloylamido groups.

They proposed that the Cu(II)-hydroperoxo complex is generated via H-atom abstraction by the Cu(II)-superoxo complex and that the ligand H_2BPPA stabilizes the Cu(II)-hydroperoxo species through hydrogen bond interactions.[15]

Iron complexes of TPA derivatives have also been studied because of their ability to mimic mononuclear iron monoxygenases. An example is the use of Fe-TPA to bind catechol as model of the enzyme 3,4- dioxygenase (3,4-PCD).[2b]

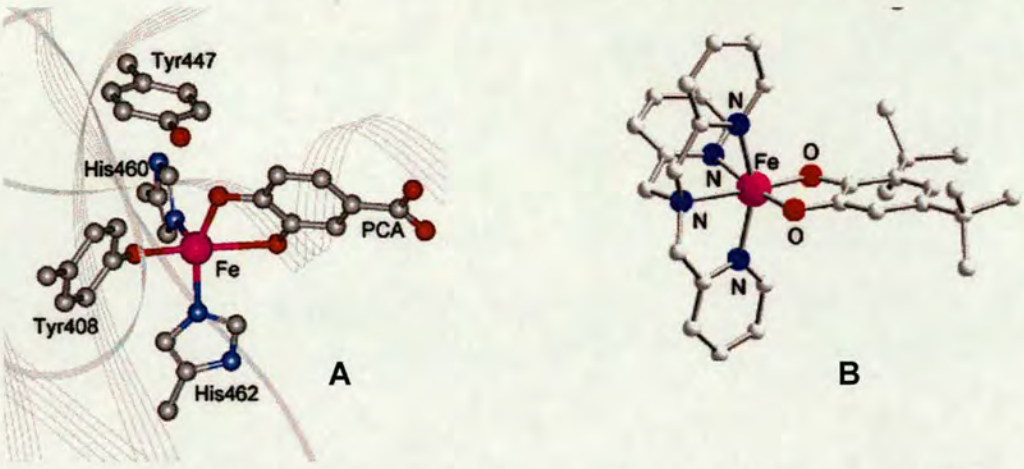

Figure 3.5: (A) Active site of enzyme 3,4-dioxygenase bound to substrate, catechol. (B) Model Fe-TPA complex bound to substrate, 3,5-di-tert-butylcatechol.

These metal complexes are important not only to understand the chemistry of the metalloenzymes, but also to develop artificial oxidation catalysts.[16]

3.1.1.2 Bis(2-pyridylmethyl)amine (BPA) based ligands and metal complexes

First reported in 1964 by Kabzinska,[17] this ligand and derivatives have been used for complexation of many metal ions.[18] Particular emphasis has been on investigating their coordination to Cu(II),[19] Zn(II)[20] and Fe(III)[21] ions.

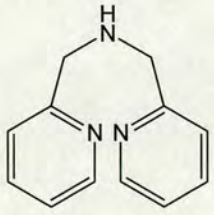

Figure 3.6: Bis(2-pyridylmethyl)amine (BPA).

The Zn-BPA combination is good for molecular recognition. Zn(II) is particularly attractive metal cation for chemosensing because unlike other transition metal cations, it does not quench the fluorescence of an attached dye as it is not redox active. The three nitrogens of BPA can coordinate strongly to a Zn(II) cation, with an association constant of around 10^7 M^{-1} in water, leaving one or two vacant coordination sites for an anionic guest. Furthermore, it is synthetically straightforward to incorporate multiple BPA units into a single organic scaffold to seek the cooperativity of two or more metal ions.

Properties in molecular recognition

Hamachi et al. used Zn(II)-BPA units linked by organic scaffolds for the design of artificial peptide receptors. They showed that the Zn(II)-BPA complex provides a good binding site for histidine residues[22] and ATP.[23]

Important Zn(II)-BPA based receptors developed by this group are anthracene derivatives having Zn(II)-BPA moieties (Figure 3.7), which selectively coordinate phosphorylated amino acids and peptides and signal binding by a change in fluorescence emission.[24]

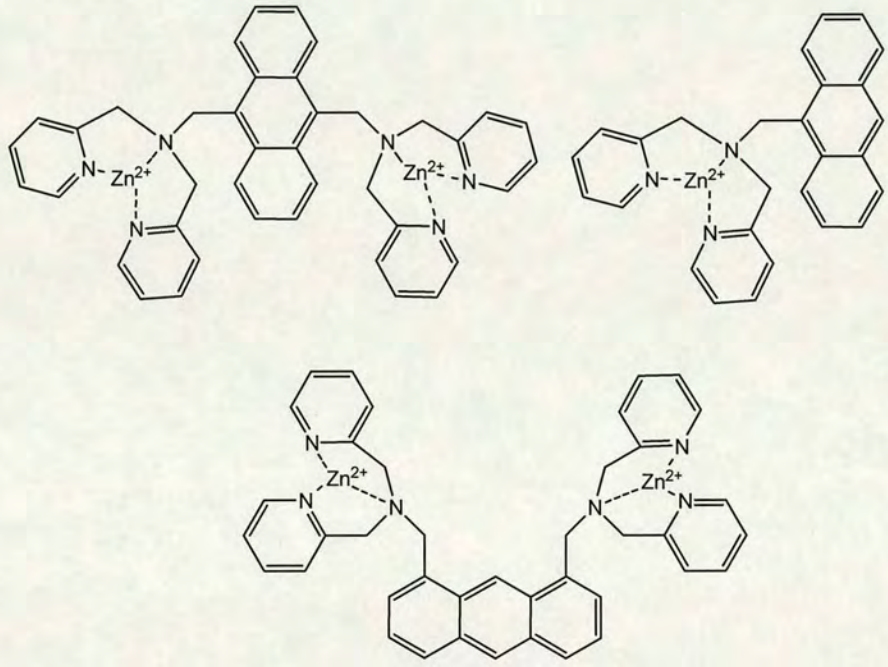

Figure 3.7: Structures of anthracene derivatives having Zn(II)-BPA moieties.

Kim et al. synthesized related BPA ligands to bind phosphate anions (Figure 3.8). In this case a 4-methyl-phenyl group is used as linker to bridge the BPA units and create a dimetallic complex. This complex combined with the dye pyrocatechol violet provides a colorimetric sensor for inorganic phosphate[25] and AMP.[26]

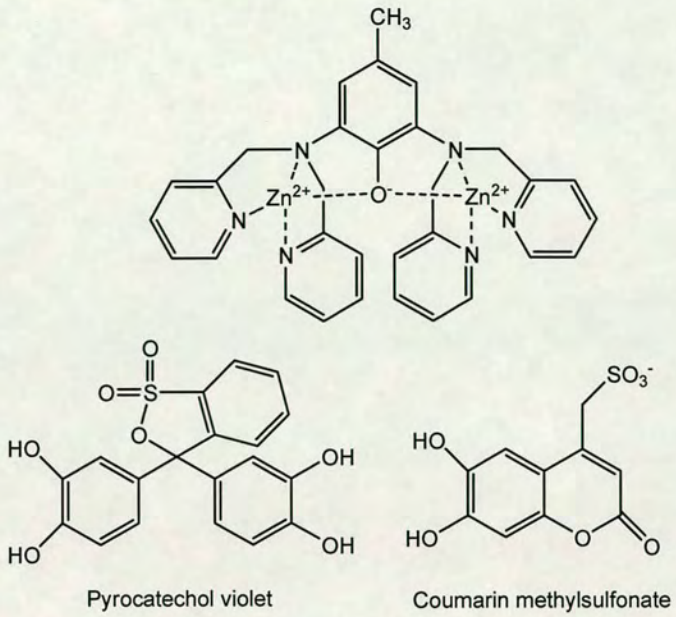

Pyrocatechol violet Coumarin methylsulfonate

Figure 3.8: Structure of Zn(II)-BPA based receptor and the molecules used as indicators in the displacements assays .

Smith et al. developed a fluorescent version of this indicator displacement system by using coumarin methylsulfonate.[27] The fluorescence of the indicator is quenched when it binds to the Zn(II)-BPA receptor and it is restored when it is displaced by a suitable phosphate derivative. This fluorescence ensemble detects pyrophosphate over hydrogen phosphate with a selectivity of nearly two orders of magnitude.

Properties as catalysts

Similar dimetallic complexes have been investigated as catalysts for the hydrolysis of phosphoesters (Figure 3.9).

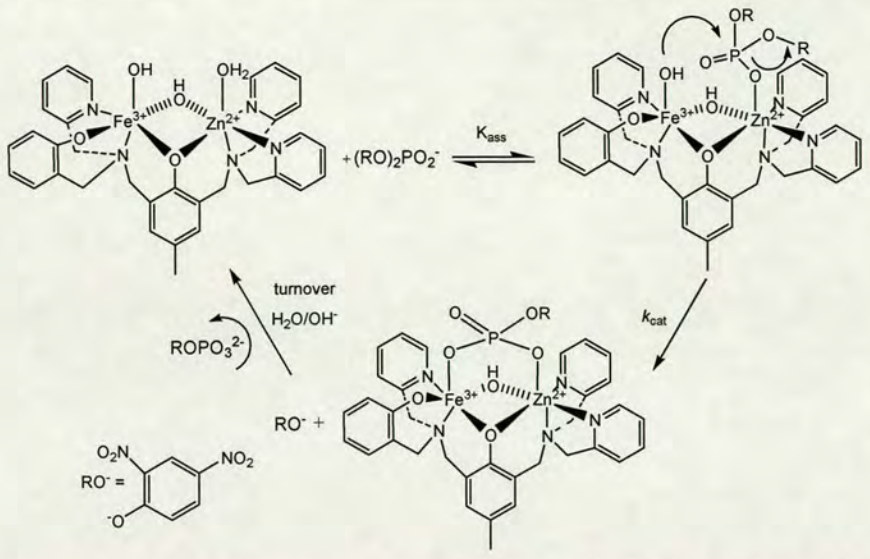

Figure 3.9: Mechanism of phosphate hydrolysis by hetero bimetallic complexes of BPA.[28]

The system shown in Figure 3.9[28] mimics the enzyme purple acid phosphatases, a family of binuclear metallohydrolases that catalyze the hydrolysis of a variety of phosphoester substrates within the pH range of 4-7.

These studies showed that these metal complexes have very good properties as sensors and catalysts in solution. Modification of gold electrodes with metal complexes of TPA and BPA derivatives could improve their chemical properties due to surface induced preorganisation.

3.1.2 Interfaces and thiolates linkages selected

In a SAM, the nature of the bridge that connects the electrode with the terminal functional group affects the rate of the interfacial electron-transfer process (see Chapter 1). Therefore, it is also important to select an appropriate interface and a thiolate linkage. The applications, properties and robustness of the SAM as catalyst or as sensor will be influenced by the chemical composition of the bridge, its length and the type of group used for attachment to the gold surface.

Several research groups have studied ferrocene terminated oligo(phenyleneethynylene) (OPE) thiols deposited as self-assembled monolayers on gold,[29] and show that they exhibit faster electron transport than their ferrocene alkanethiol

counterparts.[30] This particular type of molecule has recently attracted much attention because of their high electron conductivity, which makes them applicable as molecular wires in molecular electronics.[31]

SAMs formed with long alkane thiol chains (10 or more carbon atoms) favour a more ordered packing and higher monomer density. The disadvantage of long chain thiols for electrochemistry is that the site of redox activity will be distant from the electrode, giving a slower rate of electron transfer and hence any current due to the redox process at the SAM-solution interface will be small. A good compromise between sensitivity and stability is the use of thioctic acid (or dihydrolipoic acid). This molecule has a large disulfide-containing base, a short alkyl chain with four $-CH_2$ units and a carboxylic acid termination (Figure 3.10).

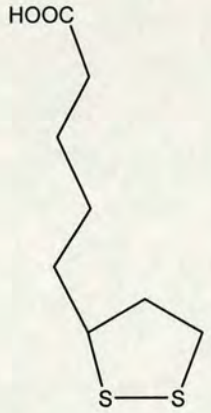

Figure 3.10: Thioctic acid molecule

SAMs of thioctic acid have been studied by electrochemical methods such as cyclic voltammetry (CV) and electrochemical impedance spectroscopy (EIS)[32] and with surface techniques such as X-ray photoelectron spectroscopy (XPS) and near-edge X-ray absorption fine structure (NEXAFS).[33] These studies reveal that this molecule can be used for immobilization of receptors onto gold electrodes. The two thiol groups which chemisorb to the electrode provide greater stability than that obtained with the single gold-sulphur bond formed by alkanethiols. Also the recognition molecule is located near the electrode allowing a good rate of electron-transfer.

Thioctic acid-based systems have been used to anchor a variety of molecules on gold surfaces.[34] Echegoyen et al. used thioctic acid to immobilize receptors based on

calix[6]crown-4,[35] calix[4]arene[36] and cyclotriveratrylene[37] derivatives to detect specific anions and cations (see Figure 3.11 (a)). Another example is the use of thioctic acid for carbohydrate immobilization on gold surfaces (Figure 3.11 (b)), which was used to achieve high specific protein binding.[38]

Nakamura et al. used binary SAMs composed of thioctic acid and thioctic amine to adsorb cytochrome c via electrostatic interactions[39] and exploit this to detect superoxide radical.[40]

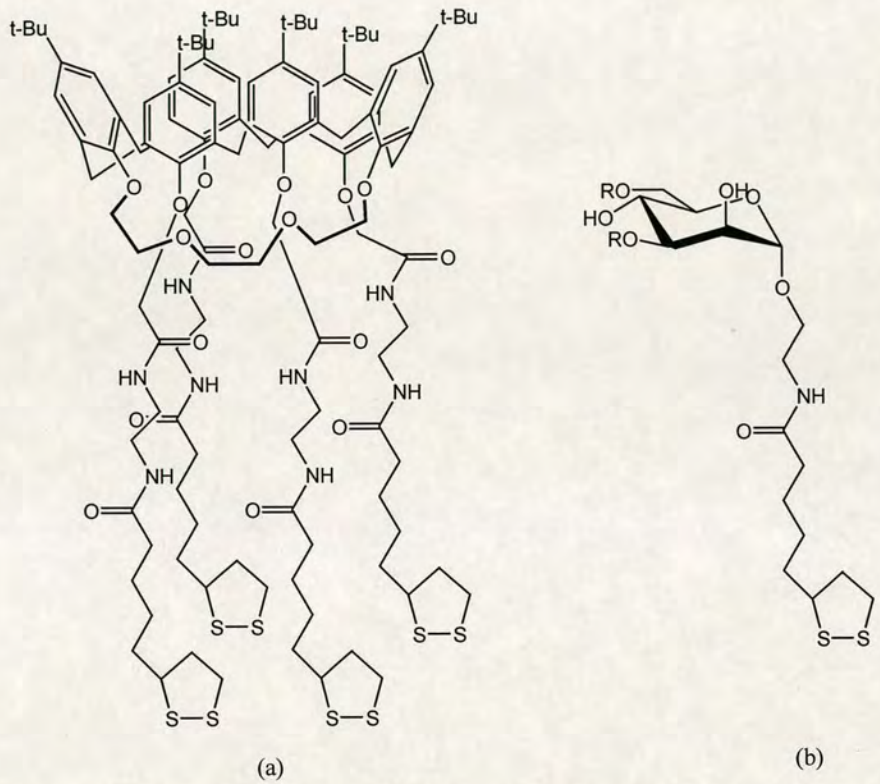

(a) (b)

Figure 3.11: (a) Structure of anion sensor based on calix[4]arene and thioctic acid derivatives; (b) Structure of the carbohydrate derivative and thioctic acid.

We have synthesized ligands having an aromatic interface and a thiol group for gold attachment and ligands where the thioctic acid group is used as the aliphatic interface.

3.2 General structure of the ligands

The ligands were designed and synthesized in such a way as to provide different domains with specific functions (Figure 3.12). They have a thiolate group for attachment to the gold surface (black), the metal binding site (blue), functional groups with the potential to participate in hydrogen bonding interactions (red) and different linkers (pink).

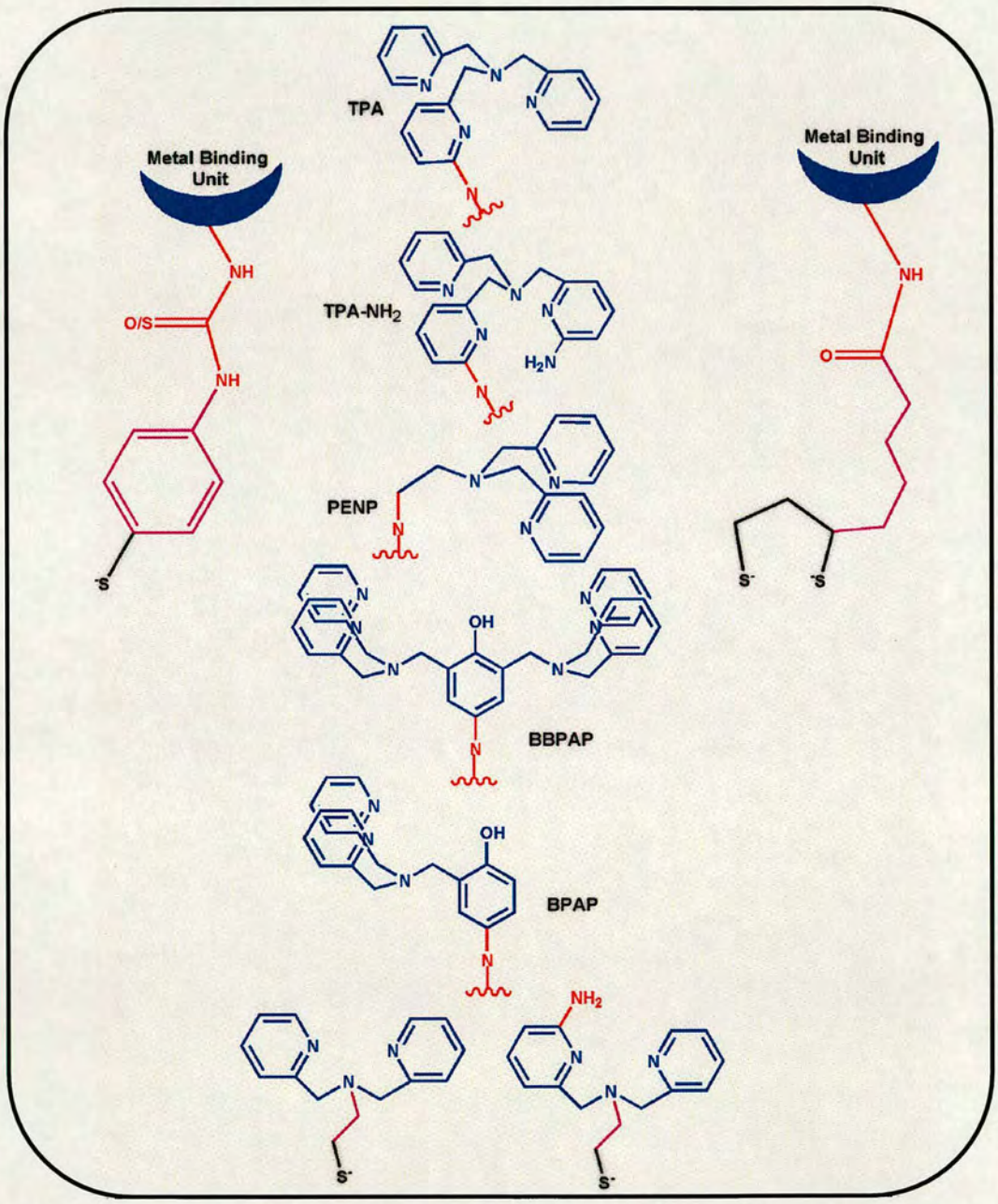

Figure 3.12: Structures of the ligands synthesized.

The metal binding sites are based on tris(2-pyridylmethyl)amine (**TPA**) and bis(2-pyridylmethyl)amine (**BPA**). The derivative of **TPA** is *N,N*-bis(2-pyridylmethyl)-*N*-(6-amino-2-pyridylmethyl)amine (**TPA-NH_2**). The dinuclear and mononuclear **BPA** based ligands are 2,6-bis[bis(2-pyridylmethyl)aminomethyl]-4-aminophenol (**BB PAP**), 2-[bis(2-pyridylmethyl)aminomethyl]-4-aminophenol (**BPAP**) and *N,N*-bis(2-pyridylmethyl)ethane-1,2-diamine (**PENP**). Two other BPA-based ligands were synthesised and these have an ethanethiol molecule attached to the **BPA** unit.

3.3 Results and discussion

All the ligands synthesised are shown in Figures 3.13-3.15. They are classified as derivatives of **TPA** and **BPA** with aromatic and aliphatic interfaces.

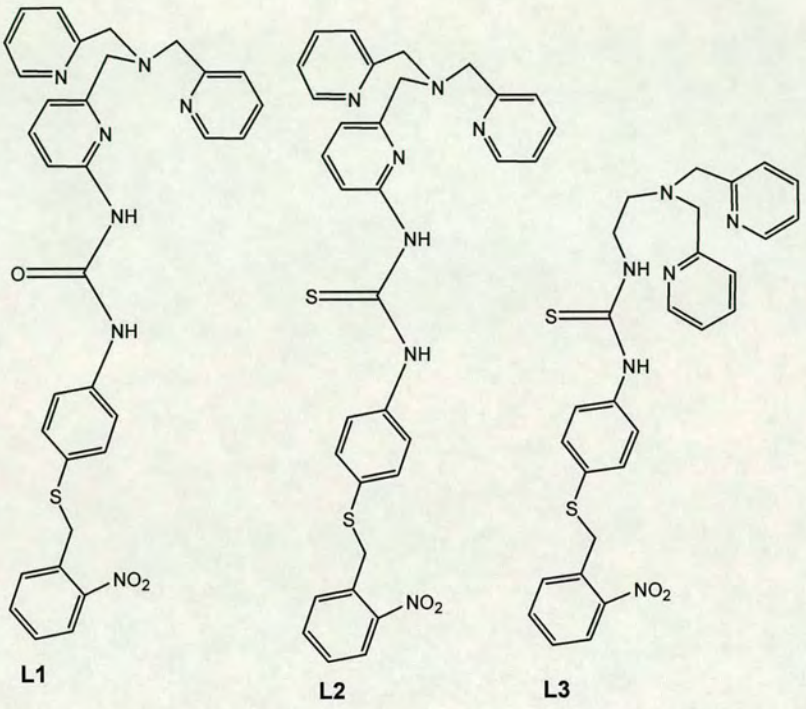

Figure 3.13: Ligands derivatives of TPA and BPA with aromatic interface.

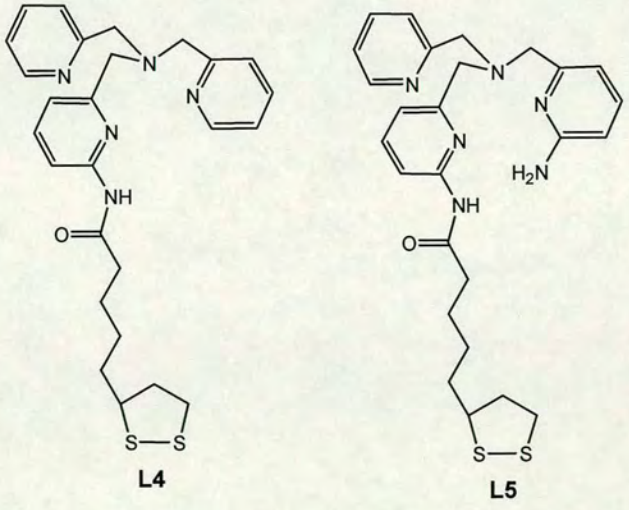

Figure 3.14: Ligands derivatives of TPA with aliphatic interface.

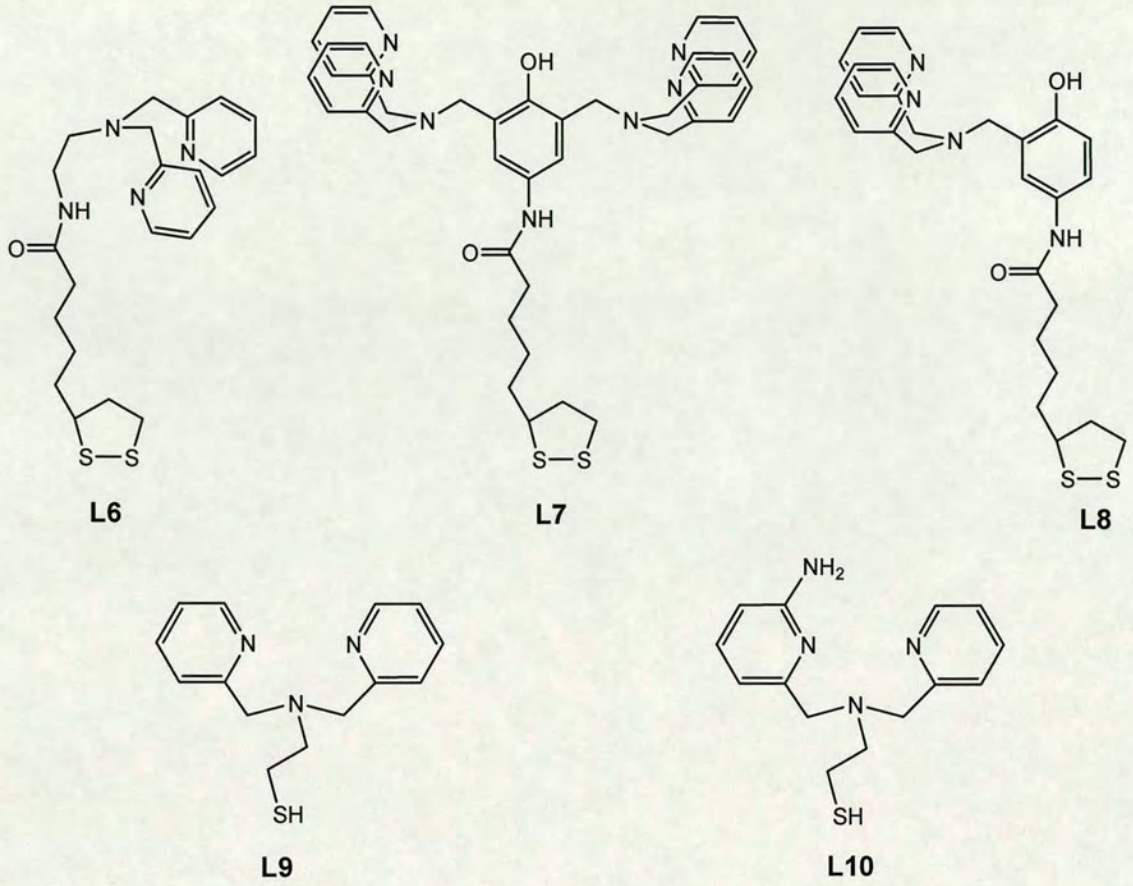

Figure 3.15: Ligands derivatives of BPA with aliphatic interface

3.3.1 Synthesis of the metal binding units

3.3.1.1 TPA derivative units

The synthetic scheme for *N,N*-bis(2-pyridylmethyl)-*N*-(6-amino-2-pyridylmethyl)amine (**TPA-NH_2**) and *N,N*-bis(6-amino-2-pyridylmethyl)-*N*-(2-pyridylmethyl)amine (**TPA-$(NH_2)_2$**) is shown in Figure 3.16.

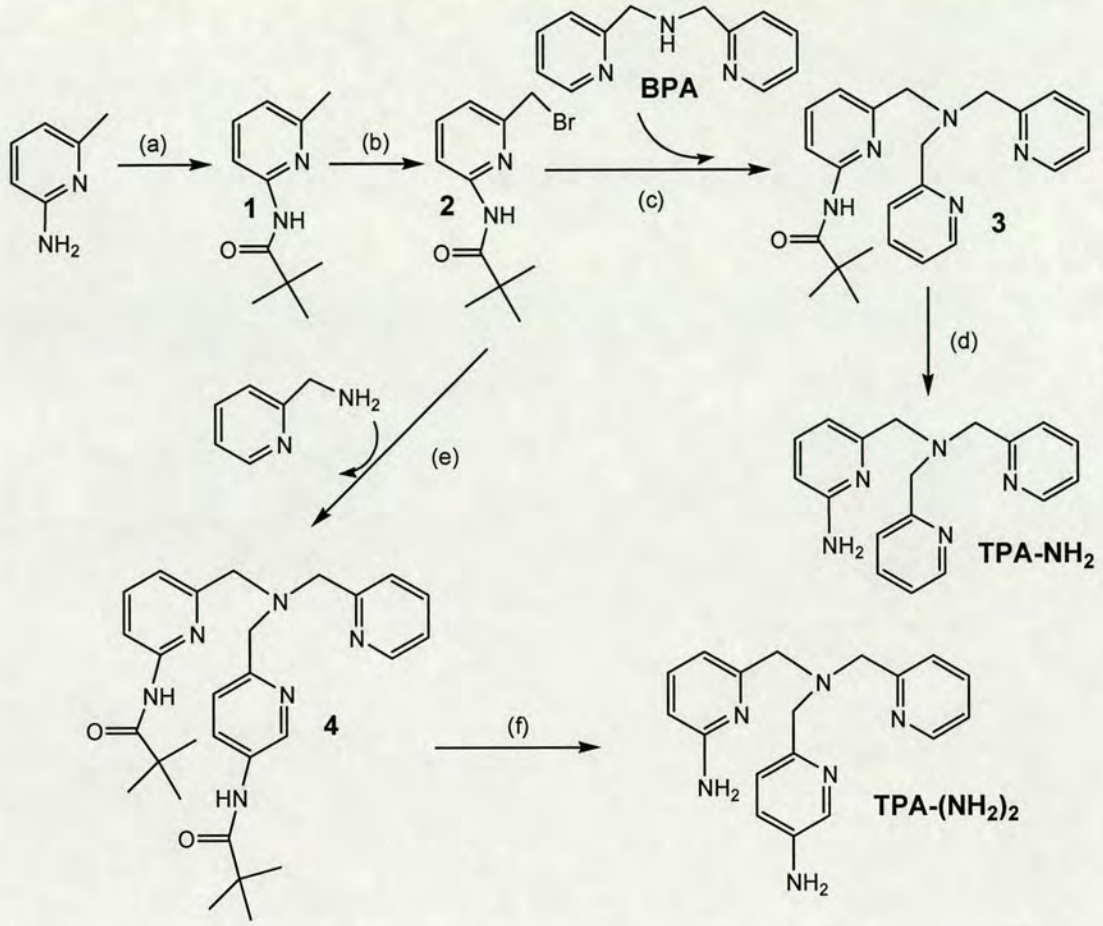

Figure 3.16: Reagents and conditions: (a) ^{t}BuCOCl (1.5 equiv), CH_2Cl_2, NEt_3, 22 h, 83%; (b) NBS (1.5 equiv), AIBN (0.5 equiv), CCl_4, 80 °C, 3.5 h, 43%; (c) CH_3CN, Na_2CO_3, 3h, rt, 80%; (d) 2 M HCl(aq), 100 °C, 16 h, 73%; (e) CH_3CN, Na_2CO_3, (^{t}Bu)NH_4Br, 48h, 44 °C, 66%; (f) 2 M HCl(aq), 100 °C, 72 h, 71%.

The first step is the synthesis of 2-(pivaloylamido)-6-(bromomethyl)pyridine[41] **2** which involves two reactions. The first one is the protection of the amino group of 2-amino-6-methylpyridine with trimethylacetyl chloride using triethylamine as a base. This reaction yields the desired pure product in good yield (83%) after flash chromatography. The second step is the bromination of the picoline methyl group of **1** using N-bromosuccinimide (NBS) as a bromination agent and a catalytic amount of 2, 2'-azobis(2-methyl-propionitrile) (AIBN) as a radical initiator in refluxing carbon tetrachloride. This reaction proceeds in low yield (43%) and requires flash chromatography to separate the mono from the bis and non-brominated products.

The asymmetric tripodal ligand *N,N*-bis(2-pyridylmethyl)-*N*-(6-pivaloylamido-2-pyridylmethyl)amine **3** was prepared by coupling 1 equivalent of **BPA** with 1

equivalent of 2-(pivaloylamido)-6-(bromoethyl) pyridine **2** in acetonitrile using 2 equivalents of Na_2CO_3.[42]

The synthesis of **TPA-NH$_2$** was carried out by hydrolysis of **3**. The trimethylacetyl protecting group of **3** was cleaved by refluxing in 2 M HCl(aq) for 16 h to yield the unprotected amine. This reaction proceeds in good yields (78%) after doing an acid/base extraction to purify the product.

A similar procedure[10] was adopted for the synthesis of **TPA-(NH$_2$)$_2$**.

3.3.1.2 BPA derivative units

The synthesis of *N*,*N*-bis(2-pyridylmethyl)ethane-1,2-diamine (**PENP**) was carried out in two steps (Figure 3.17).[43]

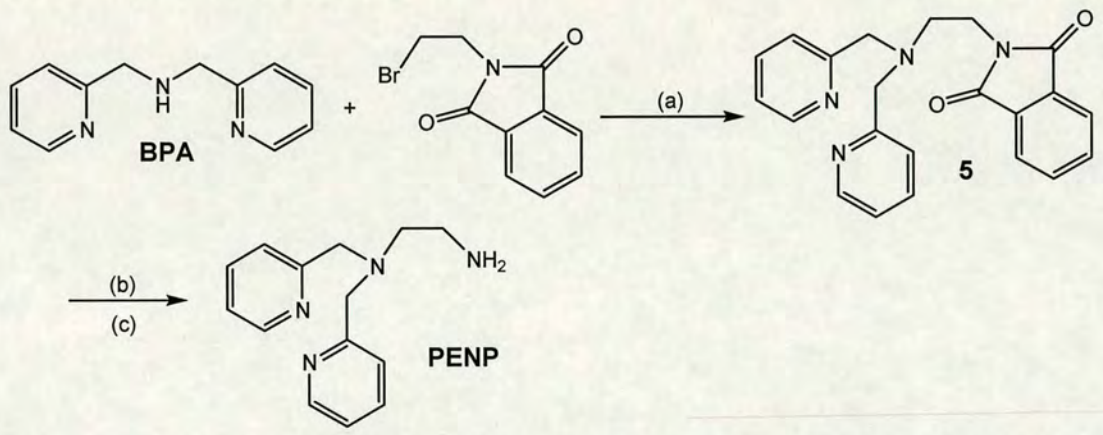

Figure 3.17: Reagents and conditions: (a) CH_3CN, K_2CO_3, KI, 1 week, 65 °C; (b) EtOH, $N_2H_4 \cdot H_2O$, 3h; (c) HCl, 1h, 0 °C, 30 %.

A mixture of **BPA**, *N*-(2-bromoethyl)-phathalimide, anhydrous K_2CO_3 and KI was dissolved in acetonitrile to obtain the intermediate product **5**, which upon reaction with $N_2H_4 \cdot H_2O$ in absolute ethanol gives the final product **PENP** in a yield of 30%.

The synthesis of the **BPA**-based dinuclear metal binding unit is illustrated in Figure 3.18.

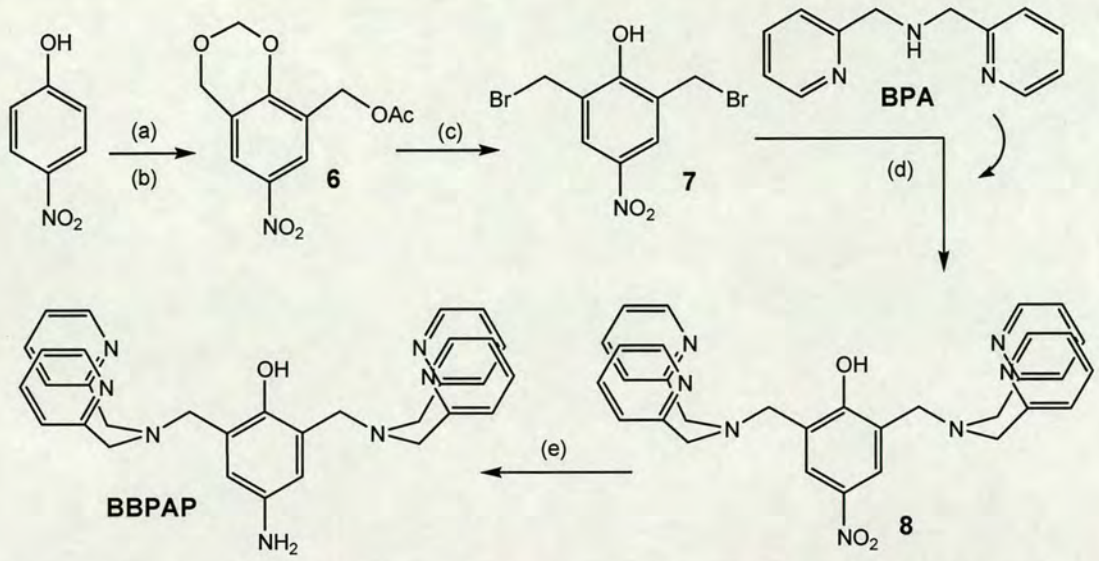

Figure 3.18: Reagents and conditions: (a) Paraformaldehyde, Acetic acid, H_2SO_4, 52%; (b) K_2CO_3(aq); (c) HBr,70 °C, 6 h, 54%; (d) Na_2CO_3, CH_3CN, N_2, 60 °C, 16 h, 67%; (e) H_2(Pd/C), CH_3OH, RT, 48 h, 77%.

The bridging unit **7** (synthesised in a two step reaction according to a published procedure[44]) was reacted with 2 equivalents of **BPA** in the presence of anhydrous Na_2CO_3 and in dry acetonitrile to give **8**. The reduction of the nitro group to obtain **BBPAP** is done in methanol using H_2 as a reducing agent and Pd/C as a catalyst.

The mononuclear metal binding unit **BPAP** was synthesised according to the steps shown in Figure 3.19:

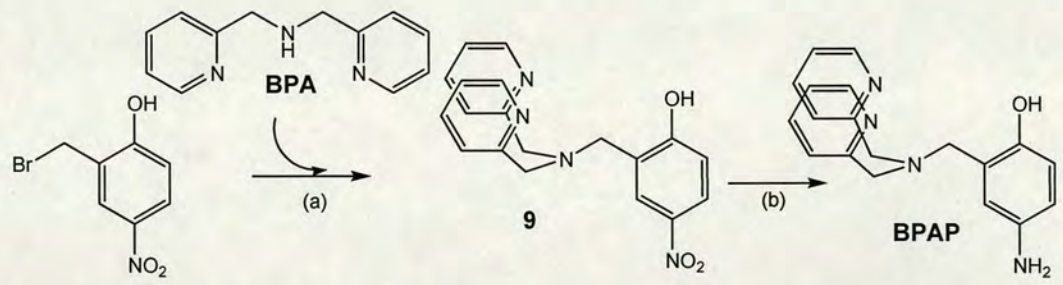

Figure 3.19: Reagents and conditions: (a) THF, Et_3N, RT; (b) H_2 (Pd/C), CH_3OH.

The first one consists of synthesising 2-[bis(2-pyridylmethyl)aminomethyl]-4-nitrophenol **9**[45] by reaction of equimolar amounts of 2-bromomethyl-4-nitrophenol and **BPA** in the presence of triethylamine in THF. **BPAP** was obtained by reducing the nitro group using H_2 as a reducing agent and Pd/C as a catalyst in methanol.

3.3.2 Synthesis of the TPA and BPA based ligands with aromatic interface

Ligands with the aromatic interface were synthesised following the procedures shown in Figure 3.20.

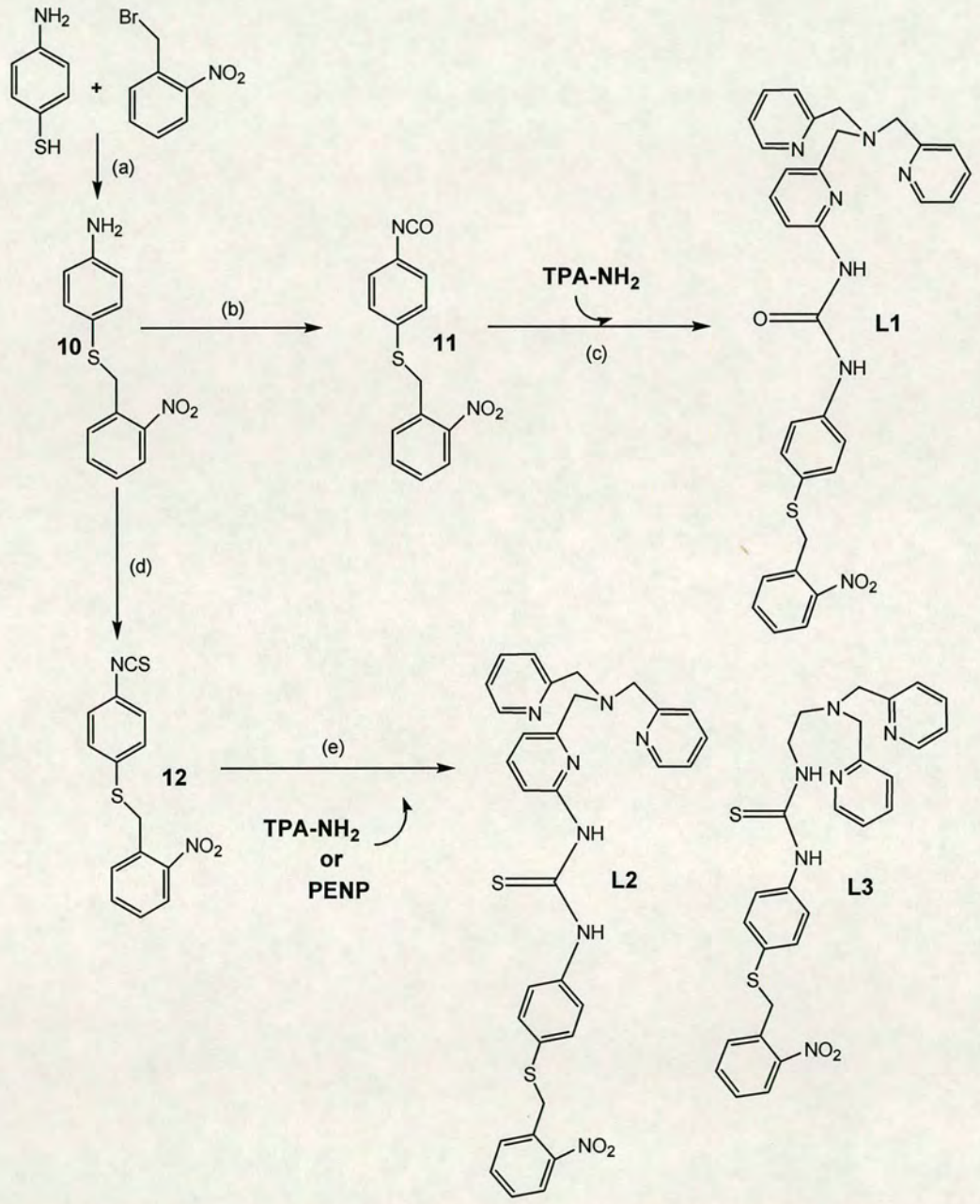

Figure 3.20: Reagents and conditions: (a) CH_3CN, Na_2CO_3, RT, 80%; (b) $CHCl_3$, $COCl_2$, $CaCO_3$, RT, 88%; (c) THF, 50 °C, 2 d, 38 %; (d) $CHCl_3$, $CSCl_2$, $CaCO_3$, RT, 72%; (e) THF, 50 °C, 2 d, 44.8 % for **TPA-$(NH_2)_2$** and 41% for **PENP**.

The synthesis of **10** involved the reaction of p-aminothiophenol with 2-nitrobenzylbromide in acetonitrile in the presence of Na_2CO_3 as a base. The ligand **10** was then reacted with phosgene or thiophosgene in a mixture of water and chloroform in the presence of $CaCO_3$ to obtain **11** and **12**.

L1 was prepared by coupling 1 equivalent of **11** with 1 equivalent of **TPA-NH$_2$** in THF at 50 °C. **L2** and **L3** were synthesised the same way but using **TPA-NH$_2$** or **PENP**.

3.3.3 Synthesis of the TPA and BPA based ligands with aliphatic interface

The **TPA** and **BPA** based ligands having thioctic acid as a aliphatic interface, such as **L4**, were synthesized as shown in Figure 3.21.

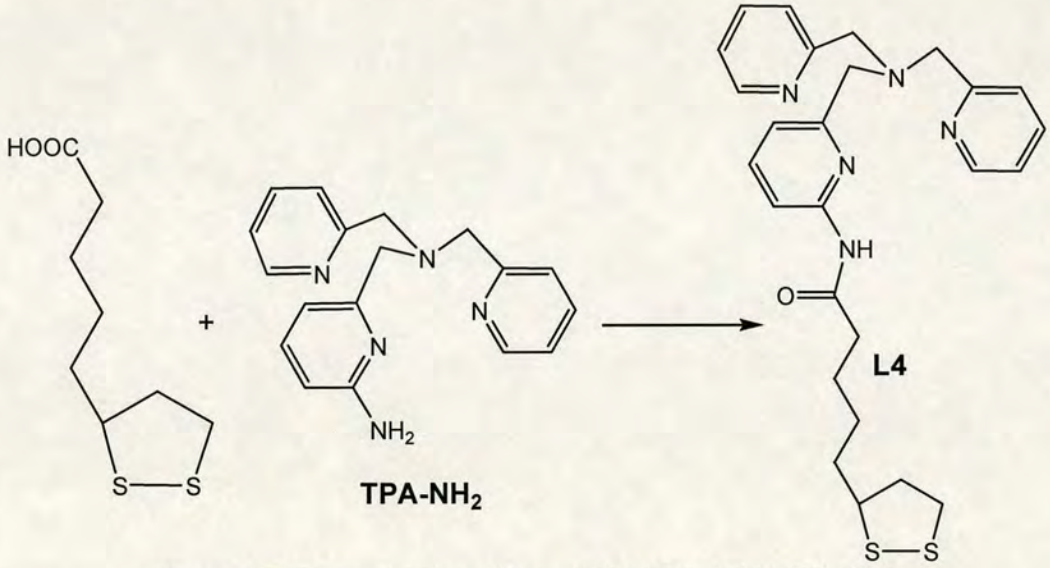

Figure 3.21: Reagents and conditions: DCM, DCC, 40°C, 72 h, 30 %.

TPA-NH$_2$ was reacted with 1 equivalent of thioctic acid in the presence of the coupling agent 1,3-dicyclohexylcarbodiimide (DCC) in dichloromethane. The final product was obtained in a 30% yield after purification by an acid/basic extraction.

L5, **L6**, **L7** and **L8** were prepared in the same way but using **TPA-(NH$_2$)$_2$**, **PENP**, **BBPAP** and **BPAP** respectively. **L5** was obtained in a 25.6% yield, **L6** in a 95 %, **L7** in 46.8 % and **L8** in 38.1 %.

The synthesis of *N*,*N*-bis(2-pyridylmethyl)aminoethanethiol[46] **L9** was carried out in one step (Figure 3.22) by reaction of **BPA** (1 equivalent) with ethylene sulfide (2 equivalents) in benzene and under N_2 (yield 70 %).

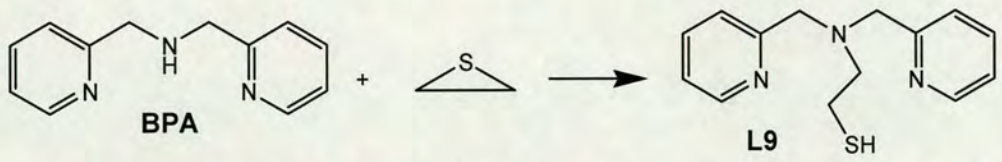

Figure 3.22: Reagents and conditions: benzene, N_2, 65 °C, 72 h, 70%.

Di-2-(*N*-(6-amino-2-pyridylmethyl)-*N*-(2-pyridylmethyl)amino)ethyl disulfide **L10** can be synthesised in 3 steps (Figure 3.23).

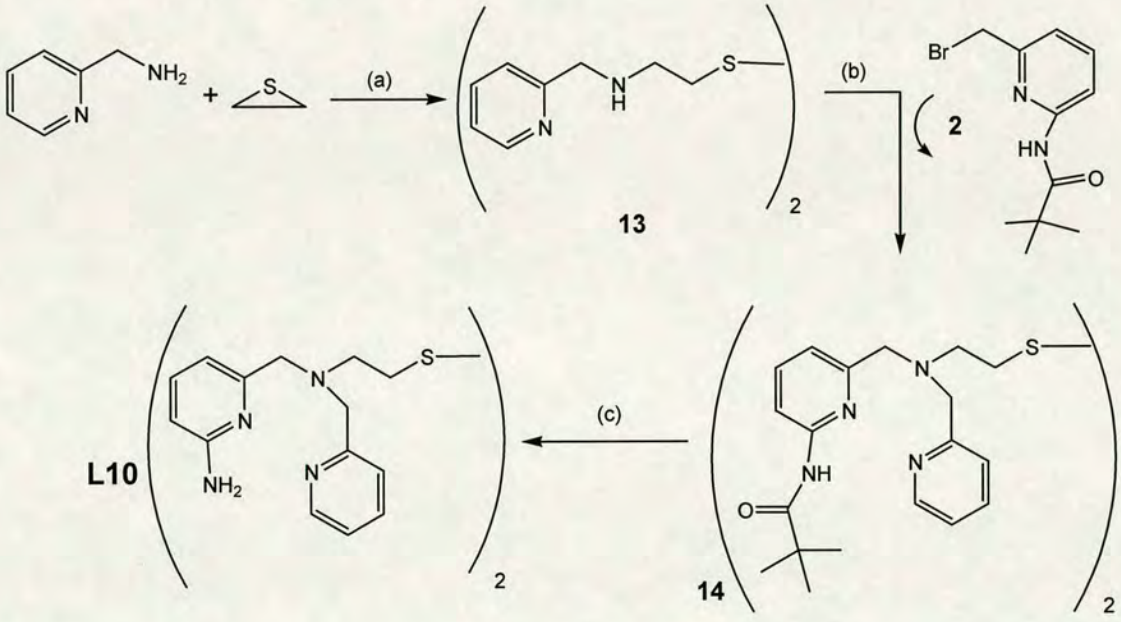

Figure 3.23: Reagents and conditions: (a) benzene, 55 °C, 16 h, 27.8%; (b) Na_2CO_3, CH_3CN, RT, 2 h; (c) 2M HCl(aq), 80 °C, 24 h, 59.97%.

The synthesis of di-2-(*N*-((2-pyridylmethyl)amino)ethyl disulfide **13** was carried out by reacting 1 equivalent of 2-(aminomethyl)pyridine with 0.5 equivalents of ethylene sulphide in benzene.[47] After one overnight, the final pure product was obtained after an extraction in HCl(aq)/dichloromethane. The second step is the reaction of 1 equivalent of **13** with 2 equivalents of 2-pivalamidopyridine-6-bromomethyl **2** in acetonitrile in the presence of Na_2CO_3 to obtain di-2-(*N*-(6-pivalamido-2-pyridylmethyl)-*N*-(2-pyridylmethyl)amino)ethyl disulfide **14**. **L10** was obtained by

hydrolysis of **14** in refluxing 2 M HCl(aq) for 24 h. This reaction proceeds in a reasonably good yield (60 %) after basifying the reaction solution and extracting the desired product with dichloromethane.

3.4 Experimental details

3.4.1 General

Reagents were obtained from commercial sources and used as received unless otherwise noted. Solvents were dried and purified under N_2 by using standard methods and were distilled immediately before use. All compounds were prepared under N_2 unless otherwise mentioned. The compounds 2-(pivalolylamido)-6-(bromomethyl)pyridine[41] **2**, *N,N*-bis-(6-pivaloylamido-2-pyridylmethyl)-*N*-(2-pyridylmethyl)amine[10] **4**, 8-acetoxymethyl-6-nitro-1,3-benzodioxene[44] **6** and 2-[bis(2-pyridylmethyl)aminomethyl]-4-nitrophenol[45] **9** were synthesized according to literature procedures. The NMR spectra were obtained using a Bruker DPX 360 at 20 °C. ^{13}C and ^{1}H chemical shifts are referenced with respect to the carbon and proton resonances of the solvent. Mass spectra were performed on a micromass Platform II system operating in Flow Injection Analysis mode with the electrospray method. Infrared spectra were recorded with JASCO FTIR-410 spectrometer between 4000 and 400 cm^{-1} as KBr pellets (solid state).

Phosgene and thiophosgene were handled with extreme care due to their high toxicity: eye and skin irritants, corrosive gases that may cause burns; inhalation can cause fatal respiratory damage. Full risk assessments were undertaken prior to use them. Impermeable gloves and safety glasses were worn at all time. Reactions were carried out in ventilated fume hood.

3.4.2 Synthesis of ligands

Synthesis of N,N-bis(2-pyridylmethyl)-N-(6-pivaloylamido-2-pyridylmethyl)amine (3)

Bis(2-pyridylmethyl)-amine (**BPA**) (0.39 g, 2 mmol) and 2-(pivaloylamido)-6-(bromoethyl)pyridine (0.54 g, 2 mmol) were dissolved in CH_3CN (20 ml). Then, Na_2CO_3 (0.43 g, 4 mmol) was added and the final solution was stirred for 3 hours at room temperature. After this, the solution was poured into 27 ml of 1 M NaOH (aq). The crude product was extracted with CH_2Cl_2 (3 × 100 ml) and the organic fractions

were dried over Na_2SO_4. The solvent was evaporated under vacuum to yield the pure product as a brown oil (0.66 g, 78 %).

^{1}H NMR($CDCl_3$, 200 MHz): δ_H/ppm 8.43 (d, 2H, J = 4.2 Hz), 8.00 (d, 1H, J = 8.2 Hz), 7.90 (s, 1H, NH), 7.61-7.46 (m, 5H), 7.22 (d, 1H, J = 7.8 Hz), 7.04-7.01 (m, 2H), 3.79 (s, 4H), 3.68 (s, 2H), 1.22 (s, 9H).

Synthesis of N,N-bis(2-pyridylmethyl)-N-(6-amino-2-pyridylmethyl)amine (TPA-NH_2)

N,*N*-bis(2-pyridylmethyl)-*N*-(6-pivaloylamido-2-pyridylmethyl)amine **3** (0.50 g, 1.63 mmol) was dissolved in 20 ml of 2 M HCl(aq) and the solution was heated to reflux for 24 h. After cooling, the solution was extracted with CH_2Cl_2 (3 × 20 ml).The aqueous solution was poured into 50 ml of 1 M NaOH(aq), and the product was extracted with CH_2Cl_2 (3 × 50 ml). The organic fractions were combined and dried over Na_2SO_4. The solvent was evaporated under vacuum and washed with diethyl ether to yield the product as brown oil (0.364 g, 73 %).

^{1}H NMR ($CDCl_3$, 200 MHz): δ_H/ppm 8.51 (d, 2H, J = 5.0 Hz), 7.62-7.57 (m, 4H), 7.39 (t, 1H, J = 7.6 Hz), 7.15-7.08 (m, 2H), 6.90 (d, 1H, J = 7.4 Hz), 6.36 (d, 1H, J = 8.2 Hz), 3.86 (s, 4H), 3.69 (s, 2H).
ESI-MS (+ion) calcd for $C_{18}H_{19}N_5$, m/e 305.38, found 306.17 $[M + H]^+$ (100 %).

Synthesis of N,N-bis(6-amino-2-pyridylmethyl)-N-(2-pyridylmethyl)-amine (TPA-$(NH_2)_2$)

N,*N*-bis(6-pivaloylamido-2-pyridylmethyl)-*N*-(2-pyridylmethyl)amine **4** (0.5 g, 0.85 mmol) was dissolved in 20 ml of 2 M HCl(aq) and the solution was heated to reflux for 72 h. After cooling, the solution was extracted with CH_2Cl_2 (3 × 50 ml). The aqueous solution was then poured into 50 ml of 1 M NaOH(aq) and the product was extracted with CH_2Cl_2 (3 × 50 ml). The organic fractions were dried over Na_2SO_4. The solvent was evaporated under vacuum and washed with diethyl ether to yield the product as brown oil (0.34 g, 68 %).

^{1}H NMR (D_2O, 200 MHz): δ_H/ppm 8.71 (d, 1H, J = 5.39 Hz), 8.51 (t, 1H, J = 7.8 Hz), 8.04 (d, 1H, J = 7.39 Hz), 7.89 (t, 1H, J = 6.9 Hz), 7.12 (t, 2H, J = 5.59 Hz), 6.79 (m, 4H), 4.29 (s, 2H), 3.97 (s, 4H).

Synthesis of N,N-bis(2-pyridylmethyl)ethane-1,2-diamine (PENP)

A mixture of bis(2-pyridylmethyl)amine (**BPA**) (1.01 g, 5.1 mmol) and *N*-(2-bromoethyl)-phathalimide (1.29 g, 5.1 mmol) were dissolved in 15 ml of CH_3CN. K_2CO_3 (1.55 g, 11.2 mmol) and KI (0.085 g, 0.5 mmol) were added to this solution and the mixture was heated to reflux under N_2 for one week. After this time the K_2CO_3 was filtered off and the solvent was evaporated. The brown oil product was washed with a few ml of ether. This product was dissolved in 15 ml of EtOH containing (0.15 ml, 5.1 mmol) of $N_2H_4 \cdot H_2O$, and refluxed for 3 h. After cooling, 5 ml of HCl (37 %) was added, and the mixture stirred for another hour, forming a white precipitate which was removed by filtration. The filtrate was evaporated under vacuum and the resulting residue was poured into 1 M NaOH(aq). The crude product was extracted three times with CH_2Cl_2 (3 × 20 ml). The combined organic fractions were dried over Na_2SO_4. The solvent was evaporated under vacuum to yield the product as brown oil (0.30 g, 30 %).

^{1}H NMR ($CDCl_3$, 200 MHz): δ_H/ppm 8.49 (d, 2H, J = 4.39 Hz), 7.6 (td, 2H, J = 7.79, 1.99 Hz), 7.42 (d, 2H, J = 7.79 Hz), 7.14 (td, 2H, J = 7.39, 1.39 Hz), 3.8 (s, 4H), 2.79-2.76 (m, 2H), 2.69-2.63 (m, 2H).

IR (KBr, cm^{-1}): 3389 (ν_{N-H}), 2934-2831 ($\nu_{CH, CH2}$), 1590-1435 ($\nu_{C=C, C=N}$).

Synthesis of 2,6-bis(bromomethyl)-4-nitrophenol (7)

A mixture of 8-acetoxymethyl-6-nitro-1,3-benzodioxene **6** (2.01 g, 7.9 mmol) and 48 % HBr (60 ml) was refluxed for 6 hours. The reaction mixture was then filtered at room temperature, and the resulting white solid was washed with cold water and dried to give 1.42 g (54 %).

^{1}HNMR ($CDCl_3$, 360 MHz): δ_H/ppm 8.22 (s, 2H), 6.50 (s, 1H) and 4.57 (s, 4H).

IR (KBr, cm^{-1}): 3420 (ν_{O-H}), 3071-2956 ($\nu_{CH, CH2}$), 1616 ($\nu_{C=C}$), 1594 (ν_{NO2}).

Synthesis of 2,6-bis[bis(2-pyridylmethyl)aminomethyl]-4-nitrophenol (8)

2,6-Bis(bromomethyl)-4-nitrophenol **7** (0.55 g, 1.7 mmol), bis(2-pyridylmethyl) amine (**BPA**) (0.67 g, 3.4 mmol), and anhydrous Na_2CO_3 (3 g, 34 mmol) were dissolved in dry CH_3CN (60 ml) and heated to reflux (T = 80 °C) under nitrogen for 18 hours. After this, the precipitate was filtered off and the solvent was removed under vacuum. The residue was redissolved in CH_2Cl_2 (30 ml) and extracted with 1 M NaOH(aq) (30 ml). The organic layer was separated, dried with $MgSO_4$, filtered and evaporated under vacuum. The residue was then washed with warm ether several times. The product is obtained as a brown solid (0.64 g, 67 %).

^1H NMR ($CDCl_3$, 200 MHz): δ_H/ppm 8.51 (d, 4H, J = 4.31 Hz), 8.20 (s, 2H), 7.59 (t, 4H, J = 6.59 Hz), 7.46 (d, 4H, J = 7.2 Hz), 7.13 (t, 4H, J = 5.99 Hz), 3.89 (s, 8H), 3.83 (s, 4H).

ESI-MS (+ ion) calcd for $C_{32}H_{31}N_7O_3$, m/e 561.25, found 561.94 (100 %).

Synthesis of 2,6-bis[bis(2-pyridylmethyl)aminomethyl]-4-aminophenol (BBPAP)

2,6-Bis[bis(2-pyridylmethyl)aminomethyl]-4-nitrophenol **8** (0.64 g, 1.14 mmol) and Pd/C (10 wt % on carbon) (0.26 g, 0.87 mmol) were added to dry MeOH (40 ml). The resulting mixture was left under H_2 (g) for 48 hours. After that, the Pd was filtered off and the solvent was evaporated to afford the final product (0.46 g, 77 %).

^1H NMR ($CDCl_3$, 200 MHz): δ_H/ppm 8.51 (dd, 4H, J = 3.79, 0.79 Hz), 7.60 (td, 4H, J = 7.39, 1.59 Hz), 7.45 (d, 4H, J = 7.8 Hz), 7.11 (td, 4H, J = 4.79, 1.19 Hz), 6.63 (s, 2H), 3.85 (s, 8H), 3.37 (s, 4H).

ESI-MS (+ion) calcd for $C_{32}H_{33}N_7O$, m/e 531.65, found 532.09 $[M + H]^+$ (100 %), 554.08 $[M + Na]^+$ (80 %).

IR (KBr, cm^{-1}): 3439 (ν_{O-H}), 3433 (ν_{N-H}), 2923-2853 (ν_{CH_2}).

Synthesis of 10

2-Nitrobenzylbromide (2.16 g, 10 mmol), Na_2CO_3 (1g ~ 0.01 mol) and 4-aminothiophenol (1.25 g, 10 mmol) were dissolved in CH_3CN (150 ml). This solution was stirred overnight at room temperature. The precipitate was then filtered

off, the solution collected and evaporated to give the pure product as a yellow solid (2.10 g, 80 %).

^{1}H NMR ($CDCl_3$, 200 MHz): δ_H/ppm 7.96 (d, 1H, J = 7.6 Hz), 7.36-7.30 (m, 2H), 7.05 (d, 3H, J = 7.4 Hz), 6.54 (d, 2H, J = 9.8 Hz), 4.25 (s, 2H).

Synthesis of 11

Phosgene (0.50 g, 5.09 mmol, 2.67 ml) was added to 20 ml of H_2O:$CHCl_3$ mixture (12:7) containing $CaCO_3$ (0.54 g, 0.87 mmol). The mixture was then cooled to 0 °C and a $CHCl_3$ solution (60 ml) containing **10** (0.88 g, 3.38 mmol) was added dropwise. The resulting mixture was allowed to warm at room temperature and stirred overnight. The organic phase was collected and the solvent was removed under reduced pressure to give the pure product as a yellow solid (0.86 g, 88 %).
The very small excess of phosgene (1.71 mmol) was destroyed by reaction with water to produce CO_2 and HCl.

^{1}H NMR ($CDCl_3$, 200 MHz): δ_H/ppm 7.99 (dd, 1H, J = 9.39, 1.99 Hz), 7.43 (td, 2H , J = 6.59, 1.59 Hz), 7.26-7.20 (m, 3H), 6.97 (d, 2H, J = 6.39 Hz), 4.39 (s, 2H).
IR (KBr, cm^{-1}): 2264.02 (ν_{NCO}).

Synthesis of 12

Thiophosgene (0.58 g, 5.09 mmol, 0.39 ml) was added to 20 ml of H_2O:$CHCl_3$ mixture (12:7) containing $CaCO_3$ (0.54 g, 0.87 mmol). The mixture was then cooled to 0 °C and a $CHCl_3$ solution (60 ml) containing **10** (0.88 g, 3.38 mmol) was added dropwise. The resulting mixture was allowed to warm at room temperature and stirred overnight. The organic phase was collected and the solvent was removed under reduced pressure to give the pure product as a yellow solid (0.74 g, 72 %).
The very small excess of thiophosgene (1.71 mmol) decomposes in water.

^{1}H NMR ($CDCl_3$, 200 MHz): δ_H/ppm 8.01 (d, 1H, J = 7.8 Hz), 7.47-7.28 (m, 2H), 7.27-7.22 (m, 3H), 7.08 (d, 2H, J = 8.2 Hz), 4.43 (s, 2H).
IR (KBr, cm^{-1}): 2124.21 (ν_{NCS}).

Synthesis of L1

N,*N*-bis(2-pyridylmethyl)-*N*-(6-amino-2-pyridylmethyl)amine (**TPA-NH$_2$**) (0.13 g, 0.42 mmol) and **11** (0.13 g, 0.42 mmol) and were dissolved in dry THF (6 ml). After stirring for 2 d at 50 °C the solution was cooled to room temperature and the solvent was removed.

The crude material was purified in the following way. First, 2 M HCl(aq) was added and the insoluble material extracted with CH_2Cl_2 (2 × 20 ml). The aqueous phase was neutralized with NaOH and the product extracted with CH_2Cl_2 (2 × 20 ml). This solution was dried under reduced pressure to afford the desired compound as a brown solid (0.094 g, 38 %).

^{1}H NMR ($CDCl_3$, 360 MHz): δ_H/ppm 12.1 (s, 1H), 8.99 (s, 1H), 8.51 (d, 2H, J = 4.32 Hz), 7.97 (d, 1H, J = 9.1 Hz), 7.64-7.59 (m, 4H), 7.38-7.35 (m, 2H), 7.28-7.26 (m, 2H), 7.20-7.18 (m, 3H), 7.14-7.11 (m, 2H), 6.89 (d, 2H, J = 7.39 Hz), 6.43 (d, 1H, J = 7.92 Hz), 4.43 (s, 2H), 3.87 (s, 4H), 3.74 (s, 2H).

ESI-MS (-ion) calcd for $C_{32}H_{29}N_7O_2S_2$, m/e 591.68, found 626.17 $[M + Cl]^-$ (50 %).

IR (KBr, cm^{-1}): 3314.07 (ν_{N-H}), 1697 ($\nu_{C=O}$), 1229.4 (ν_{C-O}).

Synthesis of L2

N,*N*-bis(2-pyridylmethyl)-*N*-(6-amino-2-pyridylmethyl)amine (**TPA-NH$_2$**) (0.20 g, 0.65 mmol) and **12** (0.20 g, 0.65 mmol) were dissolved in dry THF (~ 6 ml). This solution was stirred for 2 d at 50 °C, after which time, it was cooled to room temperature and the solvent was evaporated.

The crude material was purified in the following way. First, 2 M HCl(aq) was added and the insoluble material was extracted with CH_2Cl_2 (2 × 10 ml).The aqueous phase was neutralized with NaOH and the product was extracted with CH_2Cl_2 (2 × 10 ml).This solution was dried under reduced pressure to afford the desired compound as a brown solid (0.18 g, 44.8 %).

^{1}H NMR ($CDCl_3$, 360 MHz): δ_H/ppm 13.98 (s, 1H), 9.01 (s, 1H), 8.48 (d, 2H, J = 3.94 Hz), 8.00 (dd, 1H, J = 9.64, 1.3 Hz), 7.66 (d, 2H, J = 8.33 Hz), 7.65-7.61 (m, 1H), 7.54 (td, 2H, J = 9.64, 7.89 Hz), 7.46-7.41 (m, 2H), 7.38 (td, 2H, J = 9.64, 7.89

Hz), 7.31 (d, 2H, J = 8.76 Hz), 7.28 (dd, 1H, J = 9.20, 7.54 Hz), 7.22 (d, 1H, J = 7.98 Hz), 7.18-7.12 (m, 2H), 6.74 (d, 1H, J = 7.89 Hz), 4.43 (s, 2H), 3.87 (s, 4H), 3.82 (s, 2H).

^{13}C ($CDCl_3$, 90 MHz): δ_C/ppm 179.36, 159.38, 150.081, 140.65, 137.69, 134.22, 133.28, 133.01, 129.39, 126.42, 125.70, 124.09, 123.38, 119.8, 61.26, 60.46 and 38.73.

ESI-MS (-ion) calcd for $C_{32}H_{29}N_7O_2S_2$, m/e 607.7, found 642.1 $[M + Cl]^-$ (100 %).

IR (KBr, cm^{-1}): 3413 (ν_{N-H}), 2924-2854 (ν_{CH_2}), 1260 (ν_{C-N}), 1046 ($\nu_{C=S}$).

Synthesis of L3

N,*N*-bis(2-pyridylmethyl)ethane-1,2-diamine (**PENP**) (0.06 g, 0.24 mmol) and **12** (0.075 g, 0.24 mmol) were dissolved in 6 ml of dry THF. The reaction mixture was stirred overnight at 50 ^{0}C. The solvent was evaporated and the crude material was purified in the following way. First, 2 M HCl(aq) was added and an insoluble impurity was extracted with CH_2Cl_2 (2 × 10 ml).The aqueous phase was neutralized with NaOH and extraction with CH_2Cl_2 (2 × 10 ml) gave an oily residue which was subjected to column chromatography (SiO_2, MeOH/CH_2Cl_2 (5/95)) to afford the pure product as a brown solid (0.54 g, 41 %).

^1H NMR ($CDCl_3$, 360 MHz): δ_H/ppm 8.53 (br, s, 1H), 8.31 (d, 2H, J = 3.96 Hz), 8.10 (br, s, 1H), 7.96 (d, 1H, J = 7.20 Hz), 7.55-7.51 (m, 2H), 7.40-7.36 (m, 2H), 7.31-7.23 (m, 5H), 7.13-7.10 (m, 4H), 4.39 (s, 2H), 3.80 (m, 6H), 2.80 (s, 2H).

^{13}C ($CDCl_3$, 90 MHz,): δ_C/ppm 158.01, 148.86, 148.26, 136.64, 133.04, 132.73, 1 31.97, 131.81, 128.29, 125.22, 124.19, 123.92, 123.12, 122.25, 116.88, 59.41, 52.00, 42.94 and 37.43.

ESI-MS (+ ion) calcd for $C_{28}H_{28}N_6O_2S_2$, m/e 544.69, found 545.07 $[M + H]^+$ (75 %).

IR (KBr, cm^{-1}): 3252 (ν_{N-H}), 2924-2848 (ν_{CH, CH_2}), 1591-1308 ($\nu_{C=C, C=N}$), 1047 ($\nu_{C=S}$).

Synthesis of L4

N,*N*-bis(2-pyridylmethyl)-*N*-(6-amino-2-pyridylmethyl)amine (**TPA-NH_2**) (0.28 g, 0.92 mmol) was dissolved in 7 ml of CH_2Cl_2. Thioctic acid (0.19 g, 0.92 mmol) and

1,3-dicyclohexylcarbodiimide (DCC) (0.57 g, 2.76 mmol) were added to this solution. The mixture was allowed to stir for about 72 hours at 40 °C. Then, the solution was allowed to cool down to room temperature. The precipitate was removed by filtration and the filtrate was treated with 2 M HCl(aq) (10 ml) and CH_2Cl_2 (10 ml). The water layer was neutralized with 2 M NaOH(aq) and extracted with CH_2Cl_2 (20 ml). Finally, the organic phase was evaporated under vacuum to obtain the pure product as an oily brown solid (0.136 g, 30 %).

^{1}H NMR (CD_3OD, 360 MHz): δ_H/ppm 8.54 (d, 2H, J = 5.0 Hz), 7.93 (d, 1H, J = 7.9 Hz), 7.87 (t, 2H, J = 7.6 Hz), 7.73 (t, 1H, J = 7.6 Hz), 7.68 (m, 2H), 7.37 (m, 2H), 7.22 (d, 1H, J = 7.2 Hz), 4.08 (s, 4H), 3.92 (s, 2H), 3.61-3.42 (m, 1H), 3.20-3.10 (m, 2H), 2.51-2.46 (m, 3H), 1.95-1.46 (m, 7H).
^{13}C (CD_3OD, 90 MHz,): δ_C/ppm 172.8, 156.7, 155.0, 150.8, 147.5, 138.1, 137.3, 123.2, 122.4, 118.5, 112.1, 58.4, 58.4, 55.6, 39.4, 37.4, 35.8, 33.9, 27.9 and 24.4.
ESI-MS (+ ion) calcd for $C_{26}H_{31}N_5OS_2$, m/e 493.69, found 493.98 (100 %).
HR-MS calcd for $C_{26}H_{32}N_5OS_2$ ($M+H^+$) 494.204, found 494.2054.
IR (KBr, cm^{-1}): 3421 (ν_{N-H}), 2927-2850 (ν_{CH, CH_2}), 1684 ($\nu_{C=O}$), 1593-1302 ($\nu_{C=C, C=N}$).

Synthesis of L5

N,*N*-bis(6-amino-2-pyridylmethyl)-*N*-(2-pyridylmethyl)amine (**TPA-(NH_2)$_2$**) (0.2 g, 0.62 mmol) was dissolved in 7 ml of CH_2Cl_2. Then thioctic acid (0.24 g, 1.24 mmol) and DCC (0.38 g, 1.86 mmol) were added. The resulting solution was stirred and heated at 40 °C for 8 days. After that, the precipitate obtained was filtered off. The filtrate was treated with 2 M HCl(aq) (10 ml) and CH_2Cl_2 (10 ml). The aqueous phase was neutralized with NaOH(aq) and extracted with CH_2Cl_2 (3 × 10 ml). The solvent was evaporated and the product was obtained as a brown oil (0.08 g, 25.61 %).

^{1}H NMR (CD_3OD, 360.1 MHz): δ_H/ppm 9.99 (s, 1H), 8.51 (d, 1H, J = 5.04 Hz), 8.05 (d, 1H, J = 8.28 Hz), 7.74 (m, 2H), 7.59-7.52 (m, 2H), 7.21-7.16 (m, 1H), 6.98 (d, 1H, J = 9 Hz), 6.89 (d, 1H, J = 7.2 Hz), 6.68 (d, 1H, J = 6.5 Hz), 3.97 (s, 2H), 3.91 (s,

2H), 3.74 (s, 2H), 3.57-3.49 (m, 1H), 3.16-3.01 (m, 2H), 2.66-2.37 (m, 3H), 1.91-1.40 (m, 7H).

ESI-MS (+ ion) calcd for $C_{26}H_{32}N_6OS_2$, m/e 508.70, found 509.12 $[M + H]^+$ (100 %).

IR (KBr, cm^{-1}): 3394 (ν_{N-H}), 2927-2856 (ν_{CH, CH_2}), 1687 ($\nu_{C=O}$),1575-1300 ($\nu_{C=C, C=N}$).

Synthesis of L6

N,N-bis(2-pyridylmethyl)ethane-1,2-diamine (**PENP**) (0.1 g, 0.41 mmol) was dissolved in 5 ml of CH_2Cl_2. Then thioctic acid (0.085 g, 0.41 mmol) and DCC (0.17 g, 0.82 mmol) were added. The final mixture was left stirring overnight at room temperature. The precipitate was filtered off and the solvent was evaporated to obtain the desired product as a brown oil (0.17 g, 95 %).

^1H NMR (CD_3OD, 360 MHz): δ_H/ppm 8.53 (d, 2H, J = 4.32 Hz), 7.60 (td, 2H, J = 8.64, 1.8 Hz), 7.31 (d, 2H, J = 7.91 Hz), 7.15 (t, 2H, J = 6.12 Hz), 3.85 (s, 4H), 3.29 (m, 2H), 2.72 (t, 2H, J = 5.76 Hz), 3.67-3.44 (m, 1H), 3.18-3.05 (m, 2H), 2.37-2.19 (m, 3H), 1.97-1.41 (m, 7H).

ESI-MS (+ ion) calcd for $C_{22}H_{30}N_4OS_2$, m/e 430.19, found 431.29 $[M + H]^+$ (100 %).

IR (KBr, cm^{-1}): 3326 (ν_{N-H}), 2928-2850 (ν_{CH, CH_2}), 1700 ($\nu_{C=O}$), 1653-1311 ($\nu_{C=C, C=N}$).

Synthesis of L7

2,6-Bis[bis(2-pyridylmethyl)aminomethyl]-4-aminophenol (**BBPAP**) (0.465 g, 0.87 mmol) and of thioctic acid (0.18 g, 0.87 mmol) were dissolved in 20 ml of dry CH_2Cl_2. To this solution 0.541 g (2.62 mmol) of DCC was added. The solution was heated to reflux for 48 hours. After the reaction was completed, the solution was filtered and the filtrate was treated with 2 M HCl(aq) (20 ml). The water layer was neutralized with 2 M NaOH(aq) and extracted with CH_2Cl_2 (3 × 20 ml). The organic solution was dried with anhydrous $MgSO_4$. After that, CH_2Cl_2 was removed under vacuum to obtain the pure product as a brown oil (0.29 g, 46.8%).

^1H NMR ($CDCl_3$, 360 MHz): δ_H/ppm 8.52 (d, 4H, J = 4.4 Hz), 7.60 (t, 4H, J = 7.20 Hz), 7.45 (d, 4H, J = 7.56 Hz), 7.15-7.03 (m, 6H), 3.87 (s, 8H), 3.73 (s, 4H), 3.59-3.50 (m, 1H), 3.19-3.08 (m, 2H), 2.45-2.33 (m, 3H), 1.89-1.53 (m, 7H).

^{13}C NMR ($CDCl_3$, 90 MHz): δ_C/ppm 172.11, 159.43, 153.47, 149.80, 137.71, 130.73, 124.35, 124.18, 123.55, 122.67, 60.73, 57.32, 55.67, 41.23, 39.46, 38.17, 35.67, 29.91, 25.90.

ESI-MS (+ion) calcd for $C_{40}H_{45}N_7O_2S_2$, m/e 719.31, found 720.01 $[M + H]^+$ (100 %).

IR (KBr, cm^{-1}): 3443 (ν_{O-H}), 3408 (ν_{N-H}), 3010-2923 (ν_{CH, CH_2}), 1653 ($\nu_{C=O}$), 1590-1363 ($\nu_{C=C, C=N}$).

Synthesis of L8

2-[bis(2-pyridylmethyl)aminomethyl]-4-aminophenol (**BPAP**) (0.3 g, 0.93 mmol) and thioctic acid (0.19 g, 0.93 mmol) were dissolved in 7 ml of dry CH_2Cl_2. Then 0.58 g (2.79 mmol) of DCC was added. The final solution was heated to reflux for 48 hours. After the reaction was completed, the solution was filtered and the filtrate was treated with 2 M HCl(aq) (20 ml). The water layer was neutralized with 2 M NaOH(aq) and extracted with CH_2Cl_2 (3 × 20 ml). The organic solution was dried with anhydrous $MgSO_4$. After that, CH_2Cl_2 was removed under vacuum to obtain the pure product as a brown oil (0.18 g, 38.1 %).

^1H NMR (CD_3OD, 360 MHz): δ_H/ppm 8.56 (ddd, 2H, J = 5.02, 1.70, 0.86 Hz), 7.83 (td, 2H, J = 7.78, 1.78 Hz), 7.52-7.49 (m, 2H), 7.48 (d, 1H, J = 2.52 Hz), 7.35 (ddd, 2H, J = 7.51, 5.10, 1.11 Hz), 7.24 (dd, 1H, J = 8.67, 2.61 Hz), 6.79 (d, 1H, J = 8.64 Hz), 4.09 (s, 4H), 3.97 (s, 2H), 3.64-3.60 (m, 1H), 3.20-3.05 (m, 2H), 2.49-2.38 (m, 3H), 1.90 - 1.55 (m, 7H).

ESI-MS (+ion) calcd for $C_{27}H_{32}N_4O_2S_2$, m/e 508.7, found 509.11 $[M + H]^+$.

IR (KBr, cm^{-1}): 3397 (ν_{O-H}), 3244 (ν_{N-H}), 2925-2856 (ν_{CH, CH_2}), 1652 ($\nu_{C=O}$), 1593-1373 ($\nu_{C=C, C=N}$).

Synthesis of N,N-bis(2-pyridylmethyl)aminoethanethiol (L9)

Bis(2-pyridylmethyl)amine (**BPA**) (1g, 1.11 ml, 5 mmol) was dissolved in 2 ml of benzene in a schlenk flask and under nitrogen. Ethylene sulphide (0.60 g, 0.6 ml, 10 mmol) in benzene (2 ml) was slowly added dropwise under nitrogen and the resulting solution was stirred at 50 °C. After 72 hours, the solvent was removed under vacuum

and the residue obtained was washed with water several times to remove impurities. The pure product is obtained as a yellow oil (0.92 g, 70 %).

^{1}H NMR ($CDCl_3$, 200 MHz): δ_H/ppm 8.49 (dd, 2H, J = 3.79, 0.89 Hz), 7.6 (dd, 2H, J = 6.99, 1.59 Hz), 7.51 (d, 2H, J = 7.79 Hz), 7.14 (td, 2H, J = 4.79, 2.19 Hz), 3.76 (s, 4H), 2.74 (t, 2H, J = 8.19 Hz), 2.15 (t, 2H, J = 6.59 Hz).
ESI-MS (+ion) calcd for $C_{14}H_{17}N_3S$, m/e 259.11, found 259.98 (100 %).
IR (KBr, cm^{-1}): 3050-2940 (ν_{CH_2}), 1591-1435 ($\nu_{C=C, C=N}$), 1224 (ν_{C-N}).

Synthesis of di-2-(N-(2-pyridylmethyl)amino)ethyl disulfide (13)

2-(Aminomethyl)pyridine (0.5 g, 0.48 ml, 4.6 mmol) was dissolved in 2 ml of benzene in a schlenk flask under nitrogen. A solution of ethylene sulphide (0.14 g, 2.3 mmol, 0.138 µl) in benzene (2 ml) was slowly added dropwise under nitrogen. The final solution was heated to reflux until 55 ^{0}C overnight. After removal of the solvent by evaporation, the oily material was dissolved into 2 M HCl(aq) (5 ml), extracted with CH_2Cl_2 (3 × 5 ml), and dried over Mg_2SO_4. After removal of Mg_2SO_4 by filtration and evaporation of the solvent a brown oil was obtained (0.214 g, 27. 78 %).

^{1}H NMR ($CDCl_3$, 200 MHz): δ_H/ppm 8.50 (d, 2H, J = 5.6 Hz), 7.6 (t, 2H, J = 7.79 Hz), 7.27 (d, 2H, J = 6.99 Hz), 7.15 (t, 2H, J = 5.79 Hz), 3.90 (s, 4H), 2.89 (t, 4H, J = 5.61 Hz), 2.79 (t, 4H, J = 5.59 Hz).
ESI-MS (+ion) calcd for $C_{16}H_{22}N_4S_2$, m/e 334.13, found 334.85.

Synthesis of di-2-(N-(6-pivaloylamido-2-pyridylmethyl)-N-(2-pyridylmethyl)amino) ethyl disulfide (14)

Di-2-(*N*-(2-pyridylmethyl)amino)ethyl disulfide **13** (0.214 g, 0.63 mmol) was dissolved in 4 ml of CH_3CN previously distilled. 2-(pivaloylamido)-6-(bromomethyl) pyridine **2** (0.346 g, 1.28 mmol) and Na_2CO_3 (0.338 g, 3.1 mmol) were added. The resulting solution was stirred for 2 hours at room temperature. After removal of Na_2CO_3 by filtration, the CH_3CN was evaporated to obtain the product as a brown oil (0.45 g, 98.6 %).

^{1}H NMR ($CDCl_3$, 200 MHz): δ_H/ppm 8.46 (d, 2H, J = 3.79 Hz), 8.0 (m, 4H), 7.61 (t, 4H, J = 7.39 Hz), 7.5 (d, 2H, J = 7.79 Hz), 7.2 (t, 2H, J = 8.99 Hz), 7.13 (d, 2H, J = 5.79 Hz), 3.8 (s, 4H), 3.6 (s, 4H), 2.85-2.78 (m, 8H), 1.29 (s, 18H).
ESI-MS (+ion) calcd for $C_{38}H_{48}N_8O_2S_2$, m/e 712.33, found 736.82 $[M + Na]^+$ (100 %).

Synthesis of di-2-(N-(6-amino-2-pyridylmethyl)-N-(2-pyridylmethyl)amino)ethyl disulfide (L10)

Di-2-(*N*-(6-pivaloylamido-2-pyridylmethyl)-*N*-(2-pyridylmethyl)amino)ethyl disulfide **14** (0.45 g, 0.6 mmol) was dissolved in 2 M HCl(aq) (20 ml) and the solution was refluxed for 16 hours under nitrogen. After cooling, the solution was extracted with CH_2Cl_2 (3 × 20 ml). The aqueous solution was then poured into 1 M NaOH(aq) (final pH = 12). The crude product was the extracted with CH_2Cl_2 (3 × 20 ml) and the organic fractions were dried over Na_2SO_4. The solvent was evaporated under vacuum and the product is obtained as a brown oil (0.2 g, 59.97 %).

^{1}H NMR ($CDCl_3$, 200 MHz): δ_H/ppm 8.5 (d, 2H, J = 4.59 Hz), 7.66-7.55 (m, 4H), 7.27 (t, 2H, J = 7.79 Hz), 7.12 (d, 2H, J = 3.99 Hz), 6.86 (d, 2H, J = 6.9 Hz), 6.3 (d, 2H, J = 8.19 Hz), 4.54 (s, 4H), 3.82 (s, 4H), 3.63 (s, 4H), 2.88-2.79 (m, 8H).
ESI-MS (+ion) calcd for $C_{28}H_{34}N_8S_2$, m/e 546.23, found 546.87 (100 %).
IR (KBr, cm^{-1}): 3384 (ν_{N-H}), 2925-2853 (ν_{CH, CH_2}), 1595-1261 ($\nu_{C=C, C=N}$), 1096 (ν_{C-N}).

3.5 References

(1) S. Zahn and J. W. Canary, *J. Am. Chem. Soc.*, 2002, **124**, 9204.

(2) (a) K. D. Karlin, S. Kaderi and A. D. Zuberbuhler, *Acc. Chem. Res.*, 1997, **30**, 139; (b) M. Costas, M. P. Mehn, M. P. Jensen and Jr. L. Que, *Chem. Rev.*, 2004, **104**, 939.

(3) J. W. Canary and B. Gibb, *Prog. Inorg. Chem.*, 1997, **45**, 1.

(4) M. M. da Mota, J. Rodgers and S. M. Nelson, *J. Chem. Soc. A,* 1969, **13**, 2036.

(5) (a) U. Mukhopadhyay, I. Bernal, S. S. Massoud and F. A. Mautner, *Inorg. Chim. Acta,* 2004, **357**, 3673; (b) H. Zheng and L. Que, *Inorg. Chim. Acta*, 1997, **263**, 301; (c) A. Neubrand, F. Thaler, M. Körner, A. Zahl, C. D. Hubbard and R. V. Eldik, *J. Chem. Soc., Dalton Trans.*, 2002, **6**, 957.

(6) D. P. Madden, M. M. da Mota and S. M. Nelson, *J. Chem. Soc. A,* 1970, 790.

(7) (a) D. Mandom, A. Machkour, S. Goetz and R. Welter, *Inorg. Chem.,* 2002, **41**, 5364; (b) Y. Zang and L. Que, *Inorg. Chem.*, 1995, **34**, 1030; (c) H. Zheng, Y. Zang, Y. Dong, V. G. Young and L. Que, *J. Am. Chem. Soc.*, 1999, **121**, 2226; (d) D. M. Corsi, N. N. Murthy, V. G. Young and K. D. Karlin, *Inorg. Chem.*, 1999, **38**, 848; (d) S. V. Kryatov, A. Y. Nazarenko, P. D. Robinson and E. V. Rybak-Akimova, *Chem. Commun.*, 2000, **11**, 921; (e) R. Viswanathan, M. Palaniandavar, T. Balasubrama nian and T. P. Muthiah, *Inorg. Chem.,* 1998, **37**, 2943; (f) J. Kim, Y. Dong, E. Larka and L. Que, *Inorg. Chem.*, 1996, **35**, 2369.

(8) (a) M. Iti, K. Fujita, F. Chitose, T. Takeuchi, K. Yoshida and Y. Tacita, *Chem. Lett.,* 2002, **6**, 594; (b) H. Adams, N. A. Bailey, D. E. Fenton and Q. Yu He, *J. Chem. Soc., Dalton. Trans.*, 1995, **4**, 697; (c) L. Zhu, O. dos Santos, C. W. Koo, M. Rybstein, L. Pape and J. W. Canary, *Inorg. Chem.*, 2003, **42**, 7912; (d) M. Merkel, M. Pascaly, M. Wieting, M. Duda and A. Rompel, *Z. Anorg. Allg. Chem.,* 2003, **629**, 2216; (e) R. E. Norman, S. Yan, L. Que, G. Backes, J. Ling, J. Sanders-Loehr, J. H. Zhang and C. O'Connor, *J. Am. Chem. Soc.,* 1990, **112**, 1554.

(9) S. Menage, Y. Zang, M. P. Hendrich and L. Que, *J. Am. Chem. Soc.*, 1992, **114**, 7786.

(10) J. C. Mareque-Rivas, R. Prabaharan and R. T. Martin de Rosales, *Chem. Commun.*, 2004, 76.

(11) (a) S. L. Tobey and E. V. Anslyn, *Org. Lett.,* 2003, **5**, 2029; (b) S. L. Tobey, B. D. Jones and E.V. Anyslyn, *J. Am. Chem. Soc.*, 2003, **125**, 4026; (c) S. L. Tobey and E. V. Anslyn, *J. Am. Chem. Soc.*, 2003, **125**, 14807.

(12) Z. Tyeklár, R. R. Jacobson, N. Wei, N. N. Murthy, J. Zubieta and K. D. Karlin, *J. Am. Chem. Soc.,* 1993, **115**, 2677.

(13) (a) D. H. Lee, L. Q. Hatcher, M. A. Vance, A. Sarangi, A. E. Miligan, A. N. Sarjeant, C. D. Incarvito, A. Rheingold, K. O. Hodgson, B. Hedman, E. I. Solomon and K. D. Karlin, *Inorg. Chem.*, 2007, **46**, 6056; (b) H. Hayashi, K. Uozumi, S. Fujinami, S. Nagatomo, K. Shiren, H. Furutachi, M. Suzuki, A. Uehara and T. Kitagwa, *Chem. Lett.*, 2002, 416; (c) M. Suzuki, *Acc. Chem. Res.*, 2007, **40**, 609.

(14) T. Fujii, S. Yamaguchi, Y. Funahashi, T. Ozawa, T. Tosha, T. Kitagwa and H. Masuda, *Chem. Commun.*, 2006, 4428.

(15) A.Wada, M. Harata, K. Hasegawa, K. Jitsukawa, M. Masuda, M. Mukai, T. Kitagawa and H. Einaga, *Angew. Chem. Int. Ed.*, 1988, **37**, 798.

(16) G. J. P. Britovsek, J. England and A. J. P. White, *Inorg. Chem.*, 2005, **44**, 8125.

(17) B. Kabzinska, *Ann. Pharm. Fr.*, 1964, **22**, 685.

(18) J. K. Romary, J. D. Barger and J. E. Bunds, *Inorg. Chem.*, 1968, **7**, 1142.

(19) (a) J. A. R. Hartman, R. W. Vachet, W. Pearson, R. J. Wheat and J. H. Callahan, *Inorg. Chim. Acta*, 2003, **343**, 119; (b) N. Niklas, F. W. Heinemann, F. Hampel, T. Clark and R. Alsfasser, *Inorg. Chem.*, 2004, **43**, 4663.

(20) M. Yashiro, H. Kaneiwa, K. Onaka and M. Komiyama, *Dalton Trans.*, 2004, **4**, 605.

(21) M. Goto, N. Koga, Y. Ohse, Y. Kudoh, M. Kukihara, Y. Okuno and H. Kurosaki, *Inorg. Chem.*, 2004, **43**, 5120.

(22) Y. Mito-oka, S. Tsukiji, T. Hiraoka, N. Kasagi, S. Shinkai and I. Hamachi, *Tetrahedron Lett.*, 2001, **42**, 7059.

(23) (a) A. Ojida, S. Park, Y. Mito-Oka and I. Hamachi, *Tetrahedron Lett.*, 2002, **43**, 6193; (b) A. Ojida, M. Inoue, Y. Mito-Oka and I. Hamachi, *J. Am. Chem. Soc.*, 2003, **125**, 10184.

(24) A. Ojida, Y. Mito-oka, M. Inoue and I. Hamachi, *J. Am. Chem. Soc.*, 2002, **124**, 6256.

(25) M. S. Han and D. H. Kim, *Angew. Chem. Int. Ed.*, 2002, **41**, 3809.

(26) M. S. Han and D. H. Kim, *Bioorg. Med. Chem. Lett.*, 2003, **13**, 1079.

(27) R. G. Hanshaw, S. M. Hilkert, H. Jiang and B. D. Smith, *Tetrahedron Lett.*, 2004, **45**, 8721.

(28) A. Neves, M Lanzanaster, A. J. Bortoluzzi, R. A. Peralta, A. Casellato, E. E. Castellano, P. Herrald, M. J. Riley and G. Schenk, *J. Am. Chem. Soc.*, 2007, **129**, 7486.

(29) (a) S. B. Sachs, S. P. Dudek, R. P. Hsung, L. R. Sita, J. F. Smalley, M. D. Newton, S. W. Feldberg and C. E. D. Chidsey, *J. Am. Chem. Soc.*, 1997, **119**, 10563. (b) S. Creager, C. J. Yu, C. Bamdad, S. O'Conner, T. MacLean, E. Lam, Y. Chong, G. T. Olsen, J. Y. Luo, M. Gozin and J. F. Kayyem, *J. Am. Chem. Soc.*, 1999, **121**, 1059.

(30) (a) K. Weber, L. Hockett and S. Creager, *J. Phys. Chem. B*, 1997, **101**, 8286; (b) H. O. Finklea and D. D. Hanhew, *J. Am. Chem. Soc.*, 1992, **114**, 3173.

(31) (a) D. Vuillaume and S. Lenfant, *Microelectronic Engineering*, 2003, **70**, 539; (b) N. J. Tao, *Nature Nanotechnology*, 2006, **1**, 173.

(32) (a) M. Dijksma, B. A. Boukamp, B. Kamp and W. P. Bennekom, *Langmuir*, 2002, **18**, 3105; (b) Y. Dong, S. Abaci and C. Shannon, *Langmuir*, 2003, **19**, 8922.

(33) T. M. Willey, A. L. Vance, C. Bostedt, T. van Buuren, R. W. Meulenberg, L. J. Terminello and C. S. Fadley, *Langmuir*, 2004, **20**, 4939.

(34) (a) Y. Miura, S. Kimura, Y. Imanishi and J. Umemura, *Langmuir*, 1998, **14**, 6935; (b) Y. Dong and C. Shannon, *Anal. Chem.*, 2000, **72**, 2371.

(35) S. Zhang, A. Palkar and L. Echegoyen, *Langmuir*, 2006, **22**, 10732.

(36) S. Zhang, F. Song and L. Echegoyen, *Eur. J. Org. Chem.*, 2004, 2936.

(37) S. Zhang and L. Echegoyen, *J. Am. Chem. Soc.*, 2005, **127**, 2006.

(38) R. Karamanska, B. Mukhopadhyay, D. A. Russell and R. A. Field, *Chem. Commun.*, 2005, 3334.

(39) X. Ji, B. Jin, J. Jin and T. Nakamura, *J. Electro. Chem.*, 2006, **590**, 173.

(40) X. Ji, J. Ren, J. Jin and T. Nakamura, *Biosensors and Bioelectronics*, 2007, **23**, 241.

(41) M. Harata, K. Hasegawa, L. Jitsukawa, H. Masuda and H. Einaga, *Bull. Chem. Soc. Jpn.*, 1998, **71**, 1031.

(42) E. Szajna, M. Makowska-Grzyska, C. C. Wasde, A. M. Arif and L. M. Berreau, *Inorg. Chem.,* 2005, **44**, 7595.

(43) O. Horner, E. Anxolabehere-Mallart, M. F. Charlot, L. Tchertanov, J. Guilhem, A. T. Mattioli, A. Boussac and J. Girerd, *Inorg. Chem.,* 1999, **38**, 1222.

(44) J. De Mendoza, P. M. Nieto, P. Prados and C. Sànchez, *Tetrahedron*, 1990, **46**, 671.

(45) Y. Nishida, H. Shimo and S. Kida, *J. Chem. Soc., Chem. Commun.*, 1984, 1611.

(46) N. Lazarova, J. Babich, J. Valliant, P. Scaffer, S. James and J. Zubieta, *Inorg. Chem.*, 2005, **44**, 6763.

(47) U. Brand and H. Vahrenkamp, *Inorg. Chem.*, 1995, **34**, 3285.

Chapter 4

Metal mediated transport of electrons across SAMs

4.1 Introduction

Recent studies have shown that the incorporation of metal binding units and metals with desired electrical, magnetic, optical, molecular recognition and catalytic properties into SAMs of thiols on gold can be exploited for the development of sensors,[1] catalysts[2] and molecular electronics.[3] The incorporation of redox active units is important because it allows electrochemistry to be applied to control and study the properties of the SAM.[4] Fundamental to this diverse chemistry is the ability to regulate the transport of electrons through the molecular film. Although recent reports have suggested that metal(s) can facilitate electron transfer, the extent to which this occurs and the mechanism(s) involved are unclear.

In a recent study aimed at the formation of highly ordered films by non-covalent interactions, McGimpsey et al. studied the electron-transfer process through pyridine-capped decanethiol SAMs by cyclic voltammetry (CV) and electrochemical impedance studies (EIS) (Figure 4.1).[5] The conductivity values were measured in aqueous solutions containing $[Fe(CN)_6]^{3-/4-}$ and they found that the ligand modified electrode blocks the electron-transfer (ET) process to these redox active species, indicating the formation of an insulating monolayer with few defects. However, unexpectedly after the monolayer was exposed to a solution of Cu(II) ions, the CV of the film showed similar behaviour to that of bare gold with only a small decrease in peak current. The authors attributed this to Cu(II) ions promoting tunneling of electrons between the gold surface and the solution, but they did not give an explanation for why and how.

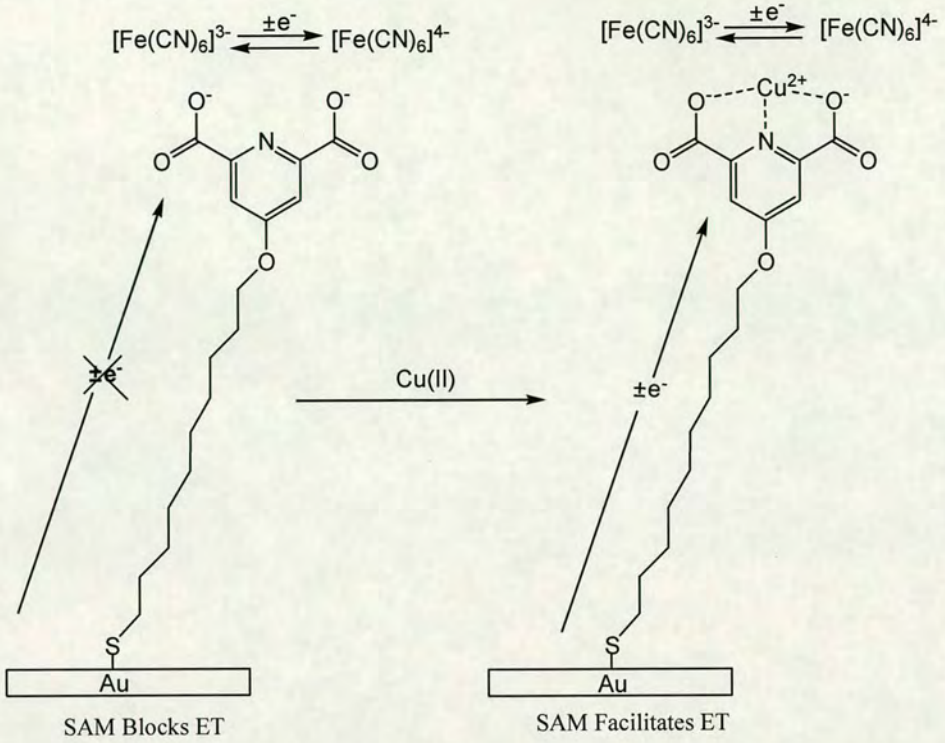

Figure 4.1: Structures of the films where SAM-Ligand blocks electron transfer and SAM-Cu complex facilitates electron-transfer.[5]

Shortly after this report, Lu et al. studied the mechanism of the electron transport through self-assembled monolayers of porphyrins (Figure 4.2), including the influence that the inclusion of metal centre ions had on the electron transport.[6] Based on these studies they proposed for first time a potential mechanism by which metals can facilitate the electron-transfer process through SAMs (Figure 4.3).

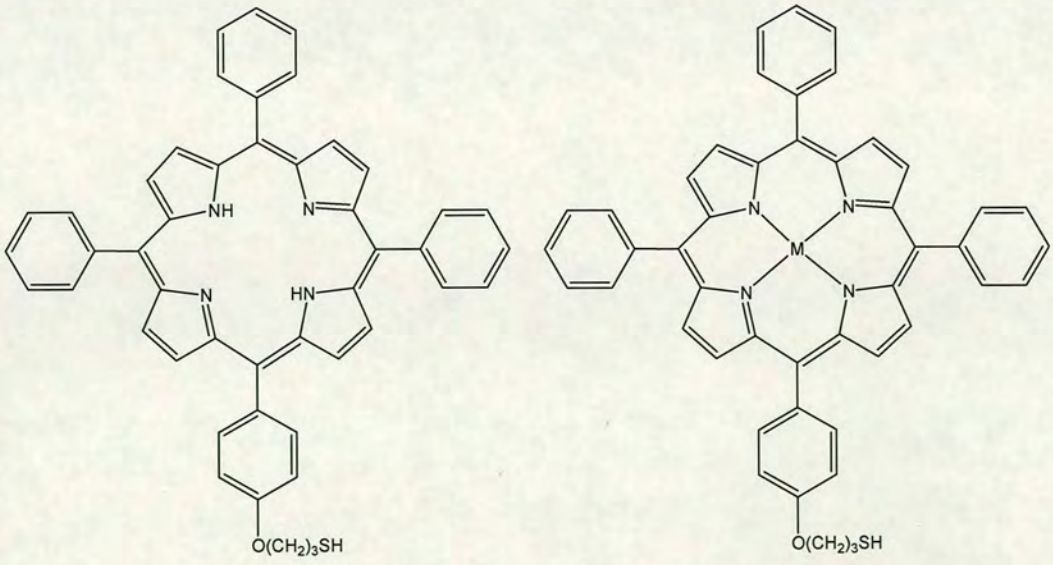

Figure 4.2: Molecular structure of SH-TPP and SH-MTPP.[6]

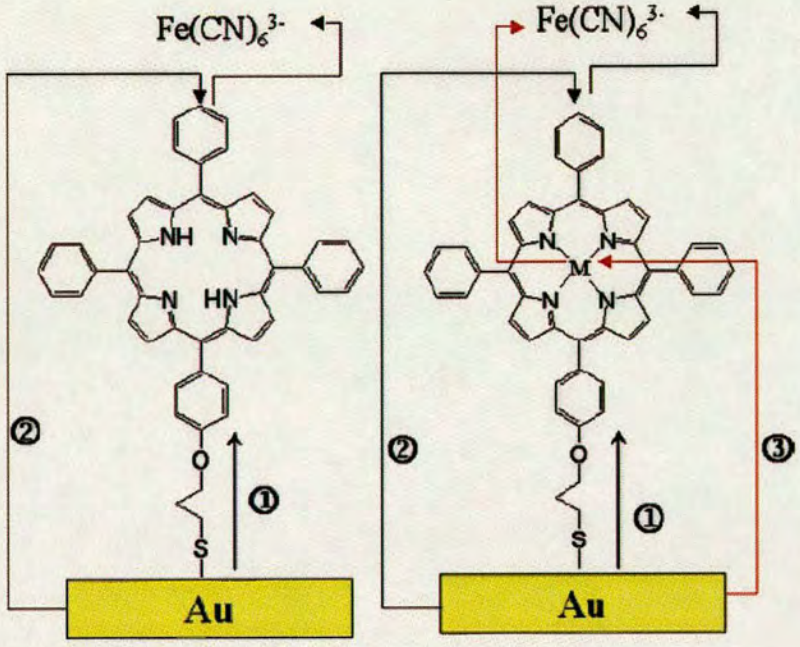

Figure 4.3: Electron-transfer processes of SAMs of SH-TPP and SH-MTPP.

In the absence of metal ions there are two possibilities:

(1) From the Au electrode tunnel through the alkyl bridge, then through the macrocycle ring and finally to the $[Fe(CN)_6]^{3-/4-}$. (2) From the Au electrode to the surface of the SAM directly and then to $[Fe(CN)_6]^{3-/4-}$.

With the insertion of metallic ions into the porphyrin ligand, electron transport through the SAM of SH-MTPP has a new possibility. (3) From the Au electrode to the metallic ion and then transfer to $[Fe(CN)_6]^{3-/4-}$.

Also recently, Masuda et al. have reported how modified electrodes with optically active (R/S) Co(III) complexes containing amino acids derivatives (phenylalanine) can promote the electron transfer process and molecular recognition between an electrode and cytochrome c (Figure 4.4).[7]

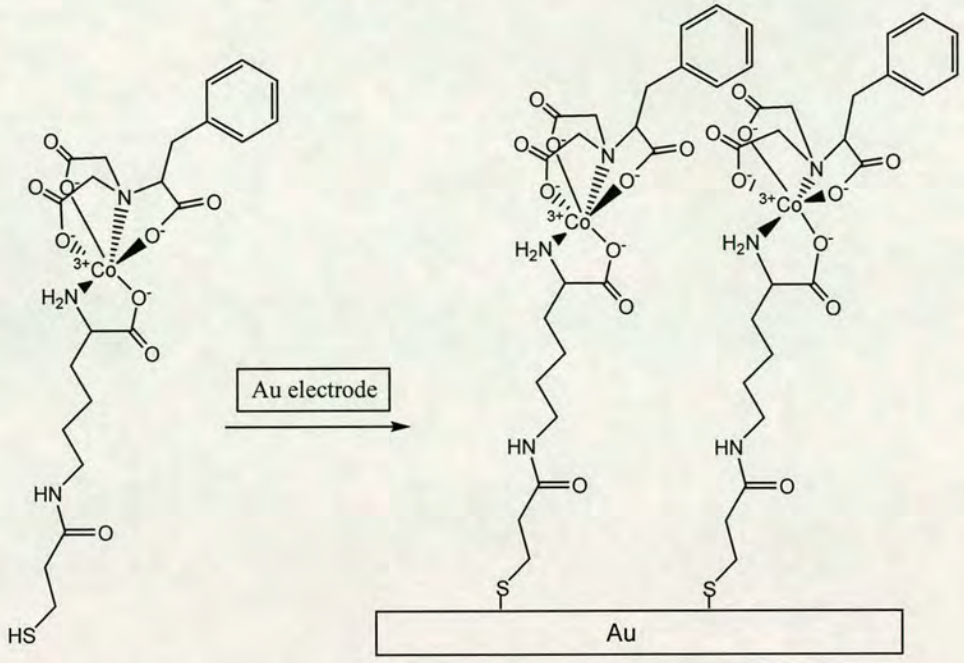

Figure 4.4: Schematic view of Co(III) complex and its modified Au electrodes.[7]

The electrochemical studies indicated that SAM-Co complex promoted the electron-transfer between cytochrome c and the Au electrode and also the redox reaction of cytochrome c. Different peak separation (ΔE_p) was obtained depending on the chirality (R or S) of the Co(III) of the SAM, indicating that cytochrome c recognized the difference in the chirality of Co(III) complexes.

They proposed that the electron-transfer process of the system could follow: (i) positively charged cytochrome c approaches the negatively charged Co(III) units on the gold electrode surface through electrostatic interactions; (ii) adsorbed cytochrome c rotates on the surface and forms the association state and (iii) the electron-transfer reaction occurs between cytochrome c and the electrode. The second process is the rate determining step of the electron-transfer between modified gold electrode and cytochrome c. The difference in the chirality of the Co(III) unit (that is the configuration of the phenylalanine) affected the interaction with the heme group of cytochrome c.

These examples show the influence of metals on the electron-transfer process through SAMs and the importance of using electrochemical techniques in order to carry out these investigations and to develop new devices.

In this chapter we describe the preparation of gold electrodes modified with self-assembled monolayers of the ligands synthesised in this thesis. The electron-transfer process of the SAM modified electrodes in the presence and absence of metals is investigated using cyclic voltammetry (CV) and electrochemical impedance spectroscopy (EIS).

These studies are complemented with surface characterization of the SAMs using X-ray photoelectron spectroscopy (XPS) and polarization-modulation reflection absorption infrared spectroscopy (PM-RAIRS).

4.2 Results and discussion: SAMs characterization

The studies are focused on two polypyridine ligands and their metal complexes shown in Figure 4.5.

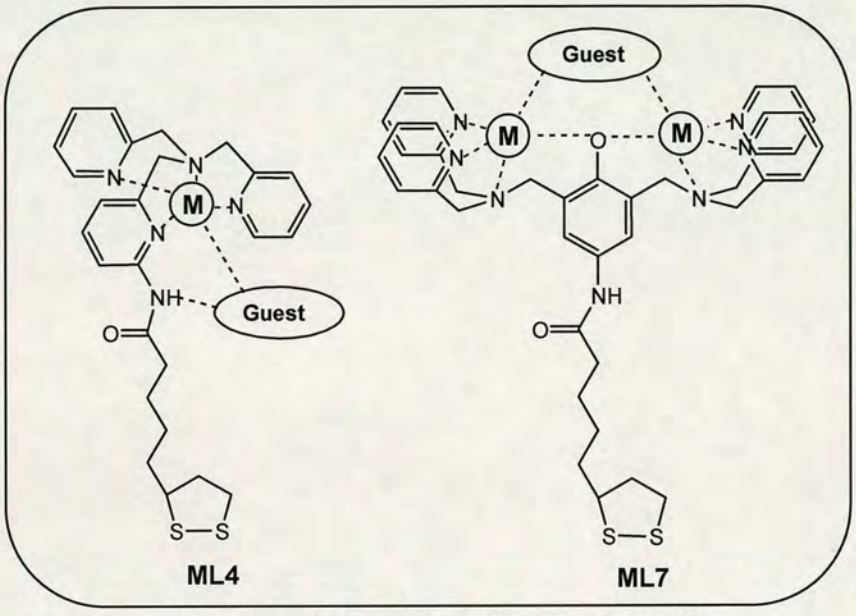

Figure 4.5: Metal complexes of the ligands studied.

The selection of these two ligands was done on the basis of the two different structures of their metal binding site. Both of them are based on tripodal ligands with interesting catalytic and anion recognition properties in solution. The metals coordinated to **L4** ligand will not be exposed to the surface of the monolayer, whereas **L7** is a dinuclear ligand which will expose the metals to the surface of the SAM. These differences should lead to different properties and electrochemical behaviour. Moreover, **L4** offers also the possibility of forming hydrogen bond interactions with possible guest molecules.

The electron-transfer properties studied by cyclic voltammetry (CV) have been carried out in 1 mM $[Fe(CN)_6]^{4-}$ aqueous solution with 0.1 M NaCl as the supporting electrolyte and at a potential scan rate of 0.1 V/s. The impedance studies were performed in equal concentrations of $[Fe(CN)_6]^{3-/4-}$ (1 or 10 mM) and with 0.1 or 1 M of NaCl as a supporting electrolyte.

4.2.1 Characterization of SAM-L4 and SAM-ML4

4.2.1.1 L4 characterization: NMR and IR studies

^{1}H NMR and IR studies were performed to characterize **L4** and its metal complexes. Figure 4.6 shows relevant sections of the ^{1}H NMR spectrum of **L4** and Zn**L4** in CD_3CN.

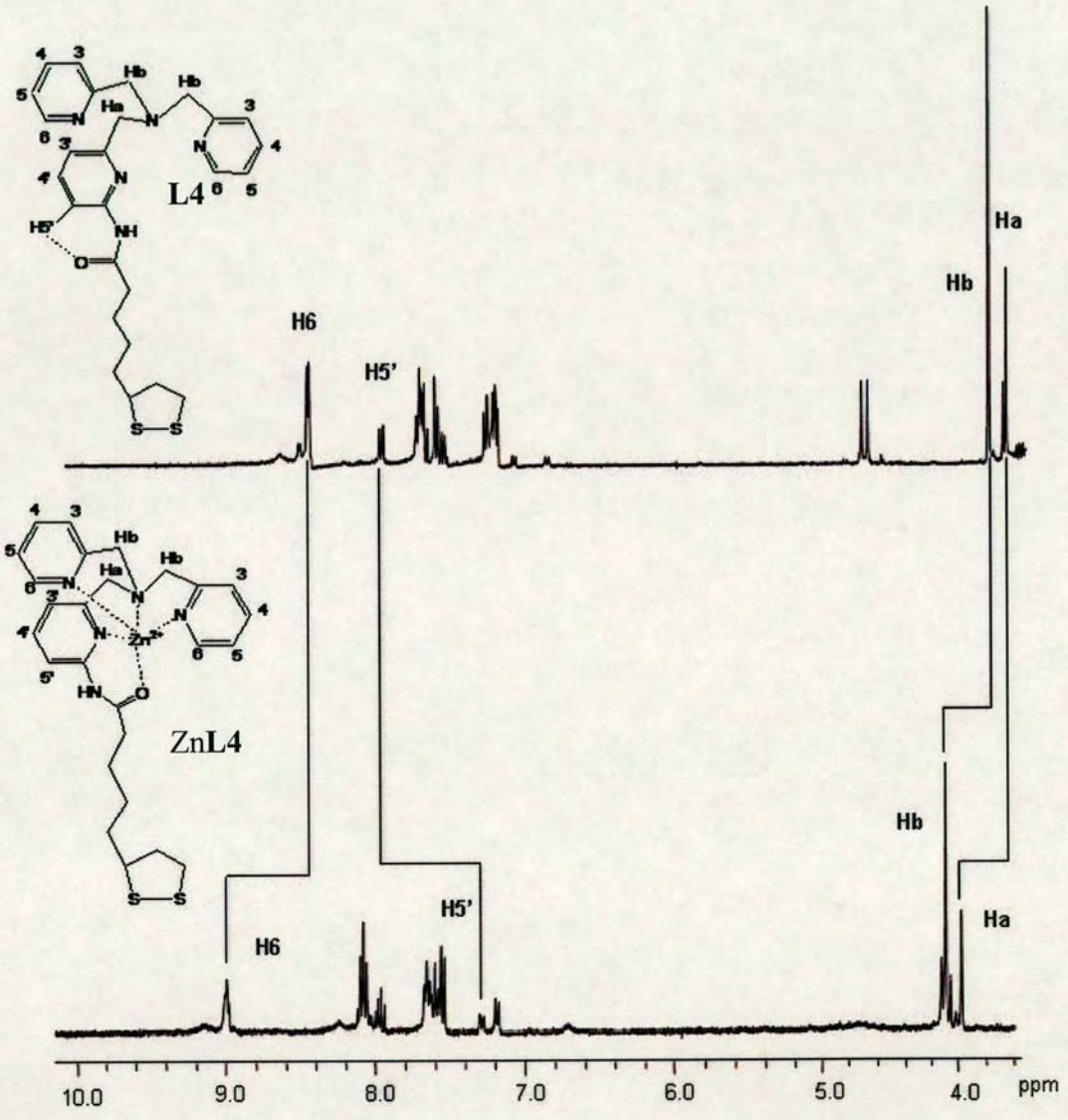

Figure 4.6: Aromatic and $PyCH_2N$ regions of the ^{1}H NMR spectrum (360.1 MHz, CD_3CN, 293 K) of **L4** (top) and Zn**L4** (bottom). See Table 1 for chemical shift values.

2D NMR ^{1}H-^{1}H COSY and ROESY spectra were obtained to assign peaks (e.g. Figure 4.7).

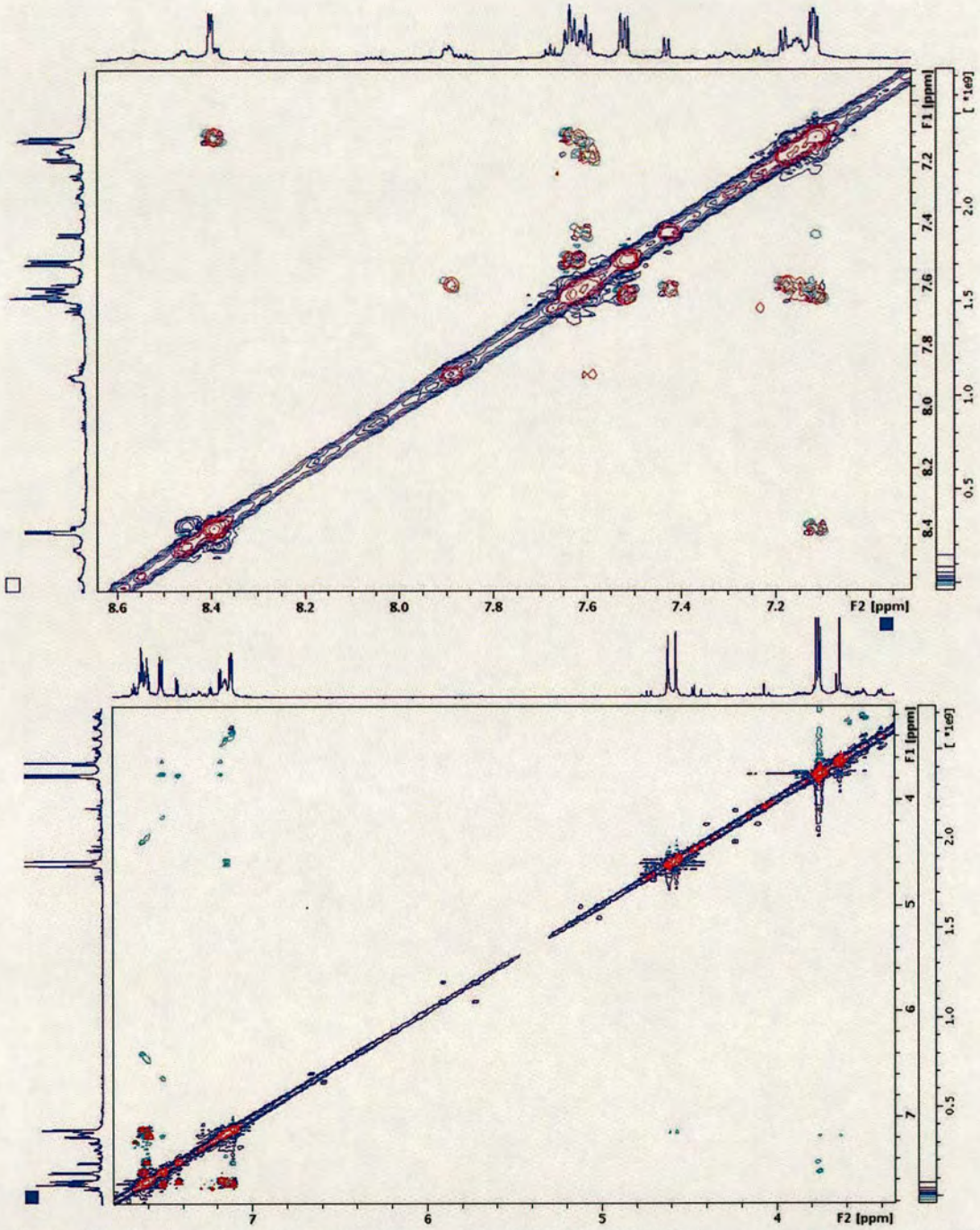

Figure 4.7: Sections (aromatic and $PyCH_2N$) of the 800 MHz ROESY (in green and blue) and COSY (in red) of **L4** in CD_3CN at 293 K.

Table 1: Summary of ^{1}H NMR (360 MHz, CD_3CN, 293K) chemical shift data for **L4** and Zn**L4**.

	L4	Zn**L4**
Py-CH_2N		
Hb	3.72	4.19 (+ 0.47)
Ha	3.64	4.08 (+ 0.44)
Py(aromatic)		
H3'	7.24	7.18 (+ 0.04)
H4'	7.60	8.05 (+ 0.45)
H5'	7.84	7.28 (-0.56)
H3	7.60	7.62 (+ 0.02)
H4	7.65	7.99 (+ 0.34)
H5	7.19	7.67 (+ 0.48)
H6	8.47	8.98 (+ 0.51)

Chemical shifts are in ppm relative to CD_3CN at 1.94 ppm. Values in parentheses denote chemical shifts downfield (positive) or upfield (negative) *versus* values in previous column.

The ^{1}H NMR spectrum of **L4** reveals a downfield shift of the H5' resonance due to the C-H5'···O=C interaction, as previously observed for related ligands.[8] In the ^{1}H NMR spectrum of Zn**L4** most proton resonances are downfield shifted relative to in **L4**, which is consistent with metal binding. A notable exception, however, is the shift by 0.56 ppm upfield of H5' (Figure 4.6, Table 1). This upfield proton chemical shift is consistent with breaking the C-H5'···O=C interaction, suggesting the possibility of forming a Zn···O=C bond, which would result from the rotation of the molecule.

IR studies of **L4** and Zn**L4** are in agreement with the conclusions derived from ^{1}H NMR studies. The IR spectra of Zn**L4** shows a ν(C=O) band shifted to lower wavenumbers by 41 cm^{-1} which may be due to the amide coordination (Table 2). In the case of Fe**L4** and Cu**L4** complexes, similar wavenumber values for ν(C=O) were obtained compared to **L4**, indicating that probably in this case the amide does not coordinate to the metal. This conclusion can not be corroborated by ^{1}H NMR because Fe**L4** and Cu**L4** are paramagnetic molecules.

The ν(N-H) band of M**L4** complexes does not shift when compared with the value of **L4**, suggesting that either no Cl^- molecules are coordinated to the complex or that if they are coordinated there is not N-H···Cl-Zn hydrogen bonding formed.

Table 2: Selected infrared vibrational data of **L4** and M**L4**.

	ν(N-H) cm^{-1}	ν(C=O) cm^{-1}
L4	3421	1684
ZnL4	3483	1643
CuL4	3452	1695
FeL4	3442	1695

The identity of these compounds was also confirmed by EIS-MS (see experimental section).

4.2.1.2 SAMs formation

SAMs of **L4** and M**L4** (M = Fe, Cu, Zn) were prepared in two different ways (Figure 4.8). In one method, SAMs were obtained by dipping the gold electrode into methanol solutions (10 mM) of **L4** for 4 days, having the disulfide unit as a gold linkage. In the other method, $NaBH_4$ was added as a reducing agent in order to cleave the disulfide bond to form the thiolate linkage, which has more affinity to gold. $NaBH_4$ was added under N_2 atmosphere to 10 mM methanol solutions of **L4** and allowing the molecular film to be formed on the gold electrode overnight. Films of the metal complexes were prepared in the same way, following the reaction of equimolar amounts of MCl_2 [M(II) = Cu, Zn and Fe] with **L4** in methanol (10 mM) for 1 h to yield $[M(\mathbf{L4})Cl]^+$.

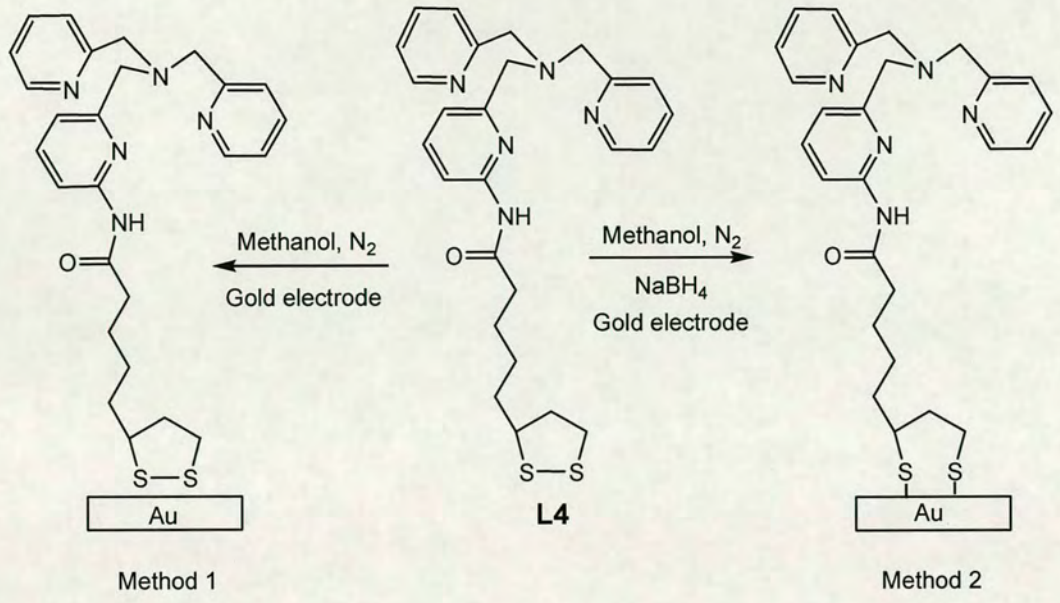

Figure 4.8: Scheme of the methods used for the formation of SAM-**L4**.

Figure 4.9 shows the carbons and the protons of **L4** affected after the $NaBH_4$ addition.

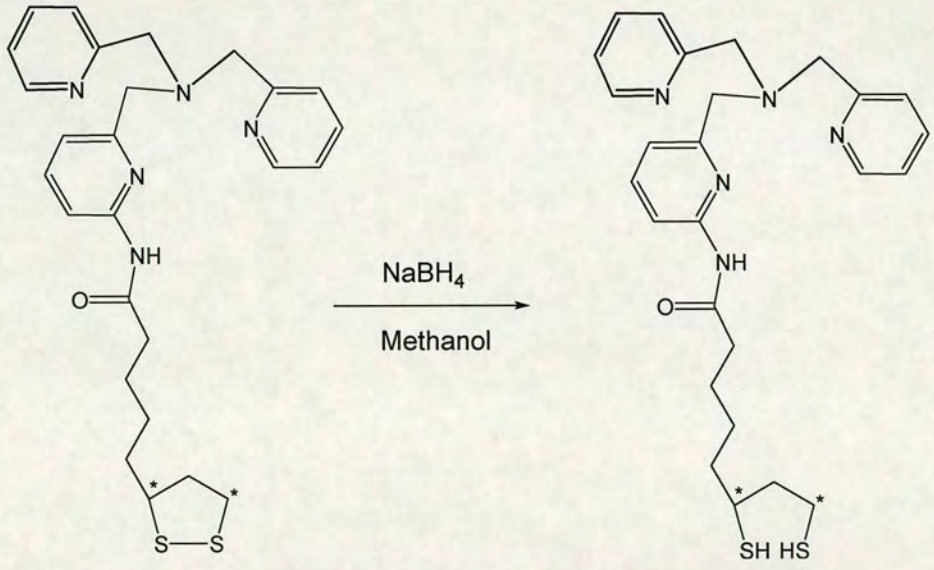

Figure 4.9: Methyl groups of **L4** affected after adding $NaBH_4$.

The disulfide cleaving reaction was monitored by NMR (CD_3OD), showing clean conversion to the dithiolate in less than 30 min (Figure 4.10 and 4.11). Over longer time (e.g. overnight), a small amount of disulphide **L4** is reformed.

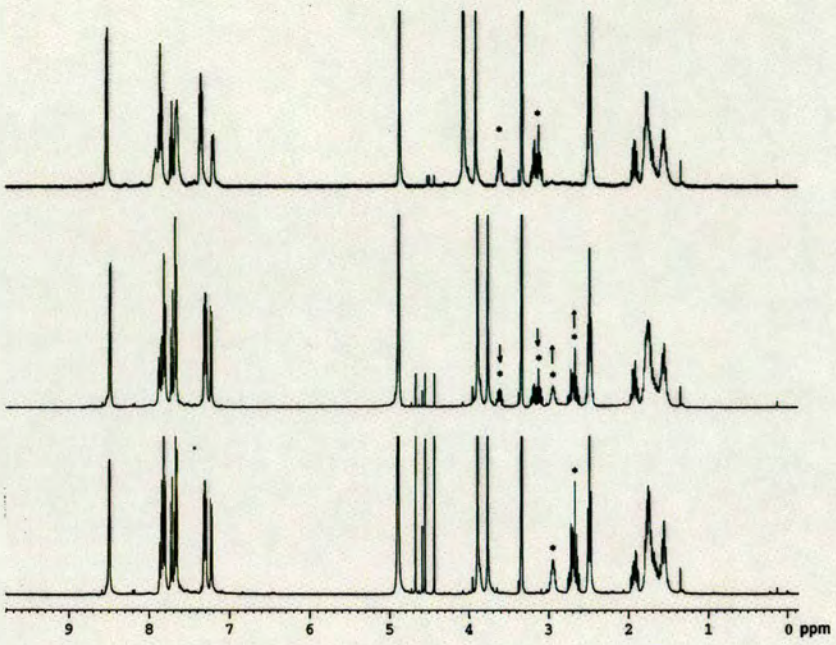

Figure 4.10: ^{1}HNMR spectrum of disulphide **L4** in CD_3OD (top) and its progressive conversion to dithiolate **L4** by reduction with $NaBH_4$ (middle and bottom).

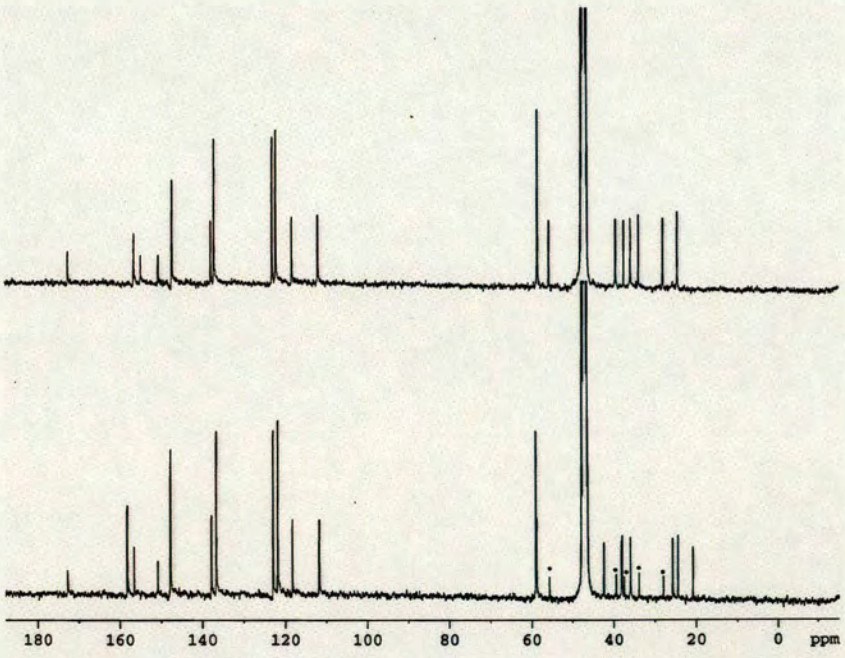

Figure 4.11: ^{13}CNMR spectrum of disulphide **L4** in CD_3OD (top) and after reduction with $NaBH_4$ (bottom, *indicates starting disulphide)

4.2.1.3 Surface characterization of SAM-L4 and SAM-ML4

Monolayers of **L4** and M**L4** complexes have been analysed using *X-ray photoelectron spectroscopy (XPS)* and by *polarization-modulation reflection absorption infrared spectroscopy (PM-RAIRS)* in order to characterize the surface composition.

Characterization using X-ray photoelectron spectroscopy (XPS)

The XPS spectra of the film formed by **L4** having disulphide as a gold linkage (Figure 4.12) shows peaks due to S, C, N and O, confirming the formation of the molecular films on the gold surface. The binding energies of 532.91 eV and 399.71 eV were used to probe the O 1s and N 1s core level regions, respectively. The S 2p peak at 163.91 eV is indicative of Au-S linkages, whereas the feature at 285.31 eV is characteristic of C 1s.

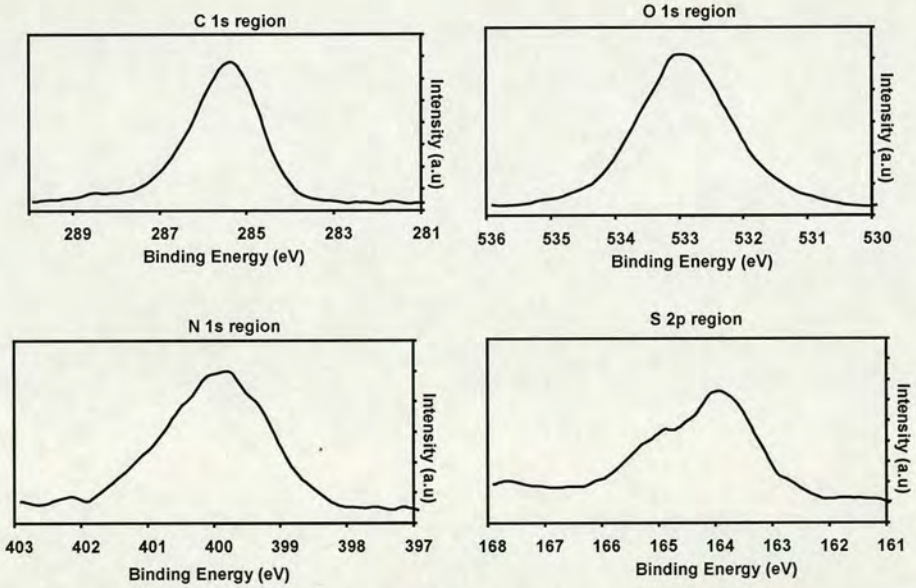

Figure 4.12: Carbon 1s, Oxygen 1s, Nitrogen 1s and Sulphur 2p X-ray photoelectron spectra of the film **L4** with disulphide linkages on Au.

The metal complexes showed in addition, peaks due to the metal and Cl^- (at 198 eV) (Figure 4.13 and 4.14), except in the case of Fe complex for which the Cl^- peaks is not observed or is very weak (Figure 4.15). For the Cu**L4** film, the peak at 932.9 eV (Cu $2p_{3/2}$) is indicative of the presence of Cu(II) centres.[9] The presence of Zn is confirmed by the peaks at 1022.91 eV and 1045.9 eV and the Fe by peaks at 710 eV

and 724 eV. The S 2p spectra of Zn and Fe**L4** complexes show an additional peak around 168 eV due to oxygenated sulphur.[10]

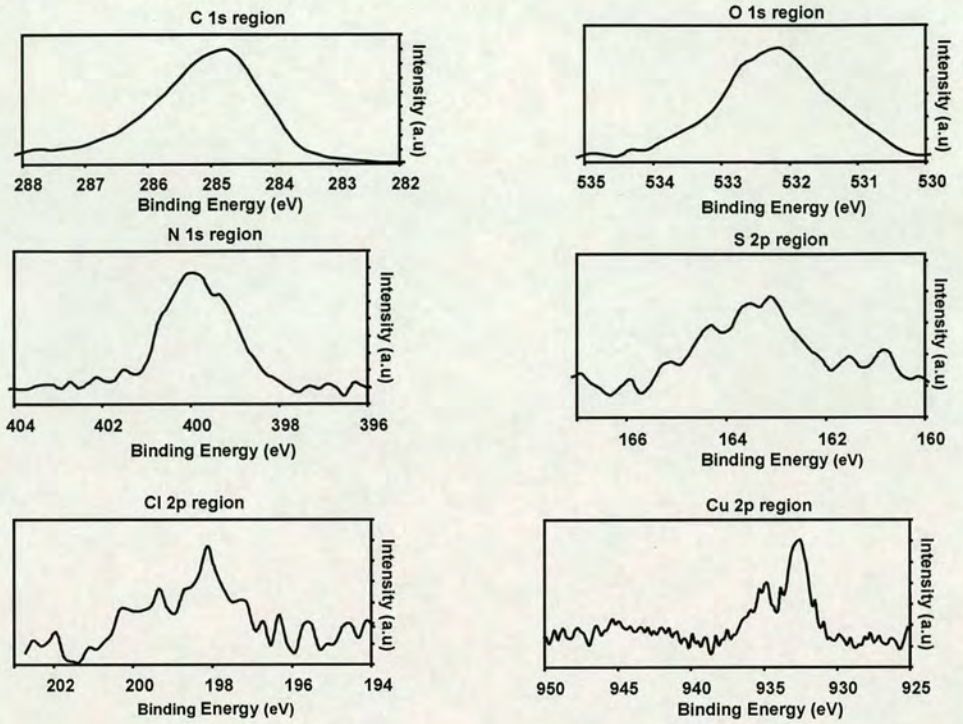

Figure 4.13: Carbon 1s, Oxygen 1s, Nitrogen 1s, Sulphur 2p, Chlorine 2p and Copper 2p X-ray photoelectron spectra of the film Cu**L4** with disulphides linkages on Au.

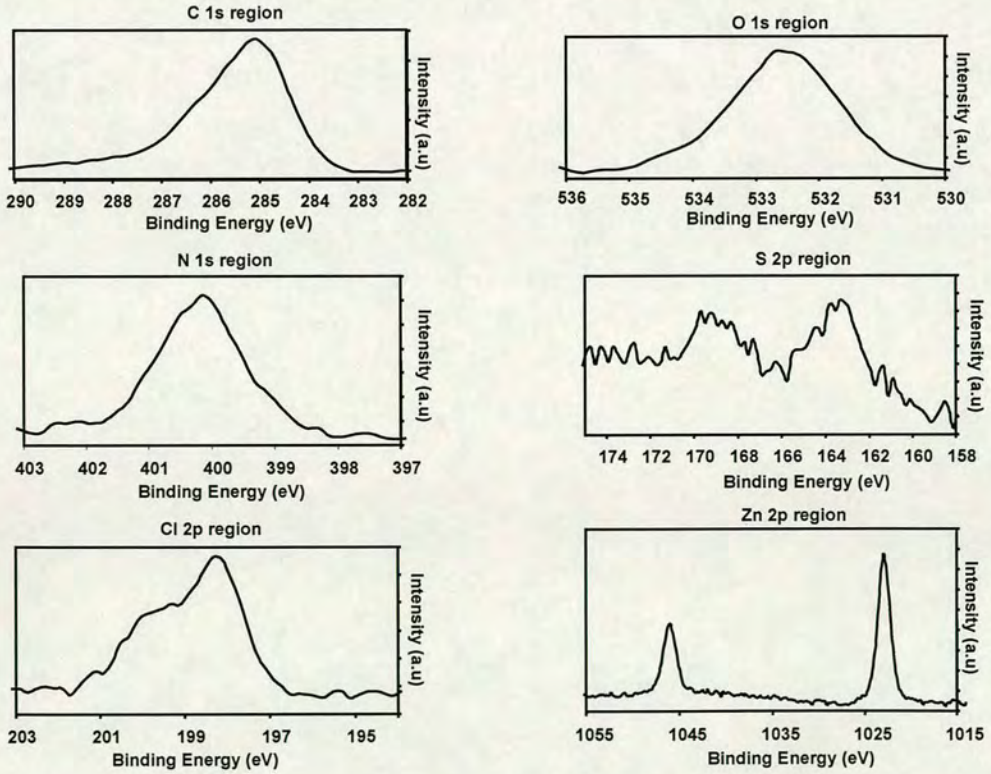

Figure 4.14: Carbon 1s, Oxygen 1s, Nitrogen 1s, Sulphur 2p, Chlorine 2p and Zinc 2p X-ray photoelectron spectra of the film Zn**L4** with disulphides linkages on Au.

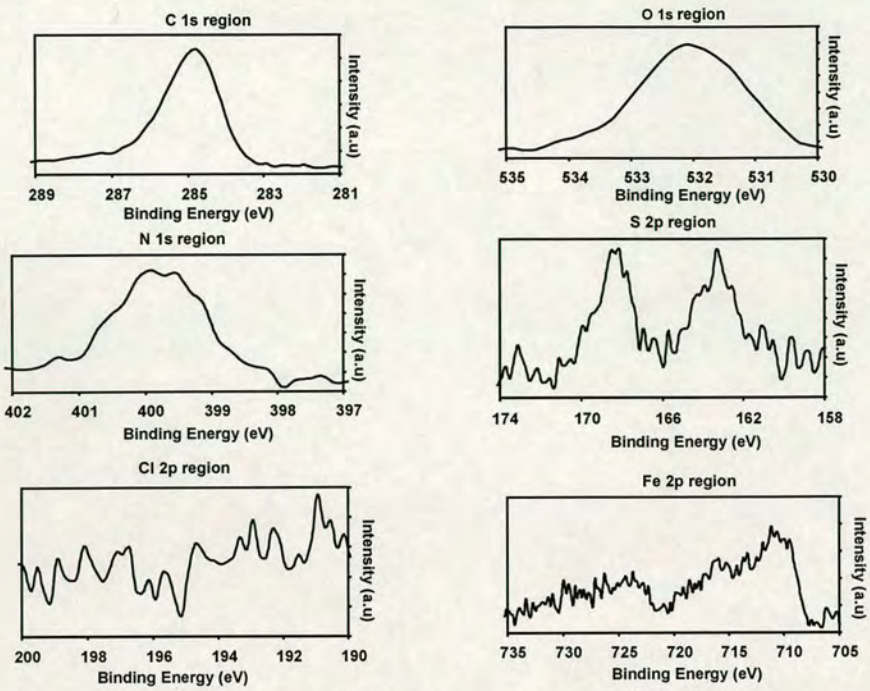

Figure 4.15: Carbon 1s, Oxygen 1s, Nitrogen 1s, Sulphur 2p, Chlorine 2p and Iron 2p X-ray photoelectron spectra of the film Fe**L4** with disulphides linkages on Au.

The XPS spectra of the film formed by **L4** having thiolate linkages (Figure 4.16) shows peaks due to S, C, N and O, confirming the formation of the molecular films on the gold surface. The binding energies of 531 eV and 399 eV were used to probe the O 1s and N 1s core level regions, respectively. The S 2p peak at 162.2 eV is indicative of Au–S bond, while in the C 1s spectrum, the peak at 284.5 eV indicated the existence of C.

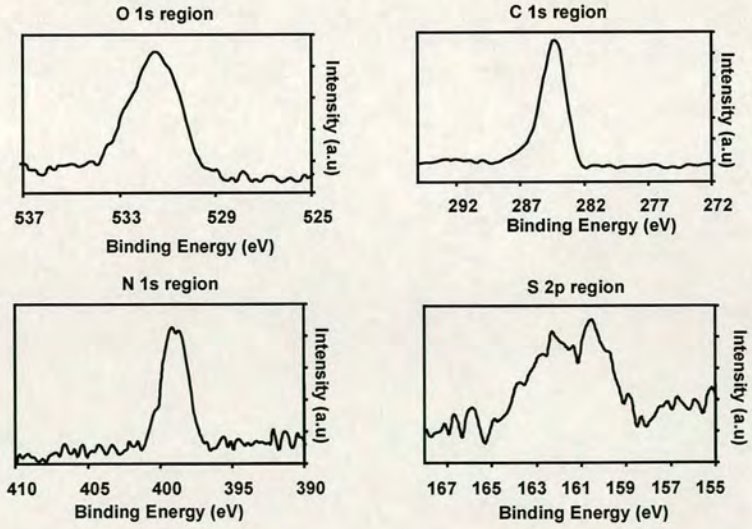

Figure 4.16: Carbon 1s, Oxygen 1s, Nitrogen 1s and Sulphur 2p X-ray photoelectron spectra of the film **L4** with dithiolate linkage on Au.

The metal complexes showed peaks due to the different metals and Cl^- (at 198 eV) (Figures 4.17, 4.18 and 4.19). For Cu**L4** film, the peaks at 932.5 eV (Cu $2p_{3/2}$) and 952.3 eV (Cu $2p_{1/2}$) are characteristic of Cu(I) centres.[9] The presence of Zn is confirmed by peaks at 1022.91 eV and 1045.9 eV. The peaks due to Fe appear at 711.11 eV and 725 eV. The sulphur peak obtained for SAM-Fe**L4** appears around 168 eV, attributed to sulfonate species (SO_3^{2-}) formed due to the oxidation in air.[10]

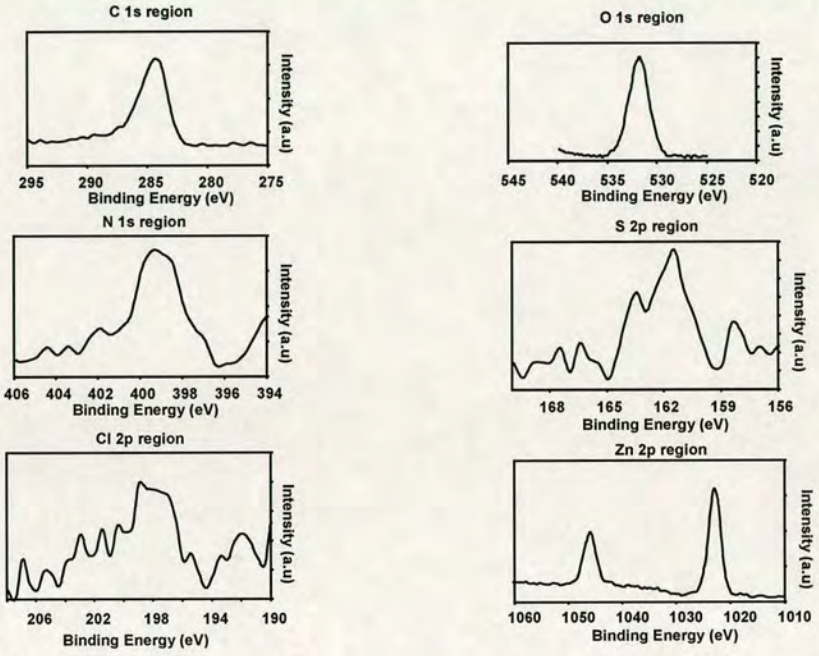

Figure 4.17: Carbon 1s, Oxygen 1s, Nitrogen 1s, Sulphur 2p, Chlorine 2p and Zinc 2p X-ray photoelectron spectra of the film Zn**L4** with dithiolate linkage on Au.

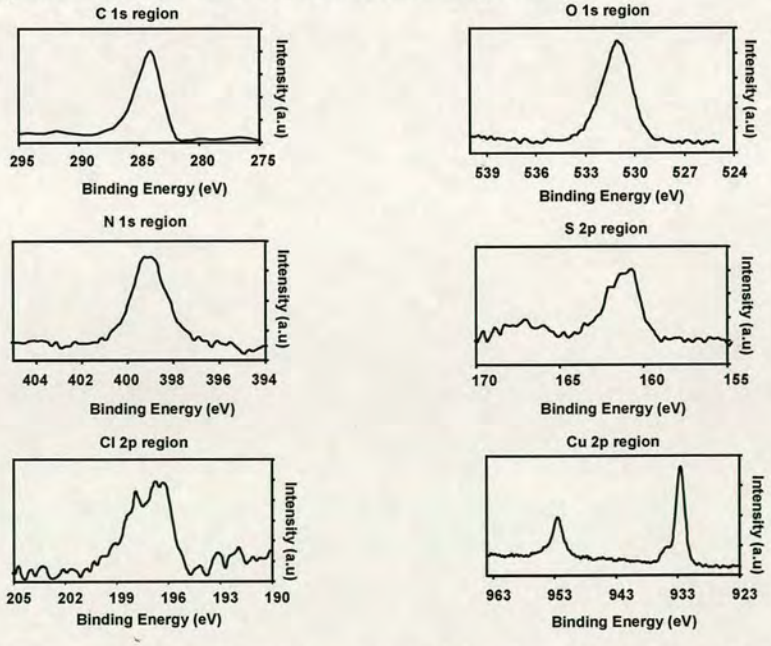

Figure 4.18: Carbon 1s, Oxygen 1s, Nitrogen 1s, Sulphur 2p, Chlorine 2p and Copper 2p X-ray photoelectron spectra of the film Cu**L4** with dithiolate linkage on Au.

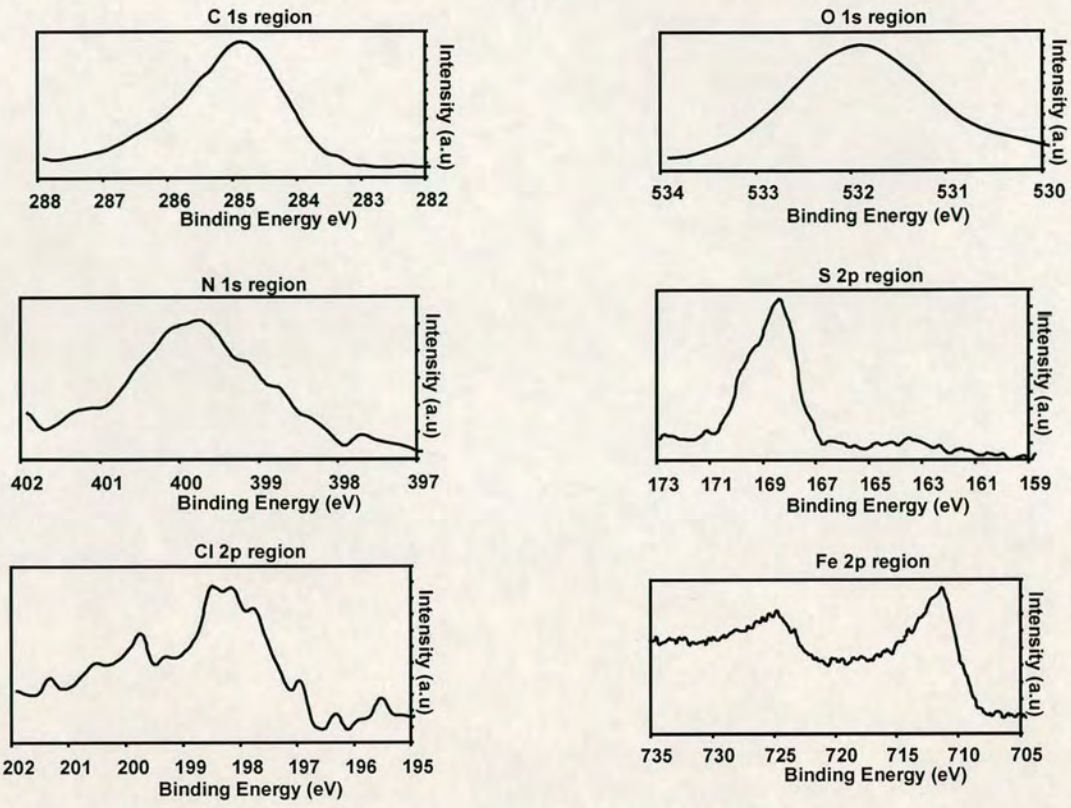

Figure 4.19: Carbon 1s, Oxygen 1s, Nitrogen 1s, Sulphur 2p, Chlorine 2p and Iron 2p X-ray photoelectron spectra of the film Fe**L4** with dithiolate linkage on Au.

Polarization-modulation reflection absorption infrared spectroscopy (PM-RAIRS) characterization

PM-RAIRS can be used also to obtain information about the structure of molecules adsorbed on solid surfaces as well as their bonding character compared to the bulk solid material. It provides further prove that the gold surface has been chemically modified.

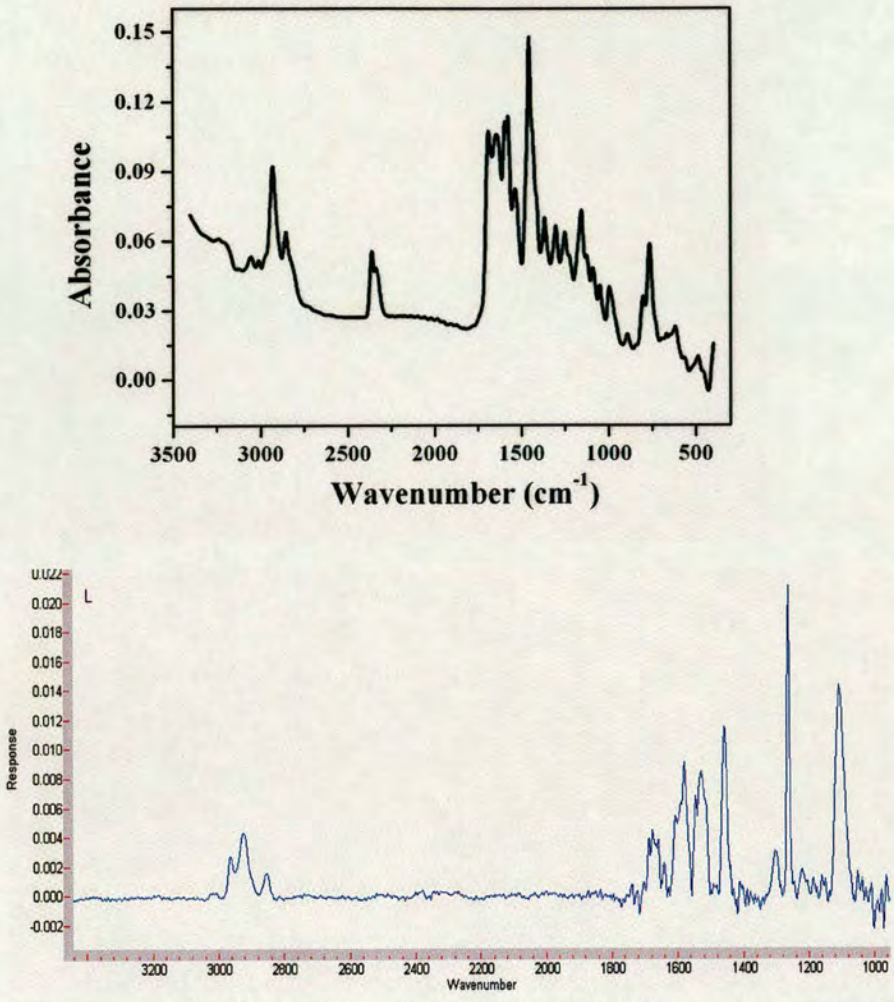

Figure 4.20: FTIR spectrum of bulk **L4** (KBr pellet) (top) and PM-RAIRS spectrum of the SAM of **L4** on gold surface (bottom).

For example, the FTIR spectrum of bulk **L4** (Figure 4.20 top) shows the bands due to CH and CH_2 stretching which appear in the 2800-3100 cm^{-1} frequency range, whereas those due to pyridine ring stretching (C-C and C-N) appear in the 1300-1600 cm^{-1} frequency range. The amide band, which results from the C=O stretching vibration of the amide group coupled to the bending of the N-H bond and the stretching of the C-N bond is centered around 1600-1700 cm^{-1}. By comparing this spectrum with the PM-RAIRS spectrum of the SAM of **L4** (Figure 4.20 bottom) on gold surface it can be seen that the bands are similar, which confirms the formation of the SAMs and that the nature of the complexes is similar (Figure 4.21).

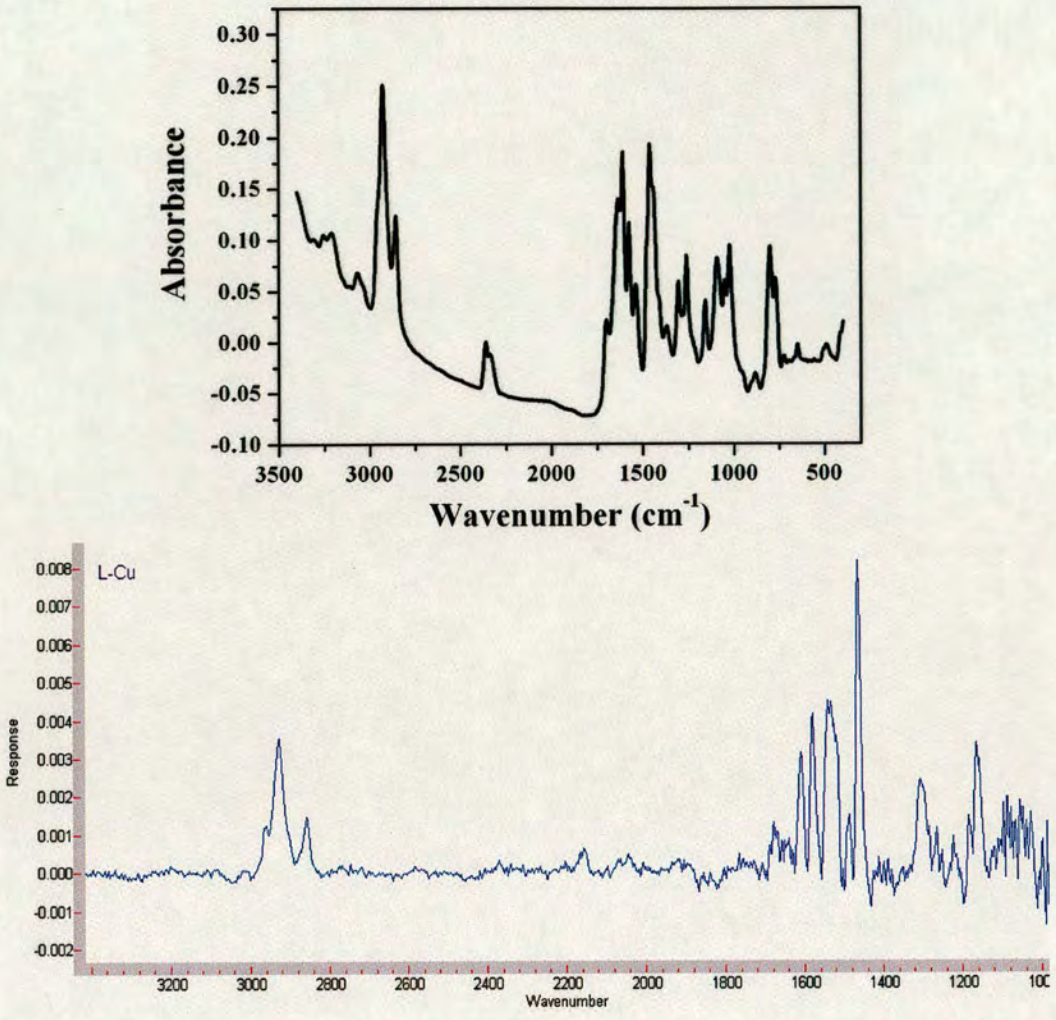

Figure 4.21: FTIR spectrum of bulk Cu**L4** (KBr pellet) (top) and PM-RAIRS spectrum of the SAM-Cu**L4** on gold surface (bottom).

4.2.1.4 Electrochemical characterization of SAM-L4 and SAM-ML4

The formation and barrier properties of the SAMs on the $[Fe(CN)_6]^{3-/4-}$ redox couple ($E_{1/2}$ = 0.20 V vs. SCE) were evaluated by *cyclic voltammetry (CV)* and *electrochemical impedance spectroscopy (EIS)*.

Cyclic voltammetry (CV) studies

The CVs were carried out in water in the presence of 1 mM $[Fe(CN)_6]^{4-}$, with 0.1 M NaCl as the supporting electrolyte.

Figure 4.22 displays the cyclic voltammogram of SAM-**L4** and SAM-M**L4** having the disulfide group as an anchor linkage.

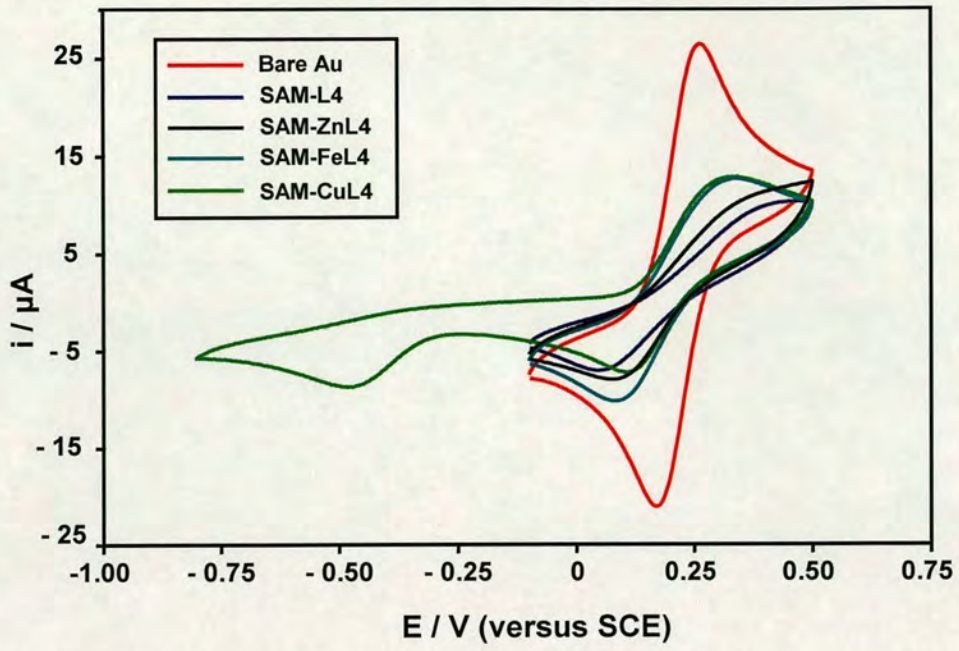

Figure 4.22: CVs of 1 mM $[Fe(CN)_6]^{4-}$ in 0.1 M NaCl at a bare gold (red) or monolayer-modified gold electrodes with **L4** (blue), Zn**L4** (black), Cu**L4** (green) and Fe**L4** (dark green) with disulphides linkages on gold. Scan rate 0.1 V s^{-1}, $T = 293$ K.

The CV of the SAM-**L4** modified electrode exhibits a redox wave due to the $[Fe(CN)_6]^{3-/4-}$ redox couple with a large peak to peak separation (Figure 4.22, blue). Such a behaviour is due to a monolayer with relatively poor blocking properties to the redox species. In the case of Zn**L4** the electron-transfer is enhanced but less than with the Cu**L4** and Fe**L4** films. Cu**L4** shows an irreversible peak at negative potential which is attributed to the dioxygen reduction as its current decreases by degassing extensively the solution with N_2. These results suggest that Cu, Zn and Fe complexes facilitate the electron-transfer reactions.

The electron-transport ability of these films formed using the thiolates was also investigated (Figure 4.23).

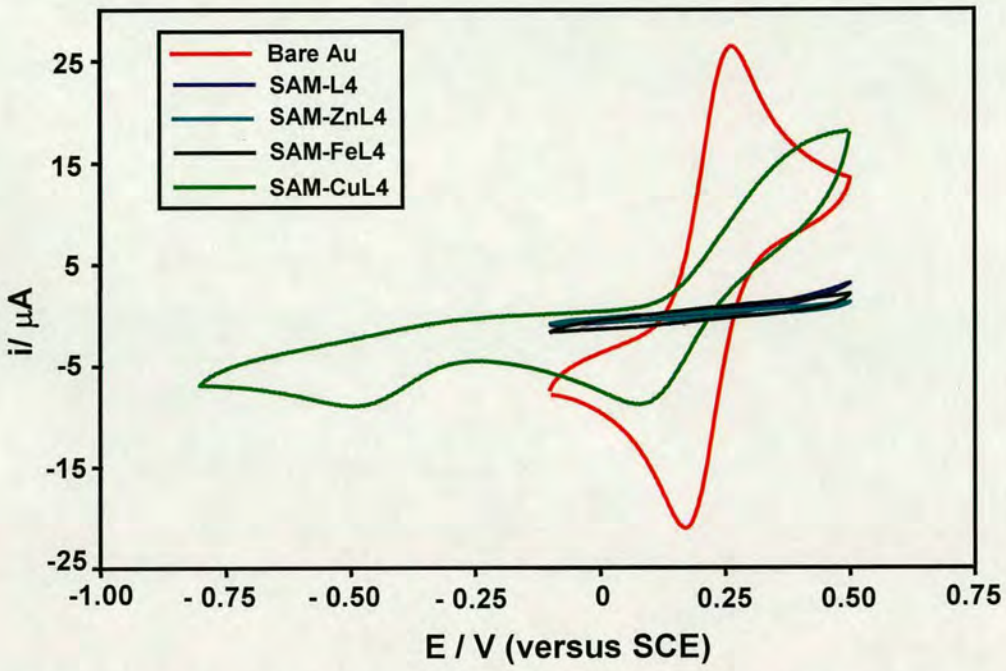

Figure 4.23: CVs of 1 mM $[Fe(CN)_6]^{4-}$ in 0.1 M NaCl at a bare gold (red) or monolayer-modified gold electrodes with **L4** (blue), Zn**L4** (light blue), Cu**L4** (green) and Fe**L4** (black) with dithiolates linkages on gold. Scan rate 0.1 V s^{-1}, T = 293 K.

In this case, for **L4** films the electron-transfer reaction to $[Fe(CN)_6]^{3-/4-}$ is completely blocked as shown in the Figure 4.23. A complete absence of the redox current reveals that a densely packed monolayer is formed on gold surface. This is most likely due to the dithiolate groups forming stronger Au-S bonds and this leading to the formation of a better monolayer. In the case of Cu**L4** we observe high electron-transfer ability to the redox couple and again the reduction peak at negative potentials was attributed to oxygen reduction. Fe**L4** and Zn**L4** monolayers produce a small increase in current indicating that these films facilitate electron-transfer to a much lesser extent. These results suggest that the metal-containing films facilitate electron transfer to the redox probe and that the magnitude of this effect is greater for those containing redox-active metals.

Electrochemical impedance spectroscopy (EIS) studies

EIS was employed to investigate the extent to which electron-transfer is facilitated. The impedance measurements were performed in the presence of 10 mM $[Fe(CN)_6]^{3-/4-}$ mixture, as the redox probe. The impedance plots (Nyquist) for bare,

SAM-**L4** and SAM-M**L4** modified Au electrodes containing disulphide linkages are shown in Figure 4.24.

The diameter of the semicircle is a measure of the charge transfer resistance across the SAMs, R_{ct}, and can be used to evaluate the rate of electron-transfer to the solution containing the redox probe.[11]

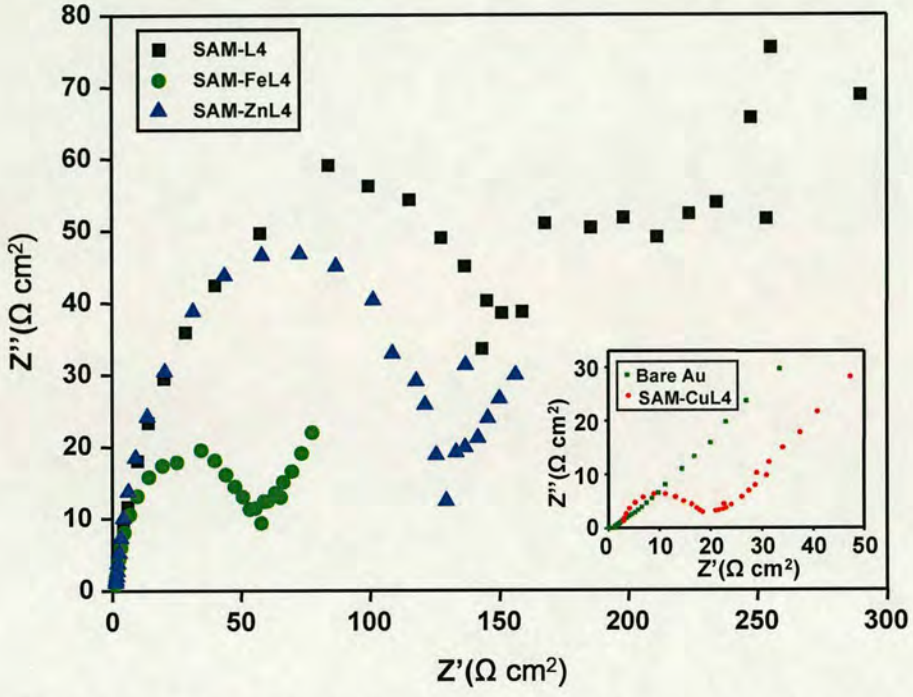

Figure 4.24: Impedance plots in 10 mM $[Fe(CN)_6]^{3-/4-}$ and 1 M NaCl at a bare (green squares) or monolayer modified gold with **L4** (black squares), Zn**L4** (blue triangles), Fe**L4** (green circles) and Cu**L4** (red circles) with disulphides linkages on gold, $T = 293$ K.

The Nyquist plot of bare gold can be described as a semicircle near the origin at high frequencies followed by a linear tail with a slope of unity, indicating that the electron-transfer process of the redox couple is essentially diffusion controlled. In contrast, the impedance plot of **L4** SAM-modified gold electrode shows the behaviour of a strongly blocking monolayer with the formation of a semicircle in the entire range of frequencies used for this study. This implies a blocking behaviour and a complete charge transfer controlled electron-transfer process.

The Zn**L4** complex has less blocking effect than SAM-**L4**, which is even less for SAM-Fe**L4**. For SAM-Cu**L4** we observe a very poor blocking ability indicating the enhancement in the electron-transfer from the gold electrode to the redox probe.

These results are in agreement with the results obtained using cyclic voltammetry. The R_{ct} values obtained from the impedance plots are listed in Table 3.

Using the R_{ct} values obtained from the impedance plots, we have calculated the apparent rate constant values (k_{app}) of $[Fe(CN)_6]^{3-/4-}$ for the SAM-modified electrodes (or real k_0 for bare gold) using equation (1), where R is the gas constant, T is the temperature, F is Faraday's constant and C is the concentration of the redox probe.

$$k_0 \text{ or } k_{app} = RT/[F^2R_{ct}C] \quad (1)$$

The k_{app} and k_0 values obtained for different monolayers and bare gold are also collected in Table 3.

Table 3: Charge transfer resistance (R_{ct}) and rate constants (k_0 and k_{app}) for bare and monolayer-modified gold electrodes obtained from EIS.

Sample	$R_{ct}(\Omega\ cm^2)$ $Fe(CN)_6^{3-}/Fe(CN)_6^{4-}$	Rate of electron-transfer k_0 and k_{app} (cm/s)
Bare gold	1.35	0.1970
SAM -L4	162.6	1.61×10^{-3}
SAM -ZnL4	134.3	1.95×10^{-3}
SAM-CuL4	17.14	1.52×10^{-2}
SAM-FeL4	62.8	4.12×10^{-3}

The blocking behaviour of these SAMs was improved when these were prepared by adding $NaBH_4$ as a disulfide reducing agent, except for SAM-Cu**L4** which gave essentially the same result (Figure 4.25).

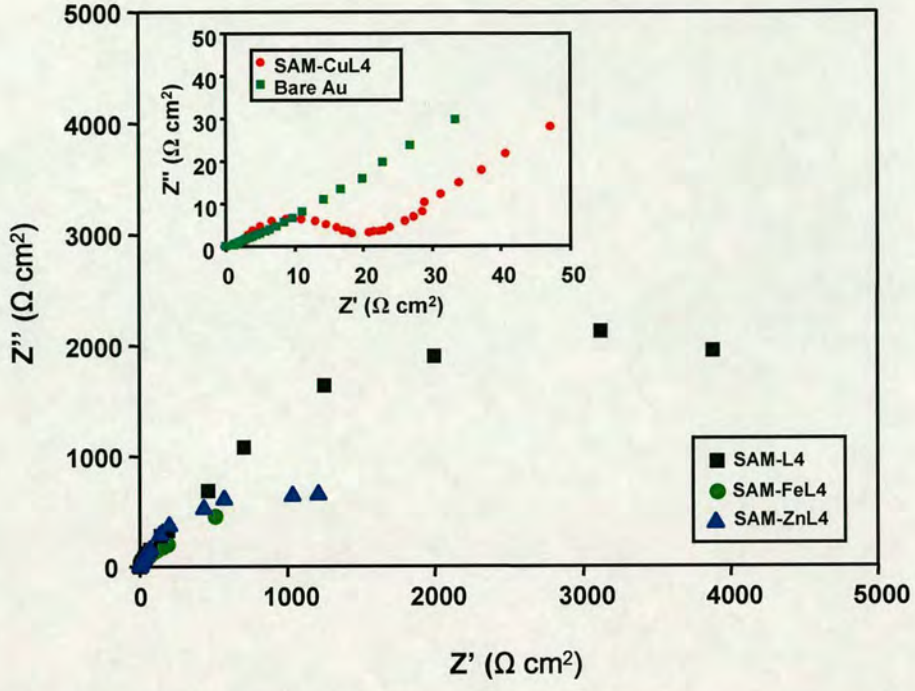

Figure 4.25: Impedance plots in 10 mM $[Fe(CN)_6]^{3-/4-}$ and 1 M NaCl at a bare (green squares) or monolayer modified gold with **L4** (black squares), Zn**L4** (blue triangles), Fe**L4** (green circles) and Cu**L4** (red circles) with dithiolates linkages on gold, $T = 293$ K.

The R_{ct} values obtained for the monolayer modified gold electrodes are shown in Table 4. For comparison, the R_{ct} values for the monolayer of decanethiol and thiophenol were also provided. As before, the apparent rate constant values (k_{app} or real, k_0, for bare gold) of $[Fe(CN)_6]^{3-/4-}$ for the SAM-modified electrodes were calculated using R_{ct} values (Table 4).

Table 4: Charge transfer resistance (R_{ct}) and rate constants (k_0 and k_{app}) for bare and monolayer-modified gold electrodes obtained from EIS.

Sample	R_{ct}(Ω cm^2) $Fe(CN)_6^{3-}/Fe(CN)_6^{4-}$	Rate of electron-transfer k_0 and k_{app}(cm/s)
Bare gold	1.35	0.1970
Decanethiol	1.70×10^3	1.54×10^{-4}
Thiophenol	440	5.95×10^{-4}
SAM-L4	6.75×10^3	3.87×10^{-5}
SAM-ZnL4	1.73×10^3	1.51×10^{-4}
SAM-CuL4	9.42	2.78×10^{-2}
SAM-FeL4	186.2	1.40×10^{-3}

Decanethiol monolayers separate the gold surface from the probe by ten saturated bonds and **L4** by at least eleven bonds (saturated and unsaturated), leading to apparent rate constants of 1.54×10^{-4} and 3.87×10^{-5} cm/s, respectively. Remarkably, for monolayers of Cu**L4**, k_{app} is 2.78×10^{-2} cm/s, much faster than across the shorter, unsaturated bridge provided by thiophenol ($k_{app} = 5.95 \times 10^{-4}$ cm/s). Thus, although Zn(II) and Fe(II) ions seem to facilitate electron transfer to the probe, redox-active Cu(II) ions are remarkably more effective.

The trend is the same like that of using disulfide linkages i.e. the blocking ability follows the order: **L4** > Zn**L4** > Fe**L4** > Cu**L4**. The magnitude of the effect, however, is greater using thiolates.

From the R_{ct} values, we have calculated the surface coverage (θ) of the monolayer on the gold electrode using equation 2.[12]

$$\theta = 1 - (R_{ct}/ R'_{ct}) \quad (2)$$

Where R_{ct} is the charge transfer resistance of bare gold electrode and R'_{ct} is the charge transfer resistance of the corresponding SAM-modified electrodes. It is assumed that the current is due to the presence of pinholes and defects within the monolayer.

Based on this method we have determined the surface coverage of the monolayers of **L4** (Table 5).

Table 5: % surface coverage for SAM-**L4** and SAM-M**L4** (M = Zn, Cu, Fe)

Sample	% Coverage SAM disulphide attachment	% Coverage SAM dithiol attachment
SAM-L4	99.16	99.98
SAM-ZnL4	98.99	99.92
SAM-CuL4	92.12	85.66
SAM-FeL4	97.85	99.27

The surface coverage of the SAMs formed by the disulfide ligands and complexes is less than by dithiol groups. Repulsive interactions between the metallated headgroups may explain the lower surface coverage of the SAMs of the preformed metal complexes.

The surface coverage (θ) values were also determined from gold oxide formation/stripping studies.[13] The cyclic voltammogram of the gold electrode in 0.1 M $HClO_4$ shows the usual features due to gold oxide formation during the positive potential scanning and oxide stripping upon reversal of the scan direction (Figure 4.26).

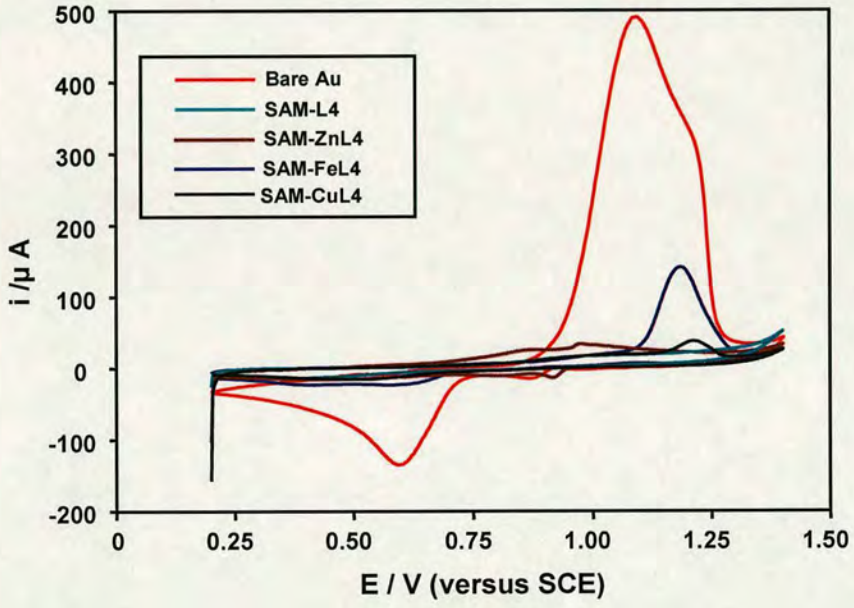

Figure 4.26: CV of the bare and monolayer modified gold electrodes with SAM-**L4** and SAM-M**L4** dithiol attachment in 0.1 M $HClO_4$. Scan rate 0.1 V s^{-1}, T = 293K.

The quantity of electric charges passed during oxide removal is proportional to the effective-electrode area. By comparing the charge of a SAM-modified electrode with the respective charge of the bare gold electrode, we can measure the surface coverage of the monolayer qualitatively:

$$\theta = 1 - (Q_{SAM} / Q_{Bare\ Au}) \quad (3)$$

where Q_{SAM} is the charge calculated from the area under the gold oxide formation peak of the SAM modified electrodes and $Q_{Bare\ Au}$ is the charge corresponding to the

unmodified Au electrode. The following values were found for SAMs with disulphide linkages: $Q_{BareAu} = 2.93 \times 10^{-4}$ C, $Q_{SAM\text{-}L4} = 1.68 \times 10^{-5}$ C, $Q_{SAM\text{-}CuL4} = 3.60 \times 10^{-5}$ C, $Q_{SAM\text{-}ZnL4} = 1.74 \times 10^{-5}$ C and $Q_{SAM\text{-}FeL4} = 7.79 \times 10^{-5}$ C. The surface coverage obtained with these values is 94.26 % for SAM-**L4**, 87.71 % for SAM-Cu**L4,** 94.06 % for SAM-Zn**L4** and 73.41 % for SAM-Fe**L4.**

In the case of SAMs prepared using thiolates linkages: $Q_{SAM\text{-}L4} = 1.59 \times 10^{-5}$ C, $Q_{SAM\text{-}CuL4} = 2.37 \times 10^{-5}$ C, $Q_{SAM\text{-}ZnL4} = 1.39 \times 10^{-5}$ C and $Q_{SAM\text{-}FeL4} = 1.45 \times 10^{-5}$ C. From these values the surface coverage was estimated to be 94.6 % for SAM-**L4**, 91.9 % for SAM-Cu**L4**, 95.2 % for SAM-Zn**L4** and 83.4 % for SAM-Fe**L4**.

These coverage fraction values are smaller than the values obtained from their corresponding impedance plots. This difference in the values can be attributed to the fact that smaller OH^- ions have easier access to the electrode than the bulkier ferrocyanide ions, which are used as coverage probes in these two methods. After several cycles in 0.1 M $HClO_4$, the voltammogram is similar to that of the bare gold electrode, indicating the complete removal of the monolayer.

From these studies we can conclude that better SAMs are formed by generating the thiol group. The surface coverage is higher so the effect of adding metals to these SAMs of thiolates derivatives is also enhanced.

4.2.1.5 Mechanism of electron-transport through SAM-CuL4

In order to study the possible effect of the chloride ions mediating the electron-transfer the CV and EIS studies were repeated using $Cu(ClO_4)_2$ as a metal precursor and $NaClO_4$ as the supporting electrolyte. The CV obtained is shown in Figure 4.27 and it is similar to that obtained with SAM-Cu**L4** formed using $CuCl_2$.

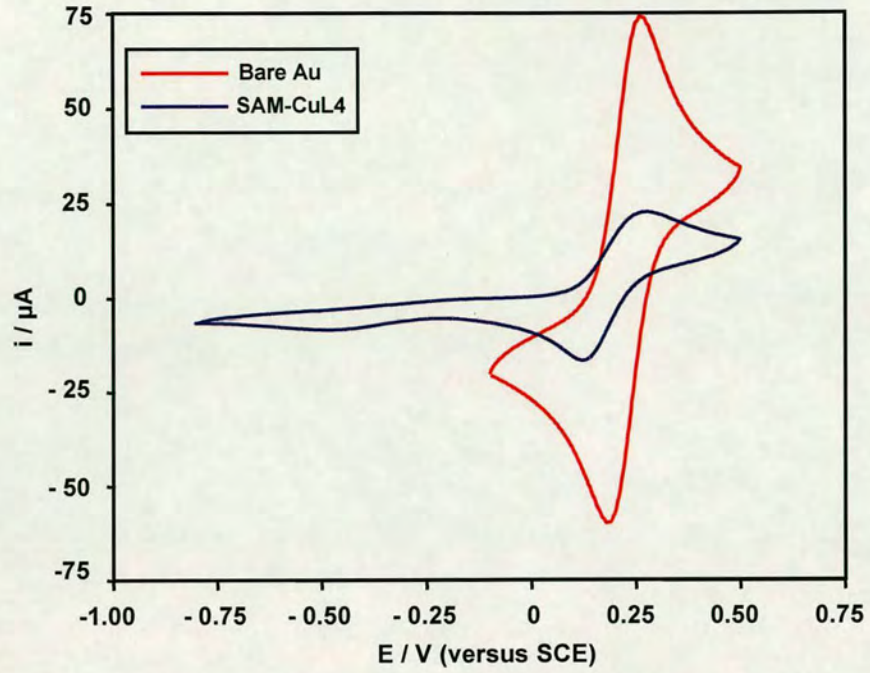

Figure 4.27: CVs of 1 mM $[Fe(CN)_6]^{4-}$ in 0.1 M $NaClO_4$ at a bare gold (red) or monolayer-modified gold electrode with Cu**L4** having dithiolate linkage (blue). Scan rate 0.1 V s^{-1}, $T = 293$K.

The impedance spectra obtained (Figure 4.28) also shows similar R_{ct} values (38.3 Ω cm^2) and rate constants (6.8×10^{-2}cm/s), suggesting that Cl^- anions are not essential to mediate electron transfer.

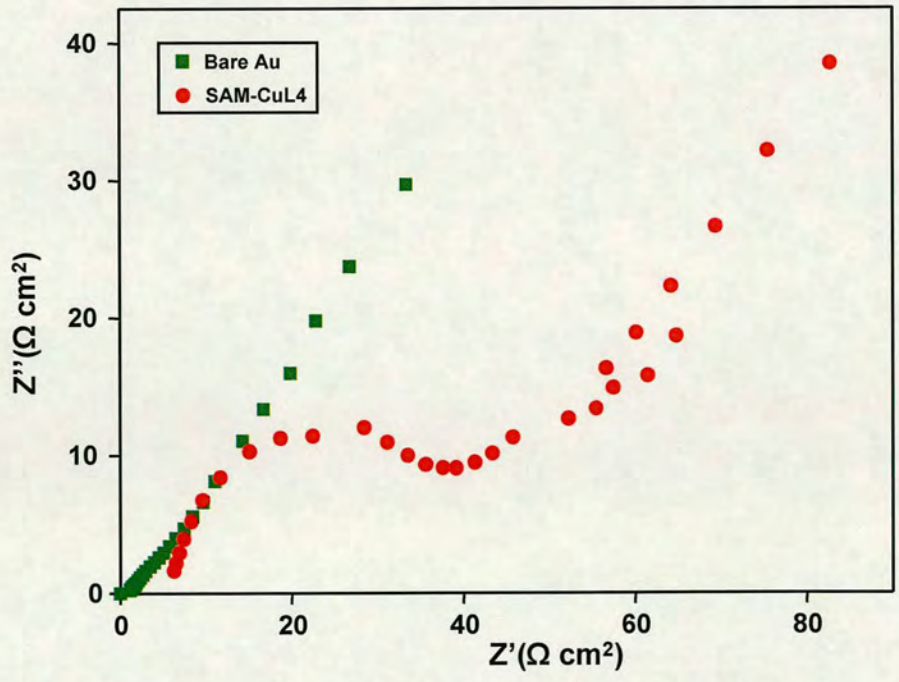

Figure 4.28: Impedance plots in 10 mM $[Fe(CN)_6]^{3-/4-}$ and 1 M $NaClO_4$ at a bare (green squares) or monolayer modified gold with Cu**L4** having dithiolate linkage (red circles), $T = 293$ K.

To determine the mechanism by which the Cu**L4** film mediates the transport of electrons to the redox probe in solution, its redox behaviour in 0.1 M NaCl as the supporting electrolyte without the redox probe was also studied (Figure 4.29).

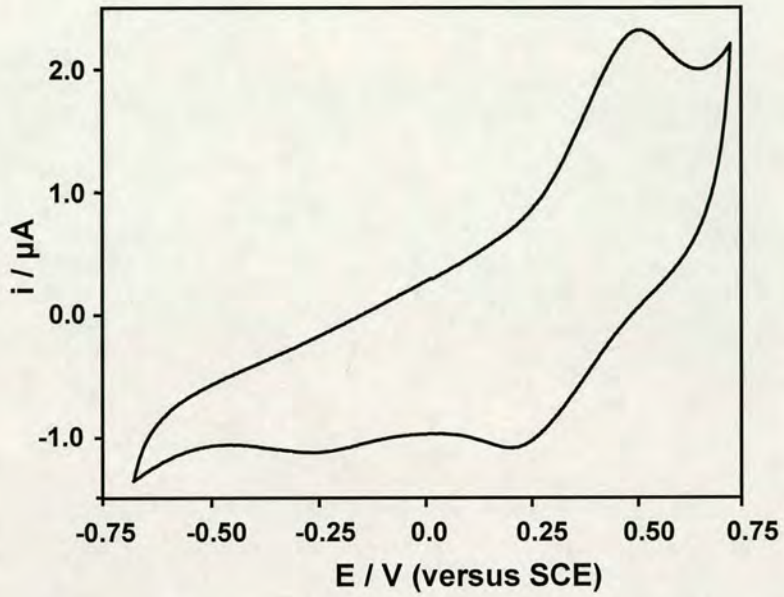

Figure 4.29: CV of the monolayer modified gold electrode with Cu**L4** in 0.1 M NaCl. Scan rate 0.1 V s^{-1}. T= 293 K.

The CV shows a non-reversible oxidation at 0.49 V and a reduction at 0.21 V and -0.28 V. Presumably this is because the copper ions are in different coordination environments. It means that there are species capable of both donating and accepting electrons at the potential of the redox probe (0.2 V). There is an apparent lack of oxidation peak for the Cu(I) complex with the lowest oxidation potential (i.e. in the high coordination number (CN) environment). This means that Cu(I) ions can rapidly change from the less favourable (high CN) coordination environment to the more favourable (low CN) one. The reduction peak at -0.28 V is smaller than that at 0.21 V. This result suggests that the conversion of Cu(II) in the higher CN to Cu(II) in the lower CN is slower and probably not complete at this scan rate.

The solid-state structures of related $[(\mathbf{L})CuCl]^{0/+}$ complexes with pivaloylamido H-bonding groups in the pyridine 6-position have been determined by X-ray crystallography.[14] They reveal that the copper centre in the 2+ oxidation state is pentacoordinated to the four ligand-base N atoms and a Cl^- ligand and in the 1+ state to only two N atoms and a Cl^-. It is reasonable to suggest that the close packing of

molecules on the electrode surface could allow a similar behaviour with the involvement of Cl^- anions or solvent molecules. On the basis of the electrochemical and crystallographic studies, a plausible mechanism for mediating electron-transfer between the electrode and the redox probe in solution is proposed (Figure 4.30).

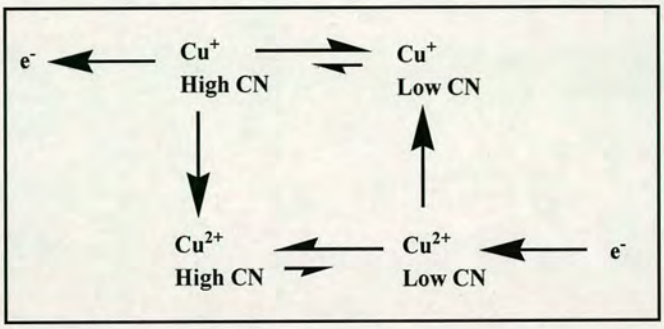

Figure 4.30: Proposed mechanism for the electron transport mediated through SAM-Cu**L4**.

In this mechanism, copper ions in different coordination environments and with different redox potentials are in rapid equilibrium in order to mediate the electron-transfer. Based on the crystallographic and electrochemical data and the coordination chemistry of copper, we propose that the Cu(I) ions are predominantly in a lower coordination number environment, whereas the Cu(II) ions prefer to be coordinated to additional ligands.

4.2.2 SAM-L7 and SAM-ZnL7

4.2.2.1 SAM formation and characterization

Our previous studies showed that better SAMs coverage is achieved by using thiolates linkages. Thus, SAM-**L7** and SAM-Zn**L7** were formed by adding $NaBH_4$ under N_2 atmosphere to 10 mM methanol solutions of **L7** and allowing the molecular film to be formed on the gold overnight.

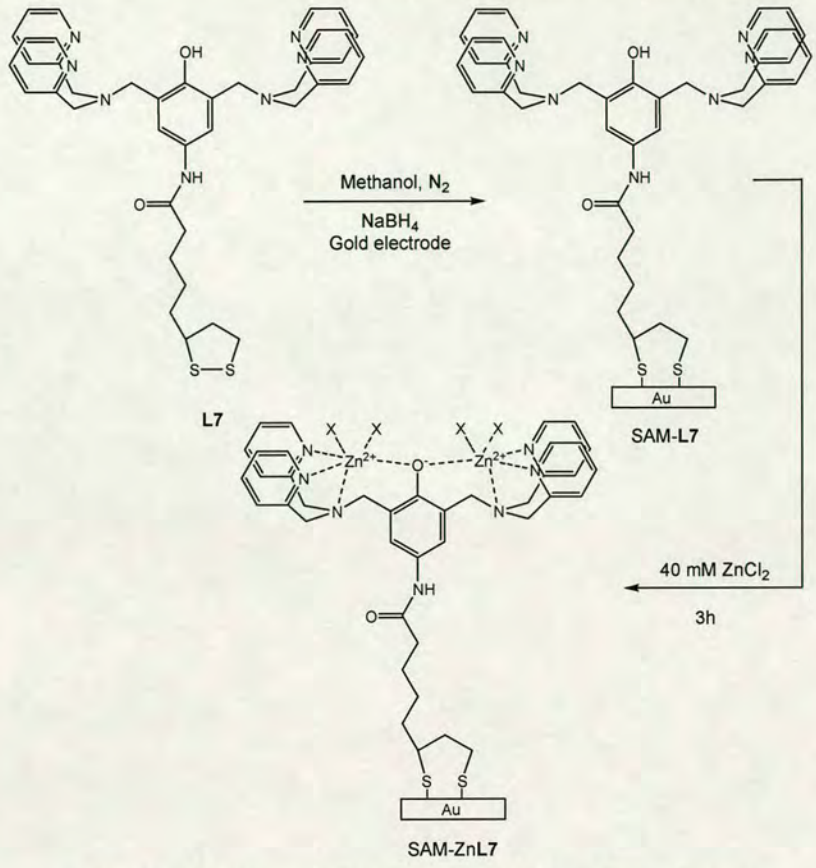

Figure 4.31: Scheme for SAM-**L7** and SAM-Zn**L7** formation.

In this case, our studies were focused on SAM-**L7** and SAM-**L7** containing Zn(II) ions. As before, we investigated the electron-transfer process to a solution containing the redox probe through SAM-**L7** and the effect that the Zn(II) metal has on it.

SAM-Zn**L7** was formed after dipping the gold electrode modified with **L7** in a solution containing 40 mM of $ZnCl_2$, exploring the capacity of the system to coordinate Zn(II) ions from the solution.

SAM-Zn**L7** formation after pre-forming Zn**L7** complex and then dipping the gold was also investigated. This method was not finally adopted due to the low solubility of Zn**L7** in methanol, which is the solvent used for monolayer formation.

Monolayers of **L7** and Zn**L7** of thiolates derivatives have been analysed using *X-ray photoelectron spectroscopy (XPS)* in order to characterize the surface composition. Films formation on the gold surface is confirmed by the presence of the peaks due to S, C, N and O in the XPS spectra (Figure 4.32).

The peaks obtained at 531 eV and 399 eV were used to probe the O 1s and N 1s core level regions, respectively. The S 2p peak at 162.5 eV is indicative of Au–thiolate linkages, whereas the feature at 284.1 eV is characteristic of C 1s.

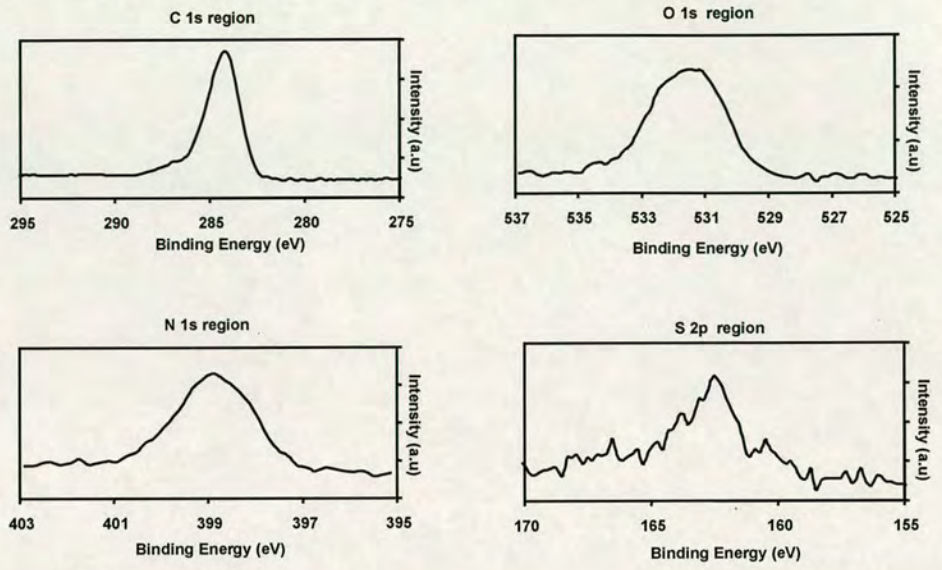

Figure 4.32: Carbon 1s, Oxygen 1s, Nitrogen 1s and Sulphur 2p X-ray photoelectron spectra of the film **L7** with dithiolate linkage on Au.

Figure 4.33 displays the XPS spectra of gold modified with SAM-Zn**L7**. Additional peaks due to the Zn at 1022.1 eV and 1045.1 eV are observed.

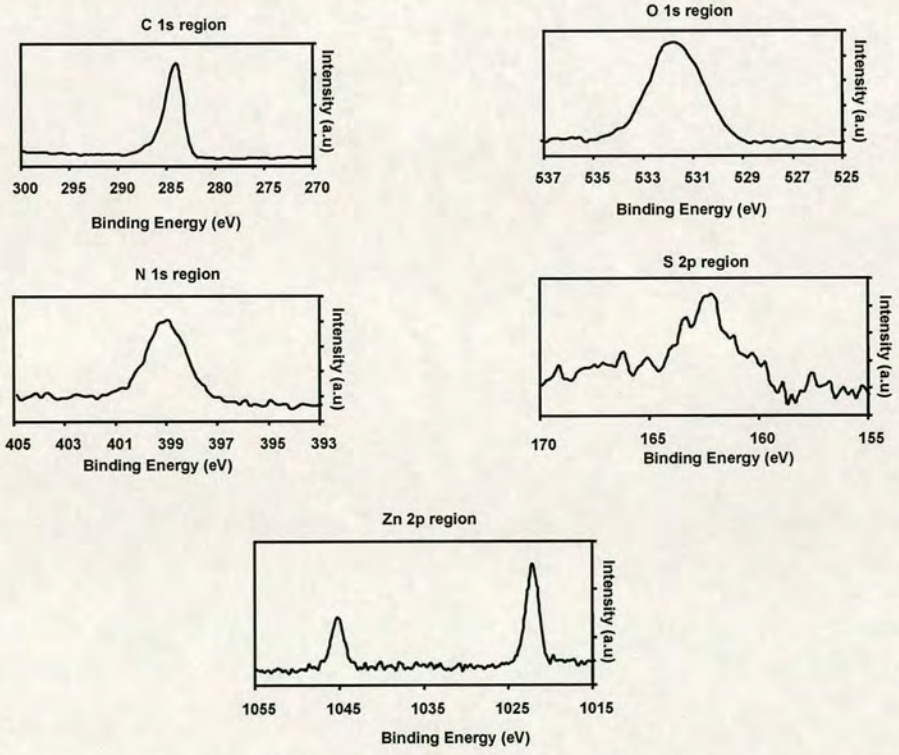

Figure 4.33: Carbon 1s, Oxygen 1s, Nitrogen 1s, Sulphur 2p and Zinc 2p X-ray photoelectron spectra of the film Zn**L7** with dithiolate linkage on Au.

4.2.2.2 Electrochemical characterization of SAM-L7 and SAM-ZnL7

Cyclic voltammetry (CV)

Figure 4.34 shows the cyclic voltammograms of SAM-**L7** and SAM-Zn**L7**.

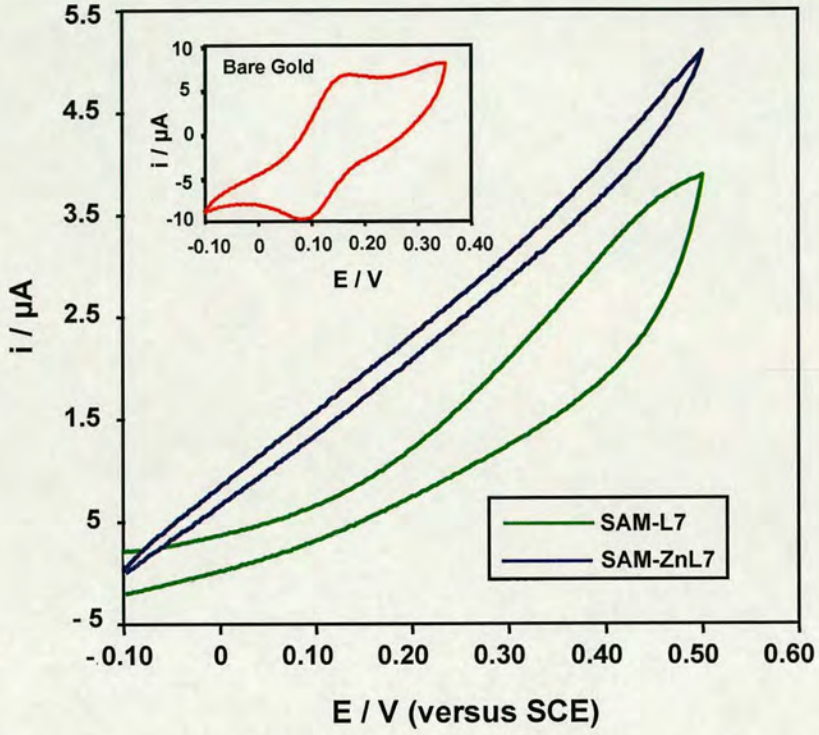

Figure 4.34: CVs of 1 mM $[Fe(CN)_6]^{4-}$ in 0.1 M NaCl at a bare gold (red) and monolayer-modified gold electrode with **L7** (green) and Zn**L7** (blue) with dithiolates linkages on gold. Scan rate 0.1 V s^{-1}, $T = 293$K.

Bare gold electrode shows the characteristic redox couple, whereas in the SAM-**L7** and SAM-Zn**L7** this process is blocked. In this case, adding a metal does not seem to increase the electron transfer process, instead it seems to inhibit it further.

Electrochemical impedance spectroscopy (EIS)

Figure 4.35 displays the EIS spectra obtained for SAM-**L7** and SAM-Zn**L7** formed after keeping SAM-**L7** in a solution of $ZnCl_2$ and Table 6 shows the corresponding R_{ct} and rate constant values (k_0 or k_{app}) obtained by fitting this data.

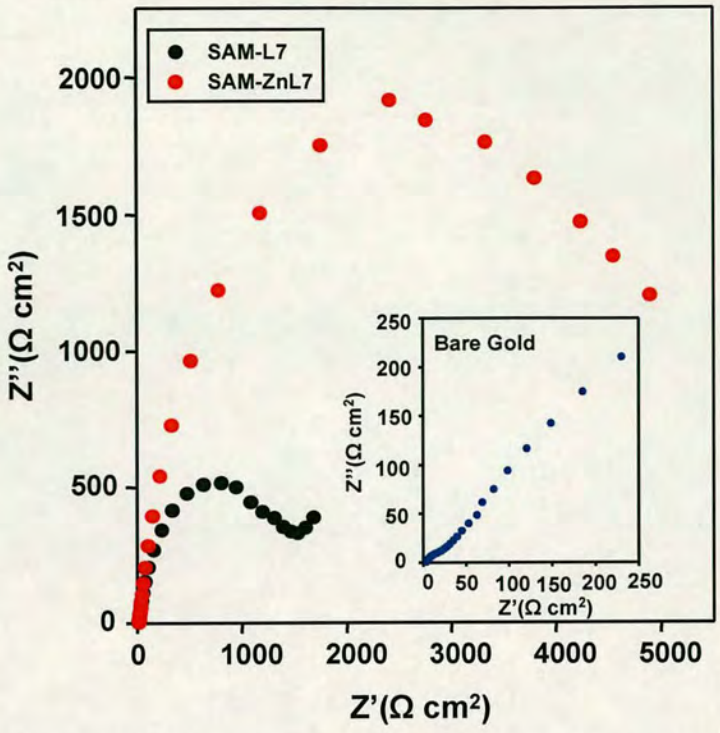

Figure 4.35: Impedance plots in 1 mM $[Fe(CN)_6]^{3-/4-}$ and 0.1 M NaCl at a bare (blue circles) and monolayer modified gold SAM-**L7** (black circles) and SAM-Zn**L7** (red circles) with **L7** and Zn**L7** having dithiolates linkages on gold, $T = 293$ K.

Table 6: Charge transfer resistance (R_{ct}) and rate constants (k_0 and k_{app}) for bare and monolayer-modified gold electrodes, obtained from EIS.

Sample	R_{ct} (Ω cm^2) $Fe(CN)_6^{3-}/Fe(CN)_6^{4-}$	Rate of electron-transfer k_0 and k_{app} (cm/s)
Bare gold	30	0.0087
SAM-L7	1488	1.75×10^{-4}
SAM-L7 + Zn	5304	4.93×10^{-5}

The monolayer-modified gold electrode with **L7** has a R_{ct} value of 1488 Ω cm^2 (k_{app} = 1.75×10^{-4} cm/s), compared to 30 Ω cm^2 (k_{app} = 0.0087 cm/s) for bare gold. Hence the SAM of **L7** thiolate linkage blocks effectively the electron-transfer process to the redox probe. For Zn**L7** monolayer R_{ct} is 5304 Ω cm^2 (k_{app} = 4.93×10^{-5} cm/s), which means that in this case the addition of Zn inhibits the electron-transfer process more.

4.2.2.3 Titration of Zn(II) with SAM-L7

The capacity of the system SAM-**L7** to coordinate Zn(II) from a solution was investigated by titrating with $ZnCl_2$. Impedance spectroscopy was employed to study the Zn(II) complexation process (Figure 4.36).

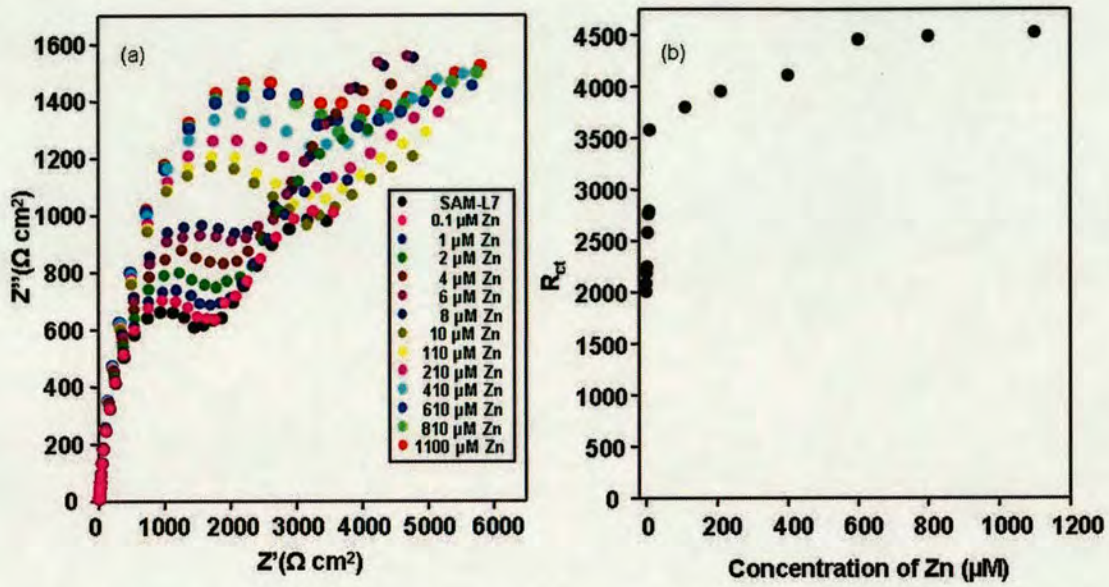

Figure 4.36: (a) Impedance plots in 1 mM $[Fe(CN)_6]^{3-/4-}$, 0.1 M NaCl and 0.1 M HEPES (pH = 7.3) at monolayer modified gold SAM-**L7** (black circles) in absence of Zn and presence of increasing concentrations of Zn; (b) Plot of R_{ct} versus increasing concentrations of Zn for SAM-**L7**. T = 293 K.

The R_{ct} of the monolayer depends on the concentration of Zn(II) added to the electrolyte solution, as [Zn] increases so does the charge transfer resistance of the monolayer. This corroborates that Zn(II) ions complexate at the interface and that this causes a decrease in the electron-transfer process to the redox probe in solution. The value of R_{ct} changes from 2009.6 Ω cm^2 in the absence of Zn(II) to 4082 Ω cm^2 in the presence of 1 mM of $ZnCl_2$. R_{ct} sharply rises until 3579 Ω cm^2 at 10 μM $ZnCl_2$ and obtains the saturation at ca. 600 μM $ZnCl_2$.

4.2.2.4 Electron transport through SAM-ZnL7

Metals containing SAM of **L4** showed an increase of the electron transport process to the redox probe as a consequence of the effect of added metal (see 4.2.1.4). These results were consistent with those obtained for other metal containing SAMs using

$[Fe(CN)_6]^{3-/4-}$ as the solution redox probe.[5-7] It was proposed that the metal bound to the SAMs attracts through electrostatic interactions; this negatively charged redox probe, so the electron-transfer is facilitated.

For SAM-Zn**L7** the results are clearly the opposite. In order to provide an explanation for this, it is useful to examine the crystal structure of a similar dinuclear Zn complex (Figure 4.37).[15]

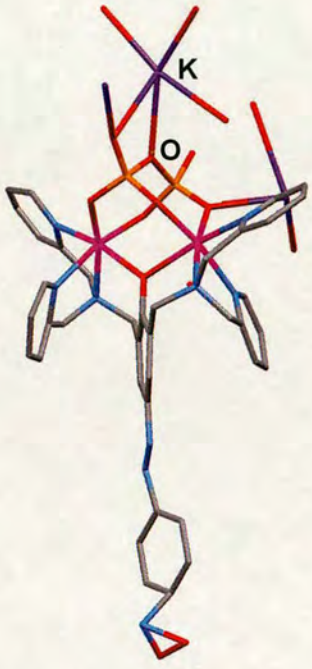

Figure 4.37: Crystal structure of a Zn(II) dinuclear metal complex derivative of BPA bound to a pyrophosphate molecule.

This Zn(II) metal complex is coordinated to a pyrophosphate molecule and as a consequence the charge of the metal complex is negative (at neutral pH the oxygen that bridges the two Zn(II) is deprotonated) and has a K^+ cation as counter ion. Based on this crystal structure and on the electrochemical studies we propose that the Zn**L7** complex immobilized on the gold surface may coordinate to 4 chloride molecules, so that the overall charge of the SAM would be negative and attracts several molecules of solvated cations present in the solution, generating a film of them between SAM-Zn**L7** and the redox probe. This layer will separate the redox probe further away from the electrode, generating a decrease in the electron transfer-process (Figure 4.38).

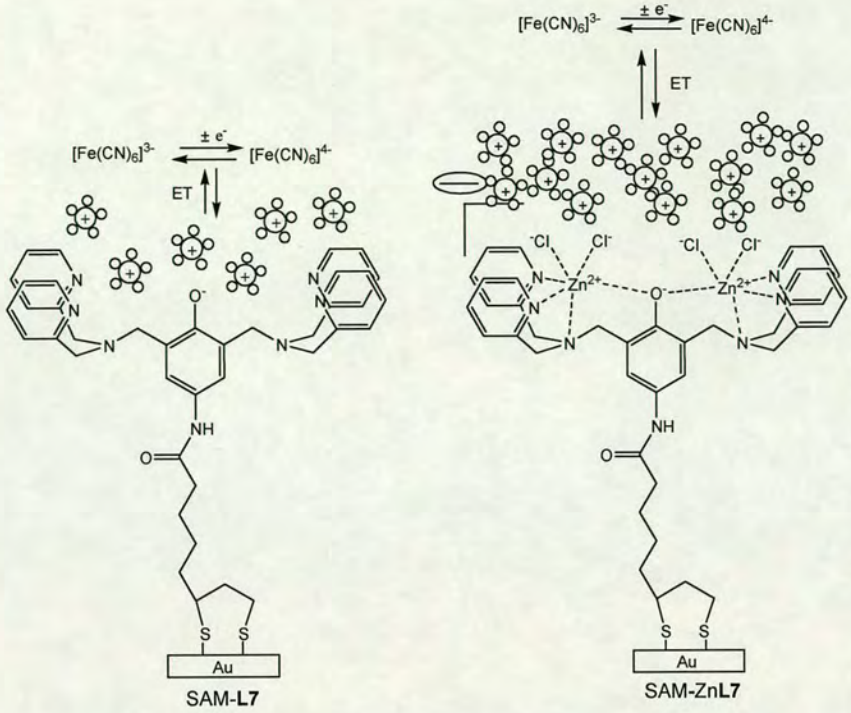

Figure 4.38: Scheme of the proposed electron-transfer process for SAM-**L7** and SAM-Zn**L7**.

If the overall charge of the SAM-Zn**L7** is negative, then the nature of the counter ion should affect the electron-transfer process. This was confirmed by measuring the impedance response of SAM-**L7** and SAM-Zn**L7** with different cations in the supporting electrolyte (Figures 4.39 and 4.40).

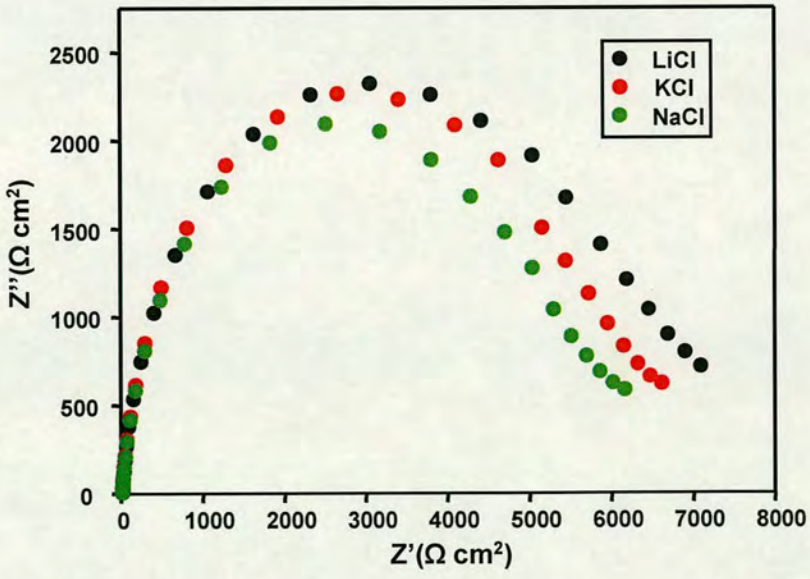

Figure 4.39: Impedance plots in 1 mM $[Fe(CN)_6]^{3-/4-}$ and 0.1 M of different electrolytes (NaCl, KCl and LiCl) at monolayer modified gold of SAM-**L7**, $T = 293$ K.

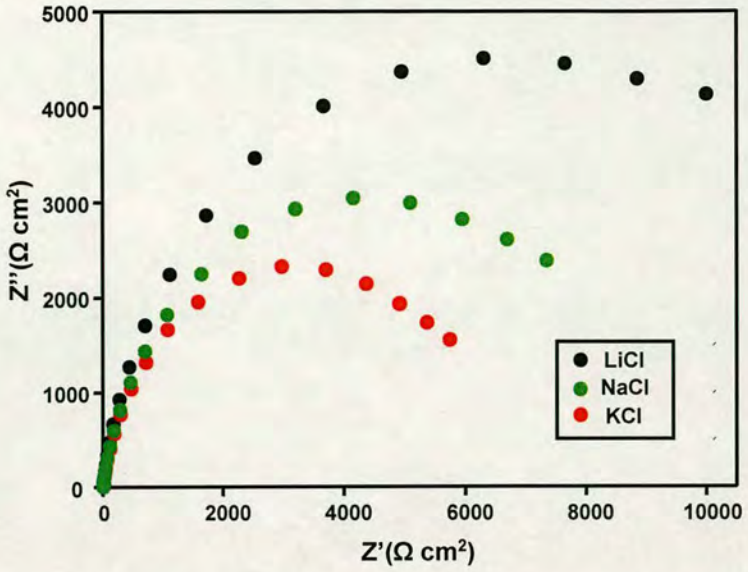

Figure 4.40: Impedance plots in 1 mM $[Fe(CN)_6]^{3-/4-}$ and 0.1 M of different electrolytes (NaCl, KCl and LiCl) at monolayer modified gold of SAM-Zn**L7**, $T = 293$ K.

The charge transfer resistance across SAM-**L7** does not change significantly in the presence of different electrolytes. In contrast, the blocking behaviour of SAM-Zn**L7** strongly depends on the nature of the cation of the electrolyte (see Figure 4.40 and Table 7).

Table 7: Charge transfer resistance (R_{ct}) and rate constants (k_{app}) of SAM-**L7** and SAM-Zn**L7** in the presence of different electrolytes.

		LiCl	NaCl	KCl
SAM-**L7**	R_{ct} (Ω cm^2)	6100	5400	5950
	k_{app} (cm/s)	4.26×10^{-5}	4.80×10^{-5}	4.37×10^{-5}
SAM-Zn**L7**	R_{ct} (Ω cm^2)	12900 >	8900 >	6500
	k_{app} (cm/s)	2.02×10^{-5}	$< 2.93 \times 10^{-5}$	$< 4.03 \times 10^{-5}$

These results can be explained by analyzing the enthalpies of hydration of the metal cations of the electrolytes Li^+ = - 515 KJ/mol > Na^+ = - 405 KJ/mol > K^+= - 321 KJ/mol. Thus, K^+ will be the less hydrated cations so their overall size will be smaller compared to Li^+ and Na^+, which are highly hydrated. Since K^+ has smaller

hydrated radii they will promote electron-transfer by facilitating close contact of the redox probe with the monolayer.[16]

4.3 Conclusions

This chapter illustrated the extent to which SAMs of metal complexes can affect the electron-transfer process to a redox probe in solution and the mechanisms involved. For all the ligands deposited on gold electrodes, good blocking properties were observed. In the case of ligands containing the thioctic acid group, better SAMs were formed by generating the thiolate linkage instead of disulfide linkage.

For monolayers containing redox-active Cu centers of **L4** the electron-transfer process to $[Fe(CN)_6]^{3-/4-}$ is considerably faster than for SAM-Fe**L7** and SAM-Zn**L7** and even faster than across SAMs providing shorter and aromatic interfaces. The electrochemical data together with crystallographic data available for related Cu(I/II) complexes, is consistent with a proposed mechanism for electron transfer where these Cu ions are in different coordination environments (i.e. with different redox potentials) and rapidly undergoing interconversion.

Our studies reveal that metals do not always facilitate the electron-transfer process to $[Fe(CN)_6]^{3-/4-}$. We found that SAM-Zn**L7** provide a bigger barrier to electron-transfer than SAM-**L7**. Based on electrochemical studies and on the crystal structure of a complex of a similar ligand, we propose that SAM-Zn**L7** is negatively charged and that this generates a layer of solvated counter ions between the SAM surface and the negative redox probe. As a result, the electron-transfer process to the redox probe is slower as this is further away from the gold electrode.

4.4 Experimental

Materials. Reagents were obtained from commercial sources and used as received unless otherwise noted. Solvents were dried and purified under N_2 by using standard methods and were distilled immediately before use. All the reactions were carried out under N_2.

Preparation of evaporated gold samples. A gold sample of 99.99% purity was used for the preparation of evaporated films of gold having a thickness of ~100 nm on glass with chromium underlayers (~ 2-5 nm thickness). The substrate was heated to 350 °C during gold evaporation under vacuum pressure of 2×10^{-5} mbar, a process that normally yields a very smooth gold substrate with predominantly Au(111) orientation. These gold samples were used as strips for the monolayer preparation and its characterization.

Synthesis of dithiolate L4. *Disulphide* **L4** (10 mg, 0.02 mmol) was dissolved in 1 ml of oxygen-free methanol solution. Then, $NaBH_4$ (approx. 2 equiv.) was added, leading to immediate bubbling of H_2.

^{1}H NMR (CD_3OD, 360.1 MHz): δ_H/ppm 8.49 (d, 2H, J = 5.8 Hz), 7.86 (d, 1H, J = 8.0 Hz), 7.80 (t, 2H, J = 7.6 Hz), 7.72 (t, 1H, J = 7.6 Hz), 7.68 (m, 2H), 7.33 (m, 2H), 7.22 (d, 1H, J = 7.2 Hz), 3.90 (s, 4H), 3.80 (s, 2H), 2.96-2.92 (m, 1H), 2.80-2.60 (m, 2H), 2.51-2.47 (m, 3H), 1.97-1.50 (m, 7H).
^{13}C NMR (CD_3OD, 90 MHz): δ_C/ppm 172.8, 158.2, 156.5, 150.8, 147.8, 137.8, 136.8, 123.0, 122.0, 118.3, 111.8, 59.0, 58.7, 42.4, 38.1, 37.9, 35.9, 25.7, 24.4 and 20.8.

Metal complexes for monolayer preparation. Copper, zinc and iron complexes of **L4** were prepared by mixing equimolar amounts of the ligand **L4** and the corresponding metal dichlorides or perchlorate salts. In a typical reaction, the ligand **L4** (10 mg, 0.02 mmol) and corresponding metal such as $CuCl_2$ (3.02 mg, 0.02 mmol), $ZnCl_2$ (2.72 mg, 0.02 mmol), $FeCl_2$ (4.02 mg, 0.02 mmol) and $Cu(ClO_4)_2$

(5.31 mg, 0.02 mmol) were dissolved in 10 ml of CH_3CN. The resulting mixture was stirred for about 1 hour under N_2 atmosphere. During the reaction a colour change from yellow to green in the case of Cu**L4** is observed (from yellow to brown in the case of Fe**L4** and no colour change in the case of Zn**L4**). Then, the solvent was removed under vacuum to prepare the methanol solutions (10 mM) for monolayer preparation.

ESI-MS (+ ion) calcd for ZnCl-**L4** ($C_{26}H_{31}ClN_5OS_2Zn$), m/e 594.53, found 593.94 (100 %); CuCl-**L4** ($C_{26}H_{31}ClCuN_5OS_2$), m/e 591.1, found 590.91(100 %); FeCl-**L4** ($C_{26}H_{31}ClFeN_5OS_2$), m/e 584.99, found 612.43 $[M\text{-}OCH_3 + CH_3OH]^+$ (95 %) and 627.16 $[M\text{-}Cl\text{+}CH_3CN]^+$ (85 %).

Monolayer preparation. Gold slides for XPS studies were chemically cleaned by immersing in a piranha solution for 5-10 minutes. *Caution: piranha solution reacts violently with organic materials and therefore must be handled with extreme care.* Then, the slides were rinsed with water and methanol, dried under N_2 and used immediately. Before SAM formation, the gold disk electrodes (Metrohm, d = 0.2 cm) were electrochemically cleaned by potential cycling in an aqueous solution of 0.1 M $HClO_4$ to obtain the characteristic Au oxide formation and stripping peaks corresponding to bare Au surface using cyclic voltammetry. After electrochemical cleaning, the electrodes were rinsed with water and methanol and dried under a stream of N_2.

Monolayers of **L4**, Cu**L4,** Zn**L4** and Fe**L4** were prepared by immersing the cleaned gold disk electrode (electrochemistry) or a gold slide (XPS) into 10 mM methanol solutions of these compounds for 4 days in the case of method 1. In method 2, the deposition of the SAMs was done in the presence of $NaBH_4$ for about 15-16 hours under N_2. After this, the SAM modified gold surfaces were rinsed with methanol and water and used immediately for the analysis.

Monolayers of **L7** were prepared by dipping the cleaned gold disk electrode /evaporated gold electrode (electrochemistry) or a gold slide (XPS) into 10 mM methanol solutions of **L7** in the presence of $NaBH_4$ for about 15-16 hours under N_2.

After this, the SAM modified gold surfaces were rinsed with methanol and water and used immediately for the analysis.

Monolayers of Zn**L7** were prepared by immersing **L7** modified gold electrode (electrochemistry) or a gold silice (XPS) into 40 mM $ZnCl_2$ or into $Zn(NO_3)_2$ for 3 and 16 hours respectively.

Physical measurements.

Electrochemistry. All electrochemical studies were performed with an Autolab PGSTAT 20 instrument. The electrochemical blocking ability of the monolayers towards electron-transfer was studied by cyclic voltammetry and electrochemical impedance spectroscopy using $[Fe(CN)_6]^{3-/4-}$ redox couple as a probe. The electrolyte solutions used for electrochemical measurements were prepared with millipore water having a resistivity of 17 MΩ. Cyclic voltammetry and impedance measurements were conducted in a three-electrode glass cell at 20 °C. A platinum rod, a saturated calomel electrode (SCE) and a monolayer-modified gold disk electrode were used as a counter, reference and working electrodes respectively. Cyclic voltammetry was performed in 1 mM $[Fe(CN)_6]^{4-}$ aqueous solution containing 0.1 M NaCl as a supporting electrolyte. Impedance measurements were carried out at the formal redox potential (as determined from cyclic voltammetry) in an aqueous solution containing equal concentrations of oxidized and reduced forms of $[Fe(CN)_6]^{3-/4-}$ with NaCl as a supporting electrolyte. The frequency range used was from 10 KHz to 0.1 Hz with an ac amplitude of 10 mV.

X-ray photoelectron spectroscopy (XPS). X-ray photoelectron spectra were obtained with a VG Scientific Sigma Probe (UK) XPS system. The Al Kα anode X-ray source (hυ = 1486.6 eV) was operated at 200 W and the take-off angle for photoelectrons was 37°. Samples were mounted with a spring clip. In a typical experiment, scans in the -10 to 1100 eV kinetic energy range were collected at a resolution of 1 eV. Then, detailed scans of 20-60 eV over a single feature were collected at a resolution of 0.2 eV. During the measurements the pressure was 10^{-9}-10^{-10} Torr.

IR spectroscopy. Infrared spectra of the bulk materials were recorded with a JASCO FTIR-410 spectrometer between 4000 and 400 cm^{-1} as KBr pellets.

Polarization-modulation reflection absorption IR spectroscopy (PM-RAIRS). PM-RAIRS data were collected using a Nicolet Nexus 860 FTIR spectrometer using a N_2(l)-cooled mercury cadmium telluride (MCT) detector. A background spectrum of bare gold surface was taken and then the monolayer modified gold surfaces were exposed to collect the respective data.

4.5 References

(1) (a) P. D. Beer, J. J. Davis, D. A. Drillsma-Milgrom and F. Szemes, *Chem. Commun.*, 2002, 1716; (b) P. D. Beer, D. P. Cormode and J. J. Davis, *Chem. Commun.*, 2004, 414; (c) D. Astruc, M. C. Daniel and J. Ruiz, *Chem. Commun.*, 2004, 2637; (d) R. K. Shervedani and S. A. Mozaffari, *Anal. Chem.*, 2006, **78**, 4957.

(2) (a) T. Hiratsu, S. Suzuki and K. Yamaguchi, *Chem. Commun.*, 2005, 4534; (b) J. P. Collman, M. S. Ennis, D. A. Offord, L. L. Chng and J. H. Griffin, *Inorg. Chem.*, 1996, **35**, 1751; (c) T. Belser, M. Stöhr and A. Pfaltz, *J. Am. Chem. Soc.*, 2005, **127**, 8720.

(3) (a) J. Park, A. N. Pasupathy, J. I. Goldsmith, C. Chang, Y. Yaish, J. R. Petta, M. Rinkoski, J. P. Sethna, H. D. Abruña, P. L. McEuen and D. C. Ralph, *Nature*, 2002, **417**, 722; (b) C. Li, W. Fan, D. A. Straus, B. Lei, S. Asano, D. Zhang, J. Han, M. Meyyappan and C. Zhou, *J. Am. Chem. Soc.*, 2004, **126**, 7750; (c) A. S. Blum, T. Ren, D. A. Parish, S. A. Trammell, M. H. Moore, J. G. Kushmerick, G.-L. Xu, J. R. Deschamps, S. K. Pollack and R. Shashidhar, *J. Am. Chem. Soc.*, 2005, **127**, 10010; (d) A. Dube, A. R. Chadeayne, M. Sharma, P. T. Wolczanski and J. R. Engstrom, *J. Am. Chem. Soc.*, 2005, **127**, 14299.

(4) G. Cooke, *Angew. Chem. Int. Ed.*, 2003, **42**, 4860.

(5) C. G. F. Cooper, J. C. MacDonald, E. Soto and W. G. McGimpsey, *J. Am. Chem. Soc.*, 2004, **126**, 1032.

(6) X. Lu, M. Li, C. Yang, L. Zhang, Y. L. Jiang, H. Li, L. Jiang, C. Liu and W. Hu, *Langmuir*, 2006, **22**, 3035.

(7) (a) I. Takahashi, T. Inomata, Y. Funahashi, T. Ozawa, K. Jitsukawa and H. Masuda, *Chem. Commun.*, 2005, 471; (b) I. Takahashi, T. Inomata, Y. Funahashi, T. Ozawa, and H. Masuda, *Chem. Eur. J.*, 2007, **13**, 8007.

(8) (a) J. C. Mareque Rivas, R. Torres Martín de Rosales and S. Parsons, *Dalton Trans.*, 2004, 172; (b) J. C. Mareque Rivas, E. Salvagni, R. Prabaharan, R. Torres Martín de Rosales and S. Parsons, *Dalton Trans.*, 2003, 3339; (c) J. C. Mareque Rivas, R. Torres Martín de Rosales and S. Parsons, *Dalton Trans.*, 2003, 2156.

(9) M. Brust, P. M. Blass and A. J. Bard, *Langmuir*, 1997, **13**, 5602.

(10) (a) P. Kohli, K. K. Taylor, J. J. Harris and G. J. Blanchard, *J. Am. Chem. Soc.*, 1998, **120**, 11962; (b) M. H. Schoenfisch and J. E. Pemberton, *J. Am. Chem. Soc.*, 1998, **120**, 4502.

(11) (a) H. O. Finklea, D. Zinder, J. Fedyk, E. Sabatini, Y. Gafni and I. Rubinstein, *Langmuir*, 1993, **9**, 3660; (b) V. Ganesh and V. Lakshminarayanan, *Langmuir*, 2006, **22**, 1561.

(12) (a) G. Sánchez-Pomales, L. Santiago-Rodríguez, N. E. Rivera-Vélez and C. R. Cabrera, *J. Electroanal. Chem.*, 2007, **611**, 80; (b) Richard P. Janek, W. Ronald Fawcett and A. Ulman, *Langmuir*, 1998, **14**, 3011.

(13) (a) H. O. Finklea, S. Avery, M. Lynch and T. Furtsch, *Langmuir*, 1987, **3**, 409; (b) E. Sabatani and I. Rubinstein, *J. Phys. Chem.*, 1987, **91**, 6663; (c) H. O. Finklea, D. A. Snider, J. Fedyk, E. Sabatani, Y. Gafni and I. Rubinstein, *Langmuir*, 1993, **9**, 3660; (d) V. Ganesh and V. Lakshminarayanan, *J. Phys. Chem. B*, 2005, **109**, 16372.

(14) (a) M. Harata, K. Jitsukawa, H. Masuda and H. Einaga, *Chem. Lett.*, 1995, 61; (b) J. C. Mareque-Rivas, S. L. Hinchley, L. Metteau and S. Parsons, *Dalton Trans.*, 2006, 2316.

(15) D. H. Lee, J. H. Im, S. U. Son, Y. K. Chung and J. I. Hong, *J. Am. Chem. Soc.*, 2003, **125**, 7752.

(16) (a) P. D. Metelski and T. W. Swaddle, *Inorg. Chem.*, 1999, **38**, 301; (b) V. A. Grigoriev, D. Cheng, C. L. Hill and I. A. Weinstock, *J. Am. Chem. Soc.*, 2001, **123**, 5292.

Chapter 5

Cyanide detection

5.1 Introduction

The development of anion sensors that work in water has become an important target in supramolecular chemistry for biological and environmental reasons.[1] Strong and selective binding of the receptor to the anion is challenging under physiological conditions, in part because most anions are highly solvated. Binding is even more difficult if the anion becomes protonated at physiological pH and so looses its charge. Metal complexes and organic molecules with hydrogen bonding groups provide some of the most effective classes of anion receptors created to date due to their ability to form strong coordination or hydrogen bonds with the anion.[2] In metal complex receptors the metal can act as a Lewis acid facilitating the deprotonation of the bound species[2] and the shape can be designed to match that of the anion,[3] improving the binding affinity and selectivity. However, the overall efficiency of a sensor depends also on the sensitivity of the method reporting the presence of the analyte. As a consequence there are few sensors capable of detecting anions in the mM–nM concentration range in water and neutral pH. Most of these exploit the sensitivity provided by fluorescence spectroscopy.[4]

Recent studies have proven that the use of self-assembled monolayers (SAMs) is an effective and convenient alternative strategy to detect cations in water due to the relative ease of preparation, fast response and pre-organisation of the receptor on the surface.[5] Anion sensing based on monolayers is comparatively much rarer and only a few recent studies have provided SAM-based sensors capable of detecting mM concentrations of anions such as phosphates, acetate and fluoride in organic solvents[6] and water.[7]

Figure 5.1 shows one of the few examples of anion receptor containing SAMs capable of detecting anions in water.

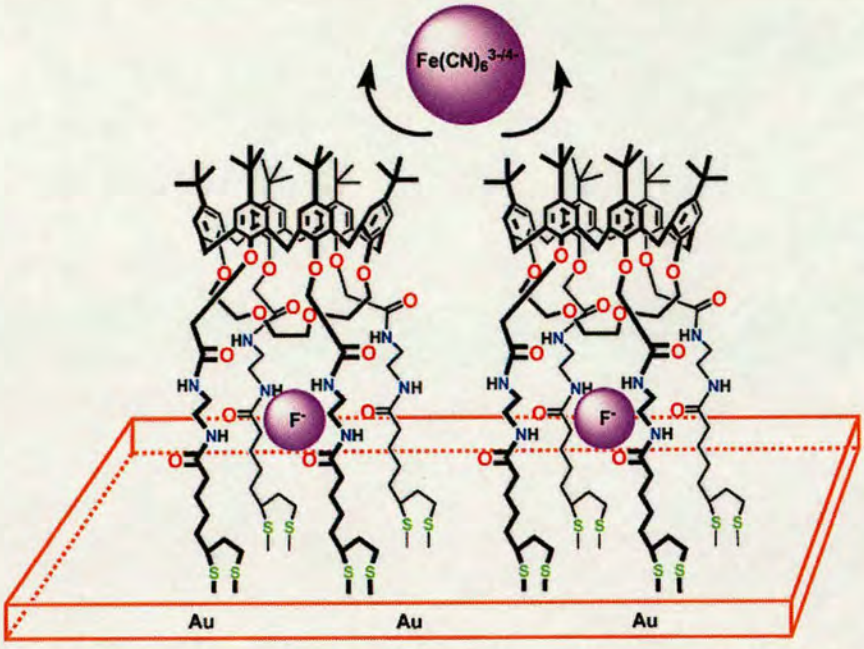

Figure 5.1: Schematic representation of F^- recognition by SAMs of a calix[6]crown-4 thioctamide derivative(C6C4TE).

In this electrochemical sensor developed by Echegoyen et al.[7b] the calix[6]crown-4 derivative (C6C4TE) with four thioctic ester groups is used to capture the anions through hydrogen bonding and impedance spectroscopy to signal anion binding. These receptor-modified surfaces were found to exhibit higher affinity for F^- anions (for which the detection limit is ca. 3 mM) than for other anions such as Cl^-, Br^-, NO_3^-, HSO_4^-, $H_2PO_4^-$ and AcO^-.

In this chapter the target anion is cyanide, which finds common industrial use in organic chemicals and polymers such as nitriles, nylon and acrylic plastics, fertilizer factories, precious metal mining and metal plating.[8] Due to the extreme toxicity of cyanide (0.5–3.5 mg per kg of body weight are lethal to humans), its concentration in drinking water cannot be greater than ca. 2 μM according to the World Health Organization.[9] Thus, there is a widespread need to develop effective cyanide sensors.[10] This is challenging because under physiological conditions cyanide exists as $HCN_{(g)}$ (The pK_a of $HCN_{(g)}$ is 9.21) and common ions such as chloride can interfere with their detection. An example of a cyanide sensor developed for detection in aqueous medium is shown in Figure 5.2.[10c]

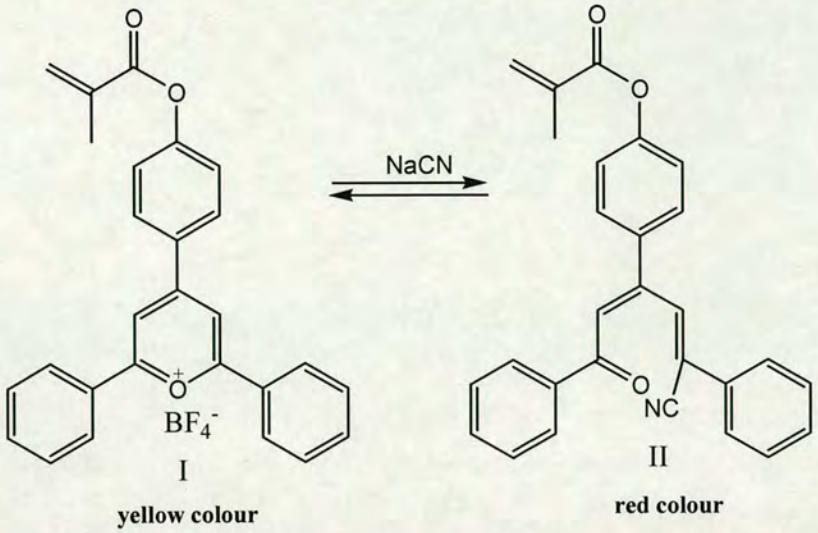

Figure 5.2: Pyrylium derivative cyanide sensor and its reactivity mechanism.

This colorimetric probe for cyanide is based on the reactivity of this anion with the pyrylium cation anchored to a polymer. After the addition of increasing concentrations of cyanide, changes in the absorbance were observed, resulting in a progressive change of colour from yellow to red. No colour change was observed in the presence of other anions such as Cl^-, Br^-, NO_3^-, $H_2PO_4^-$, SO_4^{2-} and SCN^-. The cyanide detection limit found was 4 mM at pH = 11.

Figure 5.3 shows an example of fluorescence-based cyanide detection.[10b]

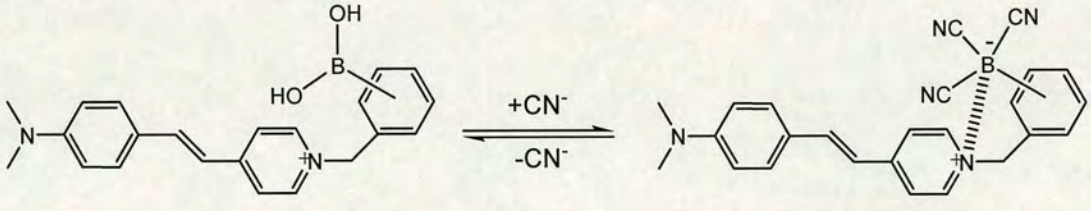

Figure 5.3: Fluorescent probe (*where $B(OH)_2$ can be orto, meta or para, respectively)* and its complexation with aqueous free cyanide (CN^-).

These water-soluble fluorescent probes were designed to determine free cyanide concentrations up to physiologically lethal levels, >20 μM, without the interference of Cl^- or oxygen. In this case cyanide binding modulates the intramolecular charge transfer within the probes and this results in enhanced fluorescence with increasing cyanide concentration.

We considered that a strategy to detect cyanide could be to exploit its metal binding properties. For example, cyanide reacts with copper ions to form very stable $[Cu(CN)_n]^{(n-1)-}$ species (Table 1).[11]

Table 1: Stability constants (β_n) of Cu-cyano-complex ions

Cu-cyano complexes,$[Cu(CN)_n]^{(n-1)-}$	Stability constant (β_n)
$[Cu(CN)_2]^-$	$5.01\times10^{21}\ M^{-2}$
$[Cu(CN)_3]^{2-}$	$6.31\times10^{26}\ M^{-1}$
$[Cu(CN)_4]^{3-}$	$7.94\times10^{27}\ M^{-1}$

This property has been used to remove copper ions from a range of ligand environments;[12] an example is illustrated in Figure 5.4.[13]

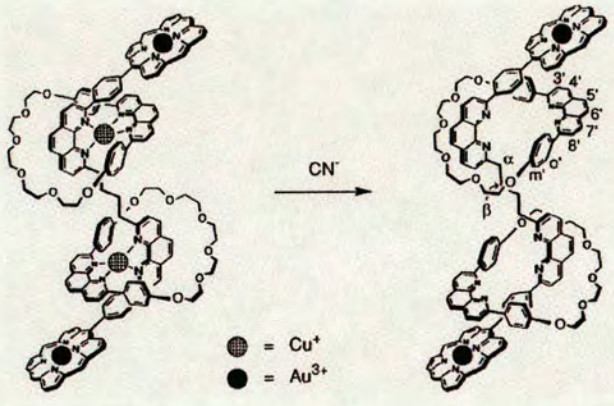

Figure 5.4: Removal of the metal template of (Cu_2)-[3]-rotaxane with CN^-.

Chapter 4 showed that in SAMs of Cu**L4**, this redox active metal affects the kinetics of electron-transfer (ET) to a negatively charged redox probe in solution,[14] $[Fe(CN)_6]^{3-/4-}$ (Figure 5.5). This chapter shows that it is possible to combine this property with the ability of (H)CN to bind copper ions to create a novel, sensitive and selective electrochemical cyanide sensor.

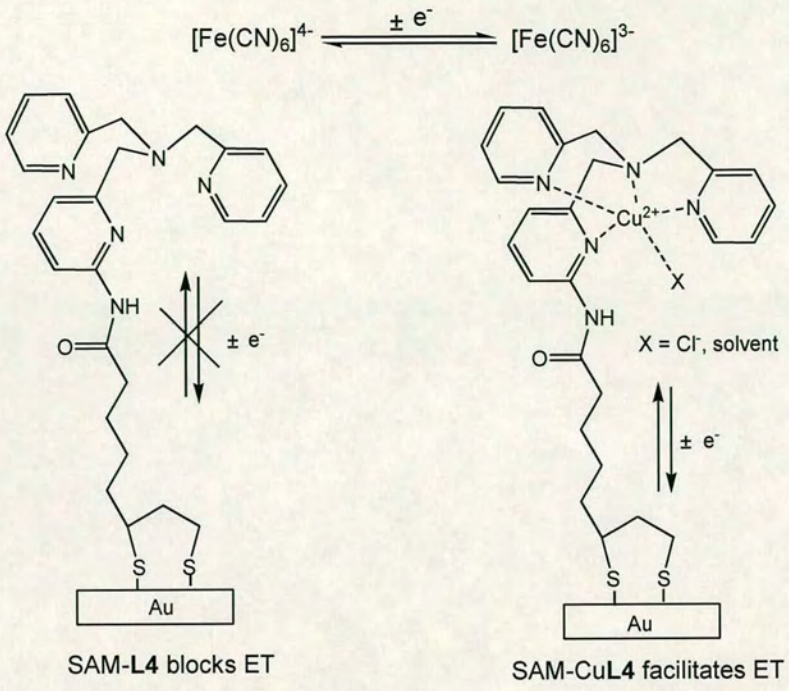

Figure 5.5: Electron-transport behaviour of SAM-**L4** and SAM-Cu**L4**.

5.2 Results and discussion

The monolayers of SAM-Cu**L4** were prepared as mentioned in Chapter 4 (illustrated Figure 5.6).

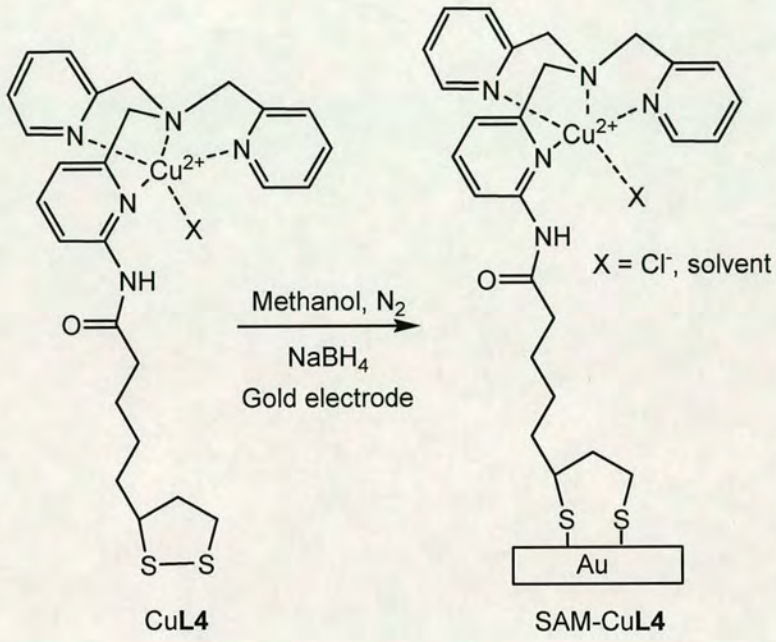

Figure 5.6: Scheme of SAM-Cu**L4** formation.

The ability of SAMs of Cu**L4** to detect different anions was investigated by cyclic voltammetry (CV) and electrochemical impedance spectroscopy (EIS). The CV and EIS studies were carried out in aqueous buffer containing 0.1 M HEPES (pH = 7.3) along with 1 mM $[Fe(CN)_6]^{3-/4-}$ and 0.1 M NaCl as supporting electrolyte.

5.2.1 SAM-CuL4 as anion sensor

5.2.1.1 Cyclic voltammetry (CV) studies

Initially, the ability of the SAM to detect different anions was investigated by cyclic voltammetry (CV). The CV is consistent with a reversible behaviour for the $[Fe(CN)_6]^{3-/4-}$ redox couple due to the copper ions of the complex facilitating the electron-transfer across the molecular film. Upon addition of cyanide (1 mM) the

shape of the CV indicates somewhat less reversible redox behaviour due to less effective electron transport across the film (Figure 5.7).

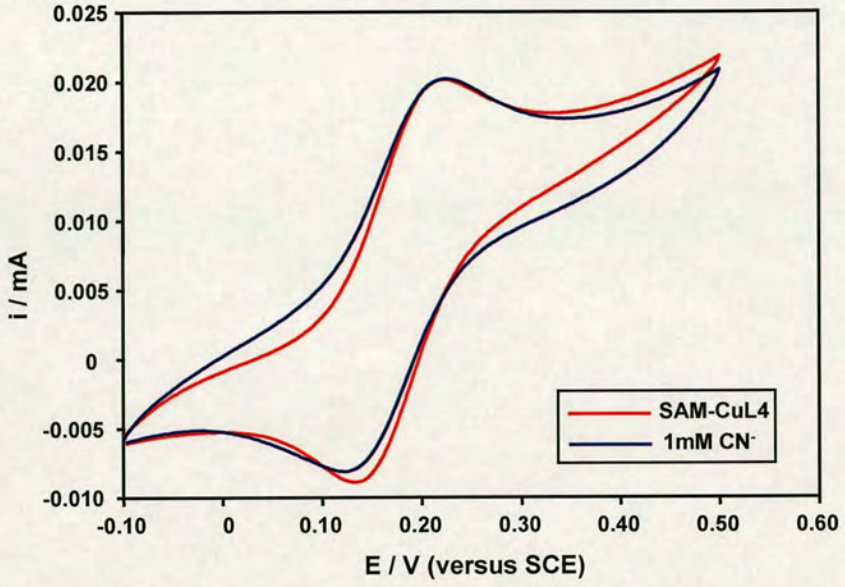

Figure 5.7: CVs of SAM-Cu**L4** in 1 mM $[Fe(CN)_6]^{3-/4-}$, 0.1 M NaCl and 0.1 M HEPES (pH = 7.3) in the absence and presence of CN^-.

In contrast no changes were observed in the presence of other potentially interfering anions (1 mM) such as $H_2PO_4^-$, NO_3^-, AcO^- and F^- (Figure 5.8).

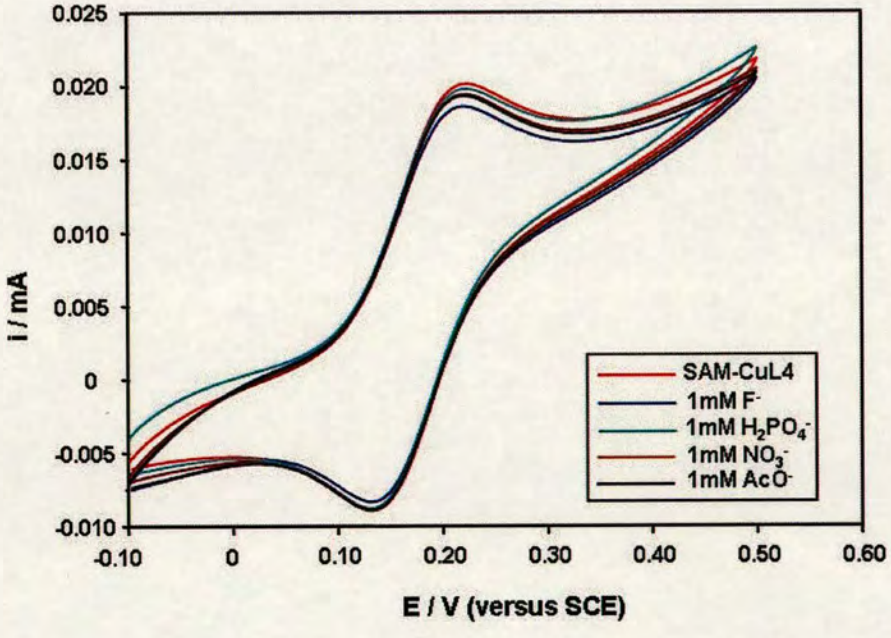

Figure 5.8: CVs of SAM-Cu**L4** in 1 mM $[Fe(CN)_6]^{3-/4-}$, 0.1 M NaCl and 0.1 M HEPES (pH = 7.3) in the absence and presence of different anions.

These results suggest that the system SAM-Cu**L4** gives some response to cyanide anions but not for the others. However, this technique was not sensitive enough to detect environmentally relevant cyanide concentrations (1–100 μM).[9]

5.2.1.2 Electrochemical impedance spectroscopy (EIS) studies

To further explore the ability of the SAM to detect anions, we used electrochemical impedance spectroscopy (EIS).[15] The impedance (Nyquist) plots for the monolayer coated gold electrode and various cyanide concentrations are shown in Figure 5.9. The charge transfer resistance, R_{ct}, was determined by fitting the experimental data to an equivalent circuit based on Randles circuit model [R(C(RW))](circuit explained and illustrated in Chapter 2). This parameter reflects the charge transfer resistance across the SAM and is used to evaluate the rate of electron-transfer to the solution containing the redox probe.[16]

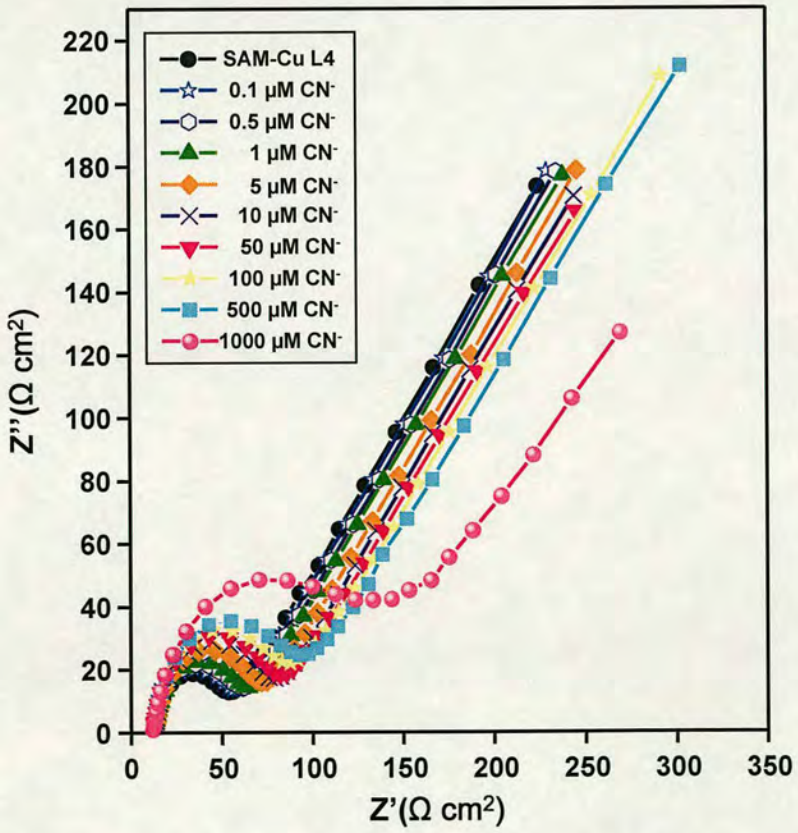

Figure 5.9: Impedance (Nyquist) plots of SAM-Cu**L4** in 1 mM $[Fe(CN)_6]^{3-/4-}$, 0.1 M NaCl and 0.1 M HEPES (pH = 7.3) in the absence and presence of increasing concentrations of CN^-, T = 293 K.

The SAM-Cu**L4** modified gold electrode exhibits a very small R_{ct} value of 32 Ω cm^2. This implies copper mediated electron-transfer across the molecular films. It can be observed from the impedance plots (Figure 5.9) that the R_{ct} values increase as the cyanide concentrations increase. Clearly, EIS is much more effective than cyclic voltammetry for detecting small changes in charge transfer resistance of SAMs. As a result, micromolar concentrations of cyanide (detection limit is 1 nM) are clearly revealed by impedance plots at pH = 7.3.

To further explore the potential of the SAM as a cyanide sensor we have investigated the response of the monolayer to other biologically important and potentially interfering anions such as $H_2PO_4^-$, NO_3^-, AcO^- and F^- using EIS in buffered aqueous solutions. Figure 5.10 shows the comparison of impedance plots obtained for the several anions studied in this work.

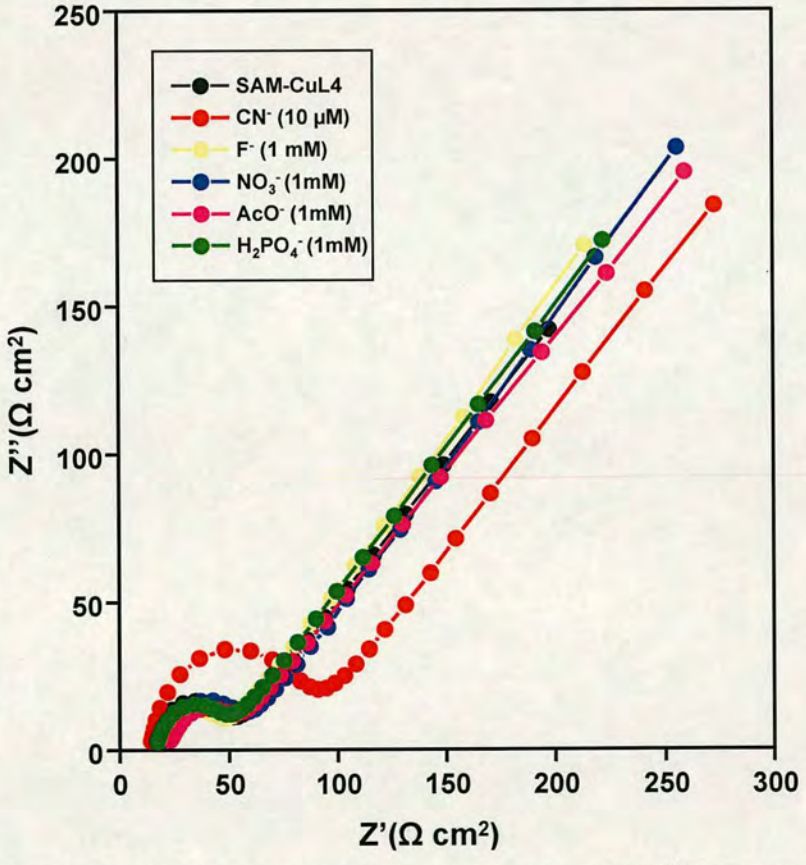

Figure 5.10: Impedance (Nyquist) plots of SAM-Cu**L4** in 1 mM $[Fe(CN)_6]^{3-/4-}$, 0.1 M NaCl and 0.1 M HEPES (pH = 7.3) in the absence and presence of different anions, T = 293 K.

With the exception of cyanide, the other anions did not change the charge transfer resistance of the SAM even at a high concentration of 1 mM. This implies that the electrochemical response of this SAM is cyanide-selective.

5.2.2 SAM-CuL4 after cyanide addition: surface characterization and cyanide sensing mechanism

The electrochemical response of the SAM on gold to cyanide in solution can arise from several processes, including one or several of the following: binding to the gold surface, binding to the Cu**L4** complex and removal of copper from the SAM to form $[Cu(CN)n]^{(n-1)-}$ species. To characterize this behaviour, we used X-ray photoelectron spectroscopy (XPS) and polarization-modulation reflection absorption IR spectroscopy (PM-RAIRS).

The PM-RAIRS spectra obtained for the adsorbed complex after the addition of CN^- ions did not show any band in the 2100–2300 cm^{-1} range that could be assigned to a cyanide stretching frequency (Figure 5.11).

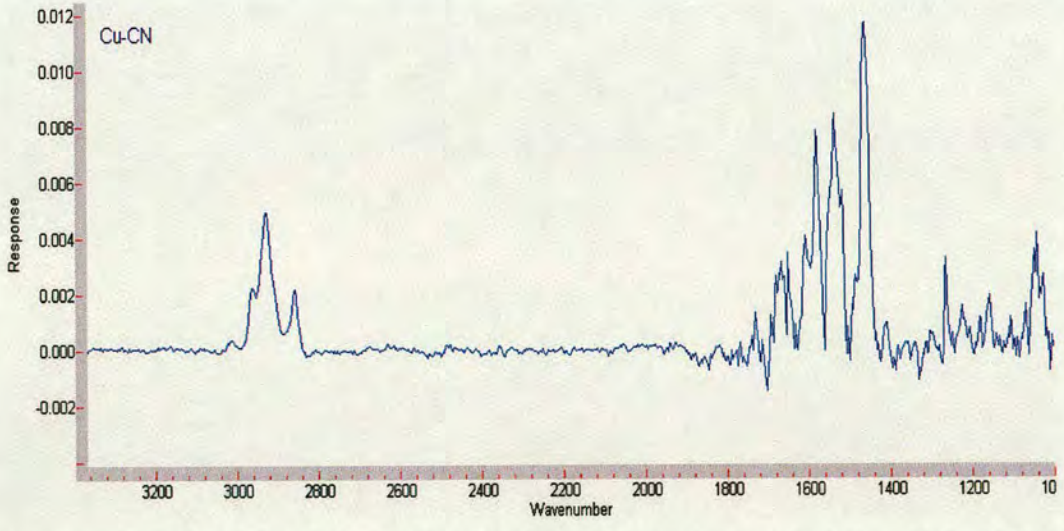

Figure 5.11: PM-RAIR spectrum of the SAM of copper complex of tris(2-pyridylmethyl)amine (TPA) based ligand (SAM-Cu**L4**) on gold surface after the addition of 100 μM CN^-.

Thus, it seems unlikely that the electrochemical behaviour is due to the formation of surface $[(\mathbf{L4})CuCN]^+$ complexes or cyanide binding to the gold surface.

XPS studies of the SAM-Cu**L4** showed peaks at 932.5 eV (Cu $2p_{3/2}$) and 952.3 eV (Cu $2p_{1/2}$) due to Cu(I) centres (see Chapter 4). After immersion of the SAM into water solutions with increasing cyanide concentrations, the intensity of these peaks progressively decreased, suggesting that copper was removed from the film, Figure 5.12.

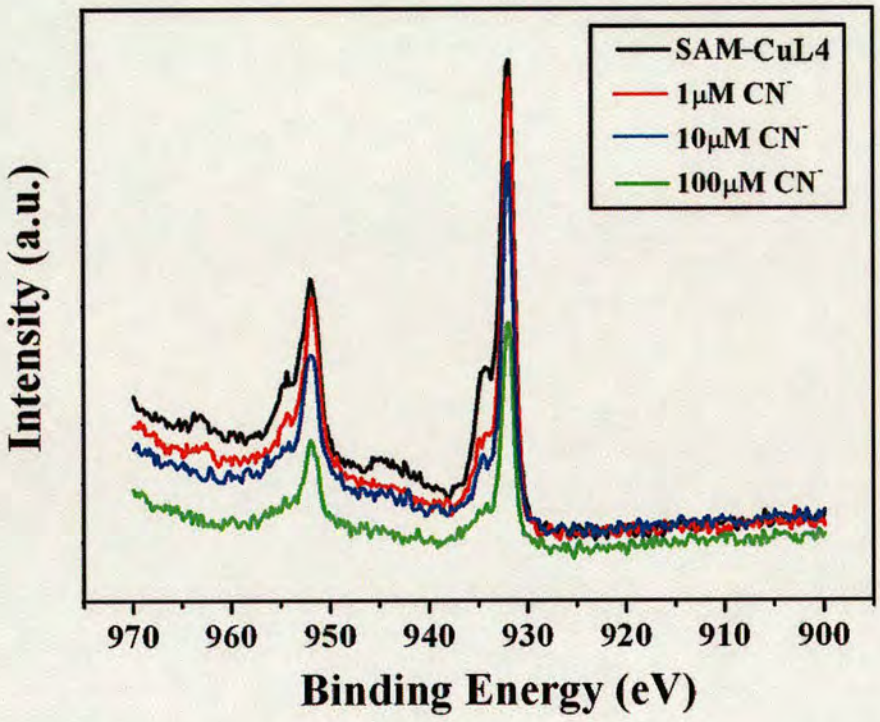

Figure 5.12: Copper 2p X-ray photoelectron spectra of the SAM-Cu**L4** before and after immersion into aqueous cyanide solutions.

This result is consistent with previous studies in which CN^- ions have been shown to remove copper ions from a range of environments.[13] The stability constants of copper complexes of ligands similar to **L4** and of $[Cu(CN)_n]^{(n-1)-}$ species have been determined,[11a,17] in bulk water, and the values suggest that copper abstraction from **L4** is feasible. In fact, after addition of cyanide the ^1H NMR of the paramagnetic $[(\mathbf{L4})CuCl]^+$ complex becomes indistinguishable from that of **L4**. The inability of cyanide to completely remove the copper from the SAM is consistent with the EIS studies, which showed that R_{ct} values in the presence of CN^- ions are lower than for the SAM of the ligand alone. This may be due to limited access of $HCN_{(g)}$ to the copper ions of the SAM.

5.3 Conclusions

In summary, in this chapter the ability of copper ions to affect the kinetics of electron- transfer across a copper binding SAM to a negatively charged redox probe in solution is combined with the ability of (H)CN to bind and remove copper ions to create a novel, sensitive and selective cyanide sensor that works under physiological conditions.

After titration of the SAM-Cu**L4** modified electrode with different anions such as CN^-, $H_2PO_4^-$, NO_3^-, AcO^- and F^-, it was found that only the CN^- anions induce changes in the R_{ct} parameter. Moreover, they do this even at nanomolar concentrations. The origin of the increase in R_{ct} could have been due to binding of CN^- to Cu**L4**, to the gold surface or due to the removal of Cu from the SAM. XPS and PM-RAIRS prove that copper ions are removed from the surface of the SAM and that CN^- anions are not bound to the SAM.

These studies also show that electrochemical impedance spectroscopy is an efficient and convenient technique to detect anions in aqueous solution. This work shows for the first time that the recently found ability of metal ions to affect electron-transfer process across SAMs can be exploited for sensing applications. Furthermore, this new sensor can detect nanomolar concentrations of CN^- using EIS. This is significant because anion sensors developed to date using SAMs have considerably worse detection limit (mM concentrations).

5.4 Experimental

Materials. Reagents were obtained from commercial sources and used as received unless otherwise noted. Solvents were dried and purified under N_2 by using standard methods and were distilled immediately before use. **L4** and $[(\mathbf{L4})CuCl]^+$ were prepared using the procedure described in previous chapter .

Preparation of evaporated gold samples. A gold sample of 99.99 % purity was used for the preparation of evaporated thin films of gold having a thickness of ~100 nm on glass with chromium underlayers (~ 2-5 nm thickness). The substrate was heated to 350°C during gold evaporation under a vacuum pressure of 2×10^{-5} mbar, a process that normally yields a very smooth gold substrate with predominantly Au(111) orientation. These gold samples were used as strips for the monolayer preparation and its characterization.

Monolayer preparation. Before SAM formation, the gold strips were chemically cleaned by immersing in a piranha solution (a mixture of H_2O_2 and conc.H_2SO_4 in 1:3 ratio) for 5-10 minutes. *Caution: piranha solution reacts violently with organic materials and therefore must be handled with extreme care.* Then, the slides were rinsed with water and methanol, dried under N_2 and used immediately.
Monolayers of Cu**L4** complex were prepared by immersing the cleaned gold strips into 10 mM methanol solutions of the complex in presence of $NaBH_4$ as a reducing agent for about 15-16 hours under N_2. After this, the SAM modified gold surfaces were rinsed with methanol and water and used immediately for the analysis.

Physical measurements.

Electrochemistry. All electrochemical studies were performed with an Autolab PGSTAT 20 instrument. The electrochemical blocking ability of the monolayers towards electron-transfer was studied by cyclic voltammetry and electrochemical impedance spectroscopy using $[Fe(CN)_6]^{3-/4-}$ redox couple as a probe. The electrolyte solutions used for electrochemical measurements were prepared using millipore

water having a resistivity of 17 M Ω. Cyclic voltammetry and impedance measurements were conducted in a three-electrode glass cell at 20 °C. A platinum rod, a saturated calomel electrode (SCE) and a monolayer-modified gold electrode were used as counter, reference and working electrodes respectively. Cyclic voltammetry was performed in 1 mM potassium ferrocyanide aqueous solution containing 0.1 M NaCl as a supporting electrolyte. Impedance measurements were carried out at the formal redox potential (as determined from cyclic voltammetry) in an aqueous solution containing equal concentrations of oxidized and reduced forms of $[Fe(CN)_6]^{3-/4-}$ (1 mM) with 0.1 M NaCl as a supporting electrolyte. The frequency ranging from 10 KHz to 0.1 Hz with an ac amplitude of 10 mV was used for the analysis. Impedance spectroscopy data were analyzed to determine the charge transfer resistance (R_{ct}), a parameter used to quantify the rate of electron-transfer across the interface.

Detection of anions. The sensitivity of monolayers to various anions such as cyanide (CN^-), phosphate ($H_2PO_4^-$), nitrate (NO_3^-), acetate (CH_3COO^-) and fluoride (F^-) were analyzed in an aqueous HEPES buffer solution (pH = 7.3) containing 1 mM $[Fe(CN)_6]^{3-/4-}$ with 0.1 M NaCl as a supporting electrolyte using cyclic voltammetry and electrochemical impedance spectroscopy. Cyanide (CN^-) salts were handled with extreme care. Risk assessments were undertaken prior to use of cyanide. The work was carried out using very small amounts of cyanide in a fume hood. Gloves and a mask and safety glasses were worn at all times when handling cyanide.
The concentration ranging from 1 nM to 1 mM was analyzed for all the anions studied in this work. The anions were added from a stock solution of their corresponding sodium salts having concentrations of 200 μM, 25 mM and 0.5 M in periodic increments to the aqueous buffer solution (20 ml) and stirred well before carrying out the analysis.

X-ray photoelectron spectroscopy (XPS). X-ray photoelectron spectra were obtained with a VG Scientific Sigma Probe (UK) XPS system. The Al Kα anode X-ray source ($h\upsilon$ = 1486.6 eV) was operated at 200 W and the take-off angle for photoelectrons was 37°. Samples were mounted with a spring clip. In a typical experiment, a few

survey scans in the -10 to 1100 eV kinetic energy range were collected at a resolution of 1 eV. Then, detailed scans of 20-60 eV over a single feature were collected at a resolution of 0.2 eV. During the measurements the pressure was 10^{-9}-10^{-10} Torr.

Polarization-modulation reflection absorption IR spectroscopy (PM-RAIRS). PM-RAIRS data were collected using a Nicolet Nexus 860 FTIR spectrometer using a N_2(l)-cooled mercury cadmium telluride (MCT) detector. A background spectrum of bare gold surface was taken and then the monolayer modified gold surfaces were exposed to collect the respective data.

5.5 References

(1) Selected reviews: (a) P. D. Beer and P.A. Gale, *Angew. Chem. Int. Ed.*, 2001, **40**, 486; (b) J. L. Sessler and J. M. Davis, *Acc. Chem. Res.*, 2001, **34**, 989; (c) P. D. Beer and S. R. Bayly, *Top. Curr. Chem.*, 2005, **255**, 125; (d) F. P. Schmidtchen, *Top. Curr. Chem.*, 2005, **255**, 1; (e) Various authors in *Anion Coordination Chemistry II*, ed. P. A. Gale, *Coord. Chem. Rev.*, 2006, **250**, 2917; (f) Various authors in 35 *Years of Synthetic Anion Receptor Chemistry*, 1968, ed. P. A. Gale, *Coord. Chem. Rev.*, 2003, **240**, 1; (g) S. O. Kang, A. R. Begum and K. Bowman-James, *Angew. Chem. Int. Ed.*, 2006, **45**, 7882; (h) J. Yoon, K. Sook, N. J. Singh and K. S. Kim, *Chem. Soc .Rev.*, 2006, **35**, 355.

(2) J. C. Mareque Rivas, R. Prabaharan and R. Torres Martin de Rosales, *Chem. Commun.*, 2004, 76.

(3) (a) S. L. Tobey, B. D. Jones and E. V. Anslyn, *J. Am. Chem. Soc.*, 2003, **125**, 4026; (b) B. P. Hay, T. K. Firman and B. A. Moyer, *J. Am. Chem. Soc.*, 2005, **127**, 1810.

(4) (a) A. Ojida,Y. Mito-oka, K. Sada and I. Hamachi, *J. Am. Chem. Soc.*, 2004, **126**, 2454; (b) H. K. Cho, D. H. Lee and J. I. Hong, *Chem. Commun.*, 2005, 1690; (c) H. N. Lee, Z. Xu, S. K. Kim, K. M. K. Swamy, Y. Kim, S. I. Kim and J. Yoon, *J. Am. Chem. Soc.*, 2007, **129**, 3828; (d) D. H. Lee, S. Y. Kim and J. I. Hong, *Angew. Chem. Int. Ed.*, 2004, **43**, 4777; (e) M. J. McDonough, A. J. Reynolds, W. Y. G. Lee and K. A. Jolliffe, *Chem. Commun.*, 2006, 2971.

(5) S. Zhang, C. M. Cardona and L. Echegoyen, *Chem. Commun.*, 2006, 4461.

(6) (a) P. D. Beer, J. J. Davis, D. A. Drillsma-Milgrom and F. Szemes, *Chem. Commun.*, 2002, 1716; (b) P. D. Beer, D. P. Cormode and J. J. Davis, *Chem. Commun.*, 2004, 414; (c) D. Astruc, M. C. Daniel and J. Ruiz, *Chem. Commun.*, 2004, 2637.

(7) (a) S. Zhang and L. Echegoyen, *J. Am. Chem. Soc.*, 2005, **127**, 2006; (b) S. Zhang, A. Palkar and L. Echegoyen, *Langmuir*, 2006, **22**, 10732.

(8) (a) C. O. Ikediobi and L. M. Latinwo, *Am. Environ. Lab.*, 1997, **9**, 20; (b) Ulmann's Encyclopedia of Industrial Chemistry, 6th edn., Wiley- VCH, New York, 1999; (c) G. C. Miller and C. A. Pritsos, *Cyanide: Social, Industrial and Economic*

Aspects, Proceedings of the TMS Annual Meeting, 2001, The Minerals, Metals and Materials Society, Warrendale, PA, USA, 2001, pp. 73–81.

(9) *Guidelines for Drinking-Water Quality*, World Health Organization, Geneva, 1996.

(10) (a) Jr. P. Anzenbacher, D. S. Tyson, K. Jursikova and F. N. Castellano, *J. Am. Chem. Soc.*, 2002, **124**, 6232; (b) R. Badugu, J. R. Lakowicz and C. D. Geddes, *J. Am. Chem. Soc.*, 2005, **127**, 3635; (c) F. García, J. M. García, B. García-Acosta, R. Martínez-Mañez, F. Sancenon and J. Soto, *Chem. Commun.*, 2005, 2790; (d) W. J. Jin, M. T. Fernández-Arguelles, J. M. Costa-Fernández, R. Pereiro and A. Sanz-Medel, *Chem. Commun.*, 2005, 883; (e) Y. G. Timofeyenki, J. J. Rosentreter and S. Mayo, *Anal. Chem.*, 2007, **79**, 251.

(11) (a) K. Kurnia, D. E. Giles, P. M. May, P. Singh and G. T. Hefter, *Talanta*, 1996, **43**, 2045; (b) N, Fujiwara, Y. L Liu, M. Takabashi and H. Kobayashi, *J. Electrochem. Soc.*, 2006, **153**, 6394.

(12) (a) N. Fujiwara, Y. L. Liu, M. Takabashi and H. Kobayashi, *J. Electrochem. Soc.*, 2006, **153**, G394; (b) R. Rahimi and P. Hambright, *J. Porphyrins Phthalocyanines*, 1998, **2**, 493.

(13) N. Solladie, J. C. Cambrón and J. P. Savage, *J. Am. Chem. Soc.*, 1999, **121**, 3684.

(14) E. Soto, J. C. MacDonald, C. G. G. Cooper and W. G. McGimpsey, *J. Am. Chem. Soc.*, 2003, **125**, 2838.

(15) (a) S. Zhang, C. M. Cardona and L. Echegoyen, *Chem. Commun.*, 2006, 4461; (b) Z. Zhang and L. Echegoyen, *J. Am. Chem. Soc.*, 2005, **127**, 2006; (c) S. Zhang, A. Palkar and L. Echegoyen, *Langmuir*, 2006, **22**, 10732; (d) S. Fink, B. A. Boukamp, A. Van den Berg, F. C. Van Veggel and D. N. Reinhoudt, *J. Am. Chem. Soc.*, 1998, **120**, 4652.

(16) (a) H. O. Finklea, D. Zinder, J. Fedyk, E. Sabatini, Y. Gafni and I. Rubinstein, *Langmuir*, 1993, **9**, 3660; (b) V. Ganesh and V. Lakshminarayanan, *Langmuir*, 2006, **22**, 1561.

(17) E. A. Ambundo, M. V. Deydier, A. J. Grall, N. Aguera-Vega, L. T. Dressel, T. H. Cooper, M. J. Heeg, L. A. Ochrymowycz and D. B. Rorabacher, *Inorg. Chem.*, 199 **38**, 4233.

Chapter 6

Phosphate detection

6.1 Introduction

We have previously discussed the importance of developing selective anion sensors due to their importance in many biological and chemical processes. Specifically, inorganic phosphate anions and their derivatives play important roles in signal transduction and energy storage in biological systems. Important examples are phosphate ($H_2PO_4^-$, Pi), pyrophosphate ($P_2O_7^{4-}$, PPi), AMP (adenosine mono-phosphate), ADP (adenosine diphosphate) and ATP (adenosine triphosphate). For instance, PPi and ATP play an important role in energy transduction in living organisms and control metabolic processes by participation in enzymatic reactions.[1] ATP hydrolysis with release of PPi is central to many biochemical reactions, such as DNA polymerization and the synthesis of cyclic adenosine monophosphate (AMPc) catalyzed by DNA polymerase.[1,2] Therefore, the detection and discrimination of these anions have been the main research focus for many research groups. Few of the sensors reported to date display high selectivity and reliability and function in water. Figure 6.1 shows the structure and the pK_a of some of these phosphoanions, which is important to understand their host: guest properties in water.

Structures of various phosphates and their pK_a values

Phosphate (Pi)

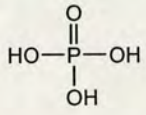

pk_a: 2.12, 7.21, 12.32

Pyrophosphate (PPi)

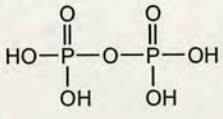

pk_a: 1.52, 2.36, 6.60, 9.25

Adenosine triphosphate (ATP)

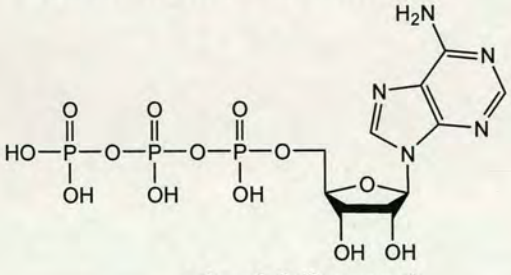

pk_a: 6.6 (3 strong)

Adenosine diphosphate (ADP)

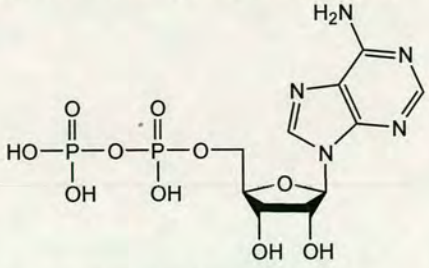

pk_a: 6.6 (2 strong)

Figure 6.1: Chemical structures of some important biological phosphates.

There are many examples in the literature of phosphate sensors based on fluorescence methods due to their simplicity and the high sensitivity of the technique.[3]

In 1994, Czarnik et al. reported the results of a pioneering study in which an anthracene derivative bearing polyamine groups was used as a PPi sensor in 100% water. This sensor was capable of discriminating between Pi (K_d = 6.3 mM) and PPi (K_d = 2.9 μM) on the basis of size (Figue 6.2 (a)).[4] However, it was difficult to apply this sensor for biological applications because the receptor unit is a polyamine ligand which chelates metal ions, and this also changes the fluorescence properties of the sensor. Almost a decade later, Kikuchi et al. used a Cd(II) cyclen coumarin system as a fluorescent chemosensor for PPi (K_d = 75 μM) in an aqueous solution (Figure 6.2 (b)),[5] but this system shows also high affinity for citrate anion (K_d = 90 μM).

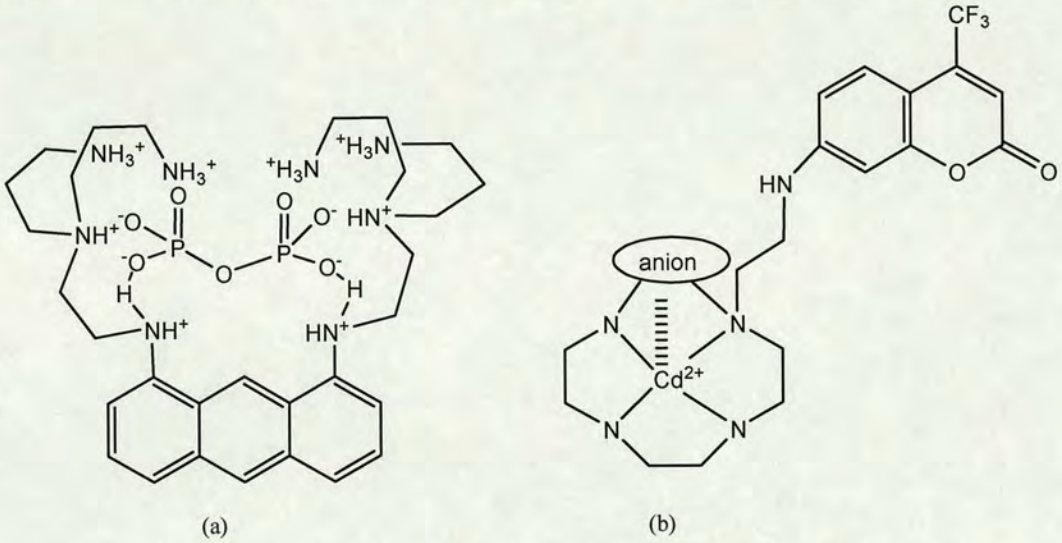

Figure 6.2: PPi sensors developed by (a) Czarnik[4] and (b) Kikuchi[5] and their co-workers.

A few indicator displacement systems for PPi using changes in fluorescence have been reported by Jolliffe et al.[6] Smith et al.[7] and Fabrizzi et al. (Figure 6.3).[8]

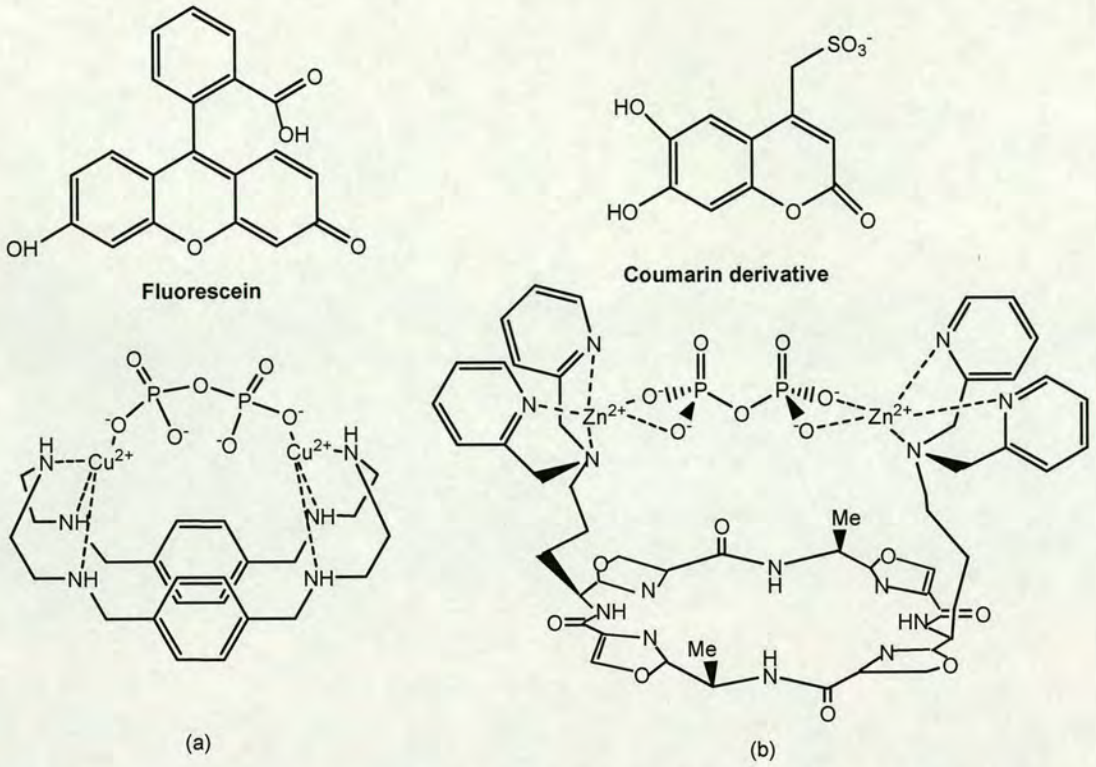

Figure 6.3: PPi fluorescent sensors developed by (a) Fabrizzi[8] and (b) Jolliffe[6] and their co-workers.

The system showed in Figure 6.3 (a) was developed by Fabrizzi et al. and uses fluorescein as an indicator. The dissociation constant (K_d) of the complex it forms with PPi is 0.06 μM, whereas the K_d for the complex with Pi is 39.8 μM. Jolliffe et al. developed a cyclic peptide receptor bearing two Zn(II)-BPA [BPA: bis(2-pyridylmethyl)amine] groups which was found to have high affinity towards phosphate derivatives (at neutral pH) in aqueous solution.[6,9] This system uses a coumarin derivative as an indicator and the complex it forms with PPi has a dissociation constant of 0.01μM, at least two orders smaller than with ATP, ADP and citrate, indicating that the system has a high selectivity for PPi over other anions. Notably, no response was observed with Pi.

Other Zn(II)-BPA sensors have been developed by Hong et al. (Figure 6.4).[10,11] In these sensors a phenoxide provides a central oxygen atom to pre-organize the binding pocket formed by the two Zn(II)-BPA units. The phenoxide also forms a conjugation pathway that electronically connects the anion association site to the chromophore.

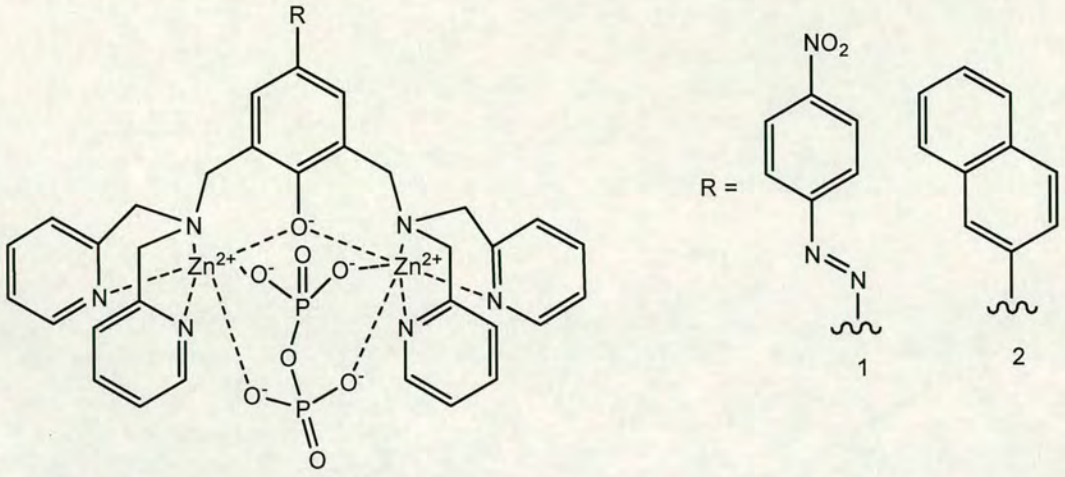

Figure 6.4: Association of PPi to Zn(II)-BPA sensors with a phenoxy bridge.[10,11]

The nature of R can be used to change the nature of the optical signal. Compound 1 is a colorimetric sensor,[10] whereas compound 2 is a fluorescence sensor.[11] Both receptors are selective to PPi in water even in the presence of other phosphate-containing compounds such as Pi and ATP.

System 1 shows changes in the UV-vis spectra upon addition of PPi and no detectable spectral change upon addition of Pi or other anions such as $CH_3CO_2^-$, F^-, HCO_3^- and Cl^-. This system shows a good selectivity for PPi with a K_d = 0.001 μM even in the presence of excess of Pi. The binding mode for the PPi-Zn complex was revealed by X-ray analysis (Figure 6.5).

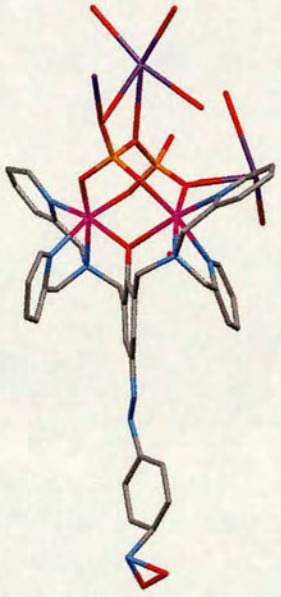

Figure 6.5: Crystal structure of PPi bound to the dinuclear Zn(II) complex of BPA derivative (Compound 1 from Figure 6.4).

In the case of system 2 the presence of PPi is signalled by changes in the emission intensity of the luminescent sensor, exhibiting high selectivity and sensitivity relative to other anions including ATP and ADP (which are structurally similar to PPi). Upon addition of PPi, a 6-fold increase of the emission intensity is noted (K_d = 0.003 μM). Added ATP leads to a 2-fold increase of emission intensity (K_d = 0.13 μM) which is 40-fold lower than PPi. Competition experiments showed selectivity for PPi over ATP, even in the presence of a large excess of ATP, with a detection limit at micromolar concentrations. This was understood to arise from the structure of the guest and differences in the charge density of the oxygen atoms involved in complexation to the Zn(II) ions.

These examples were based on strategically positioning the two metal binding units and using a suitable spacer connecting these to the signalling unit. There are other strategies in which the phosphate complexation itself induces self-assembly of the receptor and this is used for sensing.[3g,12] For instance, Yoon and al. have recently reported the PPi sensor based on the formation of an excimer (Figure 6.6).[13]

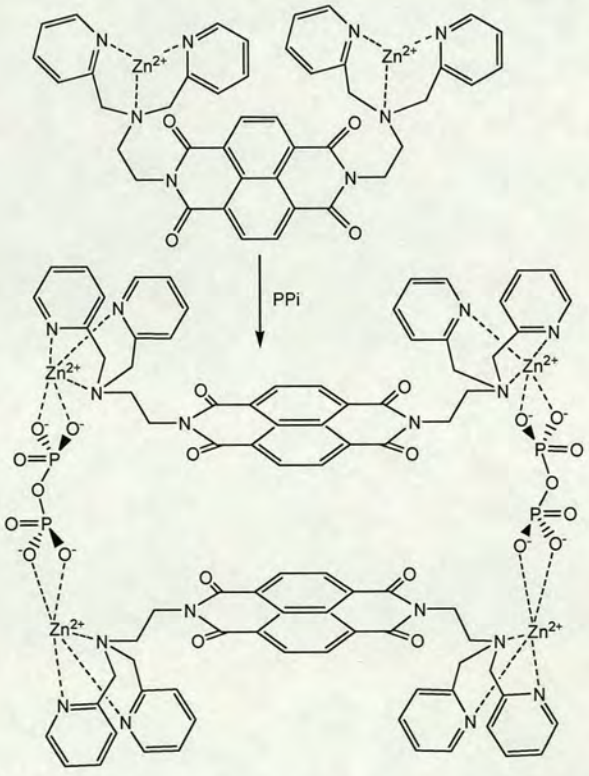

Figure 6.6: Proposed binding mechanism of the chemosensor with PPi.[13]

This chemosensor is highly selective to PPi in the presence of ATP or Pi. The low dissociation constant (2.43 μM) and high selectivity were explained by two cooperative factors. The total anionic charge density of the four O-P oxygen atoms involved in the complexation between ATP and the two Zn(II) sites is smaller than that of the four O-P oxygen atoms of PPi. In addition to the four Zn(II) binding sites for PPi, the favourable π-π interaction of two flat aromatic centre moieties can induce tight 2+2 type binding between the compound and PPi. This is the first example of PPi fluorescent sensor based on 2+2 type excimer formation.

SAM-modified gold electrodes have also been used to develop new phosphate sensors.[14] Beer et al. have reported a Pi anion sensor based upon a SAM-modified gold electrode with an amido ferrocene derivative (Figure 6.7 (a)).[15] By introducing hydrogen bond donor amide groups near the ferrocene redox centre it is possible to recognise specific anions as shown by the perturbation of the ferrocene redox potential. It was found that when these molecules with anion recognition properties are transferred from the solution to the solid state the response is amplified by the surface pre-organisation of the host.

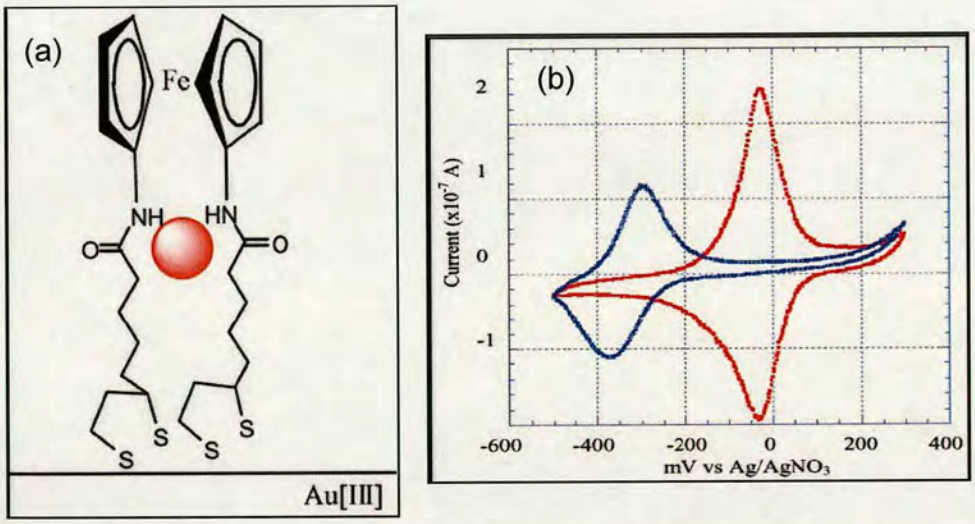

Figure 6.7: (a) Schematic representation of anion binding within the surface host 1,1'-bis(alkyl-N-amido) ferrocene; (b) Voltammetric response of the monolayer in the absence (red) and presence (blue) of $H_2PO_4^-$ (8 mM).[15]

The voltammogram of a monolayer obtained (Figure 6.7 (b)) in the absence and presence of Pi anion reveals cathodically shifted waves characterised by greater peak

separation (blue) than observed in the precursor ferrocene couple (red). The system is able to detect an 8 mM concentration of Pi in CH_2Cl_2/CH_3CN.

In this chapter, we investigate the phosphate recognition properties of Zn(II) containing SAMs of **L7** by using electrochemical techniques. Zn-BPA complexes, with a similar bridging unit, have been used to detect phosphates by fluorescence.[10,11] Here, the incorporation of this receptor unit onto gold electrodes to retain/improve the phosphate recognition properties in water due to the surface pre-organisation is studied and therefore can be used to detect these species electrochemically.

6.2 Results and discussion

As mentioned in Chapter 4, SAM-**L7** was formed by dipping the electrode in a solution containing **L7** and adding $NaBH_4$ to form dithiolate linkages. Then, SAM-**L7** was kept in a solution of $ZnCl_2$ for 3 h to obtain SAM-Zn**L7** (Figure 6.8).

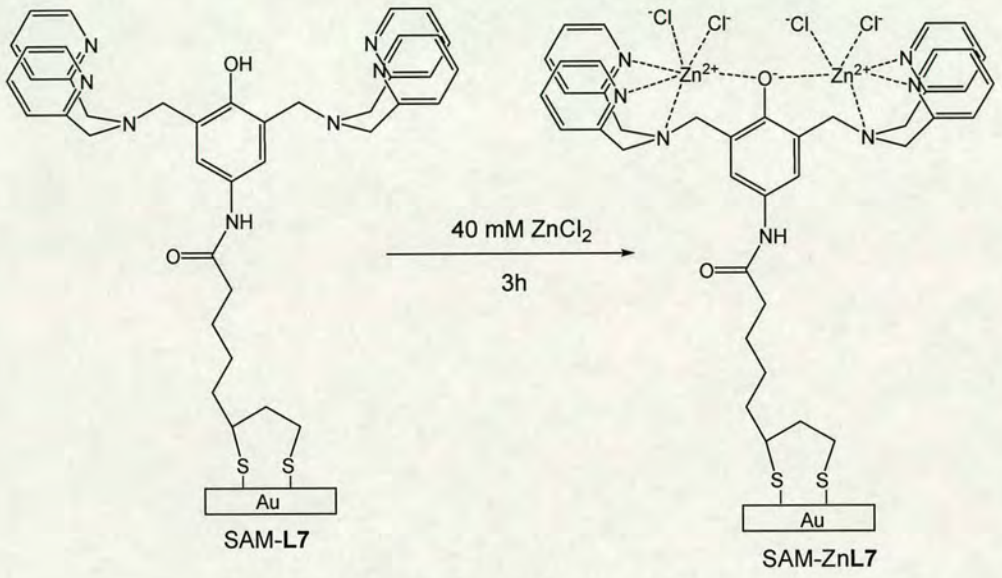

Figure 6.8: Scheme of SAM-Zn**L7** preparation.

The interfacial recognition process of Pi and PPi was followed by electrochemical impedance spectroscopy because it gives more information about the monolayer/solution interfaces than cyclic voltammetry (CV). The charge transfer resistance, R_{ct}, was used as a parameter to evaluate the electron transfer process to the solution containing the redox probe, and to detect if any change occurs at the interface after the addition of the phosphate anions.

All the impedance experiments were performed in aqueous solution of 1 mM $[Fe(CN)_6]^{3-/4-}$ as a redox probe, 0.1 M NaCl as a supporting electrolyte and in 0.1 M HEPES buffer (pH = 7.0).

6.2.1 Pyrophosphate and phosphate binding studies using SAM-ZnL7

Figure 6.9 shows the Nyquist plots for the SAM-Zn**L7** modified electrode, before and after the addition of different amounts of PPi.

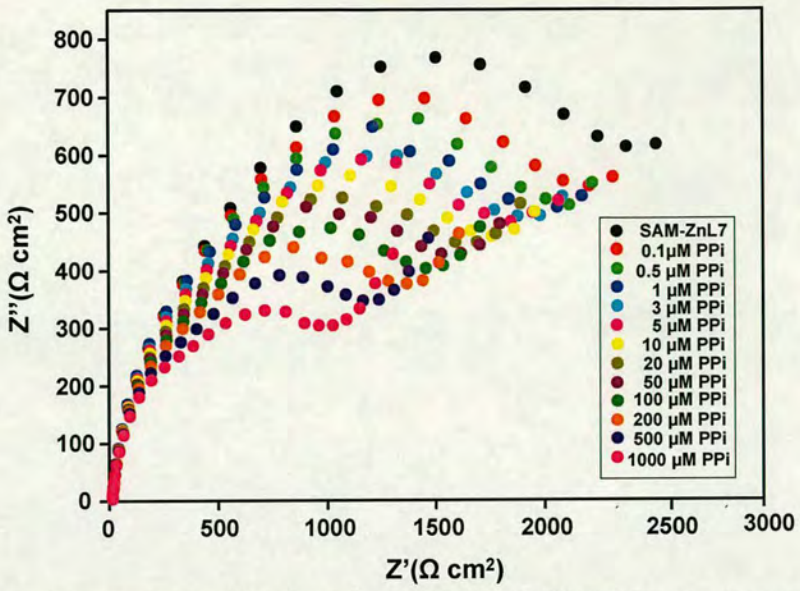

Figure 6.9: Impedance response of the electrode modified by SAM-Zn**L7** in the absence and presence of increasing concentrations of PPi. The measurements were done in 1 mM $[Fe(CN)_6]^{3-/4-}$, 0.1 M NaCl and in 0.1 M HEPES buffer (pH = 7.0).

It shows that R_{ct} decreases as PPi anion is added. For example, it decreases from 2988 Ω cm^2 in absence of PPi to 1284 Ω cm^2 at 1 mM of PPi. This suggests that PPi coordinates to the SAM-Zn**L7** complex and that this facilitates the electron transfer reaction to the redox probe.

In contrast, the titration experiments with Pi showed considerably smaller changes (Figure 6.10).

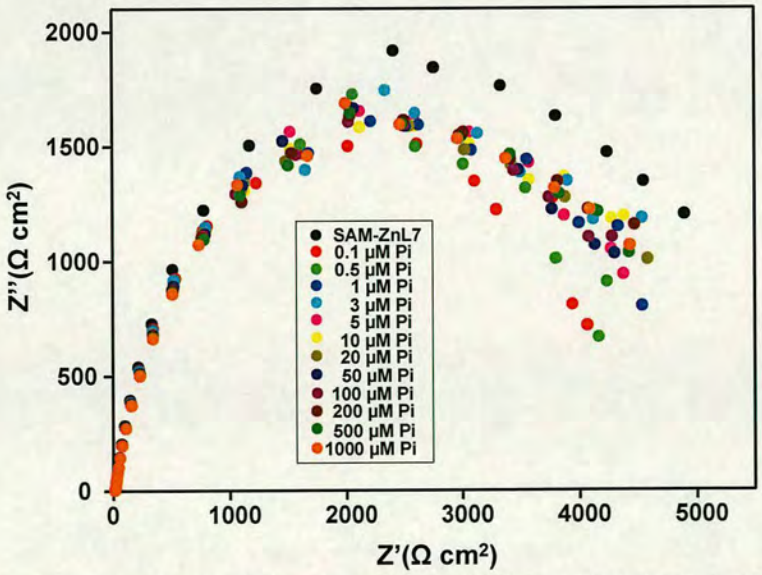

Figure 6.10: Impedance response of the electrode modified by SAM-Zn**L7** in the absence and presence of increasing concentrations of Pi. The measurements were done in 1 mM $[Fe(CN)_6]^{3-/4-}$, 0.1 M NaCl and in 0.1 M HEPES buffer (pH = 7.0).

The addition of Pi results in a small decrease in the value of R_{ct} from 5304 Ω cm^2 in the absence of Pi to 4649 Ω cm^2 in the presence of 1 mM of Pi. These results seem to suggest that either only a small amount of Pi binds to the SAM-Zn**L7** or that Pi binding induces only small changes on the electron-transfer process.

For comparison, the R_{ct} changes induced by increasing concentrations of PPi and Pi are plotted together in Figure 6.11.

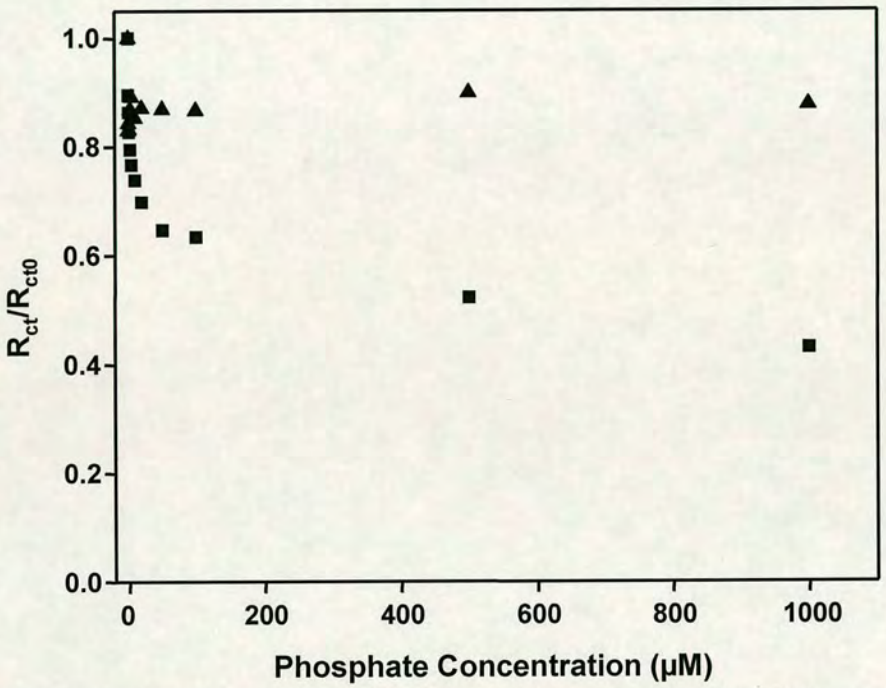

Figure 6.11: Comparative plots of the change of R_{ct} versus concentrations of the different phosphate: ▲ Pi; ■ PPi. (R_{ct0} = R_{ct} of SAM-Zn**L7** before adding phosphates).

6.2.2 Competition studies between pyrophosphate and phosphate anions

Competition studies were carried out in order to study the selectivity of the system to Pi or PPi.

6.2.2.1 Pyrophosphate detection studies in the presence of high concentration of phosphate.

To investigate the response of the system to PPi at high concentrations of Pi, SAM-Zn**L7** was first titrated with Pi until 100 μM, showing a decrease of 25 % in the value of R_{ct} (Figure 6.12).

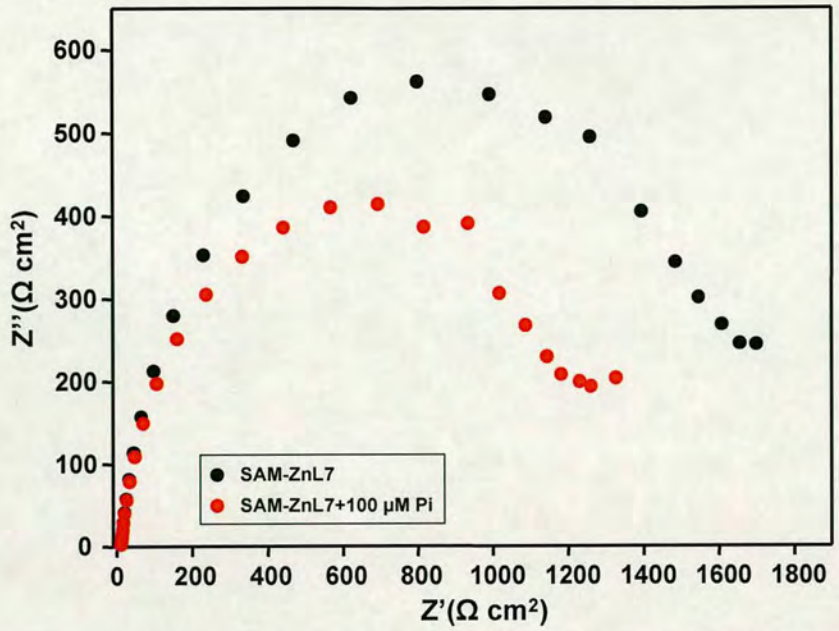

Figure 6.12: Impedance response of the electrode modified by SAM-Zn**L7** and SAM-Zn**L7** after adding 100 µM of Pi. The measurements were done in 1 mM $[Fe(CN)_6]^{3-/4-}$, 0.1 M NaCl and in 0.1 M HEPES buffer (pH = 7.0).

Then, SAM-Zn**L7** was titrated with PPi (0.1 µM-1 mM). Changes in R_{ct} were observed already at 0.1 µM PPi from 1280 to 1120 Ω cm^2 (Figure 6.13).

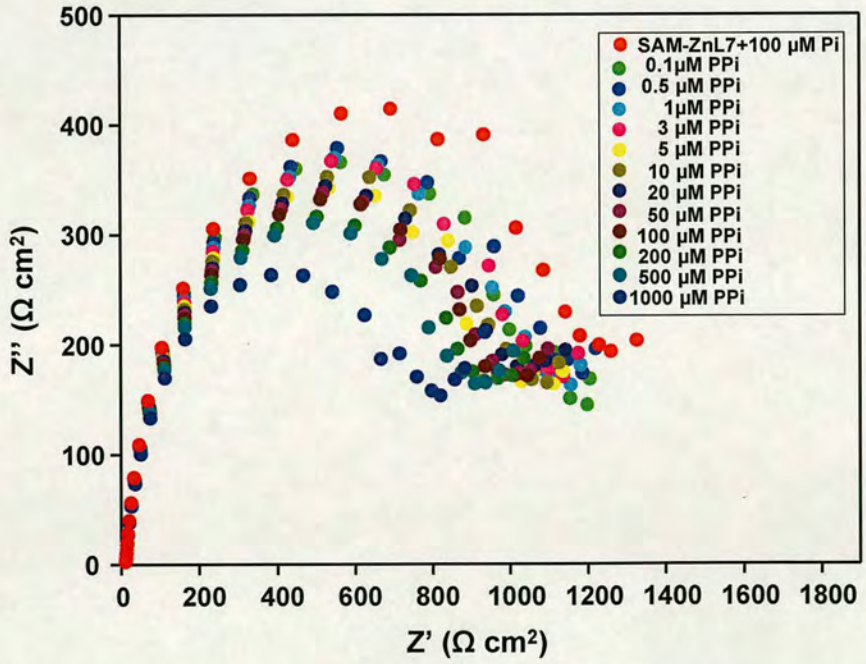

Figure 6.13: Impedance response of the electrode modified by SAM-Zn**L7** in the presence of 100 µM of Pi and after adding increasing concentration of PPi. The measurements were done in 1 mM $[Fe(CN)_6]^{3-/4-}$, 0.1 M NaCl and in 0.1 M HEPES buffer (pH = 7.0).

Considering that after the addition of 20, 50 and 100 μM of Pi R_{ct} value was almost constant, 1300, 1300 and 1280 Ω cm^2 respectively, the decrease in R_{ct} is attributed to PPi binding. In principle, PPi can bind to metal sites that are not occupied by Pi or displace Pi molecules bound to the SAM. To elucidate this, it is important to compare the R_{ct} changes induced by PPi in the presence and absence of Pi (Figure 6.14).

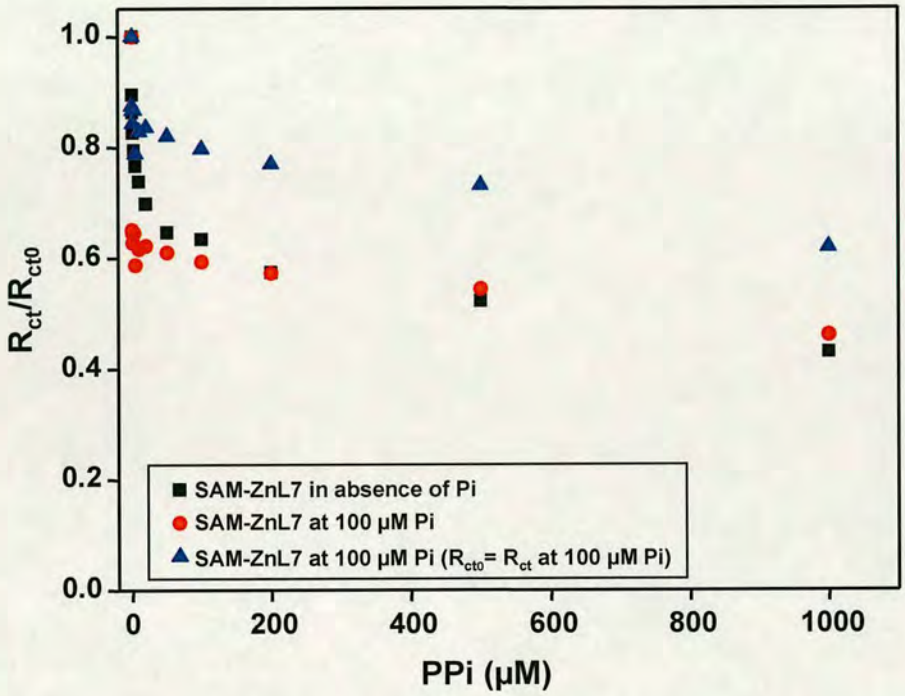

Figure 6.14: Plot of R_{ct} changes upon addition of PPi: ■, SAM-Zn**L7** titration with PPi in the absence of Pi; ▲, SAM-Zn**L7** titration with PPi in the presence of 100 μM of Pi, R_{ct0} = R_{ct} at 100 μM Pi; ●, SAM-Zn**L7** titration with PPi in the presence of 100 μM of Pi, R_{ct0} = R_{ct} before adding Pi and PPi.

The affinity of the SAM for PPi seems to be the same in the presence and in the absence of Pi (Figure 6.14). Thus, at low concentrations of PPi ([PPi] < 50μM), similar R_{ct} changes (R_{ct}/R_{ct0}) are observed for the SAM-Zn**L7** in the presence of 100 μM of Pi, (blue triangles, where R_{ct0} = R_{ct} at 100 μM of Pi) and in absence of Pi (black squares). This suggests that the PPi molecules coordinate at binding sites that are not occupied by Pi, inducing similar response and that Pi does not interfere with PPi binding. At higher concentrations of PPi ([PPi] > 50 μM), the overall changes induced by PPi (red circle, where R_{ct0} = R_{ct} before Pi and PPi) are the same as in the absence of Pi (black squares). At that concentration, competition between PPi and Pi is possible. Overall R_{ct} changes are the same compared to the values in the absence

of Pi; this is consistent with PPi being able to substitute the Pi molecules which in turn is consistent with the observations in solution.[10]

6.2.2.2 Phosphate detection studies in the presence of high concentration of pyrophosphate

The opposite studies were also carried out, that is, Pi detection studies in the presence of 100 μM PPi. As before, SAM-Zn**L7** was first titrated with PPi until 100 μM, decreasing R_{ct} value by 42.72 % (Figure 6.15), and then Pi was added (0.1 μM - 1 mM) (Figure 6.16).

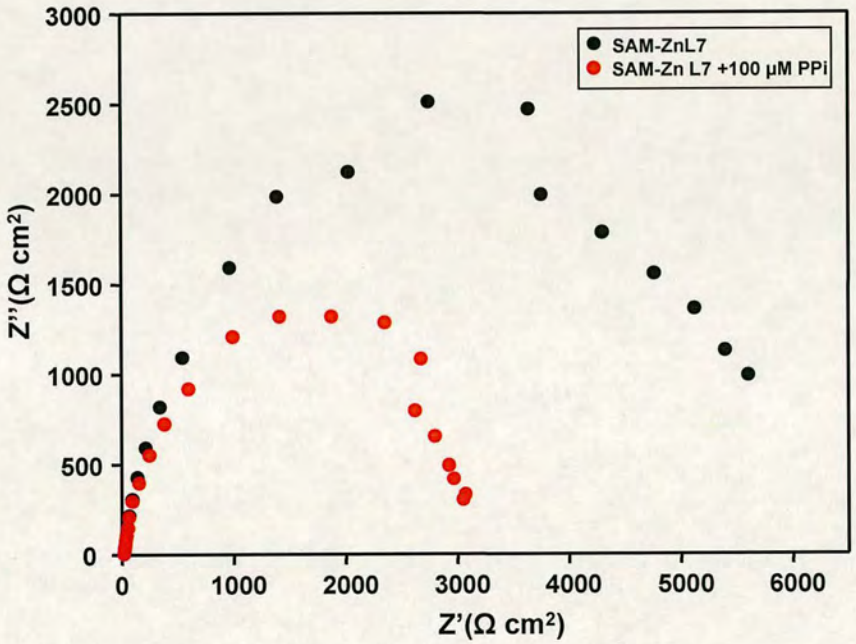

Figure 6.15: Impedance response of the electrode modified by SAM-Zn**L7** and SAM-Zn**L7** after adding 100 μM of PPi. The measurements were done in 1 mM $[Fe(CN)_6]^{3-/4-}$, 0.1 M NaCl and in 0.1 M HEPES buffer (pH = 7.0).

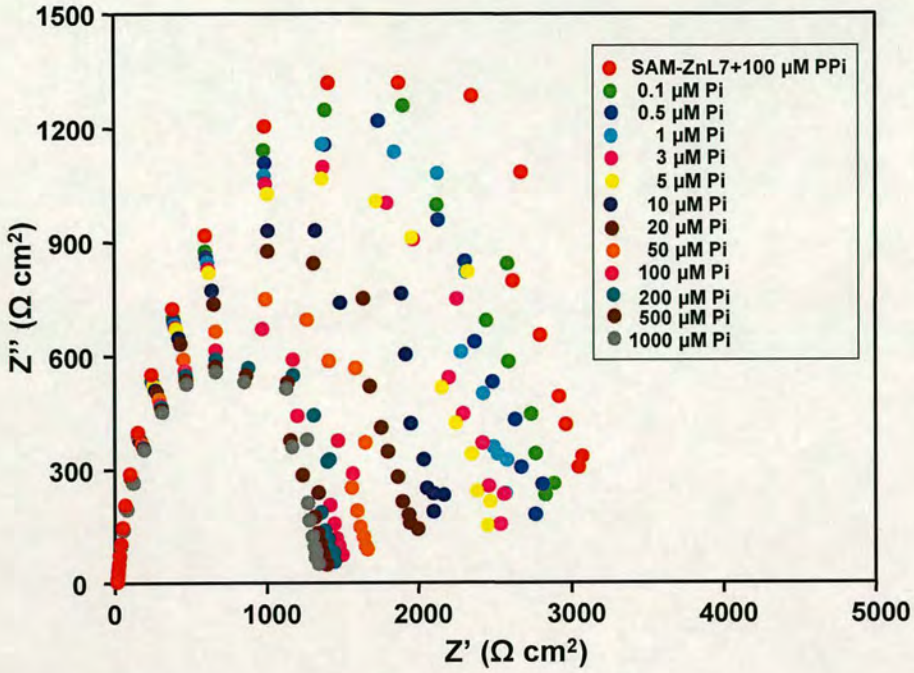

Figure 6.16: Impedance response of the electrode modified by SAM-Zn**L7** in the presence of 100 µM of PPi and after adding increasing concentrations of Pi. The measurements were done in 1 mM $[Fe(CN)_6]^{3-/4-}$, 0.1 M NaCl and in 0.1 M HEPES buffer (pH = 7.0).

According to the above mentioned results, it could have been reasonable to expect no (or very small) changes upon the addition of Pi in the presence of high concentrations of PPi, as Pi should have less affinity for the SAM than PPi.

However, as the concentration of Pi increases, R_{ct} decreases dramatically. The addition of 0.1 µM Pi induces already a small decrease in R_{ct} and as the concentration of Pi increases the R_{ct} value decreases from 3114 Ω cm^2 (at 100 µM of PPi) in the absence of Pi, to 1328.4 Ω cm^2 at 100 µM of Pi (from 100 µM of Pi R_{ct} almost does not change).

The changes observed (R_{ct}/ R_{ct0}) in the presence of 100 µM of PPi and those obtained in its absence are plotted in Figure 6.17.

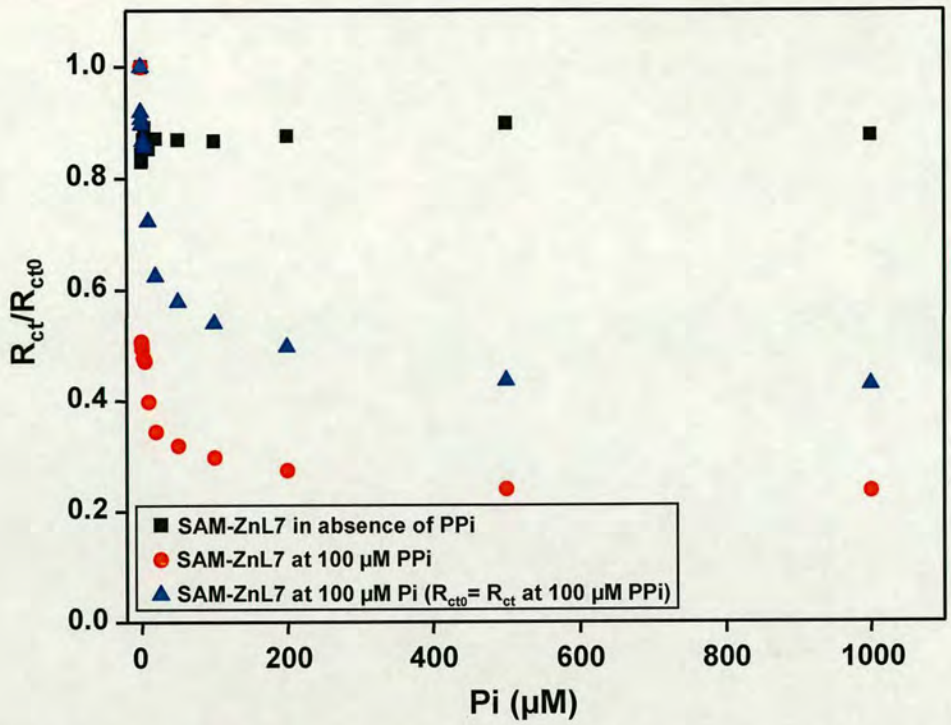

Figure 6.17: Plot of R_{ct} changes upon addition of Pi: ■, SAM-Zn**L7** titration with Pi in the absence of PPi; ▲, SAM-Zn**L7** titration with Pi in the presence of 100 μM of PPi, R_{ct0} = R_{ct} at 100 μM PPi; ●, SAM-Zn**L7** titration with PPi in the presence of 100 μM of Pi, R_{ct0} = R_{ct} before adding Pi and PPi.

In the presence of PPi the changes are surprisingly much larger, and saturate at around 100 μM Pi. This suggests that the presence of PPi at the interface of the monolayer may facilitate the coordination of Pi inducing a high response.

6.2.3 Mechanism by which phosphate anions facilitate the electron-transfer reaction

From the PPi and Pi binding studies it is clear that addition of PPi and Pi decreases R_{ct} and that this must be due to coordination to the SAM-Zn**L7**. Thus, they facilitate the electron transfer process to the redox probe. In the case of Pi, its addition decreases R_{ct} only to a very small extent. For both phosphates it could have been expected the opposite result, addition and complexation of anions at the interface should generate an electrostatic repulsion with the negative charge redox probe, decreasing the electron transfer process. The results obtained can be justified by taking into account of the counter ion effects.

In Chapter 4, the enhanced blocking effect of SAM-Zn**L7** compared to SAM-**L7** was justified as being a consequence of the overall negative charge of SAM-Zn**L7** due to chloride binding. It was proposed that a film of solvated counter ions between SAM-Zn**L7** and the negative redox probe decreases the electron transfer process (Figure 6.18).

Upon phosphate addition, the chloride anions may be replaced by the phosphates, which can interact with the counter ions via the oxygen atoms. This could help to reduce the thickness of the counter ion film (Figure 6.18) by reducing the solvation shell of the cation. This should allow a closer approach of the redox probe, facilitating the electron-transfer process.

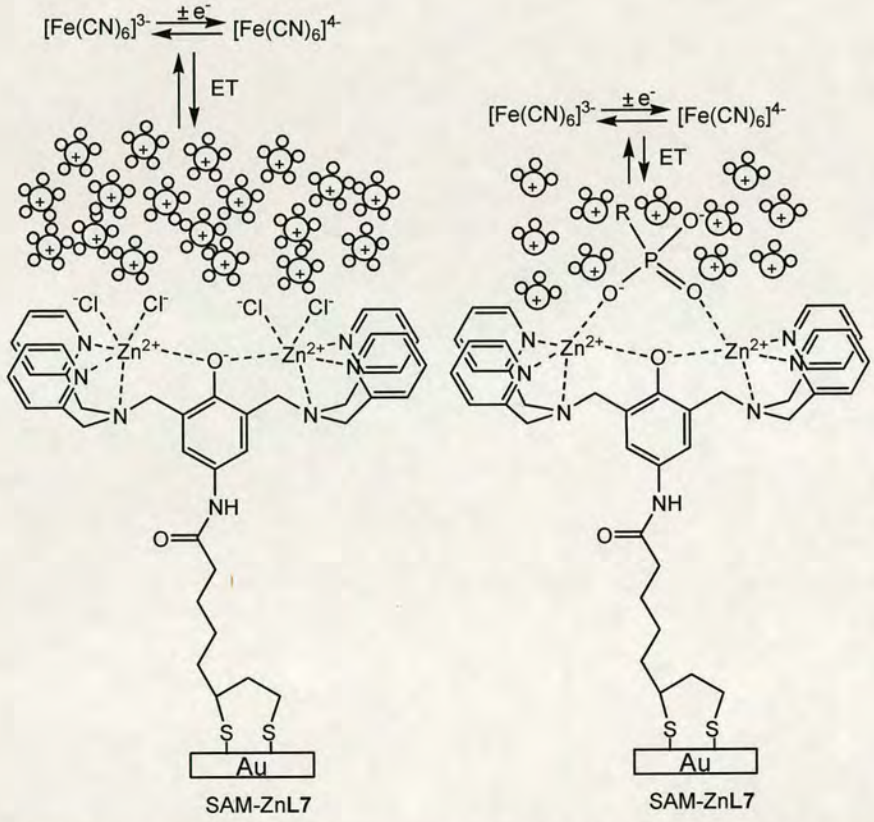

Figure 6.18: Scheme of electron-transfer process proposed for SAM-Zn**L7** before and after phosphate addition.

Among the two types of phosphates studied, SAM-Zn**L7** shows higher response to PPi than for Pi. These results agree with previous studies with a similar dinuclear Zn complexes in solution,[7,10,11] which showed more affinity for PPi than for Pi.

This was further confirmed by competition studies, even in the presence of 100 μM of excess Pi (100 μM) low concentrations of PPi (e.g. 0.1 μM) induce changes in the R_{ct} value. At higher PPi concentrations the overall changes are identical than in absence of 100 μM Pi, suggesting that PPi could replace Pi. From these studies we have also observed that the presence of PPi at the monolayer may facilitate Pi binding. The results can be also justified based on the counter-ion effect (Figure 6.19).

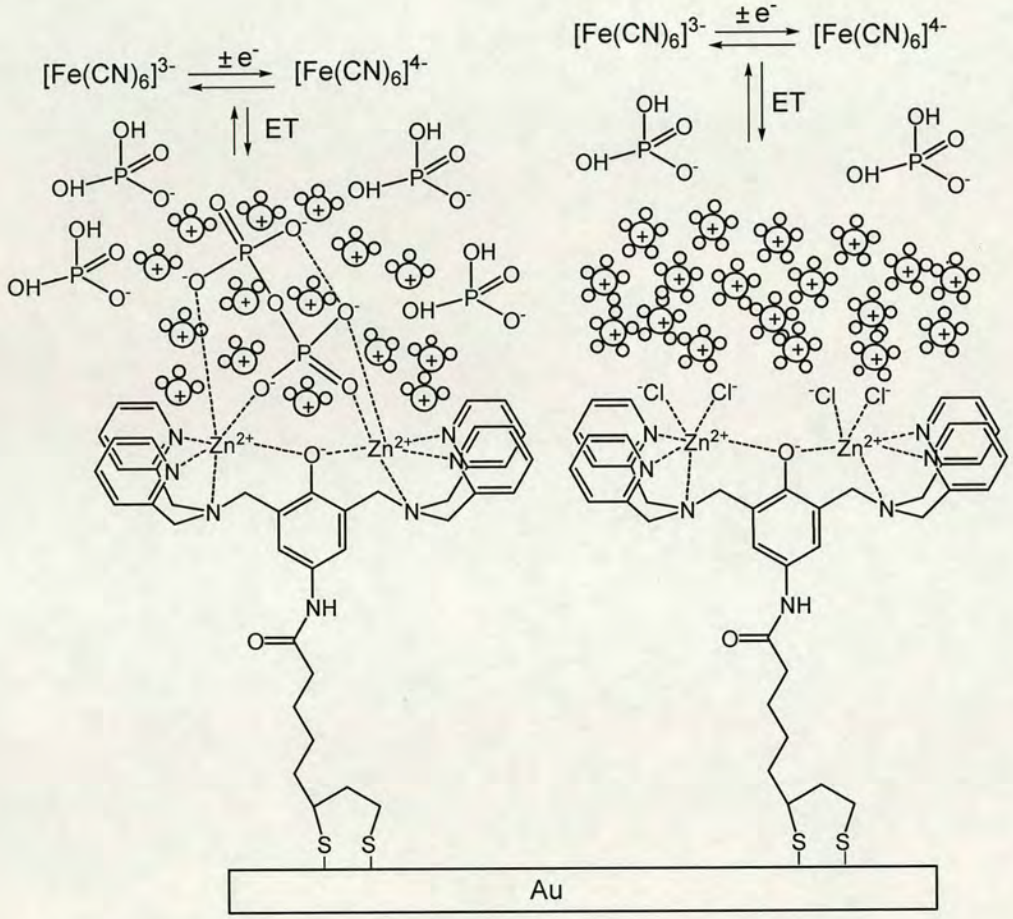

Figure 6.19: Scheme of Pi binding to a SAM-Zn**L7** containing PPi.

When PPi is bound to SAM-Zn**L7**, faster electron transfer to the redox probe is observed due to the thinner layer of counter ions formed between the SAM and the redox probe, as we discussed previously. Since Pi is also anionic, it will also be strongly attracted to SAM-Zn**L7** containing PPi. Consequently this helps in the approach of Pi to free metal binding sites available.

6.3 Conclusions

This chapter has presented the ability of SAM-Zn**L7** to recognize PPi anions. It is known that Zn(II) complexes similar to Zn**L7** can detect nanomolar and micromolar concentrations of phosphates in aqueous solution using techniques such as fluorescence or UV-vis. Here, we report the development of a new sensor for phosphate anions in aqueous solution by using electrochemical techniques such as electrochemical impedance spectroscopy (EIS).

SAM-Zn**L7** was titrated with two different phosphates: Pi and PPi. PPi induced clear changes in the R_{ct} parameter, whereas Pi generates very small changes. The changes observed were a decrease in R_{ct} value, suggesting that the phosphates complexates at the SAM-interface and as consequence the electron-transfer process to the redox probe ($[Fe(CN)_6]^{3-/4-}$) increases.

The R_{ct} changes are attributed to the capacity of the phosphates to substitute the chloride anions bound to the SAM-Zn**L7.** This suggests it has remarkably higher affinity for phosphates over chloride as the chloride concentration is 0.1 M compared to nM-μM concentrations of phosphates. The oxygen atoms of the phosphate can interact with the counter-ions and as a result these will be less solvated, creating a thinner interface between the electrode and redox probe.

Competition studies were done and suggest that SAM-Zn**L7** is selective for PPi. In the presence of 100 μM of Pi the system can detect μM concentration of PPi. The behaviour of the system is similar to in the absence of Pi, confirming that SAM-Zn**L7** has high affinity for PPi.

6.4 Experimental

Materials. Reagents were obtained from commercial sources and used as received unless otherwise noted. Solvents were dried and purified under N_2 by using standard methods and were distilled immediately before use. All the reactions were carried out under N_2.

Preparation of evaporated gold samples. A gold sample of 99.99% purity was used for the preparation of evaporated films of gold having a thickness of ~100 nm on glass with chromium underlayers (~ 2-5 nm thickness). The substrate was heated to 350 °C during gold evaporation under vacuum pressure of 2×10^{-5} mbar, a process that normally yields a very smooth gold substrate with predominantly Au(111) orientation. These gold samples were used as strips for the monolayer preparation and its characterization.

Monolayer preparation. Gold electrodes were chemically cleaned by immersing in a piranha solution for 5-10 minutes. *Caution: piranha solution reacts violently with organic materials and therefore must be handled with extreme care.* Before SAM formation, gold electrodes were electrochemically cleaned by potential cycling in an aqueous solution of 0.1 M $HClO_4$ to obtain the characteristic Au oxide formation and stripping peaks corresponding to bare Au surface using cyclic voltammetry. After electrochemical cleaning, the electrodes were rinsed with water and methanol and dried under a stream of N_2.

*SAM-Zn**L7** formation*: SAM-**L7** was previously formed by dipping the cleaned evaporated gold electrode (electrochemistry) into 10 mM methanol solutions of **L7** in the presence of $NaBH_4$ for about 15-16 hours under N_2. Then, monolayer of Zn**L7** was prepared by immersing **L7** modified gold electrode (electrochemistry) into 40 mM $ZnCl_2$. After this, SAM-modified gold surfaces were rinsed with methanol and water and used immediately for the analysis.

Physical measurements.

Electrochemistry. All electrochemical studies were performed with an Autolab PGSTAT 20 instrument. The electrochemical blocking ability of the monolayers towards electron-transfer was studied by cyclic voltammetry and electrochemical impedance spectroscopy using $[Fe(CN)_6]^{3-/4-}$ redox couple as a probe. The electrolyte solutions used for electrochemical measurements were prepared with millipore water having a resistivity of 17 M Ω. Cyclic voltammetry and impedance measurements were conducted in a three-electrode glass cell at 20 °C. A platinum rod, a saturated calomel electrode (SCE) and a monolayer-modified gold disk electrode were used as a counter, reference and working electrodes respectively. Cyclic voltammetry was performed in 1 mM $[Fe(CN)_6]^{4-}$ aqueous solution containing 0.1 M NaCl as a supporting electrolyte. Impedance measurements were carried out at the formal redox potential (as determined from cyclic voltammetry) in an aqueous solution containing equal concentrations of oxidized and reduced forms of $[Fe(CN)_6]^{3-/4-}$ with NaCl as a supporting electrolyte. The frequency ranging from 10 KHz to 0.1 Hz with an ac amplitude of 10 mV was used for the analysis. Impedance spectroscopy data were analyzed to determine the charge transfer resistance (R_{ct}), a parameter used to quantify the rate of electron transfer across the interface.

Detection of anions. The sensitivity of monolayers to the phosphates anions pyrophosphate (PPi) and phosphate (Pi) were analyzed in an aqueous HEPES buffer solution (pH = 7.3) containing 1 mM $[Fe(CN)_6]^{3-/4-}$ with 0.1 M NaCl as a supporting electrolyte using electrochemical impedance spectroscopy. The concentration ranging from 0.1 μM to 1 mM was analyzed for all the phosphates anions studied in this work. The anions were added from a stock solution of their corresponding sodium salts having concentrations of 25 mM and 0.1 M and stirred well before carrying out the analysis.

6.5 References

(1) W. N. Lipscomb and N. Sträter, *Chem. Rev.*, 1996, **96**, 2375.

(2) T. Tabary, L. Y. Ju and J. H. M. Cohen, *J. Immunol. Methods*, 1992, **156**, 55.

(3) (a) D. Aldakov and P. Anzenbacher, *Chem. Commun.*, 2003, 1394; (b) N. J. Singh, E. J. Jun, K. Chellappan, D. Thangadurai, R. P. Chandran, I. C. Hwang, J. Yoon and K. S. Kim, *Org. Lett.*, 2007, **9**, 485; (c) A. Ojida, S. Park, Y. Mito-oka and I. Hamachi, *Tetrahedron Lett.*, 2002, **43**, 6193; (d) S. K. Kim, N. J. Singh, J. Kwon, I. C. Hwang, S. J. Park, K. S. Kim and J. Yoon, *Tetrahedron*, 2006, **62**, 6065; (f) Jr. P. Anzenbacher, K. Jursíková and J. L. Sessler, *J. Am. Chem. Soc.*, 2000, **122**, 9350; (g) S. Nishizawa, Y. Kato and N. Teramae *J. Am. Chem. Soc.*, 1999, **121**, 9463.

(4) D. H. Vance and A. W. Czarnik, *J. Am. Chem. Soc.*, 1994, **116**, 9397.

(5) S. Mizukami, T. Nagano, Y. Urano, A. Ouani and K. Kikuchi, *J. Am. Chem. Soc.*, 2002, **124**, 3920.

(6) M. J. McDonough, A. J. Reynolds, W. Y. Gladys Lee and K. A. Jolliffe, *Chem. Commun.*, 2006, 2971.

(7) R. G. Hanshaw, S. M. Hilkert, H. Jiang and B. D. Smith, *Tetrahedron Lett.*, 2004, **45**, 8721.

(8) L. Fabrizzi, N. Marcotte, F. Stomeo and A. Taglietti, *Angew. Chem. Int. Ed.*, 2002, **41**, 3811.

(9) (a) R. G. Hanshaw, S. M. Hilkert, H. Jiang and B. D. Smith, *Tetrahedron Lett.*, 2004, **45**, 8721; (b) M. S. Han and D. H. Kim, *Angew. Chem. Int. Ed.*, 2002, **41**, 3809; (c) A. Ojida, Y. Mito-oka, M. Inoue and I. Hamachi, *J. Am. Chem. Soc.*, 2002, **124**, 6256; (d) A. Ojida, M. Inoue, Y. Mito-oka and I. Hamachi, *J. Am. Chem. Soc.*, 2003, **125**, 10184; (e) A. Ojida, Y. Mito-oka, K. Sada and I. Hamachi, *J. Am. Chem. Soc.*, 2004, **126**, 2454; (f) H. N. Lee, K. M. K. Swamy, S. K. Kim, J. Y. Kwon, Y. Kim, S. J. Kim, Y. J. Yoon and J. Yoon, *Org. Lett.*, 2007, **9**, 243; (g) Y. J. Jang, E. J. Jun, Y. J. Lee, Y. S. Kim, J. S. Kim and J. Yoon, *J. Org. Chem.*, 2005, **70**, 9603.

(10) D. H. Lee, J. H. Im, S. U. Son, Y. K. Chung and J. I. Hong, *J. Am. Chem. Soc.*, 2003, **125**, 7752.

(11) D. H. Lee, S. Y. Kim and J. I. Hong, *Angew. Chem. Int. Ed.*, 2004, **43**, 4777.

(12) H. K. Cho, D. H. Lee and J. I. Hong, *Chem. Commun.*, 2005, 1690.

(13) H. N. Lee, Z. Xu, S. K. Kim, K. M. Swamy, Y. Kim, S. Kim, J. Yoon, *J. Am. Chem. Soc.*, 2007, **129**, 3828.

(14) (a) H. Aoki, K. Hasegawa, K. Tohda and Y. Umezawa, *Biosensors and Bioelectronics*, 2003, **18**, 261; (b) Y. Umezawa, *J. Supramol. Chem.*, 2002, **2**, 233; (c) O. Reynes, C. Bucher, J. C. Moutet, G. Royal and E. Sait-Aman, *Inorg. Chim. Acta*, 2008, **361**, 1784; (c) S. Zhang and L. Echegoyen, *J. Am. Chem. Soc.*, 2005, **127**, 2006.

(15) P. D. Beer, J. J. Davis, D. A. Drillsma-Milgrom and F. Szemes, *Chem. Commun.*, 2002, **16**, 1716.

Future work

In this thesis formation and characterization of several self-assembled monolayers of metal complexes has been carried out.
To characterize the SAMs formed, XPS, PM-RAIRS and electrochemical techniques were used. Further studies could be carried out using complementary techniques such as atomic force microscopy (AFM) or scanning tunneling microscopy (STM), which would provide information about the structural arrangement and orientation of the molecules on the surface.

The ability of the metal to affect electron-transfer through the SAMs was investigated and used to develop new anion sensors that work in water. An alternative approach would be to investigate these sensor properties by forming mixed SAMs. For example, the bulky receptor molecules (metal complexes) can be isolated by forming mixed SAMs with alkanethiol molecules, and this strategy could improve the recognition properties of the SAM. Also interesting would be to investigate the development of SAM-based sensors which combine metal and non-metal containing receptors, as this could extend the type of molecules that can be detected.

The modification of gold electrodes with metal complexes could also be used to investigate their possible applications in the field of catalysis.
For instance, preliminary results show that SAM-Cu**L4** could be used in oxygen reduction catalysis. For these studies, other electrochemical techniques such as rotating disk and ring disk voltammetry techniques would be useful. SAMs of Cu complexes containing BPA ligands have been used for the reduction of nitrite on gold electrodes. Similar studies could be carried out using the BPA derivative ligand **L10** which contains an amino group. These studies could reveal interesting hydrogen bonding effects in the activation of small molecules.

Overall, these systems are interesting to develop new strategies for the design of novel sensors and catalysts with potential applications in nanotechnology.

Publications

1) **"Metal mediated electron transport across molecular films"**. V. Ganesh, Maria Pilar Calatayud Sanz and Juan C. Mareque-Rivas, *Chemical Communications*, 2007, 804 – 806.

2) **"Effective anion sensing based on the ability of copper to affect electron transport across self-assembled monolayers"**. V. Ganesh, Maria Pilar Calatayud Sanz and Juan C. Mareque-Rivas, *Chemical Communications,* 2007, 5010-5012.

Conferences attended

1) UK Macrocyclic and Supramolecular Chemistry Discussion Group Annual Meeting. University of Leeds, Leeds, Uk. January 4^{th}-5^{th} 2006.

2) Bioinorganic Scientific Meeting. University of Santiago de Compostela, Spain. September 16^{th}-19^{th} 2007.

3) Royal Society of Chemistry Discussion Group Meetings: Inorganic Reaction Mechanism Coordination Chemistry. University of Edinburgh, Edinburgh, UK June 18^{th}-20^{th}.

Courses Attended

1) Weekly *Inorganic Section Seminars* during terms 2005-2008.

2) *School of Chemistry Colloquia* during terms 2005-2008.

3) *How to be an effective researcher*. University of Edinburgh May 2006.

4) *Induction Course for Laboratory demonstrators in Chemistry*, University of Edinburgh, September 2006.

5) *Fire awareness and Extinguishers. Record Training. Health and safety* Department (Fire Safety Unit). University of Edinburgh, November 2006.

6) *Mass Spectrometry: Principles and Practise in the 21st* Century. University of Edinburgh, April 2008.